

**DEVELOPMENT AND CHARACTERIZATION OF BARIUM RARE-EARTH  
ZIRCONATES, A NEW GROUP OF COMPLEX PEROVSKITES, FOR  
THEIR POTENTIAL USE AS SUBSTRATES FOR  
HIGH  $T_c$  SUPERCONDUCTORS**

**THESIS SUBMITTED TO MAHATMAGANDHI UNIVERSITY  
FOR THE DEGREE OF  
DOCTOR OF PHILOSOPHY  
IN  
PHYSICS**

**BY  
R. JOSE**

**REGIONAL RESEARCH LABORATORY  
(COUNCIL OF SCIENTIFIC AND INDUSTRIAL RESEARCH)  
TRIVANDRUM - 695 019**

**APRIL 2001**

## DECLARATION

I, R. Jose, hereby declare that, this thesis entitled “DEVELOPMENT AND CHARACTERIZATION OF BARIUM RARE-EARTH ZIRCONATES, A NEW GROUP OF COMPLEX PEROVSKITES, FOR THEIR POTENTIAL USE AS SUBSTRATES FOR HIGH  $T_c$  SUPERCONDUCTORS” is a bonafied record of the research work done by me at the Electronic Ceramics division of the Regional Research Laboratory (CSIR), Trivandrum, under the guidance of Professor Jacob Koshy and that no part of this thesis has been presented earlier for any degree, diploma of any other university.



R. Jose



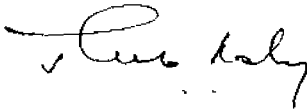
वैज्ञानिक तथा औद्योगिक अनुसन्धान परिषद्  
COUNCIL OF SCIENTIFIC & INDUSTRIAL RESEARCH  
क्षेत्रीय अनुसंधान प्रयोगशाला, तिरुवनन्तपुरम-695019  
REGIONAL RESEARCH LABORATORY  
THIRUVANANTHAPURAM 695 019  
KERALA, INDIA

Prof. J. KOSHY, Ph.D., C. Phys., F. Inst. P (Lond)

April 27, 2001

### CERTIFICATE

This is to certify that the thesis entitled "DEVELOPMENT AND CHARACTERIZATION OF BARIUM RARE-EARTH ZIRCONATES, A NEW GROUP OF COMPLEX PEROVSKITES, FOR THEIR POTENTIAL USE AS SUBSTRATES FOR HIGH  $T_c$  SUPERCONDUCTORS" is an authentic research work carried out by Mr. R. Jose, M Sc. under my supervision in partial fulfilment of the requirement for the degree of **Doctor of Philosophy** of Mahatma Gandhi University, and further that no part of this thesis has been presented before for any other degree.

  
(Jacob Koshy)

*To the loving memory of my grandmother*

## ACKNOWLEDGEMENT

*Words are insufficient to express my heartfelt thanks to my guide who has kindly suggested the problem and paved the way to the successful completion of it. His presence was every time a pleasure to me. With great love, respect and gratitude, I acknowledge my supervisor, Prof. Jacob Koshy, Dy. Director, Regional Research Laboratory, Trivandrum.*

*I am grateful to Dr. G. Vijay Nair, F.A.Sc, Director, Regional Research Laboratory, Trivandrum for providing all the facilities to carry out this work and his constant and continued support.*

*I am thankful to Ms. Asha M. John and Dr. N. Santha for their valuable help and encouragement during the course of this work.*

*My sincere thanks are due to Dr. J. James, Dr. K. G. K. Warriar, Mr. S. Suresh Kumar, Dr. P. R. S. Warriar, Dr. K. S. Kumar, Dr. J. K. Thomas, Dr. Sathy Chandrasekhar, Dr. M. T. Sebastian, Dr. H. Sreemoolanathan, Dr.M. Lalithabika, Mr. K. V. Oonnikrishnan Nair, Mr. P. Mukundan, Mr. S. K. Ghosh, Mr. S. Anantha Kumar, Mr. P. Anandan, Mr. K. S. G. Kurup, for their constant encouragement, efficacious discussions, and help with various instrumental facilities. I am very much thankful to Mr. K. P. Sadasivan, Head, Library and Informatics and all the staff members of the RRL library. I take this opportunity to express my gratitude to all the staff members of RRL*

*I am extremely thankful to Late Dr. D. Sundararaman, and Dr. V. S. Raghunathan, and Dr. E. Mohandas, Physical Metallurgy Section, IGCAR, Kalpakkam. My heartfelt thanks are due to Dr. R. Divakar, Scientific Officer, Physical Metallurgy Section and his colleagues Mr. A. Thirumurugesan and Mr. Vincent Paul Raj for their help at various stages of this work.*

*Thanks are also due to Dr. J. Kurian, Mr. P. K. Sajith, Dr. T. G. N. Babu, Dr. R. Ratheesh, Dr. Manoj Raama Varma, Ms. Maya Gopal, Mr. I. N. Jawahar, Mr. K. P. Surendran, Mr. S. Biju, Dr. V. Suresh, Dr. V. Biju, Mr. B. Praveen, Mr. A. U. Vinod, Mr. Ajay Mallia, Mr.S. Rajeshkumar, and Mr. Ramasamy, Mr. O. B. Suresh Kumar, Mr. O. B. satheesh Kumar, and Ms. Remya Korah for their helps at various stages of this work.*

*I express my deep sense of gratitude to Council of Scientific and Industrial Research, Department of Science and Technology, Govt. of India and State Committee on Science and Technology, Govt. of Kerala for financial assistance at various stages of this work.*

*Finally I thank my friends and well wishers for their encouragement and support given to me through out this work*

**R. Jose**

## PREFACE

The discovery of superconductivity in ceramic oxides has generated an enormous amount of research activities in materials with perovskite type crystal structure. It was realized that the immediate applications of the high temperature ceramic superconductors are in the form of thick and thin films. Thick films of high temperature superconductors have wide applications in microwave integrated circuits, transmission lines, and other high frequency electronic devices. Among the different copper oxide superconductors discovered,  $\text{YBa}_2\text{Cu}_3\text{O}_{7-\delta}$  (YBCO) and  $\text{Bi}_2\text{Sr}_2\text{Ca}_2\text{Cu}_3\text{O}_x$  [Bi (2223)] and  $\text{Bi}_2\text{Sr}_2\text{CaCu}_2\text{O}_x$  [Bi (2212)] (BSCCO) superconductors have gained considerable attention and a great deal of effort has been made for the production of high quality superconducting films of these compounds for suitable electronic applications. In the growth of superconducting thin films with high critical current density, the choice of a substrate is a key factor. The chemical non-reactivity between the substrate and the superconductor at the processing temperature is the most crucial factor for obtaining a superconducting film. The high chemical reactivity of these high  $T_c$  superconductors (HTS) at the processing temperature with most of the known substrate materials imposes severe restrictions on the material available as substrate for HTS films. Therefore the search for new substrate materials which satisfy the substrate requirement is undertaken on a global level.

A study on the development and characterization of a new group of complex perovskite ceramic oxides with general formula  $\text{Ba}_2\text{REZrO}_{5.5}$  for their use as substrates for high  $T_c$  superconductors and the preparation and characterization of superconducting films on the newly developed substrates are described in this thesis. These materials have an ordered cubic perovskite crystal structure and have favorable dielectric properties for substrate application at microwave frequencies. These materials do not show any phase transition up to  $1350^\circ\text{C}$  and are highly stable under atmospheric conditions. They melt congruently making it possible to grow them as single crystals from melt.  $\text{Ba}_2\text{REZrO}_{5.5}$  materials do not show any chemical reaction between YBCO, and Bi (2212) superconductors at extreme

processing conditions. Two materials in this group are non-reacting with Bi (2223) superconductor also. The suitability of these materials as substrate for high  $T_c$  superconductors was confirmed by dip-coating superconducting thick films on  $Ba_2REZrO_{5.5}$  substrates. The superconducting YBCO thick films developed on polycrystalline materials by dip-coating and melt texturing technique gave a  $T_c(0)$  of 92 K and  $J_c$  of  $\sim 3 \times 10^4$  A /  $cm^2$  at 77 K in zero applied magnetic field. Bi (2212) and Bi (2223) films developed on  $Ba_2REZrO_{5.5}$  gave a  $T_c(0)$  of 85 K and 110 K respectively. The current density of the films are  $\sim 10^3$  A /  $cm^2$  at 77 K.

In the course of this work, we have developed a modified combustion process for the synthesis of  $Ba_2REZrO_{5.5}$  materials as nanoparticles in a single step to achieve better phase purity, homogeneity and sinterability. The powders obtained through the modified combustion process were nanoparticles and no calcination at high temperature for prolonged duration was needed to obtain  $Ba_2REZrO_{5.5}$  materials as phase pure powders. The high-resolution lattice image taken on the as-prepared samples of  $Ba_2REZrO_{5.5}$  revealed that the intercrystalline boundary was sharp and free from impurities. The nanoparticles of  $Ba_2REZrO_{5.5}$  synthesized through the present method could be sintered to high density (>98%) at lower temperatures as compared to their coarse grained counterparts obtained through the solid state route.

**LIST OF PUBLICATIONS**

(SCI Journals only)

1. REBa<sub>2</sub>ZrO<sub>5.5</sub> (RE= La, Ce, Eu and Yb): Synthesis and characterization and their potential use as substrate for YBa<sub>2</sub>Cu<sub>3</sub>O<sub>7-δ</sub> superconductors.  
**R. Jose, Asha M. John, J. Kurian, P. K. Sajith and J. Koshy,**  
J. Mater. Res. **12**, 2976, 1997 (U.S.A.).
2. Superconducting Bi (2223) films [T<sub>c</sub>(0) = 110 K] by dip coating on Ba<sub>2</sub>LaZrO<sub>5.5</sub>: A newly developed ceramic substrate.  
**R. Jose, Asha M. John, J. James, K. V. O. Nair, K. V. Kurian and J. Koshy**  
Mater. Lett **41**, 112 (1999) (USA)
3. A new combustion process for nanosized YBa<sub>2</sub>ZrO<sub>5.5</sub> powders.  
**R. Jose, J. James, Asha M. John, D. Sundararaman, R. Divakar and J. Koshy,**  
Nanostruct. Mater. **11**, 623 (1999) (USA)
4. Synthesis of nanosized Ba<sub>2</sub>LaZrO<sub>5.5</sub> ceramic powders through a novel combustion route.  
**R. Jose, J. James, Asha M. John, R. Divakar and J. Koshy**  
J. Mater. Synth. Process. **8**, 1 (2000) (USA)
5. Synthesis and Characterization of nanoparticles of Ba<sub>2</sub>EuZrO<sub>5.5</sub>: A new complex perovskite ceramic oxide.  
**R. Jose, J. James, Asha M. John, R. Divakar and J. Koshy**  
J. Mater. Res. **15**, 2125 (2000) (USA)
6. Barium holmium zirconate, a new complex perovskite oxide: part I, Synthesis, characterization and potential use as substrate for high T<sub>c</sub> superconductors,  
**R. Jose, Asha M. John, and J. Koshy, (Communicated-2001)**

7. Barium holmium zirconate, a new complex perovskite oxide: part II, Synthesis as nanoparticles through a modified combustion process.  
R. Jose, Asha M. John, R. Divakar and J. Koshy , (Communicated-2001)
8. Barium Rare Earth Hafnates: Synthesis, Characterization and Potential use as substrates for YBCO superconductors  
Asha M. John, R. Jose, J. Kurian, P. K. Sajith and J. Koshy  
J. Am. Ceram. Soc. **82**, 1421, 1999 (U.S.A).
9. Synthesis and Characterization of nanoparticles of Ba<sub>2</sub>EuHfO<sub>5.5</sub>: A new complex perovskite ceramic oxide  
Asha M. John, R. Jose, J. James, R. Divakar and J. Koshy,  
Mater. Lett. (In press) (USA)
10. Synthesis and rapid densification of nanoparticles of barium praseodymium hafnium oxide: A new complex perovskite  
Asha M. John, R. Jose and J. Koshy,  
J. Nanopar. Res. (In press) (USA)
11. A new family of complex perovskites suitable as substrates for YBCO and BiSCCO superconductors  
J. Koshy, J. Kurian, K. S. Kumar, P. K. Sajith, M. J. Asha and R. Jose,  
Ind. J. Pure. Appl. Phys. **34**, 698 (1996)
12. Novel ceramic substrate for high T<sub>c</sub> superconductors  
J. Koshy, J. Kurian, R. Jose, Asha M. John, P. K. Sajith, J. James, S. P. Pai and R. Pinto  
Bull. Mater. Sci. **22**, 243 (1999)
13. Synthesis of nanoparticles of barium lanthanum hafnium oxide by a modified combustion process  
Asha M. John, R. Jose, and J. Koshy (Communicated-2001)
14. Superconducting YBCO ( $T_c(0) = 92$  K) and Bi-2223 ( $T_c(0) = 110$  K) thick films on Ba<sub>2</sub>LaHfO<sub>5.5</sub>: A new perovskite ceramic substrate  
Asha M. John, R. Jose, M. A. Ittyachen and J. Koshy, (Communicated-2001)

## PATENTS

### (a) International Patents

1. Novel Ceramic substrate for Bi-cuprate superconductors  
J.Koshy, J.Kurian, P.K.Sajith, K.S.Kumar, **R.Jose**, AshaM.John and  
A.D.Damodaran,  
**US Patent No: 5, 741, 747 dated April 21, 1998**
2. Ceramic substrate for Bi-cuprate superconductors and a process for  
preparing the same  
J.Koshy, J.Kurian, P.K.Sajith, K.S.Kumar, **R. Jose**, Asha M. John and  
A.D Damodaran  
**US Patent No: 6, 140, 275 dated Oct.31, 2000**
3. Novel Ceramic substrate for Bi-cuprate superconductors  
J.Koshy, J.Kurian, P.K.Sajith, K.S.Kumar, **R.Jose**, Asha M.John and  
A.D.Damodaran  
**European Patent File No. 96308464.5-2208 dated 28-01-1997.**
4. A novel process for the synthesis of nano particles of ceramic oxide  
powders in a single step processing using aqueous and non-aqueous  
precursor  
J.James, **R.Jose**, Asha M.John and J.Koshy  
**US Patent File No. 09 / 537 252 dated March 28, 2000**

### (b) Indian Patents

5. Process for preparation of novel ceramic substrates  $Ba_2DyMO_{5.5}$  (M = Zr,  
Sn and Hf) for Bi-cuprate superconductors and a process for the preparation  
of phase pure superconducting Bi (2223) and Bi (2223)-Ag thick film on  
this newly developed substrate  
J. Koshy, J. Kurian, P.K.Sajith, K.S. Kumar, **R. Jose**, A M. John and  
A.D. Damodaran  
**Indian Patent, 1028/DEL/96 dated 1996**
6. A novel process for the synthesis of nano particles of ceramic oxide  
powders in a single step processing using aqueous and non-aqueous  
precursor  
J.James, **R.Jose**, Asha M.John and J.Koshy  
**Indian Patent File No. NF 58 / 98 (1999)**

## CONTENTS

Preface	i
List of Publications	iii
List of patents	v
<b>I General Introduction</b>	<b>1- 49</b>
1.1 Ceramic Materials	01
1.2 Perovskites	03
1.3 High Temperature Superconductors	06
1.3.1 Superconductivity	06
1.3.2 Evolution of high temperature superconductivity	07
1.3.3 Yttrium Barium Copper Oxide Superconductor	11
1.3.4 Bismuth Strontium Calcium Copper Oxide Superconductor	15
1.3.4 Thallium Barium Calcium Copper Oxide Superconductor	19
1.3.5 Mercury Barium Calcium Copper Oxide Superconductor	20
1.4 High Temperature Superconducting Films	21
1.4.1 Superconducting thick films	22
1.4.2 Substrates for high T <sub>c</sub> superconducting films	24
1.5 Nanostructured Materials	30
1.6 Scope of the Present Work	33
References	35
<b>II Preparation and Characterization techniques</b>	<b>51-70</b>
2.1 Introduction	51
2.2 Ceramic Processing	51
2.2.1 Powder Preparation	52

2.2.2	Shaping	53
2.2.3	Sintering	54
2.3	Preparation of Superconducting thick films	54
2.4	Characterization techniques	55
2.4.1	Powder X-ray Diffraction Technique	56
2.4.2	Differential Thermal Analysis	58
2.4.3	Thermogravimetric Analysis	58
2.4.4	IR Spectroscopy	59
2.4.5	Gas Adsorption Technique	59
2.4.6	Agglomerate Size Analysis	61
2.4.7	Transmission Electron Microscopy	62
2.4.8	Dielectric Measurements	64
2.4.9	Resistance measurements	65
2.4.10	Current Density measurements	69
	References	70
<b>III</b>	<b>Synthesis of Ba<sub>2</sub>RE ZrO<sub>5.5</sub> (RE = La, Ce, Eu, Yb, Ho, and Er):A new group of complex perovskite ceramic oxide through Solid State reaction method.</b>	<b>71-101</b>
3.1	Introduction	71
3.2	Synthesis of Ba <sub>2</sub> RE ZrO <sub>5.5</sub> (RE = La, Ce, Eu, and Yb)	71
3.3	Sintering of Ba <sub>2</sub> RE ZrO <sub>5.5</sub>	73
3.4	Structural characterization of Ba <sub>2</sub> REZrO <sub>5.5</sub> ceramics	75
3.5	Synthesis of Ba <sub>2</sub> REZrO <sub>5.5</sub> (RE = Ho and Er)	83
3.6	Sintering and structural studies of Ba <sub>2</sub> REZrO <sub>5.5</sub> (RE = Ho and Er)	89
3.7	DTA studies of Ba <sub>2</sub> REZrO <sub>5.5</sub> (RE = La, Ce, Eu, Yb, Ho and Er)	93
3.8	Melting studies of Ba <sub>2</sub> REZrO <sub>5.5</sub> (RE = La, Ce, Eu, Yb, Ho and Er)	94

3.9	Stability studies of $Ba_2REZrO_{5.5}$ (RE = La, Ce, Eu, Yb, Ho and Er)	94
3.10	Dielectric studies of $Ba_2REZrO_{5.5}$ (RE = La, Ce, Eu, Yb, Ho and Er)	94
3.11	Conclusions	98
	References	100
<b>IV</b>	<b>Barium Rare-earth Zirconates as novel substrates for Superconducting <math>YBa_2Cu_3O_{7-\delta}</math> films</b>	<b>102 -125</b>
4.1	Introduction	102
4.2	Chemical reactivity between YBCO and $Ba_2REZrO_{5.5}$	104
4.2.1	The structural studies of the $Ba_2REZrO_{5.5}$ -YBCO composite	107
4.2.2	The superconducting properties of $Ba_2REZrO_{5.5}$ -YBCO composite	110
4.3	Lattice matching of $Ba_2REZrO_{5.5}$ with YBCO	114
4.4	Preparation of YBCO thick films on $Ba_2REZrO_{5.5}$	115
4.5	Characterization of YBCO thick films	117
4.6	Conclusions	123
	References	124
<b>V</b>	<b>Development of superconducting Bi- Cuprate thick films on Barium Rare-earth Zirconates by dip-coating and melt Texturing</b>	<b>126-161</b>
5.1	Introduction	126
5.2	Synthesis of Bi (2212) superconductor	127
5.3	Chemical reactivity between $Ba_2REZrO_{5.5}$ and Bi (2212)	129
5.4	Preparation of Bi (2212) thick films on $Ba_2REZrO_{5.5}$	138
5.5	Synthesis of Bi (2223) superconductor	141

5.6	Chemical reactivity between $Ba_2REZrO_{5.5}$ and Bi(2223)	144
5.7	Development of Bi (2223) thick films on $Ba_2REZrO_{5.5}$	155
5.8	Conclusions	159
	References	160
<b>VI</b>	<b>Synthesis and Characterization of nanoparticles of Barium Rare-earth Zirconates through a novel combustion route.</b>	<b>162-199</b>
6.1	Introduction	162
6.2	Wet chemical methods	163
6.3	Modified combustion process	166
6.4	Synthesis of nanoparticles of $Ba_2REZrO_{5.5}$	167
6.5	Characterization of $Ba_2REZrO_{5.5}$ powders	168
	6.5.1 Structural characterization of the combustion product	168
	6.5.2 Thermal characterization of the combustion product	173
	6.5.3 Gas adsorption studies of the combustion product	179
	6.5.4 Agglomerate size analysis of the combustion product	181
	6.5.5 TEM studies of the combustion product	182
6.6	Sintering of nanoparticle of $Ba_2REZrO_{5.5}$	191
6.8	Structural characterization of the sintered nanoparticles	193
6.9	Conclusions	195
	References	197
<b>VII</b>	<b>Summary and Conclusion</b>	<b>200-205</b>
7.1	<b>Future projections</b>	<b>204</b>

## CHAPTER 1

### GENERAL INTRODUCTION

Human civilization has gone through rapid revolutions due to the recent advancements in Material Science and Technology. Along with the exciting developments in electronics in the second half of the twentieth century, the huge potential of ceramic materials was unfolded to a fascinatingly wide spectrum of applications. This explosion includes a vast number of magnetic, electric, electronic, photonic, superconducting ceramics used in diverse domains such as transportation, industrial production, power engineering, medicine and health care, consumer electronics and communication. In the dawn of the millennium, ceramic devices are undergoing miniaturization in unimaginable pace from micro-technology to nano-technology like that of conventional semiconductors in twentieth century.

#### 1.1 Ceramic materials

The term 'ceramics' has evolved from the Greek word 'Keramos', means object made from fired clay. Ceramics are crystalline inorganic solid compounds of metal and/or nonmetals, formed by the application of heat, and some times heat and pressure [1]. The bonding in ceramics is mostly ionic but in some cases covalent or metallic bonding occurs. Ceramics, in general, are brittle, hard, wear-resistant, prone to thermal shock, refractory, electrically and thermally insulative, intrinsically transparent, non-magnetic, chemically stable and oxidation resistant [2]. As with all generalizations there will be exceptions, some ceramics are good electrical and thermal conductive and some are even electrically superconducting. Though ceramics are generally nonmagnetic, high field magnets

were developed from ceramics and the magnetic properties of certain ceramics are such that they will find tremendous applications in future. A large number of inorganic non-metallic and non water-soluble compounds including oxides, nitrides, borides, carbides and silicides of all metals and nonmetals come under the classification of ceramics.

Ceramic materials can be classified as Traditional and Advanced or Technical. Traditional ceramics include from sanitary ware to fine Chinaware and porcelains to glass products and are mostly silicate based with porous microstructures, coarse, non-uniform and multiphase. Advanced or technical ceramics are characterized by very fine microstructure, greater homogeneity and less porosity. They are synthesized using high pure raw materials through highly controlled processes [1]. Based on the application, advanced ceramics can be further divided into functional and structural ceramics. Functional ceramics are used for performing special functions, viz. electrical, magnetic, optical etc. in devices. Structural ceramics function as structural materials with high mechanical strength and stability even at high temperature. Currently ceramics are being applied for uses that were inconceivable two decades ago, like ceramic engines, electro-optic devices, laser materials, substrates in electronic circuits, electrodes in photoelectrochemical devices etc.[2].

The conventional way of advanced ceramic preparation includes powder preparation, shaping and sintering. The technical properties of ceramic materials are not only determined by its chemical composition but also by the chemical homogeneity, crystal structure and the microstructure parameters like crystallite size, aggregate/agglomerate structure of the ceramic powder [3]. The

microstructure is controlled by the preparation conditions right from the raw material powder to the final heating of the ceramic [3].

## 1.2. Perovskites

Many electronic ceramic materials belong to a large family of materials called perovskites, which derive the name from the specific mineral “perovskite”,  $\text{CaTiO}_3$ . Perovskite materials are of considerable technological importance, particularly with regard to physical properties such as pyro- and piezo-electricity, dielectric susceptibility, linear and nonlinear electro-optic effects etc.[4,5]. The compounds of the perovskite family are probably the most numerous and the most widely studied. In their ideal form, perovskites are described by the general formula  $\text{ABX}_3$ , are cubes made up of three distinct chemical elements A, B and X in the ratio 1:1:3. Of the three distinct elements, A and B are metallic cations and X is non-metallic anion. In  $\text{CaTiO}_3$ , the larger Ca occupies the A site and Ti in the B position and oxygen fills all 12 of the X sites. Barium, Potassium, Strontium and rare-earth elements can occupy the A position, more than half of the stable entries in the periodic table are known to adopt the B-position. The X position can take up not only by oxygen but also by members of the halogen family of nonmetals like fluorine, chlorine or bromine[6]. The ideal perovskite unit cell structure is illustrated in figure 1.1(a). The A cation, the larger of two kind of metals, has a 12-fold coordination in the crystal and lies at the body-centered position of the cube. The B cations have 6-fold coordination and occupy all the eight corners of the cube. The X anions are situated at the midpoint of the 12 edges of the cube [6]. Alternatively, the perovskite structure can be visualized as a collection of polyhedra as in figure 1.1(b). The anions are at the corners of the  $\text{BX}_6$  octahedra

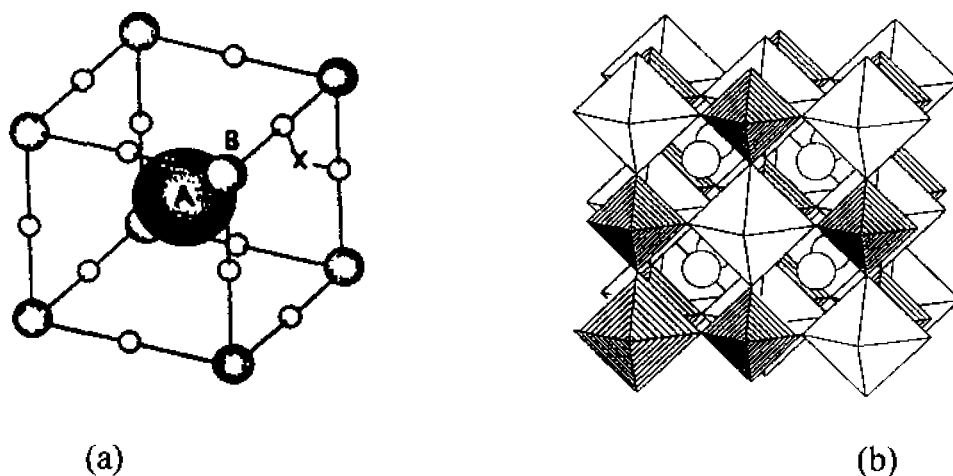


**Figure 1.1:** The perovskite structure (a) ideal, (b) as a collection of polyhedra

extending in three dimensions. The  $BX_6$  octahedra are perfect with  $90^\circ$  angles and with six equal B-X bonds. Each B-ion is surrounded by equi-distant anions. The ideal perovskite structure can also be visualized as a close-packed structure in which the X and A ions are stacked in close packed layers along the cubic (111) direction. The resulting octahedral holes are occupied by B ions.

Reducing from the ideal cubic symmetry, the unit cell structures of majority of the perovskites consist of non-ideal octahedra depending upon the relative sizes of A, B and X ions. The wide variety of properties exhibited by the perovskite family can be explained on the basis of this deviation of symmetry of octahedra. Such “off-centering” of ions give electrical polarity, called spontaneous polarization, to the perovskite crystals. Moreover, the direction of this polarization can be changed simply by subjecting to an electric field. Such materials, that have reversible spontaneous polarization are known as ferroelectrics and find extensive application in electronic devices [6]. The octahedral deviations from the ideal

structure and their relation to physical properties have been extensively studied and can be found in literature [4,5,7,8].

There are fairly a large number of compounds with the ideal perovskite structure [9-14]. In the perovskite structure, A and B sites can accommodate two or more cations, either homovalent or aliovalent, maintaining the electrical neutrality of the crystal. Such compounds are called Complex perovskites, represented by  $(A, A')(B, B')O_3$ . Here the substituted cations can either randomly or orderly occupy the A and B sites. In the random case, the substituting cations occupy the particular A or B sites of the crystal at random. Whereas, in other ordered crystal, the substituting cations occupy the A or B site in an ordered manner. In the case of two different cations, B and B', occupying the octahedral sites, the ordering of the two cations (B and B') at the octahedral sites leads to the formation of a superstructure which in turn leads to the multiplying of the basic unit cell. The ordering of the B and B' cations at the octahedral position means; B and B' cations strictly fill alternate octahedral positions through out the structure. The ordering of cations at the octahedral positions and the order-disorder transitions in complex perovskite structure as a function of annealing conditions are extensively studied and can be found in literature [15-20]. Similarly the ordering of A sites can also leads to the formation of superstructures. The ordering of the B site at  $A_2BB'O_6$  compound and the A site of  $AA'B_2O_6$  compound have been extensively investigated by different groups [9-10,15-19, 21-22].

### **1.3 High temperature superconductors:**

#### **1.3.1 Superconductivity**

Superconductivity was discovered in 1911 by a Dutch Physicist, H. Kammerlingh Onnes at the University of Lieden while he was studying the

electrical properties of metal at liquid helium temperature (4 K). He found that the electrical resistance of a rod of frozen mercury suddenly dropped to an immeasurably small value when the temperature was at 4.2 K and because of its extraordinary electrical properties, Onnes called this new state as superconductive state. Superconductors have four important characteristics [23], namely, zero resistivity, Meissner effect, Josephson effect and quantization of magnetic field. Zero resistivity means, a material in its superconducting stage offers no resistance to the flow of direct electric current or in other words superconductor is a perfect electrical conductor. Meissner effect: a superconductor will expel magnetic flux from its interior by an internally induced magnetic field. Thus a superconductor in a weak magnetic field will act as a perfect diamagnet. Josephson effect is the remarkable electrical property associated with the tunneling of superconducting electron pairs from a superconductor through a thin layer of an insulator in to another superconductor. Quantization of magnetic field: the total magnetic flux that passes through a superconducting ring may assume only quantized value, integral multiples of the flux quantum  $hc/q$ , where  $q = -2e$ , the charge of an electron pair. The first two properties are related to electric power application and the last two properties are related to microelectronic applications. In addition, superconductors have three critical parameters [23]. Critical temperature ( $T_c$ ), critical magnetic field ( $H_c$ ) and critical current density ( $J_c$ ). Critical temperature is defined as the temperature at which a specimen undergoes a transition from a state of normal electrical resistivity to the superconducting state. The value of the applied magnetic field that destroys superconductivity is called the critical magnetic field and is a function of temperature. The critical current density is the critical value of current that the superconductor can support without destroying the superconductivity and is a function of temperature and applied magnetic field. In

the years from 1911 to 1986 several hundred materials were found to be superconducting at sufficiently low temperatures. However, the highest  $T_c$  achieved in this period was 23K in  $Nb_3Ge$ , an intermetallic compound [24].

### 1.3.2 Evolution of high temperature superconductivity

In 1986, J. G. Bednorz and K. A. Muller, both from IBM laboratory in Zurich, found superconductivity at 30 K in  $La_{2-x}Ba_xCuO_4$ , which is a mixed oxide of lanthanum, barium and copper [25]. Though the transition temperature of this compound was not much higher than that was known for the best intermetallic superconductor (23 K), it was a completely different type of material and opened the way for all the subsequent work on high temperature superconductors. This discovery was confirmed by several groups as due to  $La_{2-x}Ba_xCuO_4$  phase with layered  $K_2NiF_4$  type crystal structure [26, 27] and evoked a worldwide search for new materials with higher  $T_c$  values. It was soon found that the substitution of strontium for barium in La-Ba-Cu-O compound raised  $T_c \sim 40K$  [28, 29]. Since the discovery of superconductivity in the cuprates of  $K_2NiF_4$  structure, many other cuprates with higher  $T_c$ s have been discovered, and all of them possess two-dimensional Cu-O sheets as an essential feature [24]. In December 1986, Paul Chu's group at university of Houston found  $T_C$  onset of 52.5 K for La-Ba-Cu-O compound under high pressure [30, 31]. In 1987, Paul Chu and M. K. Wu at the University of Alabama had found that a new perovskite ceramic compound, Yttrium-Barium-Copper-Oxide superconducts with a  $T_C$  of 92 K [32]. For the first time in history, superconductivity above boiling point of liquid nitrogen was discovered, representing one of the greatest triumphs of scientific endeavor. Several groups [33-39] confirmed this discovery. Although the structure and composition of this cuprate were not known initially, it was soon found that it had

the composition with oxygen deficient orthorhombic perovskite structure [40-43]. It was soon found that other rare earth cuprates of the general formula  $\text{LnBa}_2\text{Cu}_3\text{O}_7$  (Ln = Rare Earth) are also orthorhombic and superconducting with  $T_c$ s around 90K, except when Ln = La, Pr, Ce or Tb [44-47].  $\text{LnBa}_2\text{Cu}_3\text{O}_7$  compounds are often called '123' cuprates because the three metal ions are in the ratio 1:2:3. In 1987 itself Michel et al [48] substituted Bi for La in the original Bednorz and Muller formula and isolated a compound with formula  $\text{Bi}_2\text{Sr}_2\text{CuO}_{7+\delta}$  which superconduct with a maximum  $T_c$  of 22 K. Following this report, bismuth cuprates of the general formula  $\text{Bi}_2(\text{Sr,Ca})_{n-1}\text{Cu}_n\text{O}_{2n+4}$  were discovered in 1988 with  $T_c$  values of 85 K and 110 K respectively for  $n = 2$  and  $n = 3$  phases [49, 50]. The  $n = 3$  phase has three sets of nearby  $\text{CuO}_2$  planes and has the highest  $T_c$  for this series of materials. This is the point in history when it was realized that higher  $T_c$  values were more likely in compounds with a larger number of  $\text{CuO}_2$  planes in proximity. In contrast to this, superconductors with infinite layer structures where  $\text{CuO}_2$  planes are separated by Sr, Ca, Nd or La atoms were synthesized with  $T_c$  in the range 40-120 K [51-54]. The replacement of Bi by Tl and Sr by Ba in  $\text{Bi}_2(\text{Sr,Ca})_{n-1}\text{Cu}_n\text{O}_{2n+4}$  yielded a similar set of compounds with general formula  $\text{Tl}_2\text{Ba}_2\text{Ca}_{n-1}\text{Cu}_n\text{O}$  with  $T_c$  values of 80, 110 and 125 K respectively for  $n = 1, 2$  and  $3$  [55-57]. The thallium based materials had as their distinguishing characteristic of very high superconducting transition temperature, holding the record for a very long time and crossed barrier of boiling point of liquefied natural gas (120K). In 1993, Putlin [58] and co-workers reported about the synthesis of the first Hg based superconductor  $\text{HgBa}_2\text{CuO}_4$  with  $T_c = 94$  K. The mercury cuprates  $\text{HgBa}_2\text{Cu}_{n-1}\text{Cu}_n\text{O}_{2n-n}$  have a structure derived from that of the thallium cuprates  $\text{TlBa}_2\text{Ca}_{n-1}\text{Cu}_n\text{O}_{2n+3}$ . The second member of this series with  $n = 2$  has a  $T_c$  of 120 K [59]. The third member of this series with  $n = 3$

Table 1.1:  $T_C$  and Crystal structure of some Copper Oxide Superconductors

Material	$T_C$ (K)	Structure
$\text{La}_{2-x}\text{Ba}_x\text{CuO}_{4+\delta}$	30	Tetragonal
$\text{La}_{2-x}\text{Sr}_x\text{CuO}_{4+\delta}$	40	"
$\text{YBa}_2\text{Cu}_3\text{O}_{7-\delta}$	92	Orthorhombic
$\text{REBa}_2\text{Cu}_3\text{O}_{7-\delta}$ (RE = rare-earth except Ce, Pr and Tb)	~92	"
$\text{YBa}_2\text{Cu}_4\text{O}_{10}$	92	Tetragonal
$\text{Bi}_2\text{Sr}_2\text{CuO}_6$	17	Orthorhombic
$\text{Bi}_2\text{Sr}_2\text{CaCu}_2\text{O}_8$	85	"
$\text{Bi}_2\text{Sr}_2\text{Ca}_2\text{Cu}_3\text{O}_{10}$	110	"
$\text{Tl}_2\text{Ba}_2\text{CuO}_6$	20	Tetragonal
$\text{Tl}_2\text{Ba}_2\text{Ca}_2\text{Cu}_3\text{O}_x$	125	"
$\text{TlBa}_2\text{CaCu}_2\text{O}_{7+\delta}$	80	"
$\text{TlBa}_2\text{Ca}_2\text{Cu}_3\text{O}_{7+\delta}$	110	"
$\text{TlBa}_2\text{Ca}_3\text{Cu}_4\text{O}_{12+\delta}$	122	"
$\text{Tl}_2\text{Ba}_2\text{CaCu}_2\text{O}_{8+\delta}$	110	"
$\text{Tl}_2\text{Ba}_2\text{Ca}_2\text{Cu}_2\text{O}_{10+\delta}$	125	"
$\text{Tl}_2\text{Ba}_2\text{Ca}_3\text{Cu}_4\text{O}_{12+\delta}$	105	"
$\text{HgBa}_2\text{CuO}_{5+\delta}$	94	"
$\text{HgBa}_2\text{CaCu}_2\text{O}_{7+\delta}$	104	"
$\text{HgBa}_2\text{Ca}_2\text{Cu}_3\text{O}_{9+\delta}$	135	"
$\text{HgBa}_2\text{Ca}_3\text{Cu}_4\text{O}_{12+\delta}$	105	"
$\text{HgBa}_2\text{Ca}_4\text{Cu}_5\text{O}_{8+\delta}$	105	"
$\text{HgBa}_2\text{Ca}_5\text{Cu}_6\text{O}_x$	95	"

having a  $T_c$  of 134 K [60] at ambient pressure is currently the high  $T_c$  record holder. The  $T_c$  value of this material reaches to 164 K, when measured at high pressure and is not too far from the lowest temperature recorded on earth (183 K) [24]. The details of some of the important superconductors are summarized in Table 1.1. Figure 1.2 shows the evolution of high temperature superconductivity since its discovery in 1911 [24].

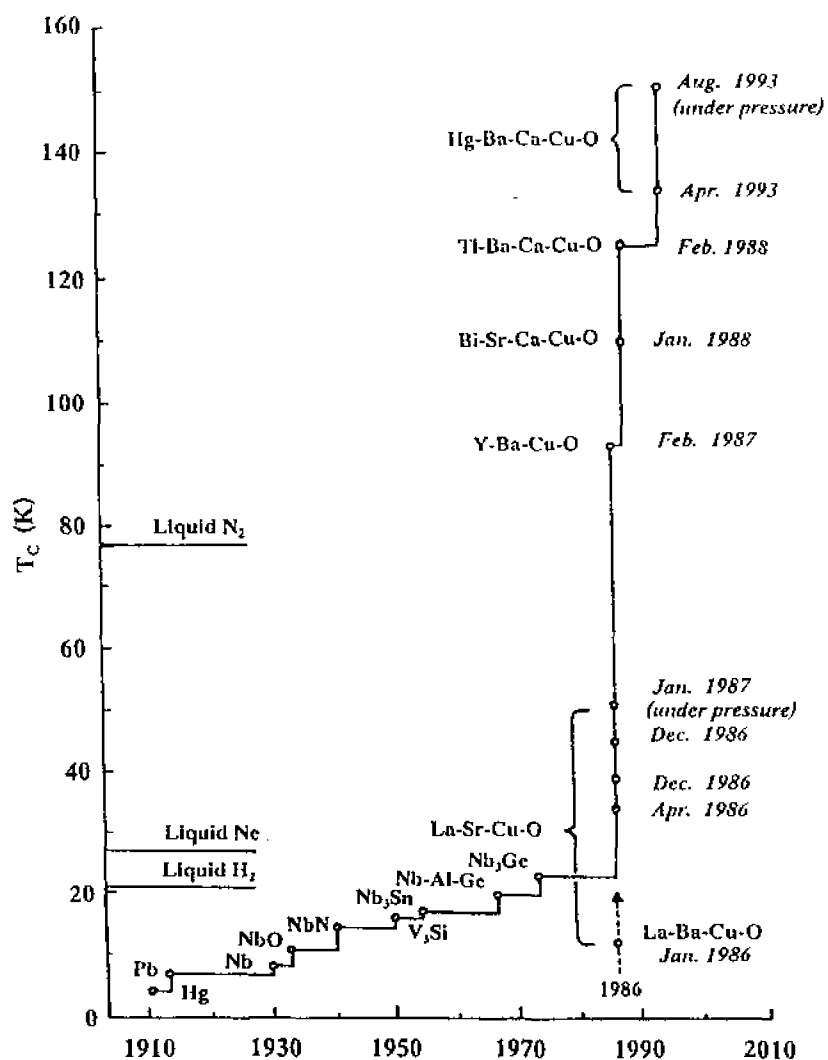


**Figure 1.2:** The evolution of superconductive transition temperature since its discovery in 1911

### 1.3.4 The Yttrium Barium Copper Oxide superconductor

Superconductivity above liquid nitrogen temperature in a mixed oxide of yttrium, barium and copper was confirmed by several groups [33-39] after its discovery by Wu *et al* [32] and the phase responsible was identified as  $\text{YBa}_2\text{Cu}_3\text{O}_{7-\delta}$  (YBCO). This is the most widely studied material among the Y-Ba-Cu-O system. YBCO has an oxygen deficient perovskite crystal structure as established by powder X-ray [40-43] and neutron diffraction studies [61-65] as well as using single crystals [66-70] studies. Two principal varieties of YBCO have been recognized. Several workers had recognized that YBCO crystallizes as tetragonal at high temperatures, but converts to an orthorhombic form by oxygen ordering on cooling [66, 71, 72]. The structure of the orthorhombic and tetragonal phases of YBCO is shown in figure 1.3.

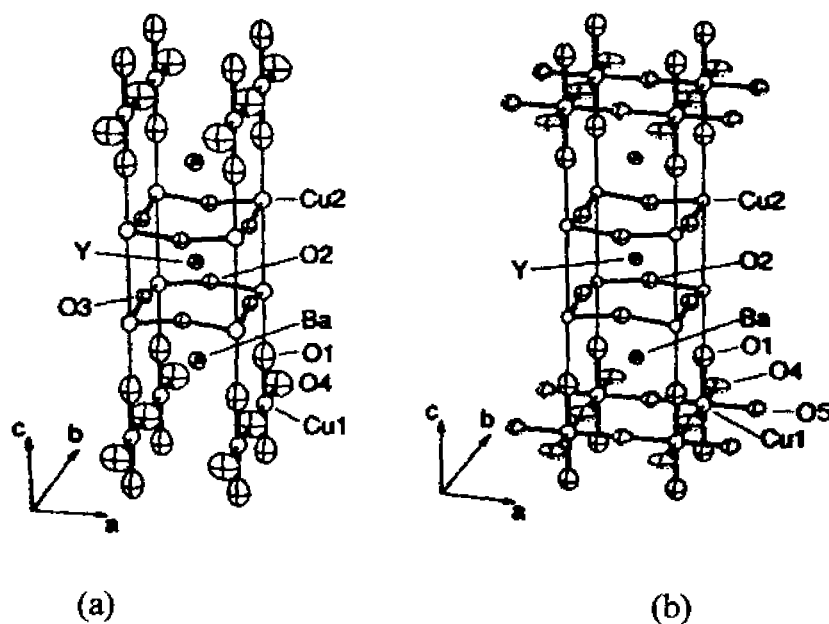
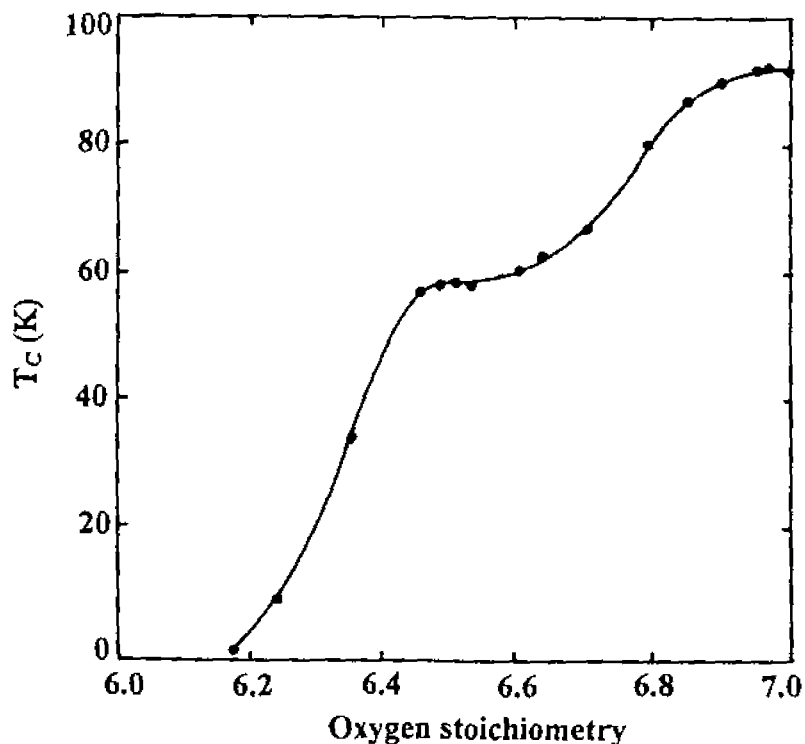


Figure 1.3: The structure of (a) orthorhombic and (b) tetragonal phase of  $\text{YBa}_2\text{Cu}_3\text{O}_{7-\delta}$

The tetragonal phase is semiconductive and the orthorhombic phase is superconductive. The structure of superconducting YBCO derives from the stoichiometric perovskite by the tripling of the basic perovskite unit cell along the c-axis, with two inequivalent Cu planes, labeled Cu1 and Cu2, sandwiched between Ba-planes and Y-planes for Cu2 and the removal of oxygen from the Cu-plane and the Cu1-plane [73]. Thus the structure consists of triple layers of corner sharing polyhedra, parallel to (001), whose cohesion is provided by planes of yttrium and barium cations [24,73]. The structure is therefore often described as an association of Cu-O chains and pyramidal copper and oxygen layers. Besides the  $\text{CuO}_2$  sheets, the superconducting phase contains Cu-O-Cu chains (or corner linked  $\text{CuO}_4$  units) which are absent in the non-superconducting sample [74, 75]. The valance of Cu in  $\text{YBa}_2\text{Cu}_3\text{O}_{7-\delta}$  is 2.33 and if no oxygen were removed the formal valance of  $\text{Cu}^{+n}$  would be  $n = 3$ . The structure has two  $\text{CuO}_2$  sheets in the a-b plane and Cu-O chains along the b-axis. The two dimensional character of this structure associated with the mixed valence of Cu is often proposed as the origin of the high temperature superconductivity in this material [24, 73].

The superconductivity in  $\text{YBa}_2\text{Cu}_3\text{O}_{7-\delta}$  is extremely sensitive to oxygen stoichiometry [40,76-80]. The structure is orthorhombic if  $\delta < 0.15$  and becomes tetragonal as  $\delta > 0.5$ . Structures of the orthorhombic and tetragonal phases differ in an interesting manner. Oxygen is readily intercalated in the  $\delta > 0.5$  sample and the stoichiometry reaches close to  $\text{YBa}_2\text{Cu}_3\text{O}_7$  on intercalation. The variation of  $T_c$  of YBCO with oxygen stoichiometry is shown in figure 1. 4. The  $T_c$  is maximized by reducing  $\delta$  to 0.1 and obtaining a fully orthorhombic phase. In both the orthorhombic and tetragonal phases, oxygen sites in the Y plane are vacant, leaving Cu2 five fold coordinated. In the ideal orthorhombic phase, in the Cu1

plane, the O4 and O5 sites are occupied differently. As  $\delta \rightarrow 0$  the O4 sites are occupied along the b-axis and the similar O5 sites are vacant along the a-axis,



**Figure 1.4:** The variation of  $T_c$  with oxygen stoichiometry for  $\text{YBa}_2\text{Cu}_3\text{O}_{7-\delta}$ .

giving b-axis Cu1-O4 chains. In the tetragonal phase  $\text{YBa}_2\text{Cu}_3\text{O}_6$  phase both O4 and O5 sites are vacant. The structural transformations and the associated superconducting properties depending on the oxygen content of YBCO have been reported by several groups [81-85]. Superconductivity of YBCO samples is greatly degraded by the interaction with water and humid air [86-88]. The lattice parameters of the orthorhombic YBCO is  $a = 3.8231 \text{ \AA}$ ,  $b = 3.8864 \text{ \AA}$ ,  $c = 11.6807 \text{ \AA}$  and the values of lattice parameter depends on the annealing conditions[89]. YBCO is a type II superconductor with upper and lower critical fields are 1T and 120 T respectively. The studies of YBCO single crystals showed marked anisotropic behavior in resistivity [88], magnetic susceptibility [90], critical

magnetic field [90] and critical current density [91, 92]. Some of the important properties of YBCO superconductor are summarized in Table 1.2.

**Table 1.2:** Physical Properties of  $\text{YBa}_2\text{Cu}_3\text{O}_{7.8}$  superconductor

Structure	: Orthorhombic perovskite
Lattice parameters (Å)	: $a = 3.8231$ , $b = 3.8864$ , $c = 11.6807$
Theoretical density (g/cc)	: 6.374
Thermal expansivity ( $\text{K}^{-1}$ )	: $11.5 \times 10^{-6}$
Specific heat capacity ( $\text{Jkg}^{-1} \text{K}^{-1}$ )	: 431
Thermal conductivity ( $\text{W m}^{-1} \text{K}^{-1}$ )	: $2.4 \times 10^{-1}$
Hall carrier density ( $\text{cm}^{-3}$ )	: $4 \times 10^{21}$ (for a material of resistivity 400 mohms just above $T_c$ )
Less coherence length (nm)	: 1.4
London Penetration depth (nm)	: 200
Mean free path (nm)	: 1.2
$T_c(0)$ (K)	: 92
$H_{c1}(0)$ (T)	: 1
$H_{c2}(0)$ (T)	: 120
Absolute thermoelectric power ( $\mu\text{VK}^{-1}$ )	: 3
TC at 77K and zero field	: $10^3 - 10^4 \text{ A/cm}^2$ (bulk)
$J_c$ at 77K and zero field	: $10^6 - 10^7 \text{ A/cm}^2$ (epitaxial thin film)

Considerable studies have been made on the substitution of different ions for all the four ions in YBCO superconductor. As mentioned earlier, the substitution of Y by any rare earth other than those of Ce, Pr and Tb show no substantial variation in  $T_c$  [44-47]. But there are reports that thin films of  $\text{PrBa}_2\text{Cu}_3\text{O}_7$  pseudomorphically grown on YBCO single crystals are superconducting with  $T_c \sim 90\text{K}$  [93, 94]. The partial substitution of barium by strontium or calcium shows a depression in  $T_c$  [95, 96]. The Cu ion in  $\text{YBa}_2\text{Cu}_3\text{O}_7$  have been partly replaced by Zn, Fe, Ni, Co, Zr etc, usually accompanied by a drastic lowering of  $T_c$  [97-101]. Although 123 cuprates are generally orthorhombic, tetragonal superconducting compositions have been prepared, when Fe, Co or Ga partly substitutes Cu [81-85]. The tetragonal cuprates generally exhibit orthorhombic microdomains. The partial substitution of oxygen by sulfur showed no change in  $T_c$  and it is reported that this has resulted in sharper transition [102]. Meanwhile, the partial substitution of Cl for O showed a depression in  $T_c$  [102]. There were reports that the partial substitution of O by F enhanced  $T_c$  ( $\sim 150\text{K}$ ) but there was no confirmation of this result afterwards [103, 104]. Another stable phase in the Y-Ba-Cu-O system is  $\text{YBa}_2\text{Cu}_4\text{O}_8$  (124) which was found to be superconducting with a  $T_c \sim 90\text{K}$  [105].

#### 1.3.4 Bismuth Strontium Calcium Copper Oxide Superconductor

Michel *et al* [48] reported the existence of superconductivity when Bi was substituted for La in the La-Sr-Cu-O system and isolated a compound with formula  $\text{Bi}_2\text{Sr}_2\text{CuO}_{7+\delta}$  with a midpoint transition between 7-22K. But this discovery did not attract much attention at that time because of its low value of  $T_c$ . Bismuth based superconductor gained attraction when superconductivity above liquid nitrogen was reported by Maeda *et al* [106] and later by Chu *et al* [49-50]. They found that the addition of Ca to this ternary led to the discovery of bulk

superconductivity at 85 K and evidence for superconductivity at 110K in the Bi-Sr-Ca-Cu-O system. Till then there have been many publications detailing the existence of superconductivity at 110K and discussing the structure of the compound containing Bi-Sr-Ca-Cu-O [51-53, 107]. The phases present in the Bi-Sr-Ca-Cu-O system is often represented by a general formula  $\text{Bi}_2\text{Sr}_2\text{Cu}_{n-1}\text{Cu}_n\text{O}_x$  with  $n = 1, 2$  and  $3$ . The first member of this series  $\text{Bi}_2\text{Sr}_2\text{CuO}_x$  [Bi (2201)] has a  $T_c = 7-22$  K depends on the Bi-Sr ratio. It had an orthorhombic symmetry with  $a = 5.32 \text{ \AA}$ ,  $b = 26.6 \text{ \AA}$  and  $c = 48.8 \text{ \AA}$  and is obtained by reacting  $\text{Bi}_2\text{O}_3$ ,  $\text{SrO}_2$  and  $\text{CuO}$  powder in a quartz tube at  $870^\circ\text{C}$  for 15 h. The crystal structure of Bi (2201) is shown in figure 1. 5(a). The second member of the series with  $n = 2$ ,  $\text{Bi}_2\text{Sr}_2\text{CaCu}_2\text{O}_x$ , (Bi-2212) had a  $T_c = 85\text{K}$  and is the most extensively studied superconductor among Bi-based superconductors. The synthesis of this material through the conventional solid state route is rather cumbersome because in most cases the powder obtained according to the nominal stoichiometry  $\text{Bi}_2\text{Sr}_2\text{CaCu}_2\text{O}_x$  is not single-phase [108]. However, a single-phase material is obtained by firing a mixture of oxides and carbonates in the nominal composition of  $\text{Bi}_4\text{Sr}_3\text{Ca}_3\text{Cu}_4\text{O}_x$  at  $850^\circ\text{C}$  for two days [101, 109]. Liu et al [110] reported the synthesis of the  $n=2$  phase by rapid calcination and post annealing. In their study, homogeneous semiconducting  $\text{Bi}_2\text{Sr}_2\text{CuO}_6$  precursor was obtained by heating at  $1200^\circ\text{C}$  under argon atmosphere for 10 seconds and the subsequent annealing at  $860^\circ\text{C}$  for 16 h transformed it in to superconducting  $\text{Bi}_2\text{Sr}_2\text{CaCu}_2\text{O}_x$  compound. It has been pointed out by Karbarz et al [111] that the phase purity of the solid state synthesized powder can be increased by either hyperbaric or hypobaric condition. Tallon et al [112] reported an increase in  $T_c$  of Bi (2212) from 80 K to 91 K produced simply by quenching and was confirmed by Almond et al [113]. This increase is sufficient to place Bi (2212) in direct competition with YBCO, which

has a similar  $T_c$  but which requires a very different and more exacting heat treatment. The crystal structure of the Bi (2212) was studied quite extensively using single crystals and using high resolution lattice imaging as well as electron X-ray and neutron diffraction techniques [50, 114-117]. The crystal structure of Bi (2212) is shown in figure 1.5(b). The structure was refined as an orthorhombic cell with lattice parameters  $a = 5.411 \text{ \AA}$ ,  $b = 5.418 \text{ \AA}$  and  $c = 30.89 \text{ \AA}$  with  $Fmmm$  symmetry [118]. The crystal structure of Bi (2212) consists of intergrowths with

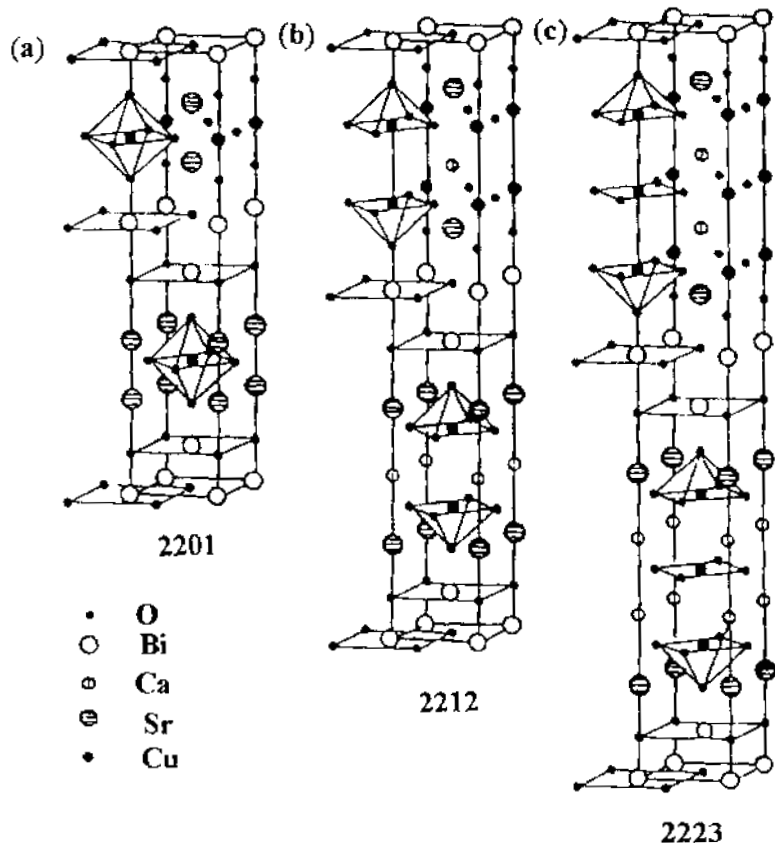


**Figure 1.5:** Crystal structure diagram of Bi-cuprate superconductors (a)  $\text{Bi}_2\text{Sr}_2\text{CuO}_5$ , (b)  $\text{Bi}_2\text{Sr}_2\text{CaCu}_2\text{O}_7$ , (c)  $\text{Bi}_2\text{Sr}_2\text{Ca}_2\text{Cu}_3\text{O}_{10}$

perovskite like units containing two  $\text{CuO}_2$  planes sandwiched between Bi-O bilayers. The perovskite unit in it is remarkably similar to that in 123 compounds. The Ca and Sr cations play the same role as the Y and Ba cations in the 123 compound. The linear chains in the 123 structure are replaced by the Bi-O layers; proving that linear chains are not essential for high  $T_c$  superconductivity. Weak bonding between Bi-O bilayers resulted in easy cleavage [119]. Bi (2212) is a type two superconductor.

The highest  $T_c$  phase in the  $\text{Bi}_2\text{Sr}_2\text{Ca}_{n-1}\text{Cu}_n\text{O}_x$  series,  $\text{Bi}_2\text{Sr}_2\text{Ca}_2\text{Cu}_3\text{O}_x$  [Bi (2223)] with  $n=3$  having a  $T_c$  of 110 K, is extremely difficult to prepare in its pure form since it is generally intergrown with the lower  $T_c$  phase corresponding to  $n=2$  and  $n=3$  [24]. Initial efforts to synthesize the Bi (2223) phase by sintering the nominal stoichiometric mixtures of oxides and carbonates at  $850^\circ\text{C}$  led to the formation of Bi (2212) as majority phase and Bi (2223) component was only a minority [120]. However, the volume fraction of Bi (2223) can be increased by heating the reaction mixture at  $880^\circ\text{C}$ , ie just below the melting temperature which suggest that the kinetics of the formation of Bi (2223) phase is closely related to the melting characteristics of the multi component mixture [120]. Numerous investigators have reported that the incorporation of Pb in the Bi-Sr-Ca-Cu-O system coupled with a prolonged sintering for more than a week increases the volume fraction of Bi (2223) [121-126]. The only single phase Bi (2223) samples reported so far have all been made by incorporation of Pb which appears to enhance the long-range diffusion of Ca and Cu, since the addition of Pb lowers the melting point of the mixture, thus accelerating the formation of Bi (2223) phase. A large number of non-conventional techniques have been proposed for the synthesis of phase pure Bi (2223) [127-131]. The structure of the compound was studied extensively using X-ray, electron and neutron diffraction [109, 116, 124, 132-135] and was reviewed extensively [120, 136, 137]. Bi (2223)

has an orthorhombic symmetry with  $a = 5.420 \text{ \AA}$ ,  $b = 5.411 \text{ \AA}$ ,  $c = 37.290 \text{ \AA}$ . The crystal structure of Bi (2223) is shown in figure 1. 5(c). Bi-2223 is a type II superconductor.

### 1.3.5 Thallium Barium Calcium Copper Oxide Superconductors:

The replacement of bismuth by thallium and strontium by barium in the Bi-Sr-Ca-Cu-O system given a similar set of superconducting compounds with general formula  $\text{Tl}_2\text{Ba}_2\text{Ca}_{n-1}\text{Cu}_n\text{O}_{2n+4}$  [55-57]. Sheng and Herman [138] discovered superconductivity in Tl-Ba-Cu-O system with a  $T_C$  above 77 K. They raised the  $T_C$  further by adding Ca to the above system and got a  $T_C$  onset of  $\sim 120 \text{ K}$  [55]. Two superconducting phases were identified in Sheng and Herman's sample by Hazen *et al* [57]  $\text{Tl}_2\text{Ba}_2\text{CaCu}_2\text{O}_{8+\delta}$  [Tl(2212)] and  $\text{Tl}_2\text{Ba}_2\text{Ca}_2\text{Cu}_3\text{O}_{10+\delta}$  [Tl(2223)]. Then Parkin *et al* [139] changed the processing conditions to greatly increase the amount of Tl (2223) and produced a  $T_C$  of 125 K. Later different superconducting compounds with the formula  $\text{TlBa}_2\text{Ca}_{n-1}\text{Cu}_n\text{O}_{2n+4}$  were discovered and this series has no Bi - analogue [140]. In the case of  $\text{Tl}_2\text{Ba}_2\text{Ca}_{n-1}\text{Cu}_n\text{O}_{2n+4}$  series, the structure consists of perovskite like units containing one, two or three  $\text{CuO}_2$  planes separated by Tl-O bilayers for  $n = 1, 2$  and  $3$  respectively. But in the case of  $\text{TlBa}_2\text{Ca}_{n-1}\text{Cu}_n\text{O}_{2n+4}$  series, the structure consists of perovskite like units containing one, two or three  $\text{CuO}_2$  planes separated by Tl-O monolayers for  $n = 1, 2$  and  $3$  respectively. All the thallium compounds have tetragonal structure at room temperature. The thallium compounds with Tl-O monolayers have primitive tetragonal cells where as the oxides with Tl-O bilayers have body centered tetragonal cells. The crystal structure of  $\text{TlBa}_2\text{CuO}_5$ ,  $\text{TlBa}_2\text{CaCu}_2\text{O}_7$ ,  $\text{TlBa}_2\text{Ca}_2\text{Cu}_3\text{O}_9$  are shown in figure 1. 6.

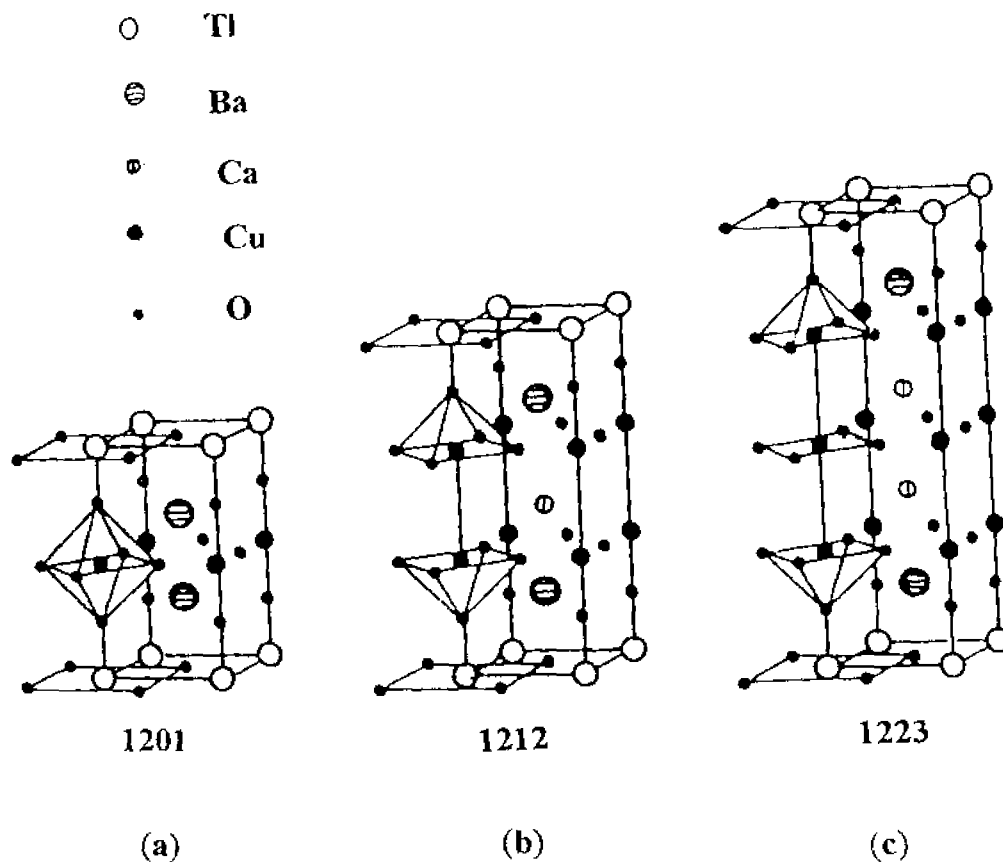


**Figure 1.6:** Crystal structure diagram of (a) Tl (1201), (b) 1212 (c) 1223

### 1.3.6 Mercury Barium Calcium Copper Oxide Superconductor

The replacement of Tl by Hg in  $\text{TlBa}_2\text{Ca}_{n-1}\text{Cu}_n\text{O}_{2n+4}$  series yielded a similar set of compounds with formula  $\text{HgBa}_2\text{Ca}_{n-1}\text{Cu}_n\text{O}_{2n+4}$  with higher  $T_C$  values than their Tl counterparts. In 1993 Putlin *et al* [58] reported the discovery of superconductivity in  $\text{HgBa}_2\text{CuO}_{4+\delta}$  with a  $T_C$  of 94 K. Later the existence of superconductivity above 130 K was reported in a multiphase compound of Hg-Ba-Ca-Cu-O system [60]. Single phase  $\text{HgBa}_2\text{Ca}_2\text{Cu}_3\text{O}_{8+\delta}$  was subsequently synthesized and found to be superconducting at a record temperature of 135 K [141]. Due to the high volatility of the mercury compounds, the synthesis of single

phase Hg based superconductor is difficult. The problem was overcome by high-pressure technique [142, 143]. The synthesis of single phase Hg-1223 by reaction sintering under high pressure and high temperature was reported by Hirabayashi *et al* [142, 143]. In this technique a precursor with the required composition of Ba, Ca and Cu was calcined and an appropriate amount of HgO is added to it. For the high-pressure synthesis, this mixture was sealed in an Au capsule and heated under a pressure of 5 GPa. The  $T_c$  value of this material reaches to 164 K, when measured at high pressure and is not too far from the lowest temperature recorded on earth [24].

#### **1.4. High Temperature Superconducting Films**

Soon after the discovery of high temperature superconductivity above liquid nitrogen in ceramic oxides, the immediate application of these new generation materials were realized to be in the form of thick and thin films [144, 145]. For practical applications, high critical current densities are required which are attainable in high quality films of high  $T_c$  superconductors [146-150]. In order to obtain high quality films of these materials, the selection of a suitable substrate and optimization of processing conditions are crucial. The research in the preparation of high quality films has been motivated by the possibilities of using these high  $T_c$  superconducting materials in various microelectronic devices like low loss microwave resonators and filters, bolometers, delay lines, flux transformers, magnetic shields, dc and r-f superconducting quantum interference devices, and various other superconducting two and three terminal devices [150]. High temperature superconducting films are also potentially suited to give an insight into the fundamental mechanisms governing high temperature superconductivity [150]. It is difficult to produce high quality films of these materials because of the sheer complexity, high anisotropic nature, close tolerance

of the composition required and the high processing temperature which make the chemical compatibility requirement of the substrate with the film more severe. Also the oxygen atmosphere required in the case of *in situ* growth of YBCO thin films imposes additional constraints for the preparation of films, as oxygen is incompatible with many aspects of traditional thin film growth methods, especially the substrate heating necessary for producing superconducting film.

High temperature superconductors offer a large number of constraints for the realization of high quality reproducible films. A major contributor to the difficulties that arise is the sheer complexity of the materials. All of the HTS compounds are composed of a minimum of four elements that must be deposited within a close tolerance of the correct ratio in order to obtain optimized films. Each high  $T_c$  material contains oxygen, an element that is incompatible with many aspects of thin film growth methods, especially the substrate heating is necessary for *in situ* annealed films, which reacts with hot filaments for evaporators. The role of oxygen is also critical in determining the properties of various film imperfections such as grain boundaries. Most of the materials are highly reactive, leading to unwanted chemical reactions that makes severe deviations from chemical purity of the films. Therefore, the selection of a suitable substrate is one of the issues that present particular challenges in the case of high temperature superconducting materials.

#### **1.4.1 Superconducting Thick Films**

The term thick film relates not so much to thickness of the film but to the method of deposition of the film [148]. Thick films are very complex non-equilibrium systems having physical properties that intimately related to their microstructure, which in turn is determined by the combination of material

properties and processing conditions. Thick film technology involves two main steps, (a) the deposition of the film of the required material in the desired pattern on to a substrate by common coating methods such as screen printing, spin coating, dip coating, spray pyrolysis, paint-on method etc. and (b) the subsequent drying followed by firing at a higher temperature to produce films of about 3 to 50 microns thick. The final electrical properties of the films depend on the material properties of the ink (homogeneous mixture consisting of the material to be coated with suitable solvents and polymers) ingredients and the substrate as well as the deposition process and time-temperature-atmosphere conditions during firing [148]. Thick films are *ex-situ* annealed films and the important requirement for good high  $T_c$  superconducting (HTS) film is the adherence to the substrate and its superconducting properties. The later are governed by the alignment and size of the superconducting grains, the presence of secondary phases and the intragrain connectivity. In order to achieve good adherence, partial melting of the high temperature superconducting materials is almost essential. One of the difficulties which come across during the preparation of high temperature superconducting thick film is the deposition of superconductor and its enhanced reaction with the substrate due to the partial melting of the superconductor at the processing temperature.

Thick films offer many advantages over thin films in certain applications. First, the preparation of thick film is inexpensive when compared with thin films, which requires expensive and sophisticated instrumentation for their deposition. Secondly, they cover large areas. Also thick film methods are simple, less costly and easy to apply. Thick films of HTS materials are of interest for many practical applications such as substrate wiring and magnetic shielding [151-155]

A survey of literature shows that considerable amount of work has been done in the preparation of superconducting YBCO [146-148, 156, 157], Bi (2223) and Bi (2212)[148, 158-161]. In the case of YBCO films developed on Si, SiO<sub>2</sub>, and Al<sub>2</sub>O<sub>3</sub> yielded poor quality films with low T<sub>C</sub> and J<sub>C</sub> values [148]. The YBCO thick films developed on MgO had low T<sub>C</sub> values of ~ 80 K but was better than the films on Si, SiO<sub>2</sub>, Al<sub>2</sub>O<sub>3</sub> etc.[162]. Bi (2223) and Bi (2212) thick films developed on Si, SiO<sub>2</sub>, and Al<sub>2</sub>O<sub>3</sub> shown interdiffusion of ions in the film and the substrate. The Bi (2223) films developed on MgO substrate always contained both low T<sub>C</sub> and high T<sub>C</sub> phases. The deterioration of superconducting properties of the commonly used conventional superconductors is due to the chemical reactivity between the substrate and the film at the partial melting temperature. Though a number of non-conventional substrates are proposed for the growth of superconducting thin films, the thick film fabrication on them are still a topic of research [148].

#### **1.4.2 Substrates for high T<sub>c</sub> superconducting films**

One of the issues that present significant challenges in the case of high T<sub>c</sub> material is the substrate. Substrates play a vital role in determining the properties of a superconducting film. A number of issues are critical in substrate selection for high T<sub>c</sub> superconducting film and are discussed herewith.

The most important requirement for the selection of any material as a substrate for high temperature superconductor is the chemical non-reactivity between the substrate and the superconductor at the processing temperature. This is true whether or not the film is epitaxial. The constraint is especially severe for high T<sub>c</sub> materials because these materials react with many substrates that otherwise be good candidates such as buffered Si or Al<sub>2</sub>O<sub>3</sub>. However oxide

materials are more likely to enhance the epitaxial growth of oxide superconductors than non-oxides because of the oxygen rich atmosphere involved in the film growth, regardless of the method used. The overriding importance of chemical compatibility over other substrate requirements in determining the suitability as substrate for HTSC film growth have been highlighted in many review articles [149, 150]. Therefore, if the chemical compatibility is poor, any other substrate requirement becomes irrelevant.

Another important criteria for the selection of a material as substrate for epitaxial films are the matching of the lattice constant values and thermal vibration. The epitaxial growth requires a misfit  $\varepsilon$  ( $\varepsilon = b - a$ ) /  $a$ , where 'a' and 'b' are the in plane lattice constant of substrate and the over grown materials) of not greater than about 15% [163]. The close lattice match between the substrate and the film is simply not enough requirements for good epitaxy, but there must also be a reasonable number of coincidence sites between the substrate material and the film. Coincidence sites are atomic positions, preferably with same or similar atomic sizes and values that coincide on either side of the interface. Thus for good epitaxy, the film and the substrate should have the same crystal structure. Since the epitaxial growth takes place at high temperature, the difference between the thermal expansion coefficient between the substrate and the film must be as minimum as possible. Since all the high  $T_c$  materials are brittle ceramic, the cracking in the film occurs if the thermal mismatch is higher. This leads to the deterioration of superconducting properties like  $T_c$  and  $J_c$ . For substrate applications the high thermal conductivity of the material is considered as an additional advantage [164].

A substrate must be thermodynamically stable within the temperature range required to grow and process the film. A phase transition within this range can

have significant effects on the surface quality of the substrates which leads to film cracks and deterioration of superconducting properties of the film. A phase transition within this region can have dramatic effects on the surface quality of the substrate and on the stresses the film must undergo. If a phase transition is inevitable, it should be as minor as possible, ie second order with no discontinuous volume change and minimal structural change [149, 150].

The quality of the surface is another important property of a substrate since it is here that the film substrate interaction occurs. An atomically flat surface is required to grow a uniform and homogeneous film. A large number of parameters can adversely affect the surface properties of the substrate such as crystal defects, polishing scratches, non-uniform sinterability of the sample, secondary phases, surface warp and cracks etc. The surface smoothness is important for a number of reasons, for example, in some cases scratches or crystallographic steps may influence the orientation of a crystal film as well as its over all microstructure. So an ideal surface would have a flat, dense, and free of twins and other structural inhomogeneties.

In the case of device application of high  $T_c$  superconducting films, another important requirement is that the substrate should have low dielectric constant and loss factor. This requirement is more severe in the case of microwave applications. The desired value of dielectric constant is related to the length of the electromagnetic wave in the substrate material and the microwave circuit fabrication tolerances. In order to avoid destruction of the electromagnetic stability of the circuit, the substrate thickness as well as the width of the coplanar lines should be sufficiently less than the wavelength [164]. By increasing the operating frequency one reduces the maximum of the allowed substrate thickness and line

width. However, the substrate thickness cannot be reduced to less than 0.3 to 0.5 mm without compromising much on its mechanical strength. This imposes restriction on the values of dielectric constant of the substrate material and extremely high value of dielectric constant and loss factor rule out their application as substrate for microwave applications [164]. Also in the case of microwave applications, where the dielectric constant of the substrate have important effect on device performance, existence of twinning transition in the processing temperature range is unacceptable as it precludes device modeling [165]. For the most of the device applications requires large area single crystal substrates. Oxide ceramic materials are usually grown as single crystals by melt growth techniques and this require that the substrate material should melt congruently making it possible to grow them as single crystals from melt.

Many commercially available substrates such as Si, SiO<sub>2</sub>, Al<sub>2</sub>O<sub>3</sub> react with both YBCO and BiSCCO superconductors at the processing temperatures thereby degrading the transition temperature of the film severely [166-168]. Though Al<sub>2</sub>O<sub>3</sub> combines outstanding dielectric properties, high mechanical strength and commercial availability in high quality twin free large diameter single crystals, the reaction between Al<sub>2</sub>O<sub>3</sub> restricts its use as substrate for YBCO and BiSCCO superconductors[150,164,168-170]. MgO is the widely used substrate for YBCO and Bi (2223) films in light of its readily availability as large area single crystals and its modest dielectric properties [150,164]. However in the case of YBCO, MgO forms an interlayer of barium salt at the YBCO-MgO interface if the processing temperature is greater than 700°C and reduces the superconducting transition temperature of the film drastically [168,171]. Also Bi (2223) films developed on MgO substrate always contained both the low T<sub>c</sub> Bi (2212) and high T<sub>c</sub> Bi (2223) phases[172,173]. SrTiO<sub>3</sub> is another substrate material used for both

BiSCCO and YBCO superconductors but its high dielectric constant restricts their use at microwave frequencies in addition to its unavailability in reasonable sizes [149,150,174].  $\text{LaAlO}_3$  is also a chemically compatible substrate but it has a phase transition in the film processing regime (800K) and its dielectric constant vary from point to point in a manner that cannot be controlled or predicated [149, 150].  $\text{LaGaO}_3$ , was identified as a potential substrate material, its lattice and thermal expansion match are quite good and have attractive dielectric properties. However it has one serious drawback that this material has a first order phase transition at 420 K [149,150,174]. Table 1.3 summarizes the list of substrate materials proposed for the growth of superconducting films and their characteristics.

Recently, a group of complex perovskite ceramic oxide with the general formula  $\text{Ba}_2\text{REMO}_6$  (RE = Rare-Earth, M = Nb, Sn, Sb and Hf) have been proposed as potential substrate for YBCO and BiSCCO superconductors [175-184]. Work on these materials are going on in regard to their single crystal growth and growth of high quality superconducting film. Progress in the identification of and utilization of substrate materials has been substantial, but less impressive than the progress in the films themselves. Considerable work is needed, since some of the remaining problems in the films are certainly connected with the lack of a suitable substrate.

Table 1.3: Summary of substrate state-of-art

Material	Structure	Lattice constant (Å)	$\epsilon'$	Tan $\delta$	Tc (K)	Jc A/cm <sup>2</sup> (77K)	Chemical compatibility
MgO	Fcc	4.20	9.65	$5 \times 10^{-4}$ (100K, 300 GHz)	90	$3.5 \times 10^6$	NO
Al <sub>2</sub> O <sub>3</sub>	Hexagonal		9.34	$3 \times 10^{-5}$ (77K, 5 GHz)	85-88	$1 \times 10^6$	"
SrTiO <sub>3</sub>	Cubic perovskite	3.905	277	$6 \times 10^{-2}$ (100K, 300 GHz)	90	$5 \times 10^6$	"
LaGaO <sub>3</sub>	Orthorhombic perovskite	A=5.519 B=5.494 C=7.770	25	$6 \times 10^{-3}$ (100K, 300 GHz)	90	$2.3 \times 10^6$	"
LaAlO <sub>3</sub>	Cubic perovskite	5.337	24	$3 \times 10^{-5}$ (77K, 5 GHz)	90	$5 \times 10^6$	"
NdGaO <sub>3</sub>	Orthorhombic perovskite	A=5.417 B=5.499 C=7.717	20	$3 \times 10^{-4}$ (77K, 5GHz)	89	$2 \times 10^6$	"
NdAlO <sub>3</sub>	Orthorhombic perovskite		17		89.7	$3 \times 10^4$	"
YAlO <sub>3</sub>	Orthorhombic perovskite	A=3.662 B=3.768 C=3.685	16	$7.3 \times 10^{-5}$ (300K, 10 GHz)	91	$7.2 \times 10^5$	"
PrGaO <sub>3</sub>	Orthorhombic perovskite	A=5.462 B=5.493 C=7.740	24	$3.6 \times 10^{-4}$ (300K, 1 KHz)	90		"
YSZ	Cubic fluorite		25	$8 \times 10^{-3}$ (100K, 300GHz)	92	$5 \times 10^6$	not severe
CaNdAlO <sub>4</sub>	K <sub>2</sub> NiF <sub>4</sub>	A = 3.69 C=12.15	19	$1 \times 10^{-4}$ (77K, 5GHz)	88	$1 \times 10^6$	no
CaYAlO <sub>4</sub>	K <sub>2</sub> NiF <sub>4</sub>	A= 3.648 C= 11.89	20	$4 \times 10^{-5}$ 77K, 5 GHz)	86	$2 \times 10^5$	"
LaSrAlO <sub>4</sub>	K <sub>2</sub> NiF <sub>4</sub>	A= 3.754 C=11.26	17	$5 \times 10^{-4}$ (100K, 8 GHz)	90	$2.3 \times 10^5$	"
LaSrGaO <sub>4</sub>	K <sub>2</sub> NiF <sub>4</sub>	A = 3.84 C=12.67	22	$5 \times 10^{-5}$ 800K, 8 GHz	91	$3.5 \times 10^6$	"
MgAl <sub>2</sub> O <sub>4</sub>	Spinal	8.083	12	$5 \times 10^{-4}$ (100K, 5 GHz)	77		"

## 1.5. Nanostructured Materials

One of the very basic results in physics and chemistry of solids is the insight that most properties of a solid depends on the microstructure, i.e., the chemical composition, the arrangement of the atoms and the size of the solid in one, two and three dimensions. If one changes one or several of these parameters, the properties of the solid vary. When the size of the solid is reduced in a considerably smaller scale, while maintaining the chemical composition and the arrangement of atoms, the properties of the solid modify dramatically. Those solids which contain high density of defects such as point defects, dislocations, grain boundaries, interface boundaries etc. and the distance between the neighboring defects approach to interatomic distance, are known as nanostructured materials or -synonymously- nanophase, nanoparticles, and nanocrystalline materials [185, 186]. Alternatively, nanostructured materials are materials with a microstructure, the characteristic length of which is of the order of a few nanometers.

Nanostructured materials have become one of the most active research fields in the area of solid state physics, chemistry and engineering. There are several reasons for it. One is the need to fabricate new materials on an ever-finer scale to continue decreasing the cost and speed of information transmission and storage [187]. Another is that, because of the very fine grain sizes, nanocrystalline materials exhibit a variety of properties that are different and often considerably improved in comparison with those of conventional polycrystalline coarse-grained materials [187]. The potential importance of these new generation materials in industry is cited in many recent review articles[185-186,188-192]. The properties of nanostructured materials deviates from those of coarse grained poly crystals and

glasses with same chemical composition. This deviation results from the reduced size and dimensionality of the nanometer sized crystals as well as from the numerous interfaces between adjacent crystallites. Nanocrystalline material exhibit increased strength / hardness [193, 194], enhanced diffusivity [195, 196], improved ductility / toughness [188], reduced elastic modulus [197, 198], higher electric resistivity [199, 200], increased specific heat [201, 202], higher thermal expansion coefficient [188, 192], lower thermal conductivity [188] and superior magnetic properties [203, 204] in comparison to conventional coarse grained materials.

The nanostructured materials are often classified in to the following three category [185]. The first category comprises materials with reduced dimensions in the form of nanometer sized particles, thin wires or thin films that are isolated, substrate supported or embedded. Chemical Vapour deposition (CVD), Physical Vapour Deposition (PVD), inert gas condensation, various aerosol techniques, precipitation from the vapour appear to be the techniques most frequently used to generate this type of microstructure. Well known examples of technological application of materials whose properties depends on this type of microstructure are catalysts and semiconductor devices utilizing single or multilayer quantum well structures [185].

The second category comprises materials in which the nanometer-sized microstructure is limited to a thin nanometer sized surface region of a bulk material. PVD, CVD, ion implantation and laser beam treatments are the most widely applied procedure to modify the chemical composition or atomic structure of solid surface on a nanometer scale. Surfaces with enhanced corrosion resistance, hardness, wear resistance or protective coatings are examples in which

the properties of thin surface layer are improved by means of creating a nanometer sized microstructure in a thin surface region. An important subgroup of this category is materials, the surface of which is structured laterally on a nanometer scale by developing a nanometer sized structural pattern on the free surface. Patterns of this type may be synthesized by lithography, means of local probes and surface precipitation processes. Patterns in the form of an array of nanometer sized islands (e.g. quantum dots) connected by nanometer sized wires are examples of this type of microstructure. Processes and devices of this type are expected to play a key role in the production of the next generation of electronic devices such as highly integrated electronic circuits, terabit memories, single electron transistor, quantum computers, etc.

The third category comprises of bulk solids with a nanometer sized microstructure and are assembled of nanometer sized building blocks-mostly crystallites- as displayed in figure 1.7. These building blocks may differ in their atomic structure, their crystallographic orientation or chemical composition. In other words, materials assembled of nanometer sized building blocks are microstructurally heterogeneous consisting of crystallites and grain boundaries. Bulk materials with a nanometer sized microstructure are called nanostructured materials. The synthesis, characterization and processing of such nanostructured materials are the part of an emerging and rapidly growing field referred to as nanotechnology. Research and development in this field emphasizes scientific discoveries in generation of materials with controlled microstructural characteristics, research on their processing in to bulk materials with engineered properties and technological functions, introduction of new device and concepts and manufacturing methods.

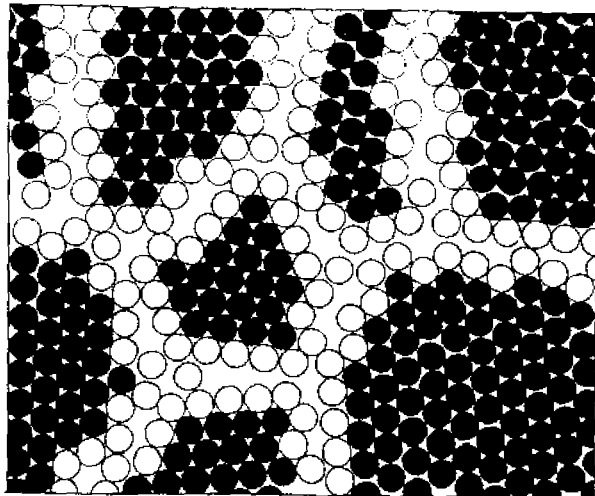


**Figure 1.7:** Two dimensional model of a nanostructured material. The atoms in the centers of the crystal are indicated in black. The ones in the boundary core regions are represented as open circle. [185]

In our present study we will focus our attention on the synthesis of a group of complex perovskite ceramic oxides, with the general formula,  $Ba_2REZrO_{5.5}$  (RE = Rare Earth) which resulted in our experiments as nanoparticles for better phase purity, homogeneity and sintering behavior.

## 1.6 Scope of the present work

It was reported that the addition of  $ZrO_2$  in YBCO did not have any detrimental effect on its superconducting properties [205-209], and this addition has eliminated the slow cooling and oxygenation steps in the synthesis of YBCO superconductor. But the addition of  $ZrO_2$  resulted in the formation of a secondary phase and was identified as  $YBa_2ZrO_6$ , which coexisted with the YBCO superconductor even after severe heat treatment conditions. Attempts were made to synthesize  $YBa_2ZrO_6$  by the conventional solid state reaction method for its potential use as substrate for YBCO superconductor, but it was reported that

$\text{YBa}_2\text{ZrO}_6$  could not be synthesized as single-phase materials without addition of CuO. In this context, studies were carried out to overcome this difficulty by substituting Y by rare-earth elements and it was found that a group of ceramic materials with the formula  $\text{Ba}_2\text{REZrO}_{5.5}$  (RE = La, Ce, Eu and Yb) could be synthesized and sintered as single phase materials through the conventional solid state route. But when RE = Ho and Er, the system crystallized in to a multiphase ceramic and it was found that the addition of CuO enhanced the formation of single phase of these compounds. The  $\text{Ba}_2\text{REZrO}_{5.5}$  materials are found to be non-reacting with high  $T_c$  superconducting materials and have favorable dielectric properties. The suitability of  $\text{Ba}_2\text{REZrO}_{5.5}$  materials was demonstrated by developing superconducting films with good superconducting characteristics. In the present research work, the difficulties with the synthesis of the newly developed  $\text{Ba}_2\text{REZrO}_{5.5}$  as well as  $\text{YBa}_2\text{ZrO}_6$  have been overcome by developing a modified combustion procedure to obtain them as nanoparticles in a single step processing by using only a hot plate as the only external heat source. The experimental details and the results obtained are described in detail in the following chapters of this thesis.

## REFERENCES

- [1] M. W. Barsoum, *Fundamentals of Ceramics*, The Mc Graw-Hill Companies Inc. 1997.
- [2] N. Ichinose, K. Koyama, N. Ogino, A. Tsuge, Y. Yokomizo, *Introduction to Fine Ceramics; Application in Engineering*, John Wiley & Sons 1987.
- [3] W. D. Kingery, H. K. Bowen, D. R. Uhlman, *Fundamentals of Ceramics*, John Wiley & Sons 1976.
- [4] A. M. Glazer, *Acta Cryst*, **B28**, (1972) 3384.
- [5] A. M. Glazer, *Acta Cryst.*, **B28**, (1975) 3384.
- [6] R. M. Hazen, *Scientific American*, **258**, (1988) 52.
- [7] M. Ahtee, A. M. Glazer, H. D. Megaw, *Phil. Mag*, **26**, (1972) 995.
- [8] H. D. Megaw, *Acta Cryst*, **A24**, (1968) 583.
- [9] F. Galasso, L. Katz, R. Ward, *J. Am. Ceram. Soc*, **81**, (1959) 820.
- [10] F. Galasso, J. R. Borrante, L. Katz, *J. Am. Ceram. Soc*, **83**, (1961) 2830.
- [11] F. S. Galasso, G. K. Lyden, D. E. Flinchbaugh, *J. Chem. Phys*, **44**, (1966) 2703.
- [12] R. S. Roth, *J. Res. NBS*, **58**, (1957) 75.
- [13] R. Roy, *J. Am. Ceram. Soc*, **37**, (1964) 581.
- [14] P. G. Casado, A. Mendiola, I. Rasines, *Z. Anorg. Allg.Chem*, **510**, (1984) 194.
- [15] X. Zhang, Q. Wang, *J. Am. Ceram. Soc.*, **74**, (1991) 2846.
- [16] N. Setter, L. E. Cross, *J. Appl. Phys.*, **51**, (1980) 4356.
- [17] N. Setter, L. E. Cross, *J. Mater. Sci.*, **15**, (1980) 2478.
- [18] P. Groves, *J. Phys. C: Solid State Phys.*, **19**, (1986) 111.
- [19] K. Endo, K. Fujimoto, K. Murakawa, *J. Am. Ceram. Soc.*, **70**, (1987) C215.
- [20] J. Chen, M. Chan, M. P. Harmer, *J. Am. Ceram. Soc.*, **72**, (1989) 593.

- [21] C. Randall, D. Barber, R. Whatmore, P. Groves, *Ferroelectrics*, **76**, (1987) 277.
- [22] G. King, E. Goo, T. Yamamoto, K. Okazaki, *J. Am. Ceram. Soc.*, **71**, (1988) 454.
- [23] V. D. Hunt, *Superconductivity Source Book*, John Wiley & Sons 1989.
- [24] T. V. Ramakrishnan, C. N. R. Rao, *Superconductivity Today; An Elementary Introduction*, University Press (India) Ltd. 1999.
- [25] J. G. Bednorz, K. A. Muller, *Z. Phys. B.- Condensed matter*, **64**, (1986) 189.
- [26] H. Tagaki, S. Uchida, K. Kitazawa, T. Tanaka, *Jpn. J. Appl. Phys.*, **26**, (1987) L123.
- [27] J. G. Bednorz, M. Tagashige, K. A. Muller, *Europhys. Lett*, **3**, (1987) 379.
- [28] S. Uchida, H. Tagaki, K. Kitazawa, S. Tanaka, *Jpn. J. Appl. Phys.*, **26**, (1987) L1.
- [29] K. Kishio, K. Kitazawa, S. Kanbe, I. Yasuda, N. Sugii, H. Tagaki, S. Uchida, K. Fueki, S. Tanaka, *Chem. Lett.*, (1987) 429.
- [30] C. W. Chu, P. H. Hor, R. L. Meng, L. Guo, Z. J. Huang, *Science*, **235**, (1987) 567.
- [31] C. W. Chu, P. H. Hor, R. L. Meng, L. Guo, Z. J. Huang, Y. Q. Wang, *Phys. Rev. Lett.*, **58**, (1987) 567.
- [32] M. K. Wu, J. R. Ashburn, C. J. Torng, P. H. Hor, R. L. Meng, Z. J. Guo, Y. Q. Wang, C. W. Chu, *Phys. Rev. Lett.*, **58**, (1987) 908.
- [33] R. J. Cava, B. Batlogg, R. B. V. Dover, D. W. Murphy, S. Sunshine, T. Seigrist, J. P. Remeika, E. A. Reitman, S. Zahurak, G. P. Espinosa, *Phys. Rev. Lett.*, **58**, (1987) 1676.

- [34] T. Seigrist, S. Sunshine, D. W. Murphy, R. J. Cava, S. Zahurak, *Phys. Rev. B*, **35**, (1987) 7137.
- [35] P. H. Hor, L. Gao, R. L. Meng, Z. J. Huang, Y. Q. Wang, K. Forster, J. Vassiliou, C. W. Chu, *Phys. Rev. Lett.*, **58**, (1987) 911.
- [36] X. Cai, R. Joynt, D. C. Jarbalestier, *Phys. Rev. Lett.*, **58**, (1987) 2798.
- [37] I. K. Gopalakrishnan, J. V. Yakhmi, R. M. Iyer, *Nature*, **327**, (1987) 604.
- [38] S. Dickman, D. Swinbanks, D. Lindley, R. Peese, *Nature*, **326**, (1987) 432.
- [39] M. Strongin, D. O. Welch, V. J. Emery, *Nature*, **326**, (1987) 540.
- [40] C. N. R. Rao, P. Ganguly, A. K. Raychaudhuri, R. A. M. Ram, K. Sreedhar, *Nature*, **326**, (1987) 856.
- [41] Y. L. Page, W. R. M. Kinnon, J. M. Tarascon, L. H. Greene, G. W. Hull, D. M. Hwang, *Phys. Rev. B*, **35**, (1987) 7245.
- [42] R. M. Hazen, L. W. Finger, R. J. Angel, C. T. Prewitt, N. L. Ross, H. K. Mao, C. G. Hadjidakis, *Phys. Rev. B*, **35**, (1987) 7238.
- [43] P. M. Grant, R. B. Beyers, E. M. Engler, G. Lim, S. P. P. Parkin, M. L. Ramirez, V. Y. Lee, A. Nazzari, J. E. Vazquez, R. J. Savoy, *Phys. Rev. B*, **35**, (1987) 7242.
- [44] R. A. M. Ram, N. Y. Vasantacharya, C. N. R. Rao, *J. Solid State Chem.*, **69**, (1987) 186.
- [45] A. K. Raychaudhuri, K. Sreedhar, K. P. Rajeev, R. A. M. Ram, P. Ganguly, C. N. R. Rao, *Philos. Mag. Lett.*, **56**, (1987) 29.
- [46] K. M. Yang, Y. Dalichaouch, J. M. Ferreira, B. W. Lee, J. J. Newmeier, M. S. Torikachvilil, H. Zhou, M. B. Maple, R. R. Hake, *Solid State Commun.*, **63**, (1987) 515.
- [47] J. M. Tarascon, W. R. Mc Kinnon, L. H. Greene, G. W. Hull, E. M. Vogel, *Phys. Rev. B*, **36**, (1987) 226.

- [48] C. Mitchell, M. Hervieu, M. M. Borel, A. Grandin, F. Deshlands, J. Provost, B. Raveau, *Z. Phys. B- Condensed Matter*, **412**, (1987) .
- [49] C. W. Chu, J. Bechtold, L. Guo, P. H. Hor, Z. J. Huang, R. L. Meng, Y. Y. Sun, Y. Q. Wang, Y. Y. Xue, *Phys. Rev. Lett.*, **60**, (1988) 941.
- [50] R. M. Hazen, C. T. Prewit, R. J. Angel, N. L. Ross, L. W. Finger, C. G. Hadidiacos, D. R. Veblen, P. J. Heaney, P. H. Hor, R. L. Meng, Y. Y. Sun, Y. Q. Wang, Y. Y. Xue, Z. J. Huang, L. Guo, J. Bechtold, C. W. Chu, *Phys. Rev. Lett.*, **60**, (1988) 1174.
- [51] C. Martin, H. Huvé, G. V. Tendeloo, A. Maignen, C. Mitchell, M. Hervieu, B. Raveau, *Physica C*, **212**, (1993) 274.
- [52] G. Er, Y. Miyamoto, F. Kanamura, S. Kikkawa, *Physica C*, **181**, (1991) 206.
- [53] M. G. Smith, A. Manthiram, J. Zhou, J. B. Goodenough, J. T. Makert, *Nature*, **351**, (1991) 549.
- [54] M. Azuma, Z. Horoi, M. Takano, Y. Brando, Y. Takeda, *Nature*, **356**, (1992) 775.
- [55] Z. Z. Sheng, A. M. Herman, *Nature*, **332**, (1988) 138.
- [56] C. C. Torardi, M. A. Subramanian, J. C. Calabrese, J. Gopalakrishnan, E. M. M. Carron, K. J. Morrissey, T. R. Askew, R. B. Flippon, U. Chowdhary, A. W. Sleight, *Phys. Rev. B*, **38**, (1988) 225.
- [57] R. M. Hazen, D. W. Finger, R. J. Angel, C. T. Prewit, N. L. Ross, C. J. Hadidiacos, P. J. Heaney, D. R. Veblen, Z. Z. Sheng, A-El-Ali, A. M. Herman, *Phys. Rev. Lett.*, **60**, (1988) 1657.
- [58] S. N. Putlin, E. V. Antipov, O. Chmaissem, M. Murezio, *Nature*, **362**, (1993) 226.
- [59] S. N. Putlin, E. V. Antipov, M. Murezio, *Physica C*, **212**, (1993) 266.

- [60] A. Schilling, M. Cantoni, J. D. Guo, H. R. Ott, *Nature*, **363**, (1993) 56.
- [61] F. Beech, S. Miraglione, A. Santoro, R. S. Roth, *Phys. Rev. B*, **35**, (1987) 8778.
- [62] M. A. Beno, L. Soderholm, R. W. Capone, D. G. Hinks, J. D. Jorgenson, I. K. Schuller, C. V. Segre, K. Zhang, J. D. Grace, *Appl. Phys. Lett.*, **51**, (1987) 57.
- [63] O. K. Anston, P. E. Hiismaki, H. O. Poyry, A. T. Tiita, K. M. Ullakko, V. A. Trunov, V. A. Ulyanov, *Solid State Commun.*, **64**, (1987) 757.
- [64] J. J. Capponi, C. Chailout, A. W. Hewat, P. Lejay, M. Marezio, N. Nguyen, B. Raveau, J. L. Soubeyroux, J. L. Tholence, R. Tourni, *Europhys Lett.*, **3**, (1987) 1301.
- [65] M. Francois, E. Walker, J. L. Jorda, K. Yvon, P. Fischer, *Solid State Commun.*, **63**, (1987) 1149.
- [66] Y. Lepage, T. Siegrist, S. A. Sunshine, L. F. Schneemeyer, D. W. Murphy, S. M. Zahurak, J. V. Waszczak, W. R. M. Kinnon, J. M. Tarascon, G. W. Hull, L. H. Greene, *Phys. Rev. B*, **36**, (1987) 3617.
- [67] G. Celestani, C. Rizzoli, *Nature*, **328**, (1987) 606.
- [68] G. J. McIntyre, A. Renault, G. Collin, *Phys. Rev. B*, **37**, (1988) 5148.
- [69] M. I. Fornasini, G. A. Costa, M. J. Ferretti, G. L. Olcese, *Solid State Commun.*, **65**, (1988) 1121.
- [70] T. Siegrist, S. A. Sunshine, D. W. Murphy, R. J. Cava, S. M. Zahurak, *Phys. Rev. B*, **36**, (1987) 7137.
- [71] Y. Syono, M. Kikuchi, K. Ohishi, K. Hiraga, H. Arai, Y. Matsui, N. Kobayashi, T. Sasaoka, Y. Muto, *Jpn. J. Appl. Phys.*, **26**, (1987) L498.
- [72] R. Beyers, G. Lim, E. M. Engler, R. J. Savoy, T. M. Shaw, T. R. Dinger, W. J. Gallagher, R. L. Sandstrom, *Appl. Phys. Lett.*, **50**, (1987) 1918.

- [73] J. C. Phillips, *Physics of High Tc Superconductors*, Academic Press, Inc. 1992.
- [74] P. Bordet, C. Chaillot, J. J. Capponi, J. Chenavas, M. Marezio, *Nature*, **327**, (1987) 687.
- [75] W. I. F. David, W. T. A. Harrison, J. M. F. Gunn, O. Moze, A. K. Soper, P. Day, J. D. Jorgensen, M. A. Beno, D. W. Capone, P. G. Hinks, I. K. Schuller, L. Soderholm, C. U. Segre, K. Zhang, J. D. Grace, *Nature*, **327**, (1987) 310.
- [76] C. N. R. Rao, P. Ganguly, *Curr. Sci*, **56**, (1987) 47.
- [77] J. E. Greedan, A. O. Reilly, C. V. Stager, *Phys. Rev. B*, **35**, (1987) 8770.
- [78] J. D. Jorgensen, M. A. Beno, D. G. Hinks, L. Soderholm, K. J. Volin, R. L. Hitterman, J. D. Grace, I. K. Schuller, C. U. Segre, K. Zhang, M. S. Kleefisch, *Phys. Rev. B*, **36**, (1987) 3608.
- [79] J. D. Jorgensen, *Jpn. J. Appl. Phys.*, **26**, (1987) 2017.
- [80] K. Kishio, J. Shimoyama, T. Hasegawa, K. Kitazawa, K. Fueiki, *Jpn. J. Appl. Phys.*, **26**, (1987) L1228.
- [81] G. Xio, M. Z. Cieplak, A. Gavrin, S. H. Streitz, A. Bkhshai, C. L. Chien, *Phys. Rev. Lett.*, **60**, (1988) 1446.
- [82] H. Ihara, H. Oyanagi, R. Sugise, E. Ohno, T. Matsubara, S. Ohashi, N. Terada, M. Jo, M. Hirabayashi, K. Murata, A. Negishi, Y. Kimura, E. Akiba, H. Hayakawa, S. Shin, *Physica C*, **153-155**, (1988) 948.
- [83] I. W. Chen, S. J. Keating, C. Y. Keating, X. Wu, J. Xu, P. E. R. Mosel, T. Y. Tien, *Solid State Commun*, **63**, (1987) 997.
- [84] A. J. Panson, A. I. Braginski, J. R. Gavler, J. R. Hulm, M. A. Jonocko, H. C. Pohl, A. M. Stewart, J. Talvacchio, G. R. Wagner, *Phys. Rev. B*, **35**, (1987) 8774.

- [85] I. K. Schuller, D. G. Hinks, M. A. Beno, D. W. C. II, L. Soderholm, J. P. Loquet, L. Bruynseraede, C. U. Segre, K. Zhang, *Solid State Commun*, **63**, (1987) 385.
- [86] M. F. Yan, R. L. Barns, H. M. O. B. Jr., P. K. Gallagher, R. C. Sherwood, S. Jin, *Appl. Phys. Lett.*, **51**, (1987) 532.
- [87] J. G. Thomson, B. G. Hyde, R. L. Withers, J. S. Anderson, J. D. F. Gerald, J. Bitmead, M. S. Paterson, A. M. Stewart, *Mater. Res. Bull.*, **22**, (1987) 1715.
- [88] S. W. Tozer, A. W. Kleinsasser, T. Penney, D. Kaiser, F. Holtzberg, *Phys. Rev. Lett.*, **59**, (1987) 1768.
- [89] X. Yu, M. Sayer, *Physica C*, **159**, (1989) 496.
- [90] T. R. McGuire, T. R. Dinger, P. J. P. Freitas, W. J. Gallagher, T. S. Plaskett, R. L. Sandstorm, J. M. Shaw, *Phys. Rev. B*, **36**, (1987) 4032.
- [91] T. R. Dinger, T. K. Worthington, W. J. Gallagher, R. L. Sandstorm, *Phys. Rev. Lett.*, **58**, (1987) 2687.
- [92] G. W. Crabtree, J. Z. Liu, A. Umezawa, M. K. Kwoke, C. H. Sowers, S. K. Maillik, *Phys. Rev. B*, **36**, (1987) 4021.
- [93] T. Ugazawa, Y. Ishimaru, J. G. Wen, S. Koyama, Y. Enomoto, *Jpn. J. Appl. Phys.*, **36**, (1997) L100.
- [94] T. Usagawa, Y. Ishimaru, J. Wen, T. Utagawa, S. Koyama, Y. Enomoto, *Jpn. J. Appl. Phys.*, **36**, (1997) L1583.
- [95] B. W. Veal, M. K. Kwoke, A. Umezawa, G. W. Crabtree, J. D. Jorgensen, J. W. Downey, L. J. Nowichi, A. W. Mitchell, A. P. Paulikas, C. H. Sowers, *Appl. Phys. Lett.*, **51**, (1987) 279.
- [96] A. Ono, T. Tanaka, H. Nozaki, Y. Ishikawa, *Jpn. J. Appl. Phys.*, **26**, (1987) 821.

- [97] M. F. Yan, W. W. Rhodes, P. K. allagher, *J. Appl. Phys.*, **63**, (1988) 821.
- [98] G. Xiao, M. Z. Cieplak, D. Masser, A. Gavrin, F. H. Streitz, C. L. Chien, J. J. Rhyne, J. A. Gotaas, *Nature*, **26**, (1988) 238.
- [99] E. T. Muromachi, Y. Uchida, K. Kato, *Jpn. J. Appl. Phys.*, **26**, (1987) L2087.
- [100] G. Xiao, F. H. streitz, A. Garvin, Y. W. Du, C. L. Chien, *Phys. Rev. B*, **35**, (1987) 8782.
- [101] J. M. Tarascon, P. Barboux, P. F. Miceli, L. H. Greene, G. W. Hull, M. Eibschutz, S. A. Sunshine, *Phys. Rev. B*, **37**, (1988) 7458.
- [102] I. Felner, I. Nowik, Y. Yeshurun, *Phys. Rev. B*, **36**, (1987) 3923.
- [103] S. R. Ovshinski, R. T. Young, D. D. Alred, G. DeMaggio, G. A. V. d. Leeden, *Phys. Rev. Lett.*, **58**, (1987) 2579.
- [104] M. Xian-Ren, R. Yan-Ru, L. Ming-zhu, T-Qing-Yun, L.-. Zhen-Jin, S. Li-Hua, D. Wei-Qiung, F. Min-Hua, M. Qing-Yun, L. Vhan-Jiang, L. Xue-hai, Q. Guan-Laing, C. Mou-Yuan, *Solid Sate Commun.*, **64**, (1987) 325.
- [105] P. Marsh, R. M. Fleming, M. L. Mandich, A. M. DeSantolo, J. Kwo, M. Hong, L. J. Martinez-Miranda, *Nature*, **334**, (1988) 141.
- [106] H. Maeda, Y. Tanaka, M. Fukutomi, T. Asano, *Jpn. J. Appl. Phys.*, **27**, (1988) L209.
- [107] M. A. Subramanian, C. C. Torardi, C. C. Calabrese, J. Gopalakrishanan, K. J. Morrissey, T. R. Askew, R. B. Flippon, U. Chowdhry, A. W. Sleight, *Science*, **239**, (1988) 225.
- [108] J. M. Tarascon, W. R. M. Kinnon, P. Barboux, D. W. Hull, Y. L. Page, N. Stoffel, M. Giround, *Phys. Rev. B*, **38**, (1988) 8885.

- [109] J. M. Tarascon, Y. LePage, P. Barboux, B. G. Bagley, L. H. Greene, W. R. M. Kinnon, G. W. Hull, M. Giroud, D. M. Hwang, *Phys. Rev. B*, **38**, (1988) 9382.
- [110] R. S. Liu, J. J. Chu, C. T. Chang, P. T. Wu, *Mater. Lett.*, **8**, (1988) 293.
- [111] F. A. Karbarz, O. D. Lacy, K. C. Goretta, U. Balachandran, D. Shi, J. G. Chen, M. Xu, M. C. Hash, *Mater. Res. Bull.*, **25**, (1990) 251.
- [112] J. L. Tallon, R. G. Buckley, P. W. Gilberd, M. R. Presland, I. W. M. Brown, M. E. Bowden, L. A. Christian, R. Goguel, *Nature*, **333**, (1988) 153.
- [113] D. P. Almond, B. Chapman, G. A. Saunders, *Supercond. Sci. Technol.*, **1**, (1988) 123.
- [114] R. M. Hazen, *Crystal Structure of High Temperature Superconductors, Vol. 2*, World Scientific Publishing Company, Pvt. Ltd 1990.
- [115] C. Namgung, J. T. S. Irvine, E. E. Lacowski, A. R. West, *Supercond. Sci. Technol.*, **2**, (1989) 140.
- [116] T. M. Shaw, S. A. Shivashankar, S. J. L. Placa, J. J. Cuomo, T. R. M. Guire, R. A. Roy, K. H. Kelleher, D. S. Yee, *Phys. Rev. B*, **37**, (1988) 8956.
- [117] C. H. Chen, D. J. Werder, S. H. Liou, H. S. Chen, M. Hong, *Phys. Rev. B*, **37**, (1988) 9834.
- [118] P. Bordet, J. J. Capponi, C. Chaillout, J. Chenavas, A. W. Hewat, J. L. Hodeau, M. Marezio, J. L. Tholence, D. Tranqui, *Physica C*, **153-155**, (1988) 623.
- [119] A. C. Vajpei, G. S. Upadhyaya, *Powder Processing of High Tc Oxide Superconductors*, Transtech publications 1992.

- [120] P. Bordet, J. J. Capponi, C. Chaillout, J. Chenavas, A. W. Hewat, E. A. Hewat, J. L. Hodeau, M. Marezio, "Studies on High Temperature Superconductors", Ed. A. V. Narlikar, *Vol. 2*, Nova Publishers 1989.
- [121] M. Takano, J. Takada, K. Oda, H. Kitaguchi, Y. Ikeda, Y. Tomii, H. Mazeki, *Jpn. J. Appl. Phys.*, **27**, (1989) 1041.
- [122] Y. Takemura, M. Hongo, S. Yamjaki, *Jpn. J. Appl. Phys.*, **28**, (1989) L916.
- [123] U. Balachandran, D. Shi, D. I. D. Stantos, S. W. Graham, M. A. Patel, B. Tani, K. Vadervoort, H. Claus, R. B. Poppel, *Physica C*, **156**, (1988) 649.
- [124] S. A. Sunshine, T. Seigrist, L. F. Schneemeyer, D. W. Murphy, R. J. Cava, B. Bratlog, R. B. v. Dover, R. M. Fleming, S. M. Glarum, S. Nakahara, R. Farrow, J. J. Krajewski, S. M. Zahurak, J. V. Waszczak, J. H. Marshall, P. Marsh, L. W. Rupp, W. F. Peck, *Phys. Rev. B*, **38**, (1988) 893.
- [125] H. K. Liu, S. X. Dou, N. Savvides, J. P. Zhou, N. X. Tan, A. J. Bourdillon, M. Kuiz, C. C. Sorrel, *Physica C*, (1989) 93.
- [126] B. Zhu, L. Lei, S. L. Yuan, S. B. Tang, W. Wang, G. G. Zhang, W. Y. Guan, J. Q. Zhen, *Physica C*, **157**, (1989) 370.
- [127] F. H. Chen, H. S. Koo, T. Y. Tseng, *J. Am. Ceram. Soc.*, **75**, (1992) 96.
- [128] F. H. Chen, H. S. Koo, T. Y. Tseng, *J. Mater. Sci.*, **25**, (1990) 3338.
- [129] T. S. Heh, J. R. Chen, T. Y. Tseng, *Jpn. J. Appl. Phys.*, **29**, (1990) 650.
- [130] F. H. Chen, H. S. Koo, T. Y. Tseng, R. S. Liu, P. T. Wu, *Mater. Lett.*, **8**, (1989) 228.
- [131] Y. K. Sun, W. Y. Lee, *Physica C*, **212**, (1993) 37.
- [132] Z. X. Zhao, *Physica C*, **153-155**, (1988) 1144.
- [133] Y. Bando, T. Kijima, Y. Kitami, J. Tanaka, F. Izumi, M. Yokoyama, *Jpn. J. Appl. Phys.*, **27**, (1988) L358.

- [134] E. A. Hewat, P. Bordet, J. J. Capponi, C. Chaillout, J. L. Hodeau, M. Marezio, *Physica C*, **153-155**, (1988) 619.
- [135] J. B. Torrance, Y. Tokura, S. J. L. Placa, T. C. Huang, R. J. Savoy, A. I. Nazzal, *Solid State Commun.*, **66**, (1988) 703.
- [136] C. Park, R. L. Snyder, *J. Am. Ceram. Soc.*, **78**, (1995) 3171.
- [137] R. J. Cava, *Science*, **247**, (1990) 656.
- [138] Z. Z. Sheng, A. M. Herman, *Nature*, **332**, (1988) 55.
- [139] S. S. P. Parkin, V. Y. Lee, E. M. Engler, A. I. Nazzal, T. C. Huang, G. Gorman, R. Savoy, R. Beyers, *Phys. Rev. Lett.*, **60**, (1988) 2539.
- [140] H. Ihara, R. Sugise, M. Hirabayashi, N. Terada, M. Jo, K. Hayashii, A. Negishi, M. Tokumoto, Y. Kimura, T. Shimomura, *Nature*, **334**, (1988) 510.
- [141] L. Guo, Z. J. Huang, R. L. Meng, J. G. Lin, F. Chen, L. Beauvais, Y. Y. Sun, Y. Y. Xue, C. W. Chu, *Physica C*, **213**, (1993) 261.
- [142] M. Hirabayashi, K. Tokiwa, M. Tokumoto, H. Ihara, *Jpn. J. Appl. Phys.*, **32**, (1993) 1206.
- [143] M. Hirabayashi, K. Tokiwa, H. Ozawa, Y. Noguchi, M. Tokumoto, H. Ihara, *Physica C*, **219**, (1994) 6.
- [144] R. E. Somekh, M. G. Blamire, Z. H. Barber, K. Butler, J. H. James, G. W. Morris, E. J. Tomlinson, A. P. Schwarzenberger, W. M. Stobbes, J. E. Evet, *Nature*, (1987) 857.
- [145] P. Chaudhuri, R. H. Koch, R. B. Laibowitz, T. R. McGuire, R. J. Gambino, *Phys. Rev. B*, **326**, (1987) 857.
- [146] N. M. Alford, T. W. Button, M. J. Adams, S. Hedges, B. Micholson, W. A. Phillips, *Nature*, **349**, (1991) 680.

- [147] N. M. Alford, T. W. Button, D. Opie, *Supercond. Sci. Technol.*, **4**, (1991) 433.
- [148] N. M. Alford, S. J. Penn, T. W. Button, *Supercond. Sci. Technol.*, **10**, (1997) 169.
- [149] R. G. Humphreys, J. S. Satchell, N. G. Chew, J. A. Edwards, S. W. Goodyear, S. E. Blenkinsop, O. D. Dosser, A. G. Cullis, *Supercond. Sci. Technol.*, **3**, (1990) 38.
- [150] J. M. Phillips, *J. Appl. Phys.*, **79**, (1996) 1829.
- [151] T. H. Tiefel, S. Jin, *J. Appl. Phys.*, **70**, (1991) 6510.
- [152] M. Yang, M. J. Giringe, C. R. M. Governor, R. Jenkins, H. Jones, *Supercond. Sci. Technol.*, **7**, (1994) 378.
- [153] C. J. Cui, S. G. Wang, H. H. Jiang, J. Z. Li, C. D. Lin, H. Z. Liu, Q. L. Zheng, Y. S. Fu, Z. L. Luo, W. C. Qiao, *IEEE Trans. Mag.*, **25**, (1988) 2506.
- [154] T. Hattori, N. Hogemoto, S. Kanazawa, H. Kobayashi, *Jpn. J. Appl. Phys.*, **27**, (1998) L1120.
- [155] O. G. Symko, W. J. Yeh, D. J. Zheng, S. Kulkarni, *J. Appl. Phys.*, **D 65**, (1989) 2142.
- [156] N. M. Alford, T. W. Button, *Adv. Mater.*, **30**, (1991) 318.
- [157] A. Bailey, G. Alvarez, G. J. Russel, K. N. R. Taylor, *Bull. Mater. Sci.*, **14**, (1991) 111.
- [158] T. G. Holsinger, D. S. Phillips, J. Y. Coulter, J. O. Willis, D. E. Peterson, *Physica C*, **243**, (1995) 93.
- [159] J. Hagberg, A. Usimaki, S. Leppavuori, *Appl. Supercond.*, **1**, (1993) 1091.
- [160] S. X. Dou, H. K. Liu, A. J. Bourdillon, N. X. Tan, C. C. Sorrell, *Physica C*, **158**, (1989) 93.

- [161] P. May, D. Jedamzik, W. Boyle, P. Miller, *Supercond. Sci. Technol.*, **1**, (1988) 1.
- [162] H. Murakami, J. Nishino, S. Yaegashi, Y. Shiohane, S. Tanaka, *Jpn. J. Appl. Phys.*, **30**, (1991) L185.
- [163] E. G. Bauer, B. W. Dodson, D. J. Ehrlich, L. C. Feldman, C. P. Flynn, M. W. Geis, J. P. Harbison, R. J. Matyi, P. S. Peercy, P. M. Petroff, J. M. Phillips, G. B. Stringfellow, A. Zhangwill, *J. Mater. Res.*, **5**, (1990) 852.
- [164] E. K. Hollman, O. G. Vendik, A. G. Zaitsev, B. T. Melekh, *Supercond. Sci. Technol.*, **7**, (1994) 609.
- [165] W. G. Lyons, R. S. Withers, J. M. Hamm, A. C. Anderson, D. E. Oates, P. M. Mankiewich, M. L. O. Malley, R. R. Bonetti, A. E. Williams, N. Newman, "Proceedings of the fifth conference on superconductivity and applications", Ed. T. H. Kao, H. S. Kowh, A. E. Kaloyeros, **251**, (1992) 639.
- [166] I. Shih, C. X. Qiu, *Processing and Application of High Tc Superconductors*, The Metallurgical Soc. Inc. 1988.
- [167] H. Koinuma, K. Fukuda, T. Hasimoto, K. Fueki, *Jpn. J. Appl. Phys.*, **27**, (1988) L1216.
- [168] C. T. Cheung, E. Ruckenstein, *J. Mater. Res.*, **4**, (1989) 1.
- [169] K. Char, D. K. Fork, T. H. Geballe, S. S. Laderman, R. C. Taber, R. D. Jacowitz, F. Bridges, G. A. N. Connel, J. B. Boycee, *Appl. Phys. Lett.*, **56**, (1990) 785.
- [170] K. Char, N. Newman, S. M. Garrison, R. W. Barton, R. C. Taber, S. S. Laderman, R. D. Jacowitz, *Appl. Phys. Lett.*, **57**, (1990) 409.
- [171] L. H. Preng, T. S. Chin, K. Chen, C. H. Lin, *Supercond. Sci. Technol.*, **3**, (1990) 233.

- [172] W. C. M. Gunnis, J. J. Briggs, *J. Mater. Res.*, **7**, (1992) 585.
- [173] A. Agrawal, R. P. Gupta, W. S. Khokale, K. D. Kundra, P. R. Deshmukh, M. Singh, P. D. Vyas, *Supercond. Sci. Technol*, **6**, (1993) 670.
- [174] C. D. Brandle, V. J. Fratello, *J. Mater. Res.*, **5**, (1990) 2160.
- [175] J. Koshy, J. K. Thomas, J. Kurian, Y. P. Yadava, A. D. Damodaran, *Materials Letters*, **17**, (1993) 393.
- [176] J. Koshy, J. Kurian, J. K. Thomas, Y. P. Yadava, A. D. Damodaran, *Jpn. J. Appl. Phys.*, **33**, (1994) 117.
- [177] J. Koshy, K.S.Kumar, J.Kurian, Y. P. Yadava, A. D. Damodaran, *Bull. Mater. Sci*, **17**, (1994) 577.
- [178] J. Koshy, K. S. Kumar, J. Kurian, Y. P. Yadava, A. D. Damodaran, *J. Am. Ceram. Soc.*, **78**, (1995) 3088.
- [179] J. Kurian, J. Koshy, P. R. S. Warriar, Y. P. Yadava, A. D. Damodaran, *J. Solid State Chem.*, **116**, (1995) 193.
- [180] J.Koshy, J. Kurian, K. S. Kumar, P. K. Sajith, M. J. Asha, R. Jose, *Ind. J. Pure Appl. Phys.*, **34**, (1996) 698.
- [181] A. M. John, R. Jose, J. Kurian, P. K. Sajith, J. Koshy, *J. Am. Ceram. Soc.*, **82**, (1999) 1421.
- [182] J. Koshy, J. Kurian, R. Jose, A. M. John, P. K. Sajith, J. James, S. P. Pai, R. Pinto, *Bull. Mater. Sci*, **22**, (1999) 246.
- [183] T. G. N. Babu, P. R. S. Warriar, J. Kurian, A. D. Damodaran, J. Koshy, *J. Mater. Sci.*, **32**, (1997) 1759.
- [184] T. G. N. Babu, J.Koshy, *J. Solid State Chem.*, **126**, (1996) .
- [185] H. Glieter, *Acta Mater.*, **48**, (2000) 1.
- [186] H. Glieter, *Nanostruct. Mater.*, **1**, (1992) 1.

- [187] A. S. Edelstein, R. C. Cammarata, *Nanomaterials, Synthesis, Properties and Applications*, Institute of Physics.
- [188] C. Suryanarayana, *Bull. Mater. Sci.*, **17**, (1994) 307.
- [189] R. A. Andrievski, *J. Mater. Sci.*, **29**, (1994) 614.
- [190] R. D. Shull, *Nanostruct. Mater.*, **2**, (1993) 213.
- [191] R. W. Siegel, *Nanostruct. Mater.*, **4**, (1994) 121.
- [192] R. Birringer, *Mater. Sci. Engg.*, **A117**, (1989) 33.
- [193] S. Li, L. Sun, Z. Wang, *Nanostruct. Mater.*, **2**, (1993) 653.
- [194] H. Chang, C. J. Altstetter, R. S. Averback, *J. Mater. Res.*, **7**, (1992) 2962.
- [195] H. Hahn, J. Logas, R. S. Averback, *J. Mater. Res.*, **5**, (1990) 609.
- [196] J. R. Groza, R. J. Dowding, *Nanostruct. Mater.*, **7**, (1996) 749.
- [197] H. Glieter, *Prog. Mater. Sci.*, **33**, (1989) 223.
- [198] G. W. Nieman, J. R. Weertman, R. W. Siegel, *J. Mater. Res.*, **6**, (1991) 1012.
- [199] Y. Z. Wang, G. W. Qiao, X. D. Liu, B. Z. Ding, Z. Q. Hu, *Mater. Lett.*, **17**, (1993) 152.
- [200] X. D. Liu, J. T. Wang, J. Zhu, *J. Mater. Sci.*, **29**, (1994) 929.
- [201] J. Rupp, R. Birringer, *Phys. Rev. B*, **36**, (1987) 7888.
- [202] E. Hellstern, H. Fetch, Z. Fu, W. L. Johnson, *J. Appl. Phys.*, **65**, (1989) 305.
- [203] Y. Yoshizawa, S. Oguma, K. J. Yamamuchi, *J. Appl. Phys.*, **64**, (1988) 6044.
- [204] S. Jin, T. H. Tiefel, M. M. Cormack, R. Ramesh, L. Chen, *Science*, **264**, (1994) 413.
- [205] K. V. Paulose, J. Koshy, P. Umadevi, A. D. Damodaran, *Appl. Phys. Lett.*, **59**, (1991) 10.

- [206] K. V. Paulose, J. Koshy, A. D. Damodaran, *Jpn. J. Appl. Phys.*, **30**, (1991) 459.
- [207] K. V. Paulose, J. Koshy, A. D. Damodaran, *Supercond. Sci. Technol*, **4**, (1991) 98.
- [208] J. Koshy, J.K.Thomas, J. Kurian, Y. P. Yadava, A. D. Damodaran, *J. Appl. Phys.*, **73**, (1993) 3402.
- [209] K. V. Paulose, P. Murugaraj, J. Koshy, A. D. Damodaran, *Jpn. J. Appl. Phys.*, **31**, (1992) 1323.

6/2056

## CHAPTER II

# PREPARATION AND CHARACTERIZATION TECHNIQUES

### 2.1 Introduction

Powder synthesis is one of the major challenges in the development of advanced ceramic materials for their various functional and structural applications. Ceramic industry requires the raw materials as powders and the quality of these powders has the strongest influence on the structure and properties of the final ceramic product. The processing of ceramics, both substrates and high Tc superconductors, involves preparation of high purity powders as single-phase materials (calcination), compaction of the single-phase powder in to the desired shape followed by densification and texturing at high temperatures (sintering). The microstructure and the final properties of ceramic powders are largely depend on the characteristics of the starting powders such as the particle size and size distribution, particle shape and shape distribution, degree of particle agglomeration, chemical composition and homogeneity [1, 2]. A brief description of the various methods used for preparation of samples and different techniques used for their characterization are given in this chapter. However, the specific details regarding the sample preparation and characterization are described in detail in the respective chapters.

### 2.2 Ceramic Processing

The conventional way of advanced ceramic fabrication includes the powder preparation, shaping and sintering.

666.3/7:621.38:042 41

### **2.2.1 Powder Preparation:**

In general the powder preparation technique fall in to three categories, viz., solid phase synthesis, liquid phase synthesis and gas phase synthesis. The solid phase synthesis (solid state reaction method) of ceramic oxides employs a series of mixing, grinding and heating cycles with varying heating schedule. In this method, the stoichiometric amount of the initial reaction mixture is calcined in a certain range of temperature for certain time. Calcination processes are endothermic decomposition reactions in which an oxysalt such as a carbonate, oxide or a hydroxide decomposes, leaving an oxide as a solid product and liberating a gas [3]. Solid state reaction is a relatively cheap technique for the production of ceramic oxide powders. The solid state reaction method, though widely used because of its simplicity, has certain disadvantages. In the case of multicomponent system, the mixing of the constituent salts or compounds is a very important part in solid state reaction method and one of the problems associated with the conventional mixing is that it may not result in sufficient transport of powders which in turn may prevent a complete solid state reaction during calcination. In the ball milled powders it is difficult to obtain reproducible uniform distribution of materials especially when one constituent fraction is present in small amounts. Inadequate mixing of powders can lead to compositional inhomogeneities, insufficient stoichiometry control and formation of extraneous phases during high temperature annealing. The presence of aggregates/agglomerates in calcined materials would result in high porosity and microstructural coarsening leading to poor sinterability and inferior physical characteristics [4-6].

In the present study, ceramic materials were synthesized by both solid state route and combustion process. In the solid state route, stoichiometric amounts of the reagents, which are oxides and/or carbonates, were thoroughly mixed in an

agate mortar with acetone as wetting medium for 2 h. The powders were dried in electric oven at 150°C for 2 to 4 h. The dried mixture was calcined in air at a desired temperature for ~ 24 h in alumina/platinum crucibles with multiple grindings. The resulting powder was ground well and the calcination step was repeated 2 to 3 times. In the present work ceramics materials were also synthesized as phase pure nanoparticles by using a modified combustion process. In this route aqueous solution of the constituent ions were prepared by dissolving stoichiometric amounts of respective nitrates/oxychloride/oxides. These solutions were mixed together and an equivalent quantity of citric acid was added. The amount of citric acid was kept at the citric acid to cation ratio unity. The oxidant/fuel ratio of the system was adjusted by the addition of ammonium hydroxide and nitric acid. The solution containing the complex precursor at neutral pH was then heated in a hot plate. Initially the solution boils and on completion of evaporation the solution turns into a foam. The foam then ignites and the product of combustion was voluminous and fluffy.

### 2.2.2 Shaping

Depending on the shape and required characteristics, numerous powder forming process have been developed. The most commonly used powder shaping techniques are die pressing, rubber mold pressing, extrusion molding, slip casting and injection molding [6]. The powder itself consists of solid brittle particles, so it is difficult to fill the powder in a die by pressure alone. As the pressure is increased, there is more strain on the compact, and cracks that can cause the compact to fracture are formed. Therefore, a binder is usually added to enhance the fluidity of the powder [5]. Polyvinyl alcohol is the commonly used binder for the forming of oxide ceramics. In the present study, the powders were pressed uniaxially pressed at a pressure of ~ 350 MPa using a hydraulic press.

### **2.2.3 Sintering**

Sintering is the most important step during ceramic processing because it is at this stage that a powder compact is exposed to the maximum temperature. When a ceramic material is heated, there is a certain temperature at which they begin to diffuse, and in most cases there is shrinkage resulting in densification. During this process, the redistribution of matter takes place in such a way that minimize the system free energy. Besides densification, many electrical, magnetic, optical and mechanical properties are determined by the physical and chemical changes during sintering at high temperature. Characteristics of the starting powder such as particle size distribution, degree of particle agglomeration, particle shape, shape distribution, particle aggregates, have a profound influence on densification and microstructural development [7]. A large number of sintering methods such as standard pressure sintering, hot pressing, hot isostatic pressing, reaction sintering, recrystallization sintering, ultra high pressure sintering are frequently employed [6]. In the present study, the sintering of the powder compacts were done in a programmable furnace in a certain temperature range.

### **2.3 Preparation of High T<sub>c</sub> Superconducting thick films**

A number of techniques has been proposed and are in use for the development of superconducting thick films. They include dip-coating, screen printing, spray pyrolysis, spin-coating, pain-on etc. All these techniques, in general, start with the preparation of a homogeneous mixture, known as ink, consisting of the superconductor powder and an organic vehicle. The vehicle is a mixture of polymers and solvents. The ink is then coated on the substrate by any of the above techniques and dried. The coated and subsequently dried coating are

fired at high temperature in order to sinter the particles in the ink so that a textured film is obtained.

In the present study, thick films of YBCO, Bi (2212) and Bi (2223) materials have been produced by dip-coating and melt texturing technique. For dip-coating, a suspension of the superconducting material was prepared by thoroughly mixing fine powders of the superconductor with isopropyl alcohol or n-butanol. For obtaining the film, the polished and cleaned substrate is dipped in the thick film suspension and the dipping process is repeated until a required thickness is achieved. The resulting film is then dried in a hot air oven and is subjected to controlled heat treatment. The actual temperature, time of annealing, rate of heating and cooling are described in the respective chapters.

#### **2.4 Characterization techniques**

The newly developed ceramic materials are crystalline and are dielectrics in nature. The structures of the materials are studied by x-ray diffraction technique and their dielectric properties are studied using an impedance analyzer. The nanoparticulate powders of the newly developed materials were characterized by differential thermal analysis, thermogravimetric analysis, FT-IR spectroscopy, BET surface area measurements, gas adsorption studies, agglomerate size analysis and high-resolution transmission electron microscopy in addition to powder x-ray and electron diffraction. Thermal analyses were also carried out on the coarse grained powders produced through the conventional solid state route. The superconducting properties of the superconductor-insulator composites and high  $T_c$  superconducting thick films were carried out by temperature-resistance measurements using four-probe technique.

### 2.4.1. Powder X-ray Diffraction Technique

Powder x-ray diffraction is one of the most important tools for the investigation of the structure of matter. This technique had its beginning in 1912 when Von Laue discovered that the crystal diffract x-rays in the same way as the visible light is diffracted by a diffraction grating. In other words, the crystal acts as a three-dimensional grating for the x-rays and the manner of the diffraction revealing the crystal structure of the matter. Later on, other uses were developed and today the method is applied, not only to the structure determination, but such diverse problems as chemical analysis, stress measurement, study of phase equilibria, measurement of particle size, determination of the orientation of one crystal or the ensemble of orientation in a polycrystalline aggregate [8,9].

The resolving power of any optical instrument limited to diffraction is proportional to the wavelength of the electromagnetic radiation used and the diffraction pattern are produced when the wavelength is comparable to the interatomic spacings in crystals. Radiations of longer wavelength are no longer diffracted by the periodic lattice of the crystal and that of shorter wavelength is diffracted through inconveniently smaller angles. x-rays have wavelengths comparable with the interatomic spacings in crystals. When x-rays of wavelengths comparable or smaller than the lattice constants are allowed to incident on a crystal, one or more diffracted beams are observed in directions quite different from that of incident beam. W. L. Bragg explained the observed angles of diffracted x-rays from a crystal in which the incident waves are reflected specularly from parallel planes of atoms in the crystal, with each plane reflecting the very small fraction of the radiation.

The diffraction of x-rays by the periodic structure of the crystal lattice is illustrated in figure 2.1. The horizontal dotted lines represent a parallel crystal plane with Miller indices (hkl) and  $W_1W_2$  and  $W_3W_4$  are the wave fronts incident and scattered by the periodic lattice of the crystal. The scattered waves undergo a constructive interference when

$$2d_{hkl} \sin\theta = n\lambda \quad (1)$$

where  $d_{hkl}$  is the spacing between crystal planes,  $n$  is the order of the spectrum and  $\lambda$  is the wave length.

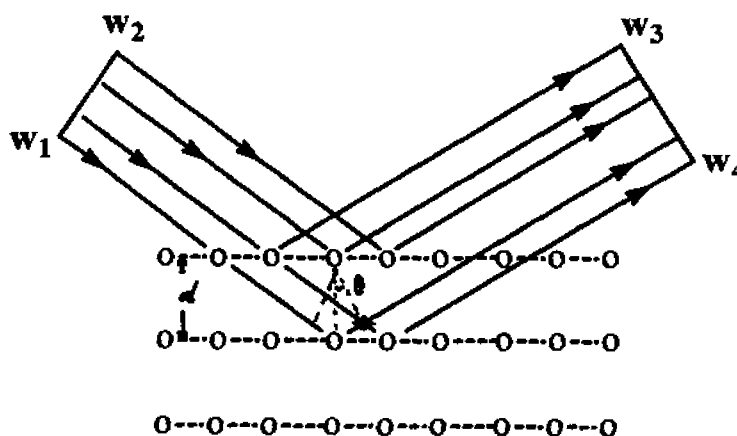


**Figure 2.1:** Reflection of a plane wave by a set of parallel planes.

For the present study, the powder X-ray diffraction (XRD) patterns were obtained using a computerized Rigaku Dmax (Japan) diffractometer employing Nickel filtered  $\text{CuK}\alpha$  radiation ( $\lambda = 1.5406 \text{ \AA}$ ). The XRD patterns were recorded at a scan speed of  $4^\circ/\text{min}$  at a step scan of  $0.01^\circ$ . Identification of the phases is done by comparing the  $d$  spacings and line strengths of the observed x-ray diffraction

pattern of the sample with standard reference data. The samples for x-ray diffractograms were prepared by smearing the finely ground powder on a standard glass plate provided with a groove.

#### **2.4.2 Differential Thermal Analysis (DTA):**

Differential thermal analysis is concerned with the detection of physical or chemical changes, which may occur when matter is heated. Specifically, DTA studies the change in absorption or liberation of heat by a sample measured as a function of the temperature. This change is compared to a reference substance that has been submitted to the same conditions. The method is especially suited for studying the structural changes within a solid at elevated temperatures and is mostly qualitative. For the present study, Differential thermal analysis was carried out using a Shimadzu DTA-50H unit with alumina as reference material. The samples were heated in nitrogen atmosphere at a heating rate of 10°C/min from room temperature to 1300°C. ~20-mg powder is used for each measurement.

#### **2.4.3 Thermogravimetric Analysis (TGA)**

Thermogravimetry studies the weight changes takesplace in a sample as the temperature is gradually raised in a certain rate. Two modes are commonly employed for thermogravimetric analysis. The first type, dynamic thermogravimetry subjects a sample to a continuous increase in temperature, usually linear with time. The second type, isothermal thermogravimetry subjects a sample to a constant temperature for a long time and the weight changes is noted. The instrument used is an automatic thermobalance. Information gained from TGA is often enhanced by the application of DTA, as the two techniques are complementary. The combination of TGA with the information from X-ray

diffraction and DTA yields a good quantitative estimation of solid state reaction. For the present study, thermogravimetric analysis was carried out using a Shimadzu TGA-50 unit at a heating rate of  $10^{\circ}\text{C}/\text{min}$  in nitrogen atmosphere from room temperature to  $1100^{\circ}\text{C}$ ,  $\sim 5$  mg powder is used for each measurement.

#### **2.4.4. IR spectroscopy**

The principle of this technique lies in the fact that when IR interacts with the materials, various chemical bonds in the material vibrate as it absorbs the IR radiation. These vibrations are either in the stretching or in the bending mode. When infrared light is passed through a material some of the frequencies are absorbed while other frequencies are transmitted through the sample without being absorbed. FT-IR spectra were recorded using a Nicolet 1 400D FT-IR spectrometer. The materials were finely dispersed in KBr using an agate mortar and pestle. The finely dispersed material was then pressed in the form of circular discs of  $\sim 10$  mm diameter and 0.5 mm thickness at a pressure 250 MPa. These pellets were then dried with IR light before the FT-IR spectrum has been recorded.

#### **2.4.5 Gas Adsorption Technique**

Analysing the surface character of powder is perhaps one of the most important and most difficult procedures in ceramics characterization. Surface phenomena are a consequence of asymmetrical or unbalanced forces between atoms and molecules at the interface of a particle and are electronic in origin. The direct means of the characterization of the surface of ceramic powder is the transmission electron microscopy and will be described later. The indirect methods include (i) interaction of the powder with a liquid and (ii) interaction of the powder with a gas.

One of the most popular techniques used for the determination of the specific surface area of fine powders is that of low temperature nitrogen gas adsorption. What is measured is the amount of nitrogen gas adsorbed by a powder sample at liquid nitrogen temperatures over a range of gas partial pressures. The amount of gas forming a monolayer of the powder surface is usually calculated using Brunauer, Emmet and Teller (BET) equation [10].

$$\frac{P}{V(P_0 - P)} = \frac{1}{V_m C} + \frac{C-1}{V_m C} \cdot \frac{P}{P_0} \quad (2)$$

Where  $V$  is the total volume of gas adsorbed,  $V_m$  is the gas adsorbed when the adsorbent surface is covered with a unimolecular layer,  $P$  is the equilibrium pressure of the system,  $P_0$  is the saturation pressure of the adsorbate gas,  $C$  is a constant dependent on the heat of adsorption and heat of liquefaction of the adsorbate gas, is in the range 50 to 300 for many adsorbents[11].

It has been shown that for  $P/P_0$  values 0.05 to 0.30, the plot of  $[P/V (P_0 - P)]$  versus  $P/P_0$  is a straight line having a slope of  $(C-1 / V_m C)$  and an intercept of  $1/V_m C$  making it possible to calculate both  $V_m$  and  $C$ . The specific surface area of the powder is obtained from the relationship

$$S = \frac{V_m \sigma N}{V_0 W} \quad (3)$$

Where  $\sigma$  is the area occupied by one molecule of adsorbate (assumed  $16.2 \text{ \AA}^2$  for nitrogen at 77 K),  $N$  is the Avagadro's number,  $W$  is the weight of the powder sample and  $V_0$  is the ideal gas volume [12].

The average particle size of the powder was calculated from surface area values by assuming they all consists of monosized hard spherical particles. The particle size is given by [12].

$$d = \frac{6}{\rho S} \quad (4)$$

Where  $\rho$  is the density of the material and  $S$  is the specific surface area.

In the present study, the ceramic powders were degassed at 200°C for 24 h using an electric oven and the nitrogen gas adsorption studies were carried out in a Micromeritics unit model Gemini 2360. For generating adsorption isotherm, relative gas pressure is increased in different steps and the volume of the nitrogen gas adsorbed for 30 min was measured. The gas adsorption studies were done at liquid nitrogen temperature.

#### 2.4.6 Agglomerate size Analysis

Agglomerate size distributions of the powders were studied using sedimentation technique. The usefulness of the sedimentation technique for agglomerate size measurement relies on the fact that the rate of fall of a particle in a fluid medium is proportional to the volume of the particle [12]. The rate of fall ( $v$ ) of a spherical particle is related to the diameter ( $d$ ) of the particle by

$$d = \left( \frac{18\eta \cdot v}{(\rho - \sigma)g} \right)^{1/2} \quad (5)$$

where,  $\eta$  is the viscosity of the fluid,  $v$  is the rate of fall (terminal velocity),  $\rho$  is the particle density,  $\sigma$  is the fluid density and  $g$  is the acceleration due to gravity.

For the present study, the agglomerate size distribution of the powders were studied by using a Micromeritics sedigraph model 5700. The powders were ultrasonically dispersed in water before the agglomerate distribution curve was recorded.

### 2.4.7 Transmission Electron Microscopy

Transmission electron microscopy is the tool for the *in situ* measurement of powder surfaces. The wave nature of moving electrons is the basis of the electron microscope. The wavelength of electron wave is equal to

$$\lambda = \frac{12.26}{\sqrt{V}} \text{ \AA} \quad (6)$$

Where V is the accelerating voltage.

The resolving power of any optical instrument, which is limited by diffraction, is proportional to the wavelength of whatever is used to illuminate the specimen. In the case of good microscope that uses visible light, maximum useful magnification is about 500X, higher magnification gives larger images but do not reveal any more details. However fast electrons have wavelengths very much shorter than those of visible light and are easily controlled by electric and magnetic fields because of their charge. This diffraction of electron beams is the principle of a Transmission Electron Microscope.

In transmission electron microscopy, electrons of higher energy ( $\sim 10^5$  eV) are allowed to transmit through the specimen surface. Some electrons will be transmitted and some will be diffracted by the specimen as the electron beam strikes it. If the transmitted beam is used for the generation of micrographs, such pictures are called bright field micrographs. In dark field mode, the diffracted electrons are used for the generation of micrographs. Both in bright and dark field images, particles with same orientation have the same gray level. The selected area electron diffraction patterns can also be utilized for the study of crystal structure. The geometry of indexing the electron diffraction pattern is shown in fig.2.2 [13].

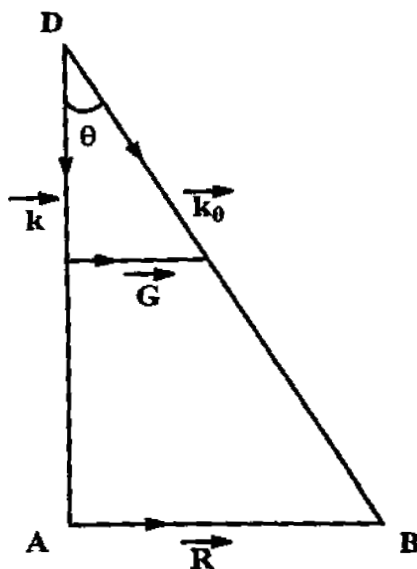


**Figure 2.2:** The Geometry for Indexing an Electron Diffraction pattern

Where,  $K_0$  is the direct wave vector ( $2\pi / \lambda$ ),  $K$  is the diffracted wave vector,  $G$  is the diffracted lattice vector ( $2\pi / d$ ),  $L$  is the camera length,  $R$  is Radius vector of the ring (spot)

From the geometry of triangles

$$\begin{aligned} \frac{k}{G} &= \frac{L}{R} \\ \Rightarrow d &= \frac{L\lambda}{R} \end{aligned} \quad (7)$$

Therefore by knowing the camera length, wavelength of electron wave and radius of the ring or spot, structure of the material can be elucidated.

In the present study the morphology and structure of the materials were studied by a JEOL 2000 EXII High Resolution Transmission Electron Microscope (HRTEM) operated at 200kV and at a vacuum of  $10^{-6}$  Torr. The powder particles were supported on a carbon film coated on a 3 mm diameter fine mesh copper grid.

The carbon films were coated by a Edward 303 vacuum coating unit at a vacuum of  $10^{-4}$  Torr. The powders were dispersed in methanol and agitated with ultrasound for 10 min. Two drops from the topmost layer of this suspension were dropped on the support film.

#### 2.4.8. Dielectric measurements

At low frequencies, the determination dielectric constant is usually based on the measurement of capacitance of a parallel plate capacitor or coaxial capacitor containing the material under test. The technique is based on the principle that when a material is introduced between the plates of a parallel plate capacitor, its capacitance increases by a factor  $\epsilon'$ , the dielectric constant of the material. The dielectric constant  $\epsilon'$  is related with the capacitance C as

$$\epsilon' = \frac{Cd}{\epsilon_0 A} \quad (8)$$

Where  $\epsilon_0$  is the permittivity of free space ( $8.85 \times 10^{-12}$  f/m), A is the cross sectional and d is the thickness of the specimen.

The dielectric properties of the viz. dielectric constant ( $\epsilon'$ ) and loss properties of the factor ( $\tan \delta$ ) of the materials have been studied using a complex impedance analyzer (Model Hewlett Packard, 4192) in the frequency range 30 Hz to 13 MHz both at room temperature and liquid nitrogen temperature. The materials used for the dielectric measurements were sintered to high density (>97%) in the form of circular discs of diameter  $\sim 10$  mm and thickness  $\sim 1$  mm. The sintered specimens were mechanically polished and cleaned the surface with acetone. Room temperature curing silver paint was pasted on both the surfaces and was dried in an electric oven at a temperature of  $\sim 100^\circ\text{C}$  for 4 h. Copper leads were taken from the silver electrode surfaces. This was used as the sample for

dielectric measurements. The capacitance and dissipation factors were directly measured from the impedance analyzer both at room temperature and liquid nitrogen temperature. For the measurements at liquid nitrogen temperature, the samples were well-immersed in liquid nitrogen taken in a thermoflask.

#### **2.4.9. Resistance measurements**

Resistance measurements are one of the important tools to characterize a superconductor sample. The superconducting transition temperature ( $T_c$ ) can be directly determined by resistance measurements of the sample as a function of temperature. In the present study standard four-point probe method was used for the resistance measurements of the superconductor-insulator and superconducting thick film samples. The four-probe method of measuring the resistance has the advantage over two-probe method that the effects due to contact resistance, lead resistance etc can be avoided.

Four probe technique in van der Pauw geometry permits the measurement of an isotropic sample of uniform flat thickness but with arbitrary shape if meet the following criteria [14, 15]. The different criteria are, (i) the contacts are at the periphery of the sample, (ii) the contacts are sufficiently small, (iii) the sample is uniform in thickness, (iv) the sample does not contain holes, and (v) the sample is homogeneous. The measurement is based on a theorem, proved by van der Pauw [14, 15], for a sample of uniform thickness and for arbitrary shape with four arbitrarily positioned contacts (A,B,C&D) on the edges as shown in figure 2.3.

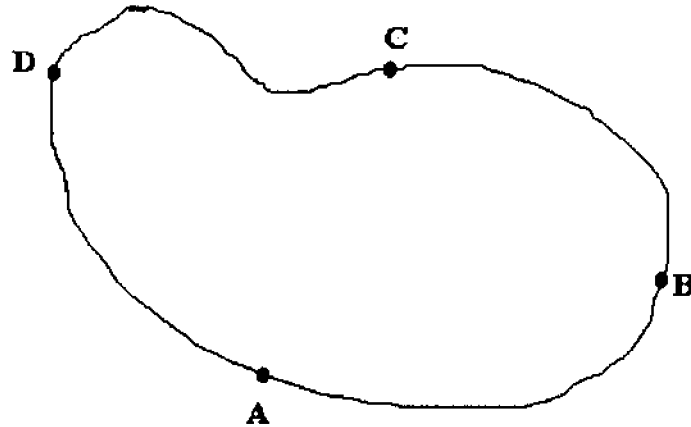


**Figure 2.3:** Lead arrangement for van der Pauw with four contacts A, B, C, and Don the periphery for resistance measurements (ref. 15)

If we define

$$R_{AB,CD} = \frac{V_D - V_C}{I_{AB}} \quad (9)$$

and

$$R_{BC,DA} = \frac{V_A - V_D}{I_{BC}} \quad (10)$$

where  $V_D - V_C$  is the potential difference between contacts D and C caused by the passage of current  $I$  from A to B, etc. van der Pauw theorem takes the form

$$\exp(-\pi R_{AB,CD} d / \rho) + \exp(-\pi R_{BC,DA} d / \rho) = 1 \quad (11)$$

Where  $\rho$  is the resistivity and  $d$  is the sample thickness. This equation can be solved for  $\rho$ , we get

$$\rho = (\pi d / \ln 2) \{ (R_{AB,CD} - R_{BC,DA}) / 2 \} \{ F(R_{AB,CD}) / (R_{BC,DA}) \} \quad (12)$$

Here  $F$  is a function of the ratio resistance such that

$$(R_{AB,CD} - R_{BC,DA}) / (R_{AB,CD} + R_{BC,DA}) = F \operatorname{arc} \cosh \{ \exp(\ln 2 / F) \} / 2 \quad (13)$$

In the special case of samples and constants which are invariant under rotation of  $90^\circ\text{C}$ , the sheet resistance  $R_s = \rho / d$  reduces to simple form

$$R_s = \rho / \ln 2) (V / I) = (\pi / \ln 2) R_{AB,CD} = (\pi / \ln 2) R_{AC,BD} \quad (14)$$

Specimens with such symmetry are often easily prepared. Here  $V$  is the voltage between two voltage contacts and  $I$  is the current flowing through two current contacts.

The resistivity measurements can be made with either direct or alternating current. With direct current care must be taken to eliminate the effects of thermoelectric voltages in the voltage circuit by frequency reversing the sample current.

In the present study, the specimen is mounted on a copper block, which is attached to one end of a copper tube. The sample is electrically insulated from the copper block applying a thin layer of insulating varnish between the specimen and copper block. Four copper leads were attached symmetrically on the periphery of the sample using conducting silver paste. The schematic diagram of the resistance measurements is shown in figure 2.4. A calibrated copper constantan thermocouple was fixed to the copper block very close to the sample to measure the temperature of the sample. The sample holder set up was introduced in to a cylindrical vessel. The vessel was evacuated and a small amount of nitrogen gas was introduced. The whole set up was then introduced in to liquid nitrogen Dewar. Resistance measurements were made at close intervals while the sample was

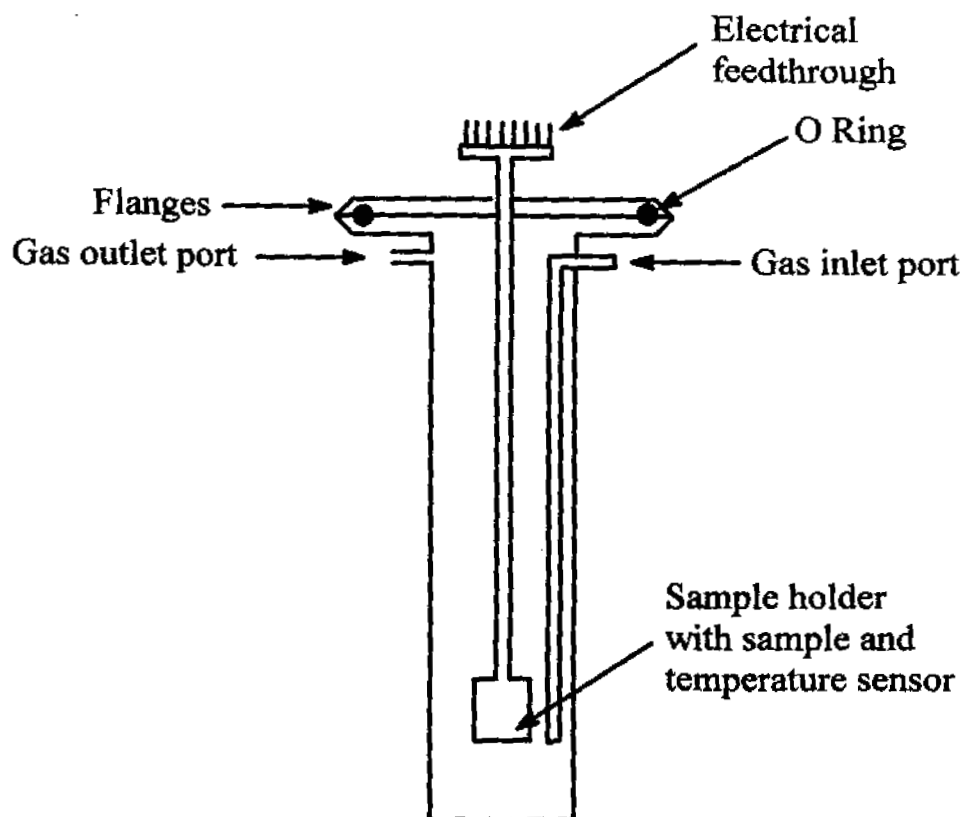


**Figure 2.4.** Schematic diagram for resistance measurement. S, Sample holder with sample and thermocouple; E, Electrical feed through; F, Flanges; R, O ring; P, pumping port; I, input for nitrogen gas

continuously cooled at a low rate. The experiment was conducted by cooling the sample continuously and taking the readings at close intervals. The rate of cooling was controlled by introducing appropriate amount of nitrogen gas in to the vessel as well as by raising the Dewar smoothly and slowly by means of a lab jack. A Keithley nanovoltmeter model 181 was used for resistance measurements. A Keithley electrometer model 602 was used for measuring higher values of resistance.

#### 2.4.10 Current density measurements

The critical current density ( $J_C$ ) of the superconducting films was measured at 77 K in zero magnetic fields by direct method. Superconducting films were developed on a rectangular substrate of dimension 15 mm (length) and 2 mm (width) was used for current density measurements. Four contacts were given linearly as shown in Figure 2.5. In the present study,  $1\mu\text{V}$  criterion was followed for the determination of  $J_C$ . All other set for current density measurements were same as that employed for resistivity measurements except the current source and the linear contacts

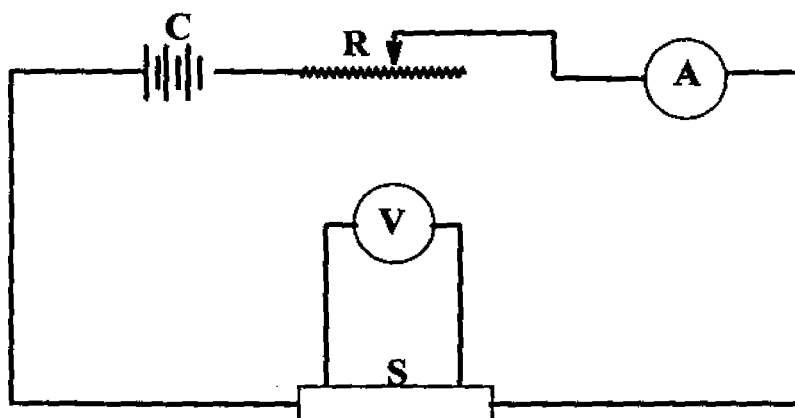


**Figure 2.6:** Schematic diagram of current density measurement showing sample (S), storage cell (C), rheostat (R), ammeter (A), and nanovoltmeter (V)

**REFERENCES**

- [1] S. G. Malghan, A. L. Dragoo, *Characterization of Ceramic Powders, Vol. 4*, ASM International 1991.
- [2] A. C. Vajpei, G. S. Upadhyaya, *Powder Processing of High Tc Oxide Superconductors*, Transtech publications 1992.
- [3] J. W. Halloran, *Calcination, Vol. 4*, ASM International 1991.
- [4] J. Wang, J. Fang, S.-C. Ng, L.-M. Gan, C.-H. Chew, X. Wang, Z. Shen, J. Am. Ceram. Soc., **82**, (1999) 873.
- [5] V. Avalacek, J. A. Puszynski, *Ind. Eng. Chem. Res.*, **35**, (1996) 349.
- [6] N. Ichinose, K. Koyama, N. Ogino, A. Tsuge, Y. Yokomizo, *Introduction to Fine Ceramics; Application in Engineering*, John Wiley & Sons 1987.
- [7] M. F. Yan, *Solid State Sintering, Vol. 4*, A. F. M. International 1991.
- [8] B. D. Cullity, *Elements of X-ray Diffraction*, Addison-Wesley Publishing Co, Inc. 1967.
- [9] H. Klug, L. E. Alexander, *X-ray Diffraction Procedure for Polycrystalline and Amorphous Materials*, Wiley, New York 1974.
- [10] S. Brunauer, P. H. Emmet, E. Teller, *J. Am. Chem. Soc.*, **60**, (1938) 309.
- [11] S. Lowel, J. E. Shields, *Powder Surface and Porosity*, Chapman and Hall, London 1984.
- [12] L. L. Hench, R. W. Gould, *Characterization of Ceramics*, Marcel Dekker, Inc., New York 1971.
- [13] L. Reimer, *Transmission Electron Microscopy: Physics of Image formation and Microanalysis*, Springer Verlag, Berlin.
- [14] L. J. Van der Pauw, *Phillips Res. Repts.*, **13**, (1958) 1.
- [15] L. J. Van der Pauw, *Phillips Tech. Rev.*, **20**, (1958) 220.

## CHAPTER III

### SYNTHESIS OF $Ba_2RE ZrO_{5.5}$ (RE = La, Ce, Eu, Yb, Ho, and Er) : A NEW GROUP OF COMPLEX PEROVSKITE CERAMIC OXIDE THROUGH SOLID STATE REACTION METHOD

#### 3.1 INTRODUCTION

In the course of our research on mixed oxides of rare-earth elements for their use as substrate for  $YBa_2Cu_3O_{7.8}$  (YBCO) superconductors [1-8], we have synthesized a new group of complex perovskites,  $Ba_2REZrO_{5.5}$  (RE = La, Ce, Eu, Yb, Ho, and Er) having general formula  $A_2(BB')O_6$  [9-12] which could be used as substrates for high  $T_C$  superconductors. In this chapter, the synthesis and sintering of  $Ba_2REZrO_{5.5}$  ceramics as single-phase material through solid state reaction method and their characterization are presented <sup>\*</sup>. The crystal structure, sintered density, resistivity measurements, dielectric properties, melting behavior and stability of these materials are studied in detail and the results also are presented.

#### 3.2 Synthesis of $Ba_2REZrO_{5.5}$ (RE =La, Ce, Eu, and Yb)

$Ba_2REZrO_{5.5}$  (RE = La, Ce, Eu, and Yb) materials have been synthesized by the solid state reaction process. High purity (99.9 %)  $BaCO_3$ ,  $RE_2O_3$  (RE = La, Ce, Eu and Yb) and  $ZrO_2$  were weighed in the precise stoichiometric ratio of  $Ba_2REZrO_{5.5}$  and wet mixed in an agate mortar with acetone as the wetting medium. The powders were then dried in an electric oven at  $\sim 100$  °C for 1 h. The dried powders were then compacted at a pressure of 2 MPa in the form of circular discs of  $\sim 25$  mm diameter. These pellets were heated at a temperature of 1200°C for 24 h and then furnace cooled to room temperature. The x-ray diffraction pattern (XRD) taken on a powdered sample heated at 1200°C showed the multiphase nature of the powder. Therefore, the powders were pressed again and subjected to

further heating at a temperature of 1350°C for 72 h with two intermediate grindings. Figure 3.1 shows the powder XRD patterns of the phase evolution of  $\text{Ba}_2\text{LaZrO}_{5.5}$  material as a typical example. The individual calcination temperature and time for the synthesis of each material as single phase is given in Table 1.1.

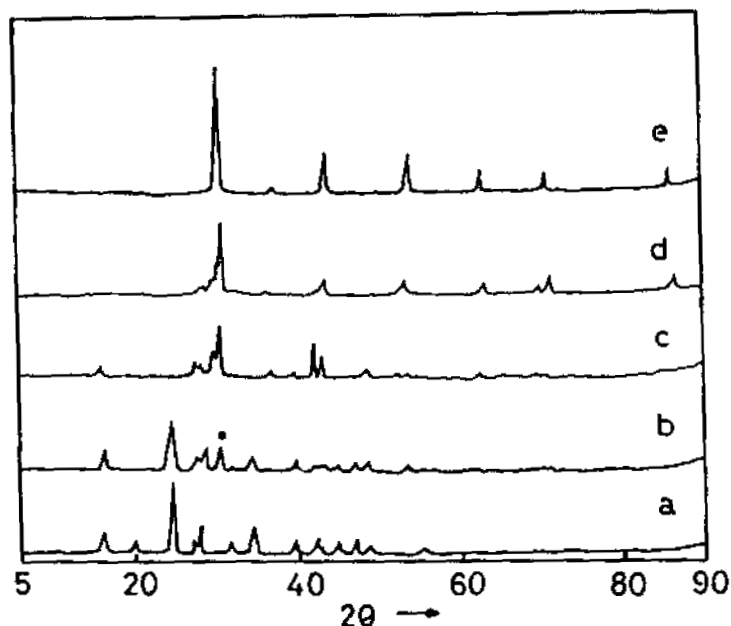


**Figure 3.1.** The XRD pattern of evolution of  $\text{Ba}_2\text{LaZrO}_{5.5}$  phase during heat treatment, (a) stoichiometric mixture containing  $\text{BaCO}_3$ ,  $\text{La}_2\text{O}_3$ , and  $\text{ZrO}_2$  (b) heated at 1350°C for 12h, (c) heated at 1350°C for 24 h (d) heated at 1350°C for 48h (e) heated at 1350°C for 48h

**Table 1.1 :** Calcination temperature and time of  $\text{Ba}_2\text{REZrO}_{5.5}$  ceramics.

Material	Temperature (°C)	Time (h)
$\text{Ba}_2\text{LaZrO}_{5.5}$	1350	40
$\text{Ba}_2\text{CeZrO}_{5.5}$	1350	48
$\text{Ba}_2\text{EuZrO}_{5.5}$	1350	72
$\text{Ba}_2\text{YbZrO}_{5.5}$	1350	72

### 3.3 Sintering of Ba<sub>2</sub>REZrO<sub>5.5</sub> ceramics

For the sintering of Ba<sub>2</sub>REZrO<sub>5.5</sub>, the single phase materials were ground well using an agate mortar and were uniaxially pressed in the form of circular discs having 13 mm diameter and ~2 mm thickness by applying a pressure of 350 MPa using poly vinyl alcohol as the binder. The green densities of the samples for this pressure were calculated from the dimensions and weight of the sample with an accuracy of  $\pm 0.02$  g/cc. The relative green density for all the samples were  $\sim 45 \pm 2\%$  of the theoretical density. These green compacts were sintered in a programmable furnace (Nabertherm, Model HT04/17, Germany) in the temperature range 1520–1675 °C. The heating schedule adopted for the sintering of Ba<sub>2</sub>EuZrO<sub>5.5</sub> is shown in Figure 3.2. The sintering temperature, sintering time, sintered density, and theoretical density for each material is given in Table 3.2. The sintered density was measured following the Archimedes method and theoretical density was calculated from the lattice constant values using the formula,

$$\rho_{\text{cal}} = \frac{ZM}{NV} \quad (3.1)$$

where Z is the number of molecules per unit cell, M is the molecular weight, N is the Avagadro Number and V is the cell volume. Figure 3.3 shows the variation of sintered density with sintering temperature for Ba<sub>2</sub>EuZrO<sub>5.5</sub> material. The sintered samples are mechanically strong and could be sliced into thin pieces of thickness 0.5 mm by a diamond cutter. Good reflecting surfaces were obtained by mechanical polishing. Organic solvents such as alcohol, and carbon tetrachloride could be used as effective cleaning agents.

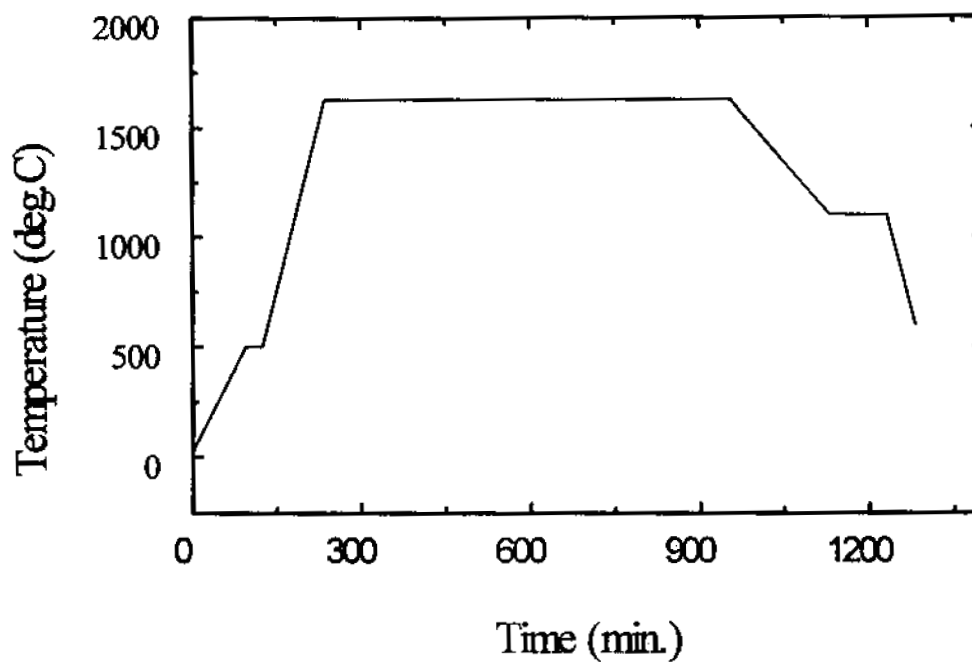


Figure 3.2 : The heating schedule adopted for the sintering of  $Ba_2EuZrO_{5.5}$

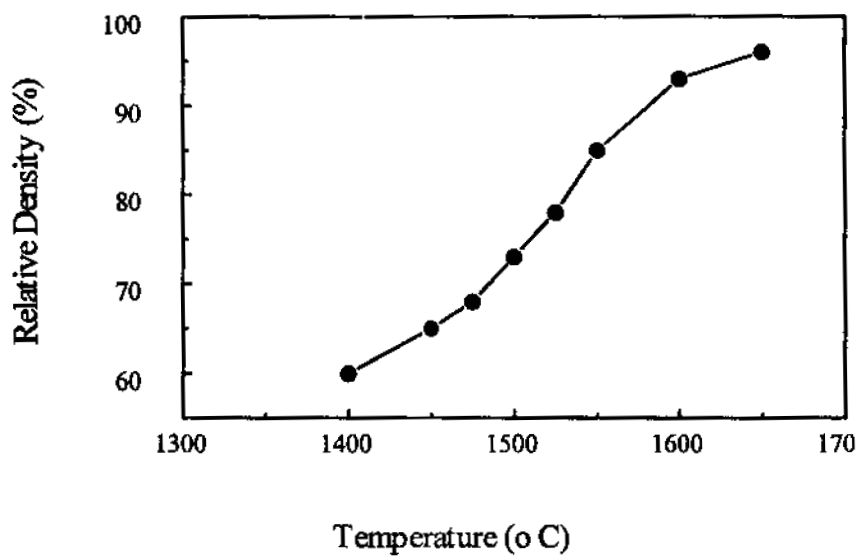


Figure 3.3: The variation of relative density of  $Ba_2EuZrO_{5.5}$  with temperature

**Table 3.2** Sintering temperature, time, theoretical density, sintered density and relative density of  $Ba_2REZrO_{5.5}$  ceramics

Material	Sintering temperature (°C)	Sintering time (h)	Theoretical density (g / cc)	Sintered density (g / cc)	Relative density (%)
$Ba_2LaZrO_{5.5}$	1550	10	6.65	6.31	97
$Ba_2CeZrO_{5.5}$	1600	10	6.30	6.05	96
$Ba_2EuZrO_{5.5}$	1625	12	6.76	6.49	96
$Ba_2YbZrO_{5.5}$	1675	12	7.04	6.76	96

### 3.4 Structural characterization of $Ba_2REZrO_{5.5}$ ceramics

The crystal structure of the newly developed materials has been studied by powder XRD using a computerized Rigaku ( $D_{max}$ , Japan) x-ray diffractometer using Ni-filtered  $CuK\alpha$  radiation. The finely ground powders of the sintered pellets were used as the samples for the x-ray diffraction studies. Figures 3. 4(a-d) show the x-ray diffraction patterns of sintered powders of  $Ba_2LaZrO_{5.5}$ ,  $Ba_2CeZrO_{5.5}$ ,  $Ba_2EuZrO_{5.5}$ , and  $Ba_2YbZrO_{5.5}$  for  $2\theta$  between 5 and  $90^\circ$ . The XRD data comprising of  $2\theta$ , d values, line widths, line strengths and (hkl) are given in Table 3.3(a-d). The XRD patterns and the data clearly show that all these materials have the same structure as judged by the similarity in intensities and positions of the lines.  $Ba_2REZrO_{5.5}$  is also found to be isostructural with other rare-earth cubic perovskites with general formula  $A_2(BB')O_6$  such as  $Ba_2EuNbO_6$ ,  $Ba_2YNbO_6$  reported in PDF cards (Powder Diffraction Files, International Center for Diffraction data (ICDD), Dept. of Commerce, USA) in which doubling of the basic

perovskite unit cell is observed [13-18]. This doubling of the basic perovskite unit cell in these materials is due to the ordering of B (RE) and B' (Zr) atoms on the octahedral sites [9,11-12,19-20]. In a substitutional solid solution, there is a random arrangement of B and B' atoms in equivalent positions in the crystal structure. If, upon suitable heat treatment the random solid solution rearranges in

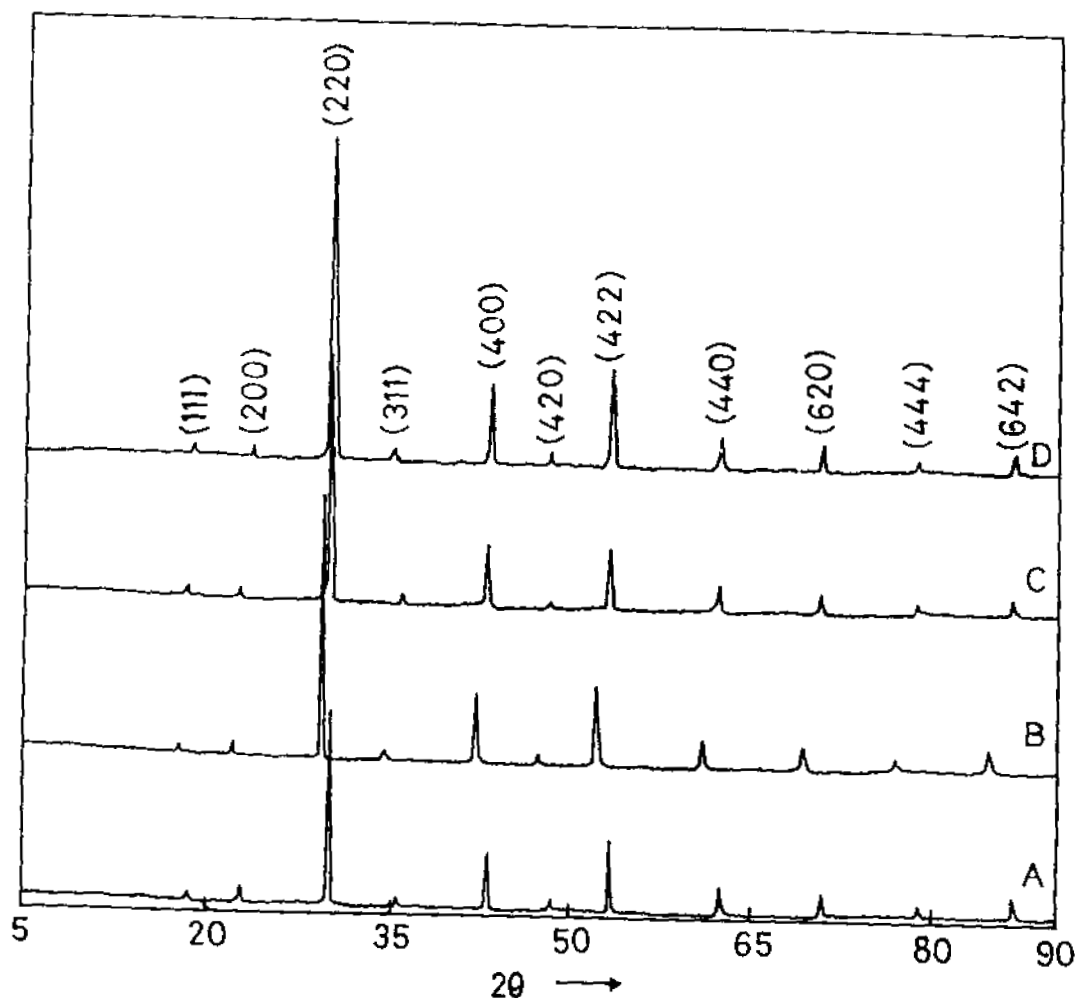


**Figure 3.4:** X-ray diffraction pattern of phase-pure sintered (A)  $\text{Ba}_2\text{LaZrO}_{5.5}$  (B)  $\text{Ba}_2\text{CeZrO}_{5.5}$ , (C)  $\text{Ba}_2\text{EuZrO}_{5.5}$ , and (D)  $\text{Ba}_2\text{YbZrO}_{5.5}$  for  $2\theta$  from  $5 - 90^\circ$

Table 3.3 (a) : X-ray diffraction data <sup>\*</sup> of Ba<sub>2</sub>LaZrO<sub>5.5</sub>

No	2θ (deg.)	Width ( deg.)	d (Å)	(hkl)	I / I <sub>o</sub>
1	18.289	0.270	4.846	111	3
2	21.149	0.465	4.197	200	8
3	30.080	0.555	2.968	220	100
4	35.439	0.360	2.531	311	6
5	37.071	0.510	2.423	222	10
6	43.090	0.525	2.098	400	31
7	48.458	0.495	1.877	420	6
8	53.426	0.555	1.713	422	40
9	62.539	0.555	1.484	440	10
10	70.948	0.630	1.327	620	15
11	78.948	0.570	1.212	444	8
12	86.713	0.795	1.122	642	15

<sup>\*</sup>Accepted in Powder Diffraction File, Published by Dept. of Commerce, ICDD (USA)

Table 3.3 (b) : X-ray diffraction data <sup>☆</sup> of Ba<sub>2</sub>CeZrO<sub>5.5</sub>

No	2θ (deg)	Width ( deg.)	d (Å)	(hkl)	I / I <sub>o</sub>
1	17.871	0.150	4.959	111	2
2	20.664	0.105	4.295	200	4
3	29.092	0.315	3.067	220	100
4	34.605	0.390	2.596	311	5
5	36.196	0.090	2.479	222	5
6	42.050	0.165	2.147	400	30
7	47.280	0.210	1.921	420	6
8	52.120	0.225	1.753	422	32
9	60.965	0.075	1.518	440	12
10	69.104	0.195	1.358	620	11
11	76.820	0.105	1.239	444	5
12	84.298	0.165	1.147	642	10

<sup>☆</sup> Accepted in Powder Diffraction File, Published by Dept. of Commerce, ICDD (USA)

**Table 3.3 (c):** X-ray diffraction data<sup>☆</sup> of Ba<sub>2</sub>EuZrO<sub>5.5</sub>

No	2 $\theta$ (deg.)	Width ( deg.)	D ( $\text{\AA}$ )	(hkl)	I / I <sub>0</sub>
1	18.234	0.090	4.861	111	8
2	21.084	0.120	4.210	200	8
3	29.990	0.405	2.977	220	100
4	35.325	0.090	2.538	311	7
5	36.970	0.120	2.430	222	10
6	42.929	0.315	2.105	400	29
7	48.299	0.075	1.882	420	6
8	53.253	0.338	1.718	422	29
9	62.329	0.285	1.488	440	15
10	70.701	0.180	1.331	620	13
11	78.663	0.120	1.215	444	7
12	86.406	0.105	1.125	642	12

<sup>☆</sup> Accepted in Powder Diffraction File, Published by Dept. of Commerce, ICDD (USA)

**Table 3.3 (d):** X-ray diffraction data <sup>☆</sup> of Ba<sub>2</sub>YbZrO<sub>5.5</sub>

No	2θ (deg)	Width ( deg.)	d (Å)	(hkl)	I / I <sub>o</sub>
1	18.284	0.180	4.848	111	4
2	21.142	0.105	4.198	200	7
3	30.070	0.345	2.969	220	100
4	35.424	0.225	2.531	311	5
5	37.054	0.090	2.424	222	10
6	43.051	0.405	2.099	400	30
7	48.438	0.135	1.877	420	6
8	53.400	0.495	1.714	422	30
9	62.516	0.355	1.484	440	10
10	70.921	0.105	1.327	620	15
11	78.916	0.105	1.212	444	8
12	86.697	0.105	1.122	642	15

<sup>☆</sup> Accepted in Powder Diffraction File, Published by Dept. of Commerce, ICDD (USA)

to a structure in which B and B' occupy the same set of positions but in a regular way, the structure is described as a superstructure [9-11]. In the superstructure, the positions occupied by B and B' are no longer equivalent, and this is exhibited in the XRD pattern by the presence of superstructure lines, i.e. the (odd, odd, odd) reflections. This 1:1 ordering in complex perovskites of the type A<sub>2</sub>(BB')O<sub>6</sub> is most probable when there exist a large difference in the valency and ion sizes of B and B' cations which result in a very strong tendency to order through electrostatic

forces [9, 12]. In the case of newly developed  $\text{Ba}_2\text{REZrO}_{5.5}$  ceramics, the difference in valency between RE and Zr are not too large but their ionic sizes differ considerably and in such cases there is always a tendency for ordering after prolonged annealing [9, 12] as observed in the present case. The XRD peaks including the minor ones are indexed for a cubic perovskite structure. The crystal structure diagram of  $\text{Ba}_2\text{REZrO}_{5.5}$  materials is shown in figure 3.5. Though  $\text{Ba}_2\text{REZrO}_{5.5}$  materials have the  $\text{A}_2(\text{BB}')\text{O}_6$  structure, taking into account the

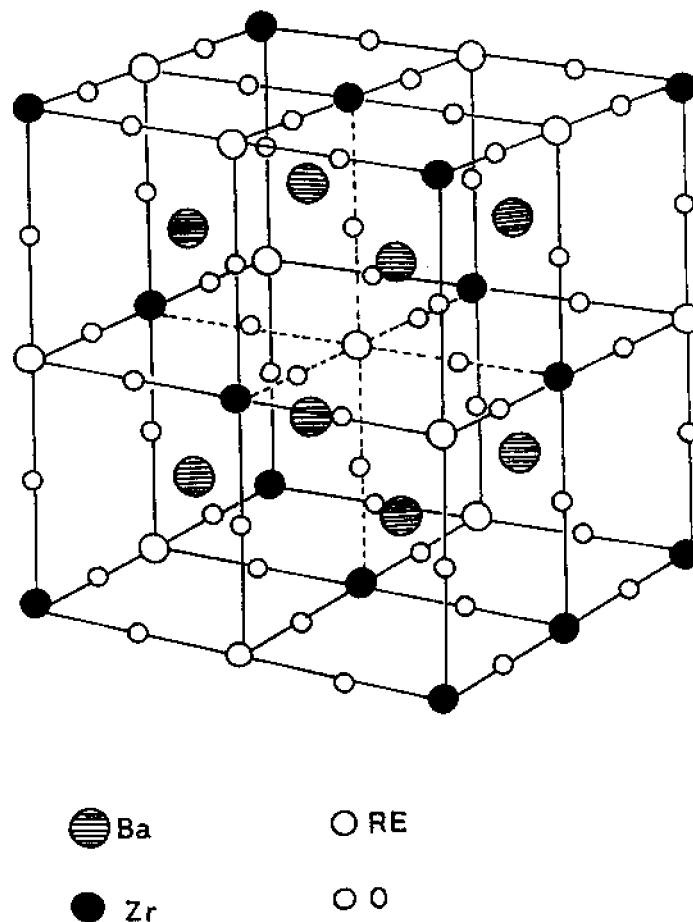


**Figure 3.5:** The Crystal structure diagram of  $\text{Ba}_2\text{REZrO}_{5.5}$

valency of Zr at +4, the chemical formulae of the compounds are written as  $\text{Ba}_2\text{LaZrO}_{5.5}$ ,  $\text{Ba}_2\text{CeZrO}_{5.5}$ ,  $\text{Ba}_2\text{EuZrO}_{5.5}$ , and  $\text{Ba}_2\text{HoZrO}_{5.5}$ . The lattice parameter was determined from the simple least square refinements using all XRD peak positions for  $2\theta$  values from 5 to  $90^\circ$ . The lattice parameter for all the materials are in the range 8.394 - 8.551 Å. The cell volumes were calculated based on the doubling of the basic  $\text{ABO}_3$  unit cell.

The lattice parameters of  $\text{Ba}_2\text{REZrO}_{5.5}$  are also calculated based on a hard sphere approximation using equations,

$$a_A = \frac{4(R_A + R_O)}{\sqrt{2}} \quad (3.2)$$

$$a_B = 2R_B + 2R_{B'} + 4R_O \quad (3.3)$$

$$a_{\text{cal}} = \frac{a_A + a_B}{2} \quad (3.4)$$

where  $R_{A^+}$ ,  $R_B$ ,  $R_{B'}$  and  $R_O$  are the ionic radii of each of the respective cations A, B, B' and anion O.  $a_A$  and  $a_B$  are the calculated lattice parameters based on A and B cations and  $a_{\text{cal}}$  is the calculated lattice parameter. The radii of the ions of the respective co-ordination were obtained from Shannon et al [21, 22] and are given in Table 3.4.  $a_A$ ,  $a_B$  and  $a_{\text{cal}}$ , observed lattice parameters and percentage of deviation between the observed and calculated lattice parameters are given in Table 3.5. The close agreement between the theoretical and observed lattice parameters confirms the structure assigned to  $\text{Ba}_2\text{REZrO}_{5.5}$  ceramics. The good agreement between the bulk density and the theoretical density of  $\text{Ba}_2\text{REZrO}_{5.5}$  ceramic materials in the present study definitely confirm that the  $\text{Ba}_2\text{REZrO}_{5.5}$  ceramics crystallize in  $\text{A}_2(\text{BB}')\text{O}_6$  type complex cubic perovskite crystal structure.

**Table 3.4:** Ionic radii for respective co-ordination and polarizabilities of elements used for the synthesis of  $Ba_2REZrO_{5.5}$  [Shannon, RD, (ref.24, 25, 26)]

Element	Ionic Radii ( $\text{\AA}$ )	Ionic Polarizability ( $\text{\AA}^3$ )
Ba	1.74	6.40
Zr	0.86	3.25
O	1.21	2.01
La	1.20	4.82
Ce	0.90	6.15
Eu	1.09	4.53
Yb	0.998	3.58

**Table 3.5:** Observed lattice parameters, Calculated lattice parameters and the % of deviation between calculated and observed lattice parameters of  $Ba_2REZrO_{5.5}$  ceramics.

Material	$a_{obs}$ ( $\text{\AA}$ )	$A_{cal}$	deviation (%)
$Ba_2LaZrO_{5.5}$	8.394	8.65	2.98
$Ba_2CeZrO_{5.5}$	8.551	8.35	2.3
$Ba_2EuZrO_{5.5}$	8.420	8.54	1.4
$Ba_2YbZrO_{5.5}$	8.395	8.39	-0.05

### 3.5 Synthesis of $Ba_2REZrO_{5.5}$ (RE = Ho and Er):

In the previous sections, the synthesis, sintering and structural characterization of a group of complex perovskite materials with general formula  $Ba_2REZrO_{5.5}$  (RE = La, Ce, Eu and Yb) are described. Attempts were also made to synthesize materials with RE = Ho and Er in the above series through the

conventional solid state reaction method. Figures 3.6 and 3.7 show the XRD patterns of the stoichiometric mixture of  $Ba_2REZrO_{5.5}$  ( $RE = Ho$  or  $Er$ ) heated at different temperatures in the range 1350 to 1650°C for different duration. It is observed that all the diffraction peaks are doublets and the doubling of the peaks

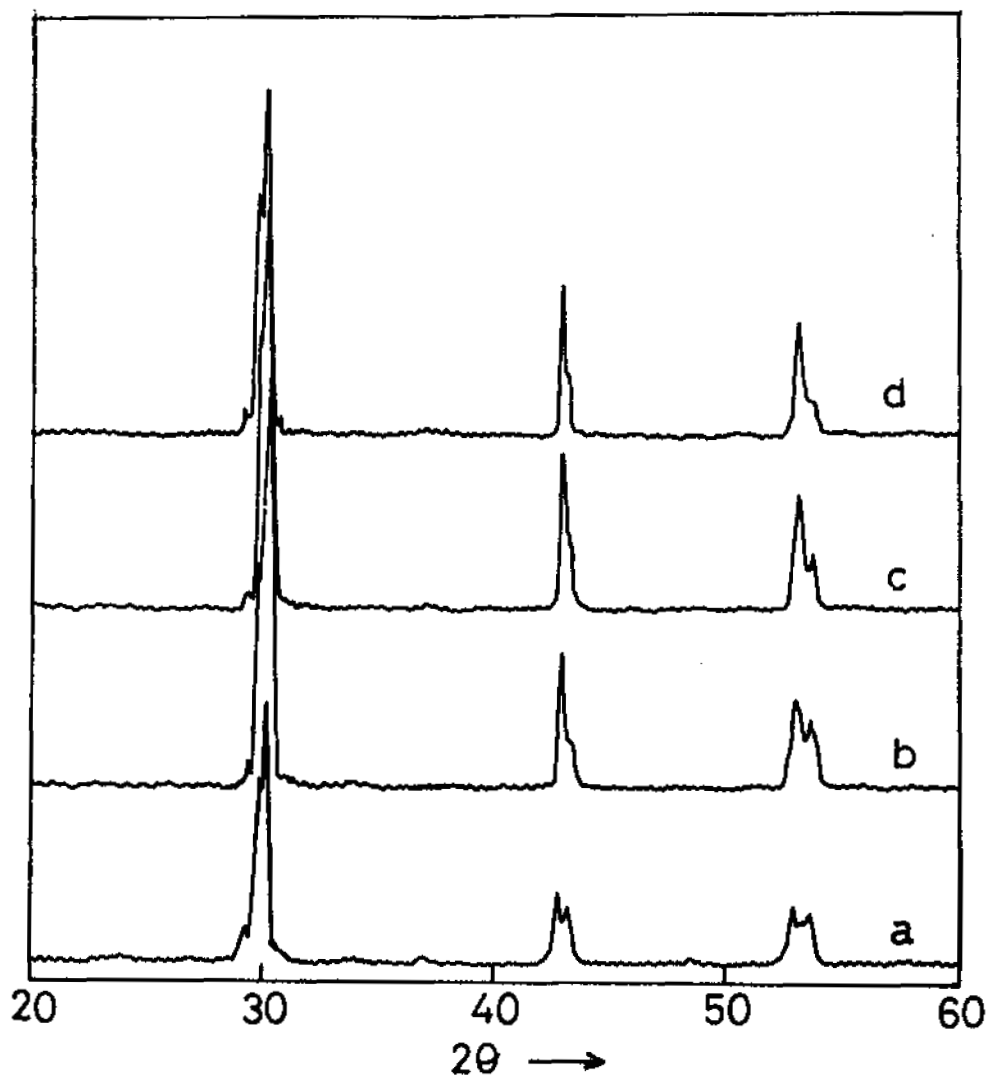


**Figure 3.6.** X-ray diffraction pattern of  $Ba_2HoZrO_{5.5}$  material calcined at (a) 1350°C for 36 h, (b) 1350°C for 72 h, (c) 1450°C for 24 h, (d) 1550°C for 15 h

could not be eliminated by increasing the annealing temperature and time. A close examination of the XRD pattern revealed that the doubling of the peaks in the XRD pattern shown in the figures 3.6 and 3.7 are due to the formation of two stable phases,  $\text{BaZrO}_3$  and  $\text{BaREO}_{2.5}$  (RE = Ho and Er) developed during the annealing process. This was confirmed by synthesizing  $\text{BaZrO}_3$  and  $\text{BaREO}_{2.5}$  (RE = Ho and Er) separately as single-phase materials through solid state reaction and comparing the XRD patterns obtained with Figures 3.6 and 3.7.

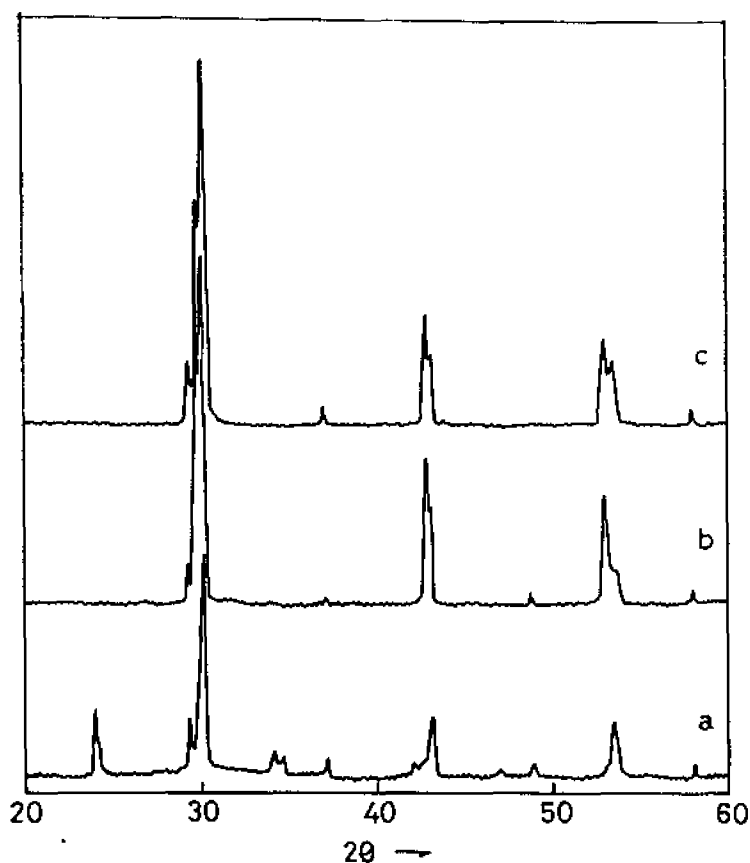


**Figure 3.7:** X-ray diffraction pattern of  $\text{Ba}_2\text{ErZrO}_{5.5}$  material calcined at (a)  $1350^\circ\text{C}$  for 36 h, (b)  $1350^\circ\text{C}$  for 72 h, (c)  $1650^\circ\text{C}$  for 12h

The stoichiometric amounts of high purity (99.9%)  $\text{Ba}(\text{CO})_3$  and  $\text{RE}_2\text{O}_3$  (RE = Ho and Er) were wet mixed in agate mortar with acetone as the wetting medium, dried and calcined in air at  $1350^\circ\text{C}$  for 72h with three intermediate grindings. Similarly,  $\text{BaZrO}_3$  has also been synthesized by the solid state reaction method by calcining the stoichiometric mixture of  $\text{Ba}(\text{CO})_3$  and  $\text{ZrO}_2$  at  $1200^\circ\text{C}$  for 12h [23]. Figure 3.8(a-b) show the XRD patterns of  $\text{BaZrO}_3$  and  $\text{BaHoO}_{2.5}$  respectively. Figure 3.8(c) is the XRD pattern of a mixture of  $\text{BaZrO}_3$  and  $\text{BaHoO}_{2.5}$  taken in 1:1 molar ratio. Figure 3.8(c) is compared with the XRD pattern obtained for the stoichiometric mixture of  $\text{Ba}_2\text{HoZrO}_{5.5}$  heated at  $1650^\circ\text{C}$  for 12h shown in figure 3.8(d).

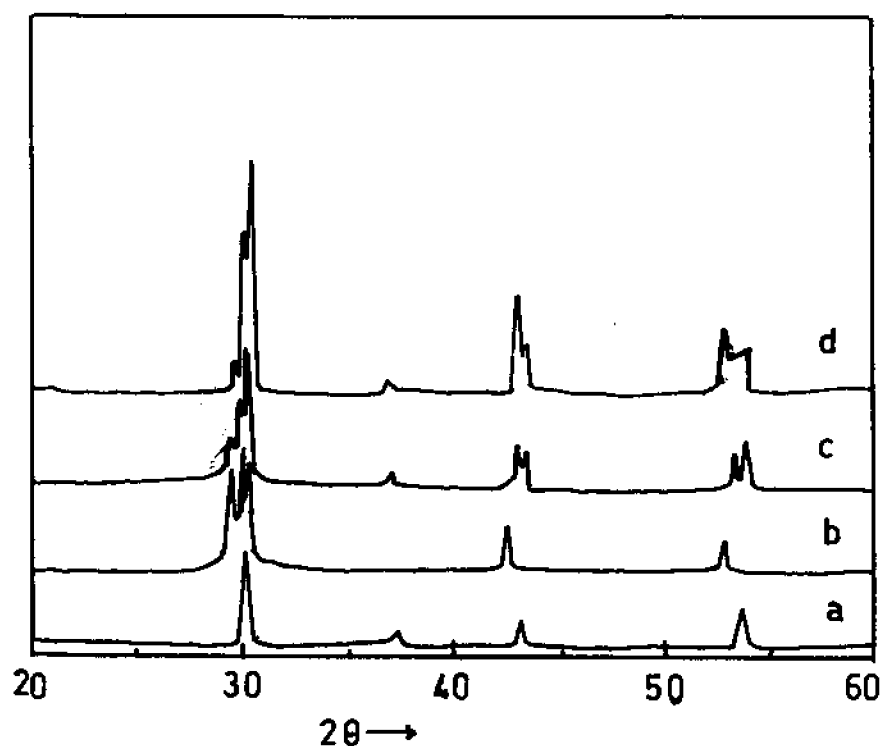


**Figure 3.8:** The XRD pattern of (a)  $\text{BaZrO}_3$ , (b)  $\text{BaHoO}_{2.5}$ , (c) 1:1 molar mixture of  $\text{BaZrO}_3$  and  $\text{BaHoO}_{2.5}$  and (d) stoichiometric amount for the preparation of  $\text{Ba}_2\text{HoZrO}_{5.5}$  heated at  $1650^\circ$  for 15 h.

The XRD patterns given in figures 3.8 (c) and 3.8 (d) are exactly identical showing that the doubling of the peak in the XRD pattern shown in Figure 3.6 can be due to the formation of a mixture consisting of  $\text{BaZrO}_3$  and  $\text{BaHoO}_{2.5}$ . Similarly, figures 3.9(a-c) show the XRD patterns of  $\text{BaZrO}_3$ ,  $\text{BaErO}_{2.5}$  and their 1:1 molar mixture respectively. Figure 3.9(c) is compared with the XRD pattern obtained for the stoichiometric mixture of  $\text{Ba}_2\text{ErZrO}_{5.5}$  heated at  $1650^\circ\text{C}$  for 12h shown in figure 3.9(d). The XRD patterns given in figures 3.9(c) and 3.9(d) are exactly identical which indicates that the doubling of the peak in the XRD pattern shown in figure 3.7 can also be explained as due to the formation of a mixture consisting of  $\text{BaZrO}_3$  and  $\text{BaErO}_{2.5}$ .

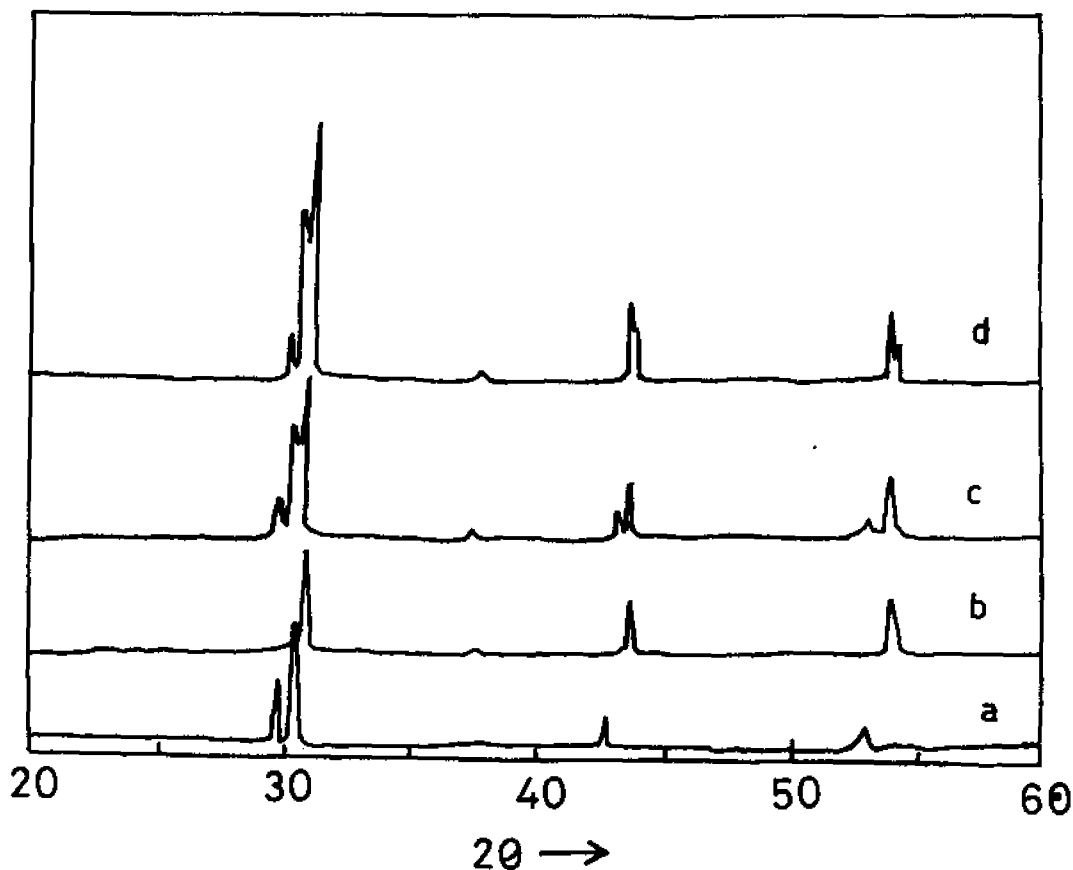


**Figure 3.9:** The XRD pattern of (a)  $\text{BaErO}_{2.5}$ , (b)  $\text{BaZrO}_3$ , (c) 1:1 molar mixture of  $\text{BaZrO}_3$  and  $\text{BaErO}_{2.5}$  and (d) stoichiometric amount for the preparation of  $\text{Ba}_2\text{ErZrO}_{5.5}$  heated at  $1650^\circ$  for 15 h.

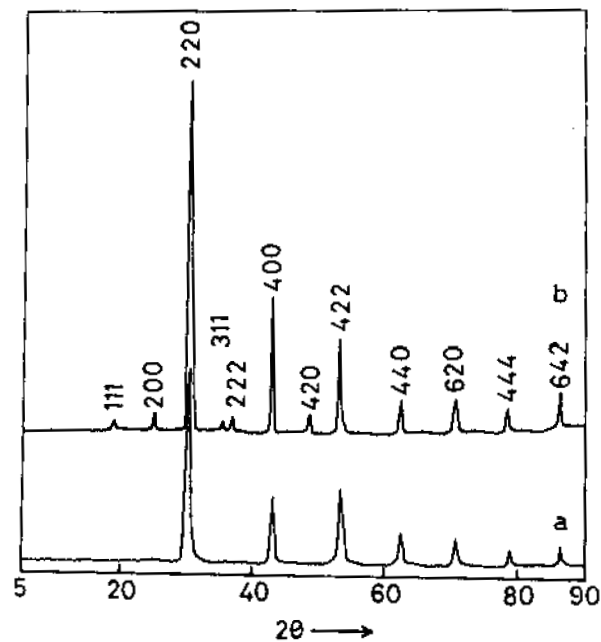


**Figure 3.10:** X-ray diffraction pattern of Ba<sub>2</sub>HoZrO<sub>5.5</sub> material (a) calcined with 1 % CuO as additive and (b) sintered at 1600°C.

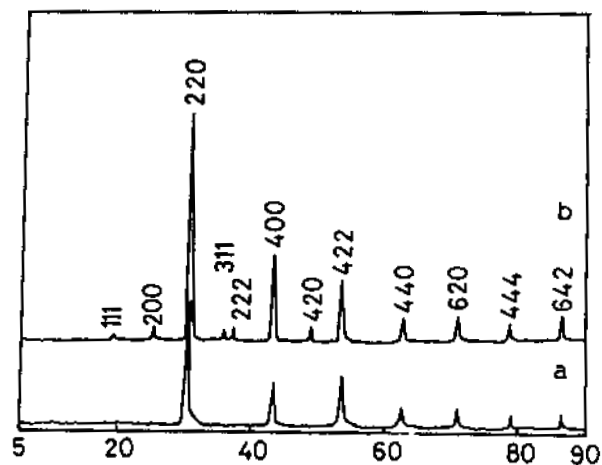


**Figure 3.11:** X-ray diffraction pattern of Ba<sub>2</sub>ErZrO<sub>5.5</sub> material (a) calcined with 1 % CuO as additive and (b) sintered at 1650°C.

As the development of these stable phases prevented the formation of  $\text{Ba}_2\text{HoZrO}_{5.5}$  and  $\text{Ba}_2\text{ErZrO}_{5.5}$  as single-phase materials, it was decided to attempt the liquid phase sintering by the addition of small amount of impurity in the reaction mixture. Addition of small amount of CuO to the reaction mixture was found to have tremendous effect on the phase formation of both  $\text{Ba}_2\text{HoZrO}_{5.5}$  and  $\text{Ba}_2\text{ErZrO}_{5.5}$ . We have added 1 wt % of CuO to the reaction mixture and then thoroughly mixed in an agate mortar for 1 h. The mixed powders were then calcined at 1350 °C for 24 h and then furnace cooled to room temperature. Figure 3.10(a) and 3.11(a) show the XRD patterns of  $\text{Ba}_2\text{HoZrO}_{5.5}$  and  $\text{Ba}_2\text{ErZrO}_{5.5}$  calcined at 1350 °C for 24 h. The XRD patterns clearly shows the formation of  $\text{Ba}_2\text{HoZrO}_{5.5}$  and  $\text{Ba}_2\text{ErZrO}_{5.5}$  as single-phase materials with virtually no secondary phases. For our present case the phase and structure developed during liquid phase sintering can be explained on the basis that CuO melts at a relatively lower temperature and this melt is likely to assist the phase formation of both  $\text{Ba}_2\text{HoZrO}_{5.5}$  and  $\text{Ba}_2\text{ErZrO}_{5.5}$  as single phase materials through a liquid phase assisted reaction mechanism [24].

### 3.6 Sintering and structural studies of $\text{Ba}_2\text{REZrO}_{5.5}$ (RE=Ho and Er)

The  $\text{Ba}_2\text{REZrO}_{5.5}$  (RE = Ho and Er) powders obtained through the addition of CuO as impurity were then ground well and pressed in the form of pellets and these pellets were sintered in the temperature range 1350-1650°C in air for 10 h. The samples were mechanically strong and could be sliced in to thin pieces by a diamond cutter. Good surfaces were obtained by mechanical polishing. The powder x-ray diffraction pattern of sintered  $\text{Ba}_2\text{HoZrO}_{5.5}$  and  $\text{Ba}_2\text{ErZrO}_{5.5}$  for  $2\theta$  between 5 ° and 90 ° are shown in figures 3.10(b) and 3.11(b) and the x-ray diffraction data are given in Table 3.6(a&b).

**Table 3.6 (a):** X-ray diffraction data <sup>☆</sup> of Ba<sub>2</sub>HoZrO<sub>5.5</sub>

No	2θ (deg.)	d (Å)	Width (deg.)	(hkl)	I / I <sub>o</sub>
1	18.217	4.865	0.244	111	2
2	21.065	4.214	0.173	200	4
3	29.960	2.980	0.296	220	100
4	35.299	2.549	0.214	311	3
5	36.916	2.432	0.352	222	5
6	42.888	2.107	0.255	400	35
7	48.252	1.885	0.206	420	13
8	53.120	1.720	0.408	422	30
9	56.706	1.622	0.267	511 / 333	2
10	62.266	1.490	0.535	440	9
11	70.627	1.333	0.497	620	10
12	78.613	1.216	0.459	444	5
13	86.307	1.126	0.704	642	8

<sup>☆</sup> Accepted in Powder Diffraction File, Published by Dept. of Commerce, ICDD (USA)

**Table 3.6(b):** X-ray diffraction data <sup>☆</sup> of Ba<sub>2</sub>ErZrO<sub>5.5</sub>

No	2θ (deg.)	d (Å)	Width (deg.)	(hkl)	I / I <sub>o</sub>
1	18.270	4.852	0.129	111	4
2	21.126	4.202	0.105	200	8
3	30.050	2.971	0.259	220	100
4	35.394	2.534	0.180	311	6
5	36.990	2.426	0.270	222	6
6	42.990	2.101	0.270	400	30
7	48.940	1.879	0.359	420	8
8	53.290	1.715	0.360	422	29
9	56.898	1.617	0.270	511 / 333	3
10	62.380	1.485	0.540	440	11
11	70.860	1.328	0.300	620	9
12	78.870	1.213	0.400	444	4
13	86.640	1.123	0.240	642	8

<sup>☆</sup> Accepted in Powder Diffraction File, Published by Dept. of Commerce, ICDD (USA)

The XRD pattern and the XRD data clearly show that these two materials have the same structure as evident from the similarity in intensity and positions of the lines and are isostructural with other Ba<sub>2</sub>REZrO<sub>5.5</sub> (RE = La, Ce, Eu and Yb) materials. The lattice constant values of these materials were also calculated using equations 3.2, 3.3 and 3.4 and are in good agreement with the experimentally observed values. The processing conditions and structural parameters of the

$\text{Ba}_2\text{REZrO}_{5.5}$  (RE = Ho and Er) materials are summarized in Tables 3.7 and 3.8 respectively.

**Table 3.7:** The Processing parameters of  $\text{Ba}_2\text{HoZrO}_{5.5}$  and  $\text{Ba}_2\text{ErZrO}_{5.5}$  materials

Material	Calcination temperature (°C)	Duration of calcination (h)	Sintering temperature (°C)	Duration of sintering (h)
$\text{Ba}_2\text{HoZrO}_{5.5}$	1350	24	10	1600
$\text{Ba}_2\text{ErZrO}_{5.5}$	1350	24	10	1650

**Table 3.8:** Structural parameters of  $\text{Ba}_2\text{HoZrO}_{5.5}$  and  $\text{Ba}_2\text{ErZrO}_{5.5}$

Parameter	$\text{Ba}_2\text{HoZrO}_{5.5}$	$\text{Ba}_2\text{ErZrO}_{5.5}$
Observed Lattice Parameter (Å)	8.428	8.404
Calculated Lattice parameter (Å)	8.35	8.47
Deviation between observed and calculated (%)	- 0.93	0.83
Theoretical density (g / cc)	6.86	6.63
Sintered density (g / cc)	6.65	6.36
Relative sintered density (%)	97	96
Ionic radii (Å)	0.901	1.021
Ionic polarizability (Å <sup>3</sup> )	3.97	3.81

### 3.6 DTA Studies of $\text{Ba}_2\text{REZrO}_{5.5}$ (RE = La, Ce, Eu, Yb, Ho and Er)

In order to understand whether  $\text{Ba}_2\text{REZrO}_{5.5}$  materials are thermally stable, differential thermal analyses (DTA) have been carried out in the temperature range 30-1300 °C in nitrogen atmosphere. Figure 3.12 shows the DTA trace for a typical  $\text{Ba}_2\text{EuZrO}_{5.5}$  material recorded at a heating rate of 10°C/min. It is obvious from the figure that there is no enthalpy change occurring in the sample as it is heated up to 1300 °C. This observation clearly shows that there is no structural changes taking place in the sample and the materials are thermodynamically stable up to a temperature of 1300 °C.

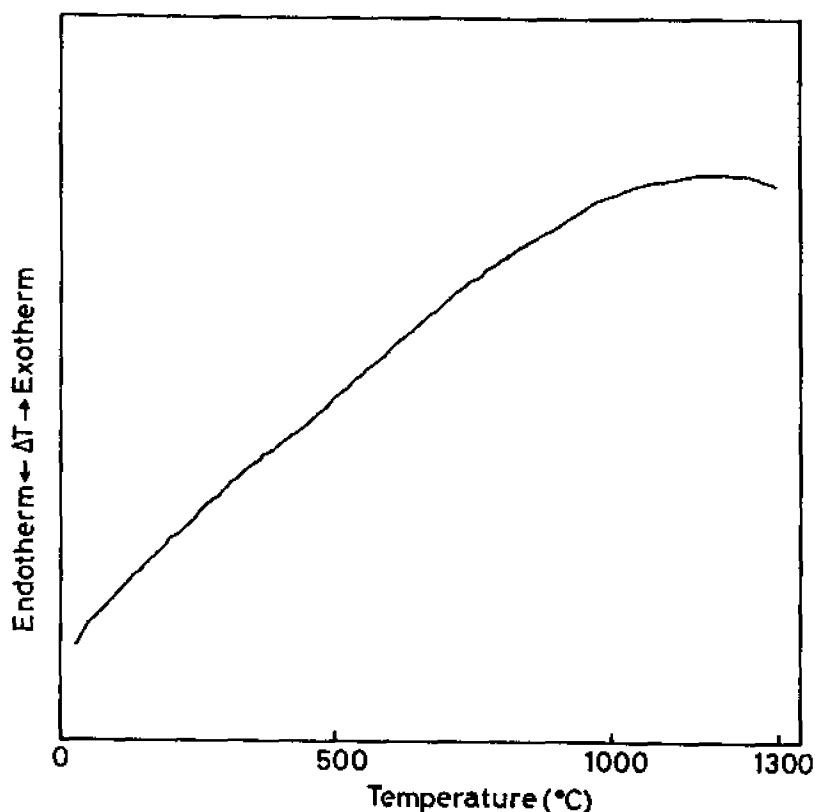


Figure 3.12: DTA trace of  $\text{Ba}_2\text{EuZrO}_{5.5}$

### **3.7 Melting studies of Ba<sub>2</sub>REZrO<sub>5.5</sub> (RE= La, Ce, Eu, Yb, Ho and Er)**

Melting studies were carried out in order to see whether Ba<sub>2</sub>REZrO<sub>5.5</sub> ceramic materials melt congruently and the growth of single crystals from melt is possible. Single phase Ba<sub>2</sub>REZrO<sub>5.5</sub> materials were completely melted using an oxy-hydrogen flame. The melted and subsequently quenched samples were then crushed to fine powder and the structure was studied by powder X-ray diffraction techniques. The XRD patterns of these samples are identical to the sintered sample, which indicate that Ba<sub>2</sub>REZrO<sub>5.5</sub> materials melt congruently and the growth of the single crystal from melt is possible.

### **3.8 Stability studies of Ba<sub>2</sub>REZrO<sub>5.5</sub> (RE = La, Ce, Eu, Yb, Ho and Er)**

The atmospheric stability and resistance to degradation of the Ba<sub>2</sub>REZrO<sub>5.5</sub> ceramics were studied by humidity treatment. Well-sintered samples of Ba<sub>2</sub>REZrO<sub>5.5</sub> were kept in boiling water for 30 minutes. The electrical resistivity and density of the humidity treated specimens measured after drying were the same as those of sintered samples. This clearly revealed that Ba<sub>2</sub>REZrO<sub>5.5</sub> showed high stability and resistance to degradation under atmospheric conditions. The electrical resistivity measurements of Ba<sub>2</sub>REZrO<sub>5.5</sub> samples were carried out using Keithley solid state electrometer model 602. The resistivity of the sintered as well as humidity treated Ba<sub>2</sub>REZrO<sub>5.5</sub> specimens were  $\sim 10^{10}$   $\Omega$  cm at room temperature.

### **3.9 Dielectric studies of Ba<sub>2</sub>REZrO<sub>5.5</sub> (RE = La, Ce, Eu, Yb, Ho and Er)**

The dielectric properties such as dielectric constant ( $\epsilon'$ ) and dielectric loss factor ( $\tan \delta$ ) of the newly synthesized Ba<sub>2</sub>REZrO<sub>5.5</sub> ceramic materials have been

studied in the frequency range 30 Hz to 13 MHz at room temperature and at liquid nitrogen temperature using a complex impedance analyzer (HP 4192, USA). Sintered circular discs of  $\text{Ba}_2\text{REZrO}_{5.5}$  having a diameter of 13 mm and thickness of  $\sim 1$  mm with silver electrodes on both sides were used for dielectric measurements. Figures 3.14 and 3.15 show the variation of dielectric constant and loss factor with frequency at room temperature for  $\text{Ba}_2\text{REZrO}_{5.5}$  materials. The study of the variation of  $\epsilon'$  and  $\tan\delta$  of  $\text{Ba}_2\text{REZrO}_{5.5}$  materials with frequency at liquid nitrogen temperature in the frequency range 13 Hz to 13 MHz showed that there was no substantial change in the value of  $\epsilon'$  of  $\text{Ba}_2\text{REZrO}_{5.5}$  materials. However, the value of  $\tan\delta$  decreased almost by one order and the variation of  $\tan\delta$  with frequency is shown in figure 3.16.

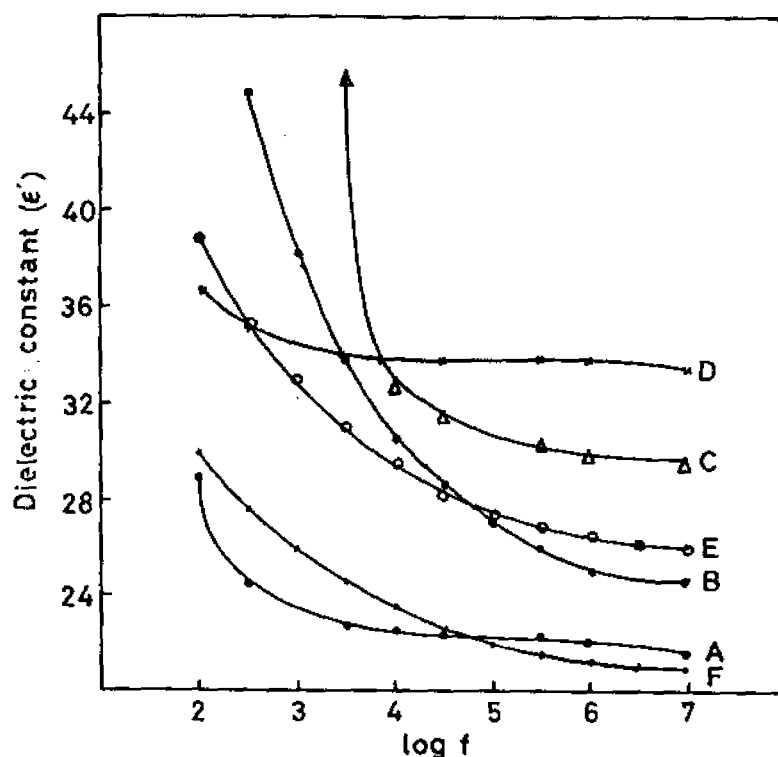


**Figure 14:** Variation of dielectric constant ( $\epsilon'$ ) with frequency for (A) $\text{Ba}_2\text{LaZrO}_{5.5}$ , (B) $\text{Ba}_2\text{CeZrO}_{5.5}$ , (C) $\text{Ba}_2\text{EuZrO}_{5.5}$ , (D) $\text{Ba}_2\text{YbZrO}_{5.5}$ , (E) $\text{Ba}_2\text{HoZrO}_{5.5}$ , (F) $\text{Ba}_2\text{ErZrO}_{5.5}$

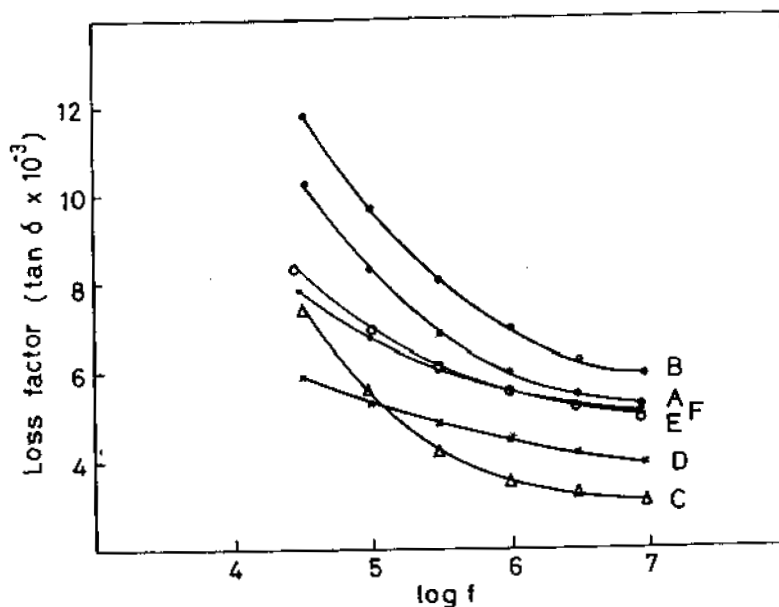


**Figure 15:** Variation of loss factor ( $\tan\delta$ ) with frequency for (A) $\text{Ba}_2\text{LaZrO}_{5.5}$ , (B) $\text{Ba}_2\text{CeZrO}_{5.5}$ , (C) $\text{Ba}_2\text{EuZrO}_{5.5}$ , (D) $\text{Ba}_2\text{YbZrO}_{5.5}$ , (E) $\text{Ba}_2\text{HoZrO}_{5.5}$ , (F) $\text{Ba}_2\text{ErZrO}_{5.5}$  at room temperature

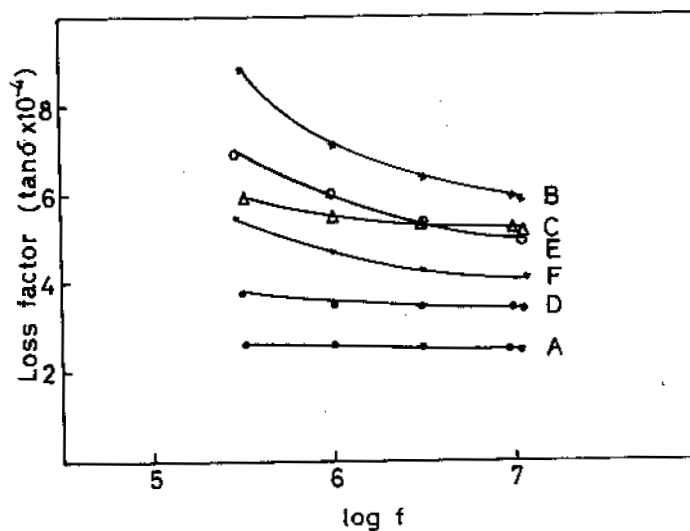


**Figure 15:** Variation of loss factor ( $\tan\delta$ ) with frequency for (A) $\text{Ba}_2\text{LaZrO}_{5.5}$ , (B) $\text{Ba}_2\text{CeZrO}_{5.5}$ , (C) $\text{Ba}_2\text{EuZrO}_{5.5}$ , (D) $\text{Ba}_2\text{YbZrO}_{5.5}$ , (E) $\text{Ba}_2\text{HoZrO}_{5.5}$ , (F) $\text{Ba}_2\text{ErZrO}_{5.5}$  at 77K

The dielectric constants have also been calculated using Clausius-Mossotti equation and dielectric polarizabilities [25].

$$\varepsilon = \frac{3V_m + 8\pi\alpha}{3V_m - 4\pi\alpha} \quad (3.5)$$

where  $V_m$  is the unit cell volume and  $\alpha$  is the total dielectric polarizability. The ionic polarizabilities of the elements under study were obtained from Shannon *et al* and are given in table 3.4. The dielectric constant and loss factor values and total dielectric polarizability and dielectric constant based on the Clausius-Mosotti equation is given in Table 3.9. The dielectric constant values calculated using equation (3.5) agree very well with that observed.

**Table 3.9:** Dielectric constant calculated and measured dielectric loss at 10 MHz and total dielectric polarizability of  $Ba_2REZrO_{5.5}$  ceramics.

Material	Total dielectric polarizabilty	Dielectric constant (calculated)	Dielectric constant (measured at 10 MHz)	Dielectric loss (tan $\delta$ ) at 10MHz	
				Room temp.	77 K
$Ba_2LaZrO_{5.5}$	132.7	29.13	21.37	$5.7 \times 10^{-3}$	$3 \times 10^{-4}$
$Ba_2CeZrO_{5.5}$	133.03	25.64	33.18	$6 \times 10^{-3}$	$4 \times 10^{-4}$
$Ba_2EuZrO_{5.5}$	126.65	24.98	24.98	$3.5 \times 10^{-3}$	$6 \times 10^{-4}$
$Ba_2YbZrO_{5.5}$	124.3	22.57	29.03	$4 \times 10^{-3}$	$3.5 \times 10^{-4}$
$Ba_2HoZrO_{5.5}$	124.4	23.53	23.53	$2.4 \times 10^{-3}$	$5 \times 10^{-4}$
$Ba_2ErZrO_{5.5}$	123.66	21.56	21.62	$5.3 \times 10^{-3}$	$4.1 \times 10^{-4}$

### 3.10 Conclusions

A new group of ceramic oxides with the general formula  $Ba_2REZrO_{5.5}$  (RE= La, Ce, Eu, Yb, Ho and Er) has been synthesized and sintered as single phase materials by solid state reaction method for the first time. The structure of the materials were studied by XRD and found that they are isostructural and have an ordered complex cubic perovskite structure of the general formula  $A_2(BB')O_6$ . The presence of the superstructure lines in the XRD pattern of  $Ba_2REZrO_{5.5}$  indicates the doubling of basic  $ABO_3$  perovskite unit cell. Two materials in this group, viz.,  $Ba_2HoZrO_{5.5}$  and  $Ba_2ErZrO_{5.5}$  could not be synthesized as single-phase materials through solid state reaction method by using only the constituent oxides or carbonates. During high temperature annealing, the development of stable  $BaZrO_3$  and  $BaREO_{2.5}$  (RE = Ho and Er) phases prevented the formation of  $Ba_2REZrO_{5.5}$  (RE = Ho and Er) as a single-phase materials even at  $1650^\circ\text{C}$ . However, an addition of small amount of CuO (1 wt.%) in the reaction mixture has resulted in the formation of an ordered complex perovskite phase during the heating process. The phase and structural development during liquid phase sintering in the present case can be explained on the basis that CuO melts at a relatively lower temperature and this melt is likely to assist the phase formation of both  $Ba_2HoZrO_{5.5}$  and  $Ba_2ErZrO_{5.5}$  as single phase materials through a liquid phase assisted reaction mechanism.

The crystal structure diagram of the  $Ba_2REZrO_{5.5}$  is studied from the XRD pattern. The lattice parameters of  $Ba_2REZrO_{5.5}$  materials measured by x-ray diffraction are in the range 8.394 - 8.551 Å. Based on the proposed crystal structure, the lattice parameters of the  $Ba_2REZrO_{5.5}$  materials were calculated by using a hard sphere approximation and is in good agreement with the values observed experimentally. These new materials are thermally stable and do not undergo any phase transition in the temperature range 30 -  $1300^\circ\text{C}$ . These materials melt congruently making the

single crystal growth from melt possible and are stable under atmospheric conditions. The dielectric constant and loss factor values of these materials are studied at room temperature and liquid nitrogen temperature and are in a range suitable for electronic applications at microwave frequencies. There was no substantial difference in the value of the dielectric constant measured at room temperature and liquid nitrogen temperature, but the dielectric loss decreased almost by one order of magnitude at 77 K. The dielectric constants of the  $\text{Ba}_2\text{REZrO}_{5.5}$  materials were also calculated using the Clausius-Mossotti equation and dielectric polarizabilities of the elements and are in agreement with that measured.

**Reference**

- [1] J. Koshy, J. K. Thomas, J. Kurian, Y. P. Yadava, A. D. Damodaran, *Mater. Lett.*, **17**, (1993) 393.
- [2] J. Koshy, J.K.Thomas, J. Kurian, Y. P. Yadava, A. D. Damodaran, *J. Appl. Phys.*, **73**, (1993) 3402.
- [3] J. Koshy, K.S.Kumar, J.Kurian, Y. P. Yadava, A. D. Damodaran, *Bull. Mater. Sci*, **17**, (1994) 577.
- [4] J. Koshy, J. Kurian, J. K. Thomas, Y. P. Yadava, A. D. Damodaran, *Jpn. J. Appl. Phys.*, **33**, (1994) 117.
- [5] J. Koshy, K. S. Kumar, J. Kurian, Y. P. Yadava, A. D. Damodaran, *J. Am. Ceram. Soc.*, **78**, (1995) 3088.
- [6] J. Koshy, J. Kurian, R. Jose, A. M. John, P. K. Sajith, J. James, S. P. Pai, R. Pinto, *Bull. Mater. Sci*, **22**, (1999) 246.
- [7] K. V. Paulose, M. K. Jayaraj, J. Koshy, A. D. Damodaran, *Solid State Commun.*, **87**, (1993) 147.
- [8] K. V. Paulose, M. T. Sebastian, R. R. Nair, J. Koshy, A. D. Damodaran, *Solid State Commun.*, (1992) 985.
- [9] X. Zhang, Q. Wang, *J. Am. Ceram. Soc.*, **74**, (1991) 2846.
- [10] A. F. Wells, *Structural Inorganic Chemistry*, Clarendon Press, Oxford, UK 1986.
- [11] N. Setter, L. E. Cross, *J. Appl. Phys.*, **51**, (1980) 4356.
- [12] N. Setter, L. E. Cross, *J. Mater. Sci.*, **15**, (1980) 2478.
- [13] P. G. Casado, A. Mendiola, I. rasines, *Z. anorg. allg.chem*, **510**, (1984) 194.
- [14] C. D. Brandle, V. J. Fratello, *J. Mater. Res.*, **5**, (1990) 2160.
- [15] F. Galasso, L. Katz, R. Ward, *J. Am. Ceram. Soc*, **81**, (1959) 820.
- [16] F. Galasso, J. R. Borrante, L. Katz, *J. Am. Ceram. Soc*, **83**, (1961) 2830.
- [17] F. Galasso, W. Darby, *J. Phys. Chem.*, **66**, (1962) 131.

- [18] F. S. Galasso, G. K. Lyden, D. E. Flinchbaugh, *J. Chem. Phys.*, **44**, (1966) 2703.
- [19] P. Groves, *J. Phys. C: Solid State Phys.*, **19**, (1986) 111.
- [20] K. Endo, K. Fujimoto, K. Murakawa, *J. Am. Ceram. Soc.*, **70**, (1987) C215.
- [21] R. D. Shannon, C. T. Prewitt, *Acta Cryst.*, **B 25**, (1969) 925.
- [22] R. D. Shannon, *Acta Cryst.*, **A 32**, (1976) 751.
- [23] J. L. Zhang, J. E. Evetts, *J. Mater. Sci.*, **29**, (1994) 778.
- [24] T. H. Courtney, *Metallurgical Transactions*, **15 A1**, (1984) 1065
- [25] R. D. Shannon, *J. Appl. Phys.*, **73**, (1993) 348.

## CHAPTER IV

### BARIUM RARE-EARTH ZIRCONATES AS NOVEL SUBSTRATE FOR SUPERCONDUCTING $\text{YBa}_2\text{Cu}_3\text{O}_{7-\delta}$ FILMS

#### 4.1 Introduction

The discovery of high temperature superconductivity above liquid nitrogen temperature in  $\text{YBa}_2\text{Cu}_3\text{O}_{7-\delta}$  (YBCO) has led considerable amount of research activities on the preparation of these materials in the form of thick and thin films for device applications [1]. Thick films of high  $T_C$  superconductors are of interest for many applications such as magnetic shielding, substrate wiring, various high-speed microelectronic devices and microwave electronic circuits [2-9]. The particular advantages of thick film route are simplicity, low cost of process and the ability to apply coating on large area and on curved surfaces [2,10-11]. For the preparation of superconducting YBCO thick film different techniques such as screen printing, dip-coating, spin-coating, spray pyrolysis, paint-on-method etc. are used.

In the fabrication of a superconducting film, the selection of a substrate is a crucial factor. One of the most important requirements for the selection of a material as substrate for high temperature superconductors is the chemical non-reactivity between the substrate and the film at the processing temperature. The overriding importance of chemical non-reactivity of the substrate with the film over other substrate requirements has been highlighted in many articles [1,10,12-14]. In addition to the chemical non-reactivity, the substrate should have low dielectric constant and loss factor for their application in microwave devices [10, 12-13]. Also the substrate should have thermal and lattice match with HTSC film and be free from any phase transitions. Perovskite oxides are preferred as substrate

materials because the ceramic superconductors have perovskite structure and therefore a reasonable number of coincidence sites exist between the substrate and the superconductor which enhance epitaxial growth [1]. All the currently available substrates represent some kind of compromise, i.e. they either offer a good lattice match and a high dielectric constant, or a low dielectric constant and a poor lattice match or twinning. Therefore, the search for a suitable and economically viable substrate for high temperature superconductor is an active area of research.

The conventional substrates such as  $\text{Al}_2\text{O}_3$ , Si,  $\text{SiO}_2$ , react with YBCO superconductor at the processing temperature and reduce the transition temperature of the film drastically [5-6,14-19]. Even MgO, the most widely used substrate for YBCO, forms an interlayer of Ba-salt at YBCO-MgO interface if the processing temperature is above  $700^\circ\text{C}$  thereby reducing the transition temperature of the film drastically [5-6,20-22].  $\text{SrTiO}_3$ , though has a good lattice matching with YBCO, its high dielectric constant and loss factor values restricts its use for microwave device applications [1,13,23]. Presently,  $\text{LaAlO}_3$  has become a substrate of choice for the growth of YBCO films. Though  $\text{LaAlO}_3$  has a moderately low dielectric constant and loss factor, it has the disadvantage that it is available only in twinned crystalline form [1,13] and its dielectric constant vary from point to point in a manner that cannot be controlled or predicted [1]. The newly developed materials  $\text{Ba}_2\text{REZrO}_{5.5}$  (RE = La, Ce, Eu, Ho, Er) are found to be potentially suited as substrate for YBCO superconductor\*. This chapter describes chemical reactivity studies between  $\text{Ba}_2\text{REZrO}_{5.5}$  and YBCO superconductor and the development of superconducting YBCO thick films on  $\text{Ba}_2\text{REZrO}_{5.5}$  substrates by dip-coating and melt texturing. The lattice matching of  $\text{Ba}_2\text{REZrO}_{5.5}$  with YBCO is also discussed in this chapter.

#### 4.2 Chemical reactivity between YBCO and Ba<sub>2</sub>REZrO<sub>5.5</sub>

One of the primary concerns about a material to be selected as a substrate for high T<sub>c</sub> superconductor is the chemical non-reactivity between the substrate and the superconductor at the processing temperature. In order to understand whether the newly developed Ba<sub>2</sub>REZrO<sub>5.5</sub> ceramics are chemically non-reacting with YBCO superconductor, a detailed chemical reactivity study have been carried out. The single phase YBCO samples for the present study has been synthesized by the conventional solid state reaction method. Stoichiometric amounts of high purity (99.99%) Y<sub>2</sub>O<sub>3</sub>, BaCO<sub>3</sub> and CuO were weighed in the precise ratio YBa<sub>2</sub>Cu<sub>3</sub>O<sub>7.8</sub> and thoroughly mixed in an agate mortar using acetone as wetting medium. The mixture is then dried in an electric oven at 100°C for 2h and calcined at 930°C for 48 h with two intermediate grindings. The finely ground calcined powder was pressed in the form of circular discs with dimensions of 13 mm diameter and ~ 1.5 mm thickness by applying a pressure of 300 MPa. These discs were sintered in air at 950 °C for 15h and then cooled slowly at the rate of 2°C / min from the sintering temperature to 550 °C for oxygenation. The samples were annealed at this temperature for 24 h and then furnace cooled to room temperature. The phase purity of the sample has been examined by XRD and the superconductivity of the sintered samples was studied by temperature-resistance measurements. The sintered samples were single phase and the pure YBCO samples gave a T<sub>c (0)</sub> of 92 K. The chemical reactivity studies between Ba<sub>2</sub>REZrO<sub>5.5</sub> and YBCO have been performed in two different approaches. The

---

\*Published in *Journal of Materials Research*, 12 (1997) 2976

first is to examine whether there is any structural change taking place in YBCO due to the presence of  $\text{Ba}_2\text{REZrO}_{5.5}$  in the composite and the second is to study the effect of addition of  $\text{Ba}_2\text{REZrO}_{5.5}$  on the superconducting properties of YBCO in the YBCO- $\text{Ba}_2\text{REZrO}_{5.5}$  composite.

#### 4.2.1 The structural studies of the $\text{Ba}_2\text{REZrO}_{5.5}$ -YBCO composites

In the present study, single phase YBCO and  $\text{Ba}_2\text{REZrO}_{5.5}$  powders were mixed in different volume ratio and pressed in the form of circular discs of 10 mm

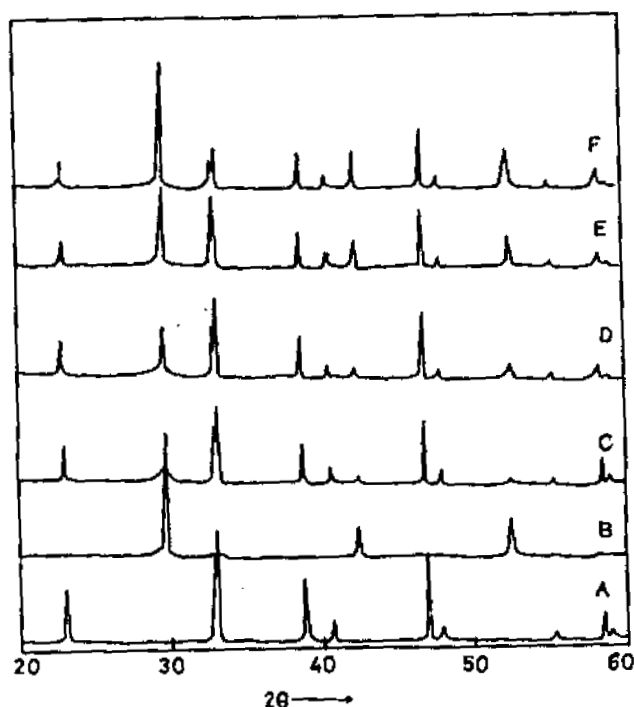
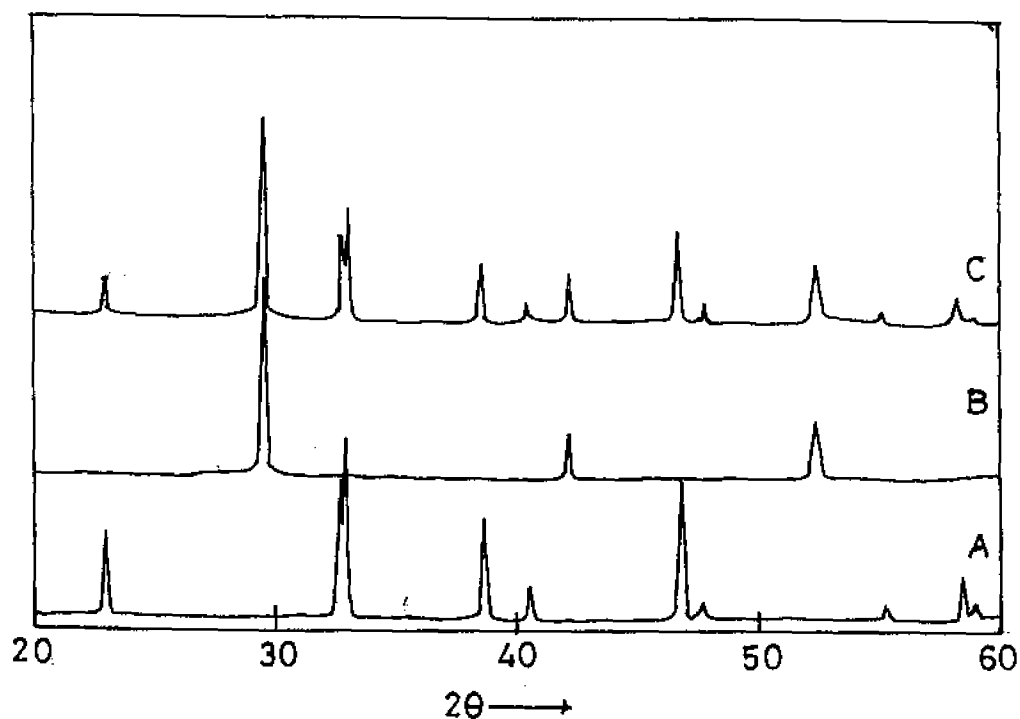


Figure 4.1 (a): X-ray diffraction pattern of (A) pure YBCO, (B) pure  $\text{Ba}_2\text{LaZrO}_{5.5}$ , (C) 10 vol.% of  $\text{Ba}_2\text{LaZrO}_{5.5}$ -YBCO, (D) 20 vol.% of  $\text{Ba}_2\text{LaZrO}_{5.5}$ -YBCO (E) 30 vol.% of  $\text{Ba}_2\text{LaZrO}_{5.5}$ -YBCO and (F) 50 vol.% of  $\text{Ba}_2\text{LaZrO}_{5.5}$ -YBCO composite systems after annealing at  $950^\circ\text{C}$  for 15 h.

diameter and  $\sim 2$  mm thickness. These discs were then annealed at  $950^{\circ}\text{C}$  for 12 h and cooled slowly to room temperature. The structure of the  $\text{Ba}_2\text{REZrO}_{5.5}$ -YBCO composite has been studied by powder XRD. If YBCO reacted with such annealing conditions, additional phases besides YBCO and  $\text{Ba}_2\text{REZrO}_{5.5}$  or change in lattice constant values would be observed in the X-ray diffraction pattern. On the other hand if YBCO does not react with  $\text{Ba}_2\text{REZrO}_{5.5}$  the crystalline phases after annealing will be just two identical phases of YBCO and  $\text{Ba}_2\text{REZrO}_{5.5}$ . Powder XRD patterns of annealed samples of different volume mixture of YBCO and  $\text{Ba}_2\text{REZrO}_{5.5}$  are shown in figures 4.1(a-f). In these figures, the XRD patterns of the two phases in the annealed samples were compared with those of pure



**Figure 4.1 (b):** X-ray diffraction pattern of (A) pure YBCO, (B) pure  $\text{Ba}_2\text{CeZrO}_{5.5}$ , (C) 1:1 volume mixture of  $\text{Ba}_2\text{CeZrO}_{5.5}$ -YBCO annealed at  $950^{\circ}\text{C}$  for 15 h.

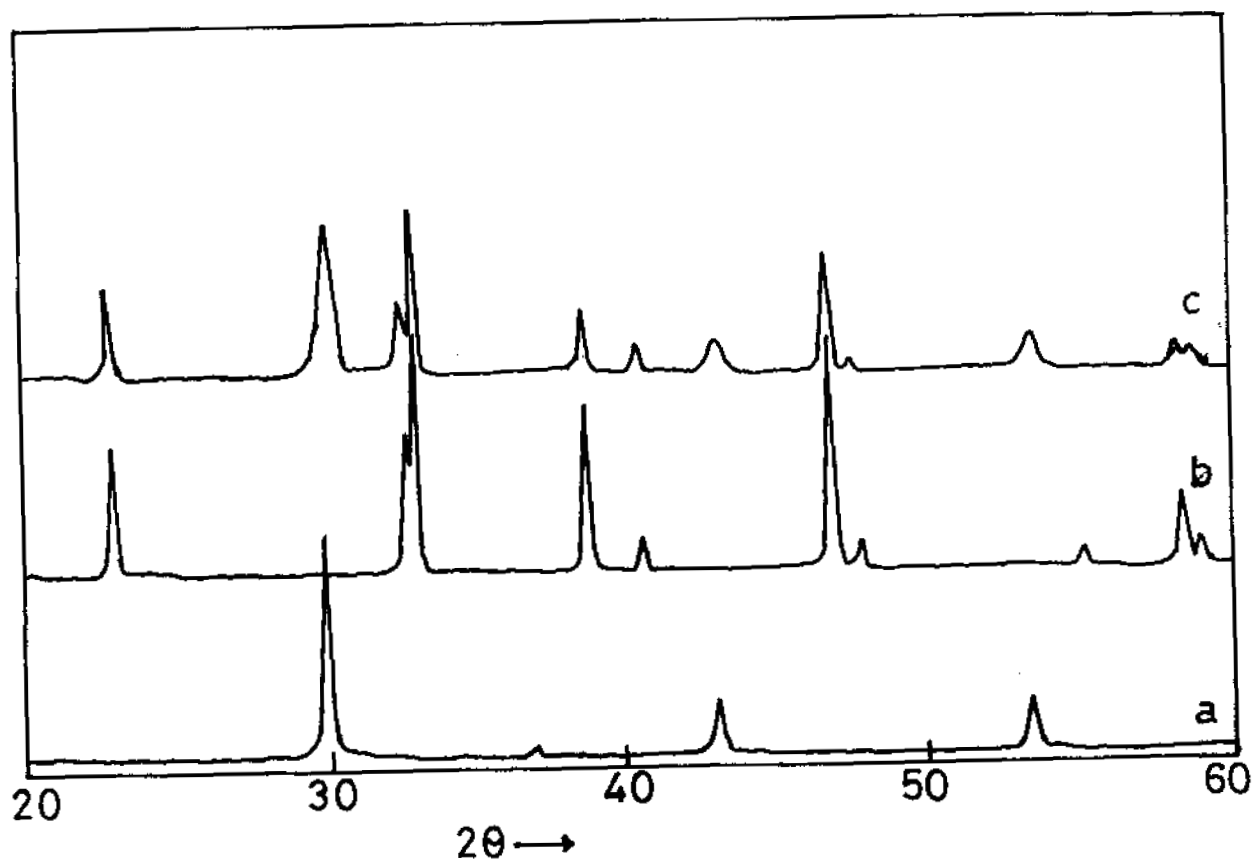
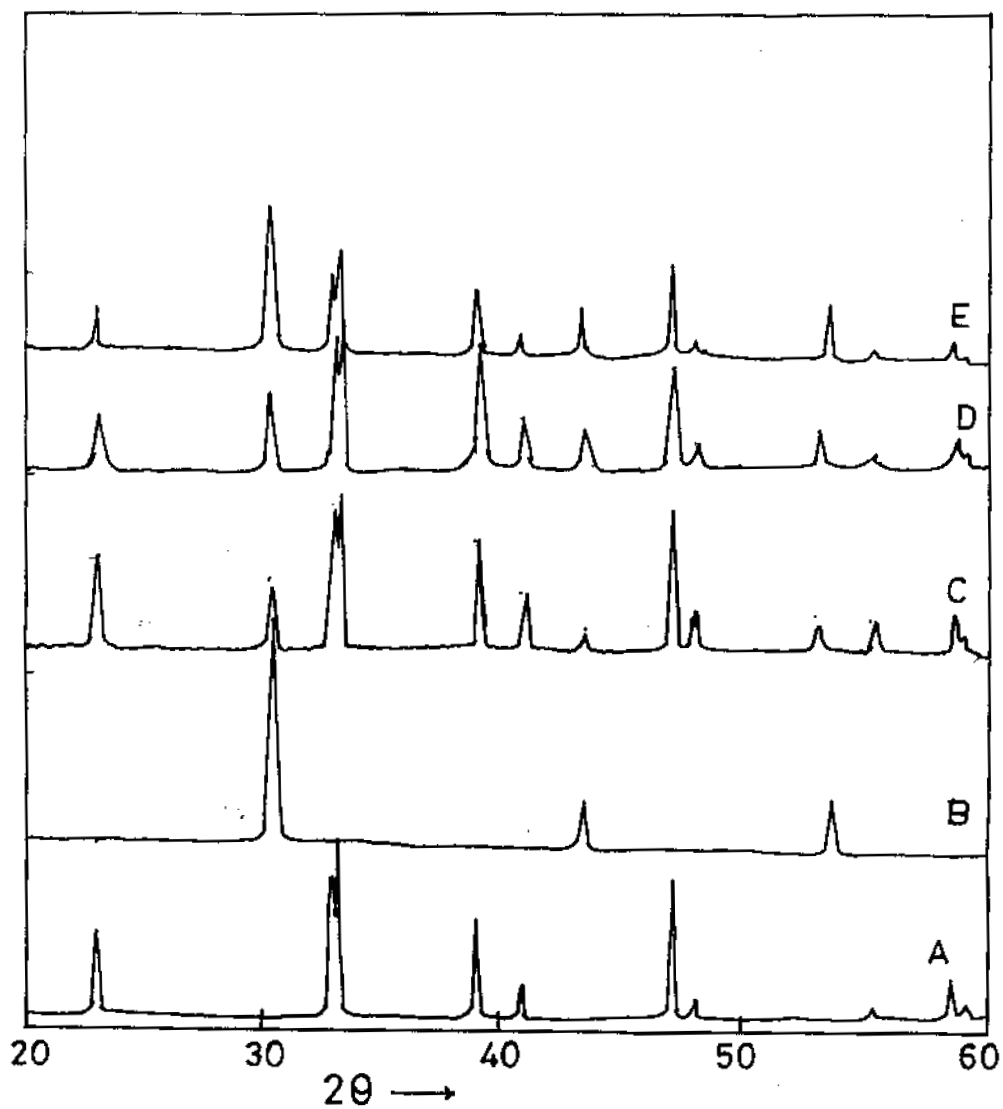
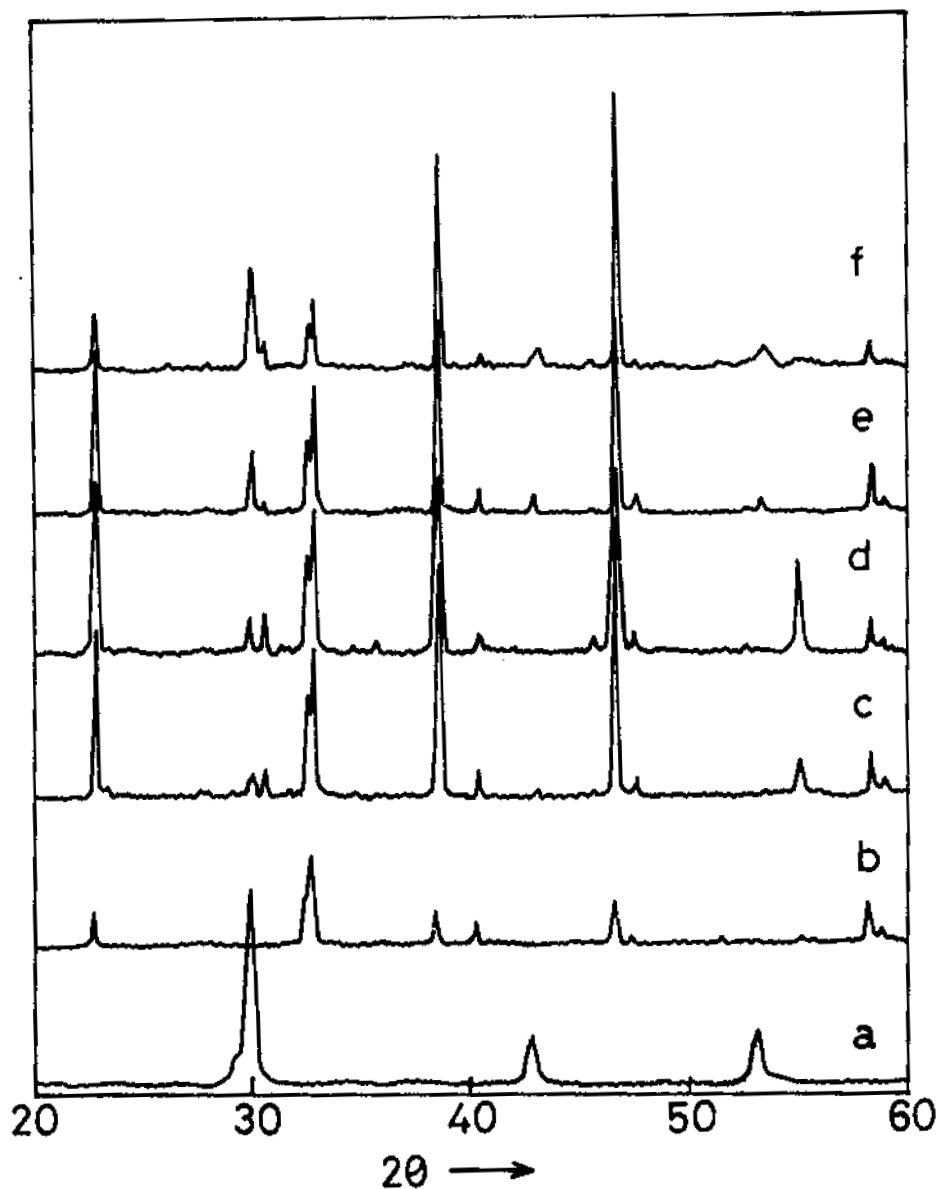


Figure 4.1 (c): X-ray diffraction pattern of (a) pure  $\text{Ba}_2\text{EuZrO}_{5.5}$ , (b) pure YBCO, (c) 1:1 volume mixture of  $\text{Ba}_2\text{EuZrO}_{5.5}$ -YBCO annealed at 950°C for 15 h.

YBCO and pure  $\text{Ba}_2\text{REZrO}_{5.5}$ . It is clear from these figures that there is no new additional phase formed (within the precision of X-ray diffraction technique) besides YBCO and  $\text{Ba}_2\text{REZrO}_{5.5}$  in the YBCO- $\text{Ba}_2\text{REZrO}_{5.5}$  composite. This indicates that there is no detectable chemical reaction taking place between YBCO and  $\text{Ba}_2\text{REZrO}_{5.5}$ .



**Figure 4.1 (d):** X-ray diffraction pattern of (A) pure YBCO, (B) pure  $\text{Ba}_2\text{YbZrO}_{5.5}$ , (C) 10 vol.% of  $\text{Ba}_2\text{YbZrO}_{5.5}$ -YBCO, (D) 20 vol.% of  $\text{Ba}_2\text{YbZrO}_{5.5}$ -YBCO (E) 30 vol.% of  $\text{Ba}_2\text{YbZrO}_{5.5}$ -YBCO and (F) 50 vol.% of  $\text{Ba}_2\text{YbZrO}_{5.5}$ -YBCO composite systems after annealing at  $950^\circ\text{C}$  for 15 h.



**Figure 4.1 (e):** X-ray diffraction pattern of (a) pure  $\text{Ba}_2\text{HoZrO}_{5.5}$  (b) pure YBCO (c) 10 vol.% of  $\text{Ba}_2\text{HoZrO}_{5.5}$ -YBCO, (d) 20 vol.% of  $\text{Ba}_2\text{HoZrO}_{5.5}$ -YBCO (e) 30 vol.% of  $\text{Ba}_2\text{HoZrO}_{5.5}$ -YBCO and (f) 50 vol.% of  $\text{Ba}_2\text{HoZrO}_{5.5}$ -YBCO composite systems after annealing at  $950^\circ\text{C}$  for 15 h.

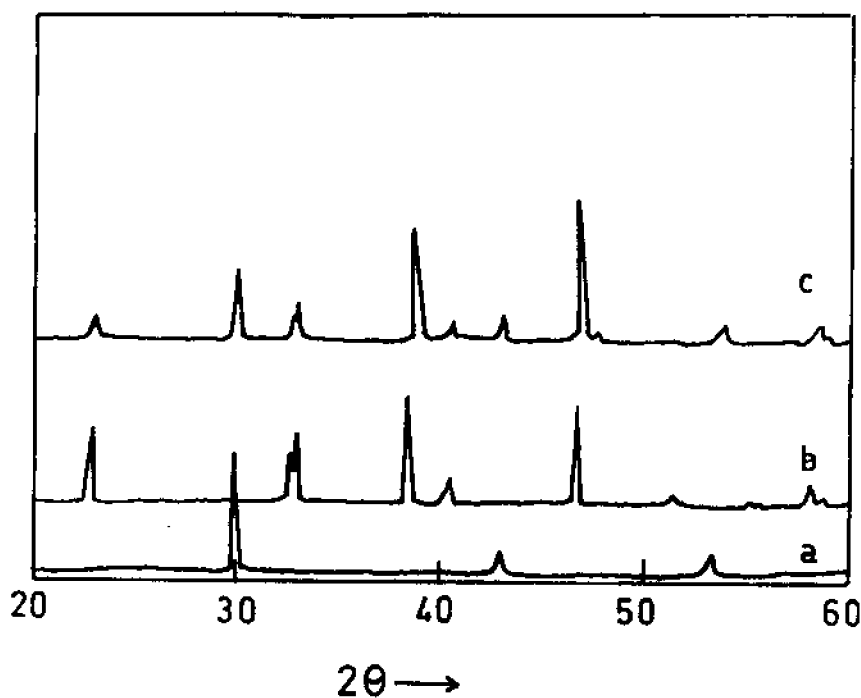


**Figure 4.1 (f):** X-ray diffraction pattern of (a) pure  $\text{Ba}_2\text{ErZrO}_{5.5}$ , (b) pure YBCO, (c) 1:1 volume mixture of  $\text{Ba}_2\text{ErZrO}_{5.5}$ -YBCO annealed at  $950^\circ\text{C}$  for 15 h.

#### 4.2.2 The superconducting properties of $\text{Ba}_2\text{REZrO}_{5.5}$ -YBCO composite

The effect of  $\text{Ba}_2\text{REZrO}_{5.5}$  addition on the superconducting properties of YBCO was studied by temperature-resistance measurements. Superconducting YBCO and  $\text{Ba}_2\text{REZrO}_{5.5}$  were mixed in different volume ratio and pressed in the form of pellets at a pressure of 250 MPa. These discs were sintered at  $950^\circ\text{C}$  for 12 h and then slow cooled at the rate of  $2^\circ\text{C}/\text{min}$  to  $550^\circ\text{C}$ . The samples were then oxygenated at this temperature for 24 h and then furnace cooled to room temperature. The resistance measurements of the composites were made by standard four-probe technique

using a nanovoltmeter (model 181, Kiethley Instruments, Cleveland, OH) and a current source (model 220, Kiethley). The temperature of the sample was measured by a calibrated copper Constantine thermocouple calibrated with an RF 800 rhodium-iron resistance sensor with an accuracy of  $\pm 0.2\text{K}$ . Figures 2(a-f) show the resistivity versus temperature curves for the YBCO- $\text{Ba}_2\text{REZrO}_{5.5}$  composites containing different vol.% of  $\text{Ba}_2\text{REZrO}_{5.5}$  annealed at  $950^\circ\text{C}$  for 12 h. A superconducting transition of  $\sim 92\text{ K}$  in all these composites indicate that a substantial addition of  $\text{Ba}_2\text{REZrO}_{5.5}$  in YBCO did not have any detrimental effect on the superconducting transition temperature of YBCO even after severe heat treatment.

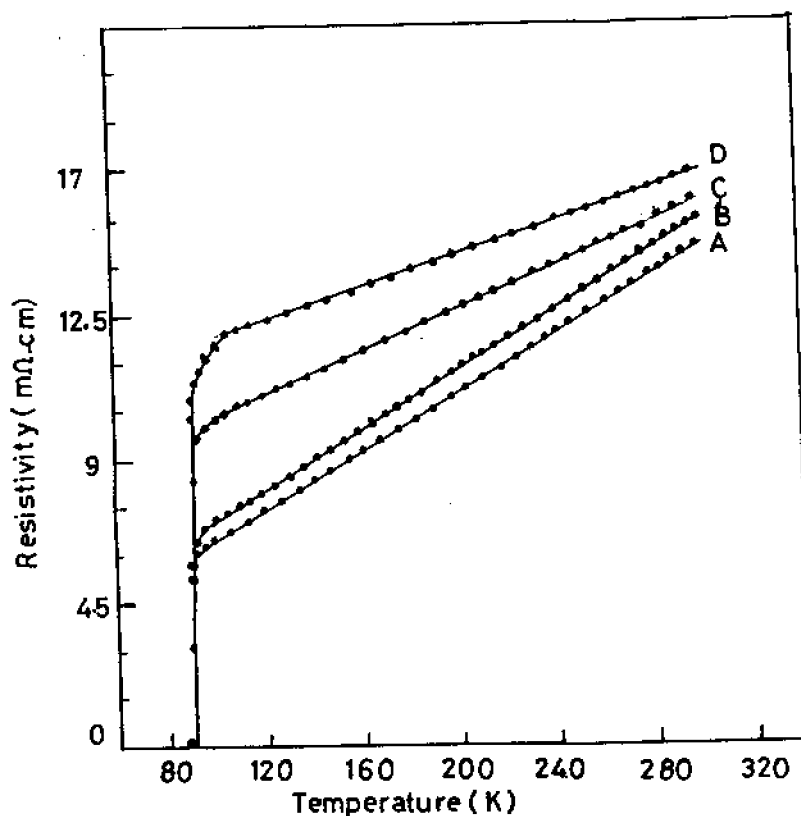


**Figure 4.2(a):** The electrical resistivity vs. temperature curves for composites containing (A) 10 vol.% of  $\text{Ba}_2\text{LaZrO}_{5.5}$ -YBCO, (B) 20 vol.% of  $\text{Ba}_2\text{LaZrO}_{5.5}$ -YBCO (C) 30 vol.% of  $\text{Ba}_2\text{LaZrO}_{5.5}$ -YBCO and (D) 40 vol.% of  $\text{Ba}_2\text{LaZrO}_{5.5}$ -YBCO.

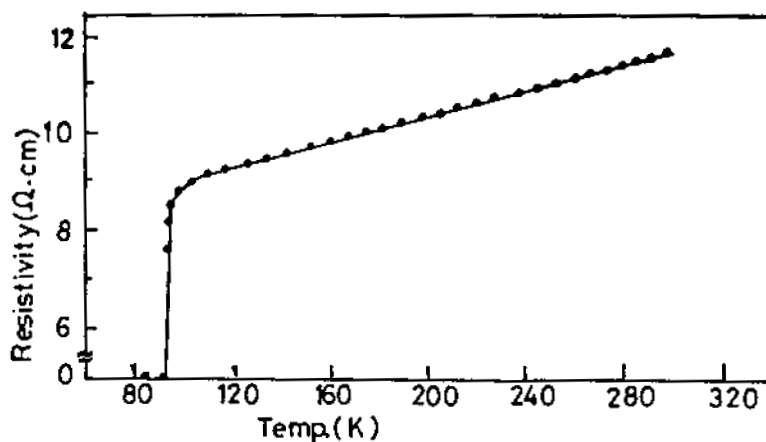


Figure 4.2 (b): Temperature-Resistivity curve of composite containing 20 vol.% of  $\text{Ba}_2\text{CeZrO}_{5.5}$  and 80 vol.% of YBCO

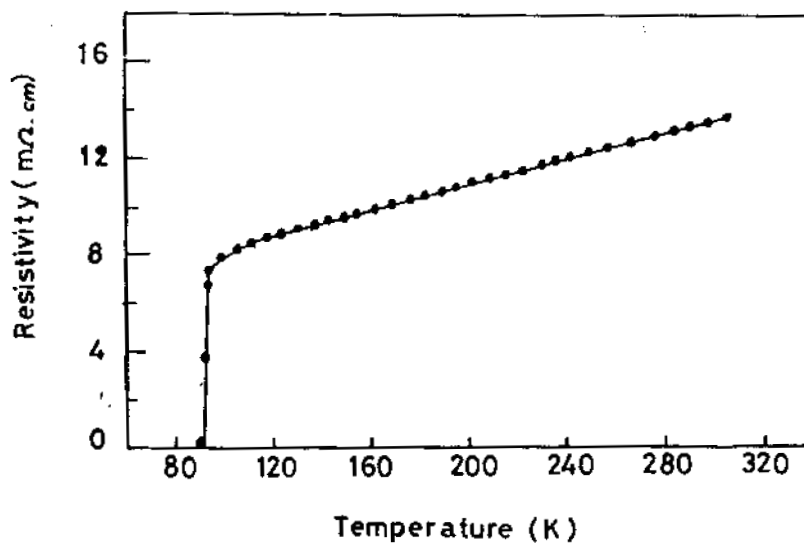


Figure 4.2 (c): Temperature-Resistivity curve of composite containing 20 vol.% of  $\text{Ba}_2\text{EuZrO}_{5.5}$  and 80 vol.% of YBCO

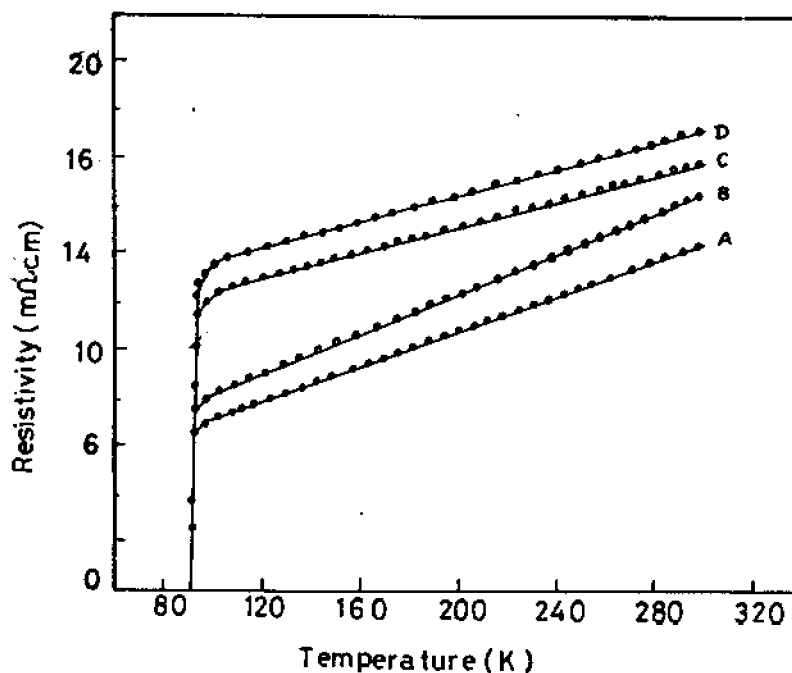


Figure 4.2(d): The electrical resistivity vs. temperature curves for composites containing (A) 10 vol.% of  $\text{Ba}_2\text{YbZrO}_{5.5}$ -YBCO, (B) 20 vol.% of  $\text{Ba}_2\text{YbZrO}_{5.5}$ -YBCO (C) 30 vol.% of  $\text{Ba}_2\text{YbZrO}_{5.5}$ -YBCO and (D) 40 vol.% of  $\text{Ba}_2\text{YbZrO}_{5.5}$ -YBCO.

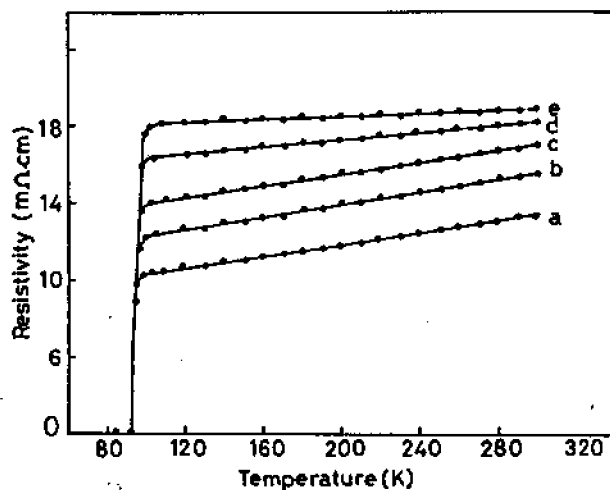


Figure 4.2 (e): The electrical resistivity vs. temperature curves YBCO (c) 10 vol.% of  $\text{Ba}_2\text{HoZrO}_{5.5}$ -YBCO, (d) 20 vol.% of  $\text{Ba}_2\text{HoZrO}_{5.5}$ -YBCO (e) 30 vol.% of  $\text{Ba}_2\text{HoZrO}_{5.5}$ -YBCO and (f) 40 vol.% of  $\text{Ba}_2\text{HoZrO}_{5.5}$ -YBCO (f) 50 vol.% of  $\text{Ba}_2\text{HoZrO}_{5.5}$ -YBCO composite systems.

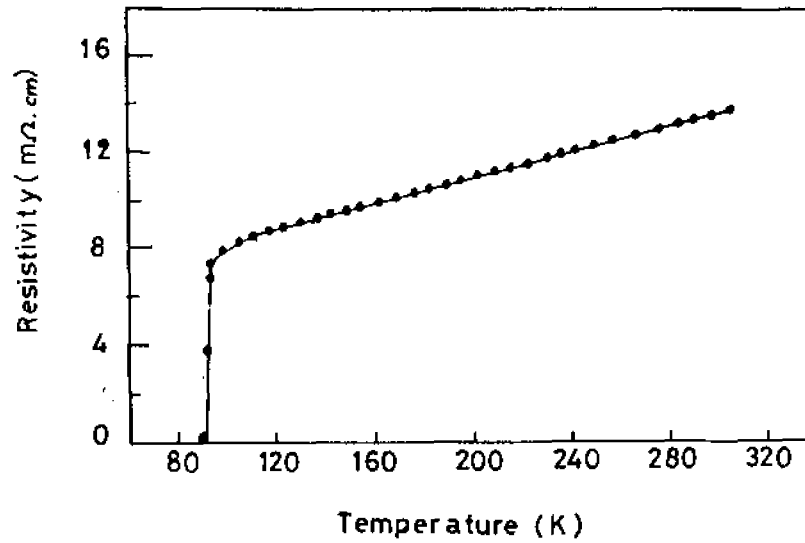


Figure 4.3 (c): Temperature-Resistivity curve of composite containing 20 vol.% of  $\text{Ba}_2\text{ErZrO}_{5.5}$  and 80 vol.% of YBCO

#### 4.3 The Lattice matching of $\text{Ba}_2\text{REZrO}_{5.5}$ with YBCO

Another important criteria for the selection of a material as a substrate for the epitaxial growth is the matching of lattice constant between the substrate and the material to be grown on the top of it. It was reported that for any material to be grown as an epitaxial layer on a substrate the minimum lattice mismatch between the substrate material and the overgrown film is about 15 % [24]. The lattice mismatch is given by

$$\varepsilon = \frac{a-b}{a} \quad (4.1)$$

where 'a' and 'b' are the in plane lattice constant of the substrate and the overgrown material. The crystalline structure of superconducting YBCO is of orthorhombic type symmetry with  $a = 3.82 \text{ \AA}$ ,  $b = 3.88 \text{ \AA}$ , and  $c = 11.68 \text{ \AA}$  [25]. The lattice mismatch between the newly developed  $\text{Ba}_2\text{REZrO}_{5.5}$  material and YBCO in the a-b plane was calculated using equation (4.1) with  $a = (a/2)$  taking

the doubling of the basic perovskite unit cell in  $\text{Ba}_2\text{REZrO}_{5.5}$  material in to account and are given in Table 4.1.

**Table 4.1 : Lattice mismatch between  $\text{Ba}_2\text{REZrO}_{5.5}$  and YBCO**

Material	Lattice constant (Å)	$\Delta a / a$ (%)	$\Delta b / a$ (%)
$\text{Ba}_2\text{LaZrO}_{5.5}$	8.394	8.9	7.5
$\text{Ba}_2\text{CeZrO}_{5.5}$	8.550	10.6	9.2
$\text{Ba}_2\text{EuZrO}_{5.5}$	8.420	9.3	7.8
$\text{Ba}_2\text{YbZrO}_{5.5}$	8.395	8.9	7.5
$\text{Ba}_2\text{HoZrO}_{5.5}$	8.428	9.3	7.9
$\text{Ba}_2\text{ErZrO}_{5.5}$	8.404	9	7.7

It is clear from Table 4.1 that the lattice match between  $\text{Ba}_2\text{REZrO}_{5.5}$  and YBCO is within the tolerable limit for epitaxial growth and is in a range comparable to that of MgO (4.208 Å) which is extensively used as substrate for epitaxial films of YBCO.

#### 4.4 Preparation of YBCO thick films on $\text{Ba}_2\text{REZrO}_{5.5}$

The suitability of  $\text{Ba}_2\text{REZrO}_{5.5}$  as substrates for high  $T_c$  YBCO superconducting films has been confirmed by developing YBCO films on  $\text{Ba}_2\text{REZrO}_{5.5}$  substrates by dip-coating and melt texturing. The YBCO suspension for dip-coating was prepared by thoroughly mixing fine superconducting YBCO powder with isopropyl alcohol or n-butanol and the viscosity of the suspension was controlled by the addition of commercially available fish oil. The polished and cleaned  $\text{Ba}_2\text{REZrO}_{5.5}$  substrates were then dipped in the YBCO suspension and

then dried. This step was repeated until a required thickness is attained. The dip-coated films were then dried in an oven to avoid organic dispersants and subjected to controlled heat treatments.

As mentioned earlier, for the successful fabrication of superconducting YBCO thick film, optimization and close control of heat treatment conditions are essential. In the present study, for the preparation of YBCO thick films on  $\text{Ba}_2\text{REZrO}_{5.5}$ , the following optimized processing conditions are developed. The dried dip-coated films were heated in a programmable furnace at the rate of  $5^\circ\text{C}/\text{min}$  in air up to  $1000^\circ\text{C}$  and kept at this temperature for 2 min. The films were cooled from  $1000^\circ\text{C}$  at a rate of  $2^\circ\text{C}/\text{min}$  up to  $950^\circ\text{C}$  and were annealed at  $950^\circ\text{C}$  for 2 to 3 h. The films were then slow cooled at the rate of  $1^\circ\text{C}/\text{min}$  to room temperature. The diagrammatic representation of heating and cooling schedule adopted for the preparation of YBCO thick films on  $\text{Ba}_2\text{REZrO}_{5.5}$  is shown in figure 4. 3. The heating of YBCO films up to the partial melting temperature of YBCO ( $1000^\circ\text{C}$ ) was necessary to obtain good adhesion between the substrate and the film and also for obtaining highly textured films with smooth surfaces. The slow cooling procedure adopted was essential to facilitate oxygenation. Also it has been found that annealing temperature close to the melting point of YBCO and relatively short annealing time enhanced the c-axis orientation of the YBCO film. The surface of the dip-coated and melt-textured film looked black and the peel off test carried out using an adhesive tape showed that the films on  $\text{Ba}_2\text{REZrO}_{5.5}$  had good adhesion to the film.

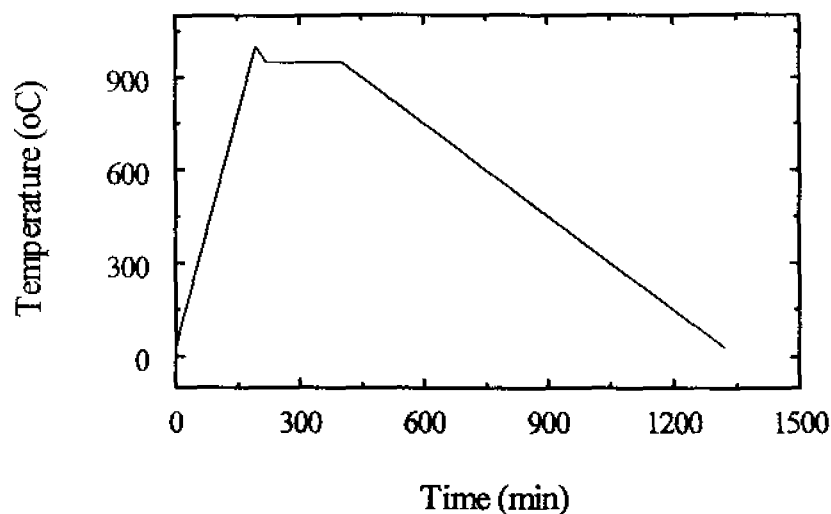


**Figure 4.3:** The heating schedule adopted for the preparation of YBCO thick films

#### 4.5 Characterization of the YBCO thick films

The structure of the YBCO films dip-coated and melt textured on  $\text{Ba}_2\text{REZrO}_{5.5}$  substrate were studied by x-ray diffraction and the superconductivity of the films were studied by temperature-resistance and critical current density measurements.

Figures 4.4 (a-d) show the XRD patterns of YBCO films dip-coated on  $\text{Ba}_2\text{REZrO}_{5.5}$  substrates. Except for the characteristic peaks of  $\text{Ba}_2\text{REZrO}_{5.5}$  all the other peaks in figs. 4.4 (a-d) are those of orthorhombic YBCO. The absence of any other peaks other than those of  $\text{Ba}_2\text{REZrO}_{5.5}$  and YBCO indicate that there is no detectable chemical reaction between  $\text{Ba}_2\text{REZrO}_{5.5}$  and YBCO even at the partial melting temperature of YBCO.

The superconductivity of the YBCO thick films developed prepared on  $\text{Ba}_2\text{REZrO}_{5.5}$  was studied by standard four-probe technique. A Kiethley current

source model 220 and Keithley nanovoltmeter model 181 was used for resistance measurements. The temperature of the films was measured by a copper-Constantine thermocouple with an accuracy of  $\pm 0.2$  K. Figs 4. 5 (a-d) show the temperature-resistance curves for dip-coated YBCO films on  $\text{Ba}_2\text{REZrO}_{5.5}$  substrates. The films showed metallic behavior in the normal state and gave a zero resistivity transition of 92 K with transition width ( $\Delta T$ ) of  $\sim 2$  K. The critical current density ( $J_C$ ) of the film under zero applied magnetic field were  $\sim 10^4$  A/cm<sup>2</sup>. The values of  $T_C$ ,  $J_C$  and  $\Delta T$  obtained for YBCO thick films on  $\text{Ba}_2\text{REZrO}_{5.5}$  substrates are summarized in Table 4.2. These results clearly confirm that the newly developed  $\text{Ba}_2\text{REZrO}_{5.5}$  materials are potentially suited for their application as substrates for superconducting YBCO films for various device applications.

**Table 4.2:** The superconducting transition temperature ( $T_C$ ), transition width ( $\Delta T$ ) and critical current density at 77 K for YBCO films on  $\text{Ba}_2\text{REZrO}_{5.5}$  substrates

Substrate	$T_C$ (0) (K)	$\Delta T$ (K)	$J_C$ (A/cm <sup>2</sup> )
$\text{Ba}_2\text{LaZrO}_{5.5}$	92	2.0	$1.1 \times 10^4$
$\text{Ba}_2\text{EuZrO}_{5.5}$	92	1.9	$5.4 \times 10^4$
$\text{Ba}_2\text{YbZrO}_{5.5}$	92	2.1	$3.2 \times 10^3$
$\text{Ba}_2\text{HoZrO}_{5.5}$	92	2.0	$3.7 \times 10^4$

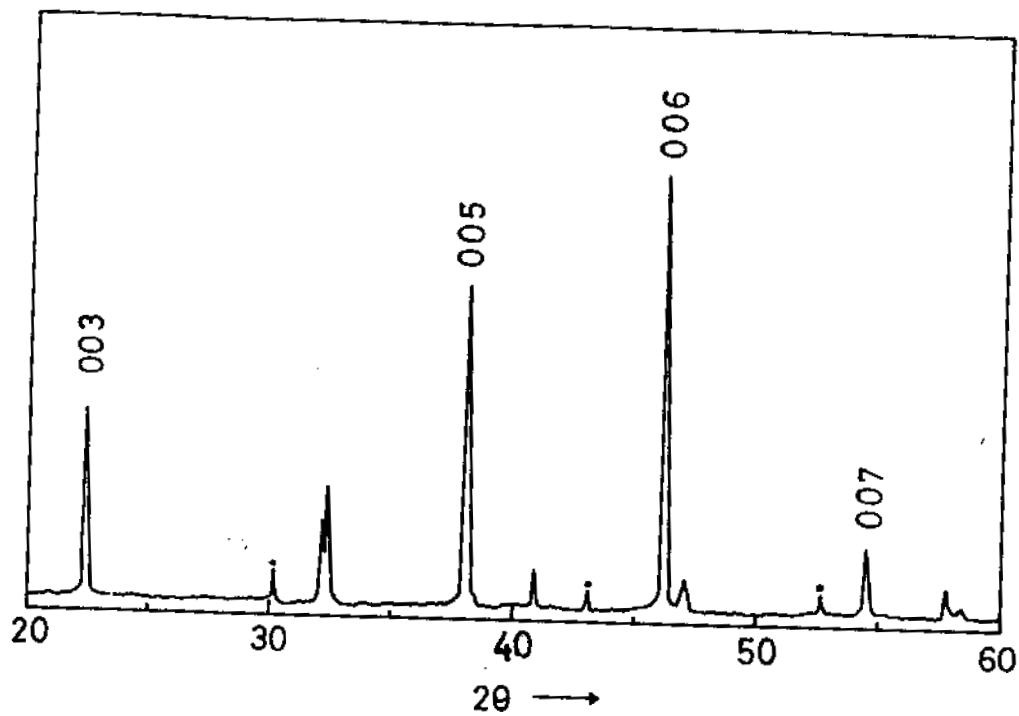


Figure 4.4 (a): XRD pattern of dip-coated YBCO film on  $\text{Ba}_2\text{LaZrO}_{5.5}$  substrate

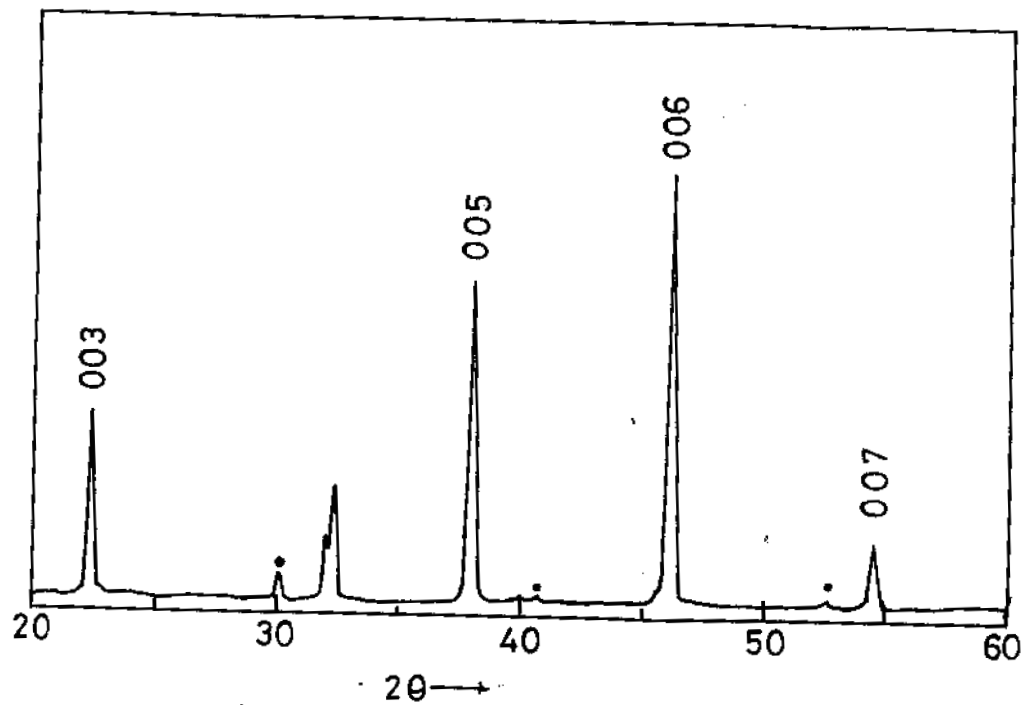


Figure 4.4 (b): XRD pattern of dip-coated YBCO film on  $\text{Ba}_2\text{EuZrO}_{5.5}$  substrate

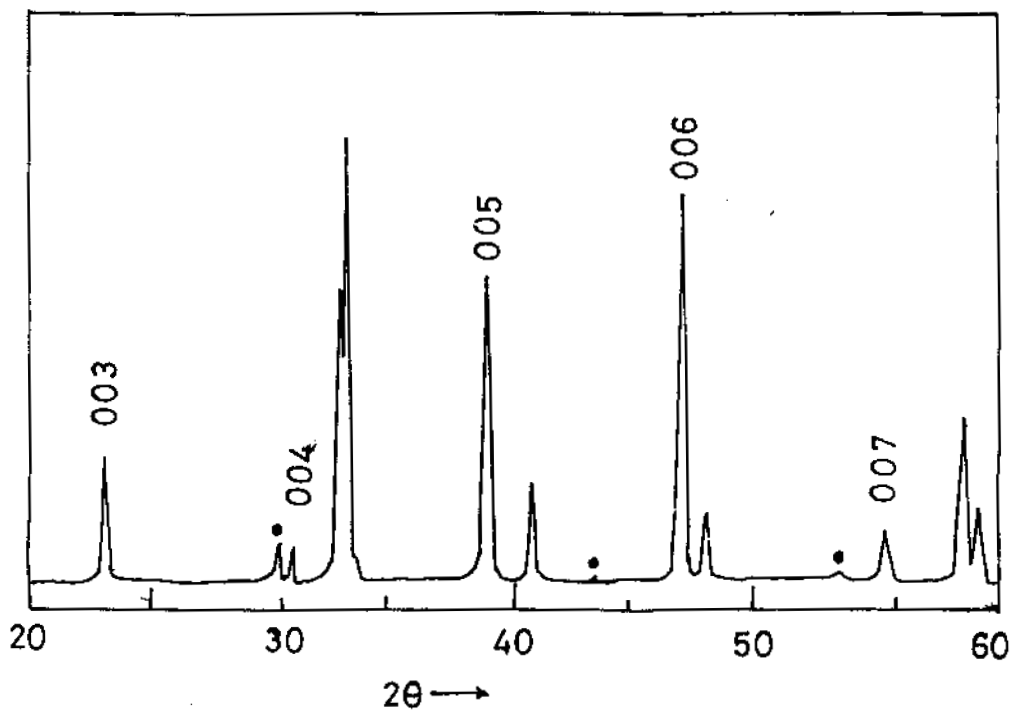


Figure 4.4 (c): XRD pattern of dip-coated YBCO film on Ba<sub>2</sub>YbZrO<sub>5.5</sub> substrate

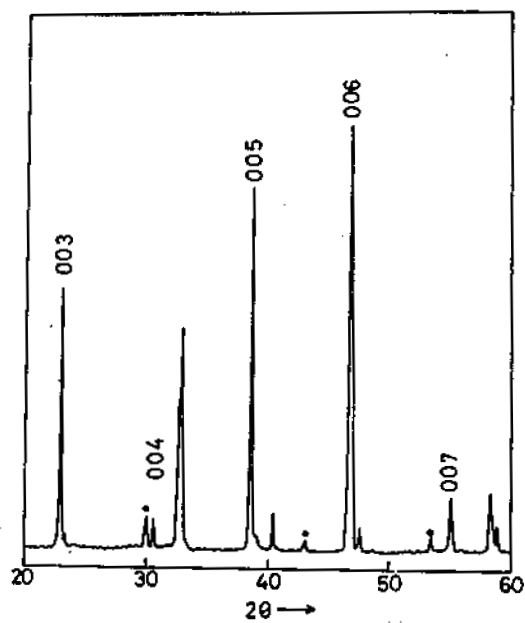


Figure 4.4 (d): XRD pattern of dip-coated YBCO film on Ba<sub>2</sub>HoZrO<sub>5.5</sub> substrate

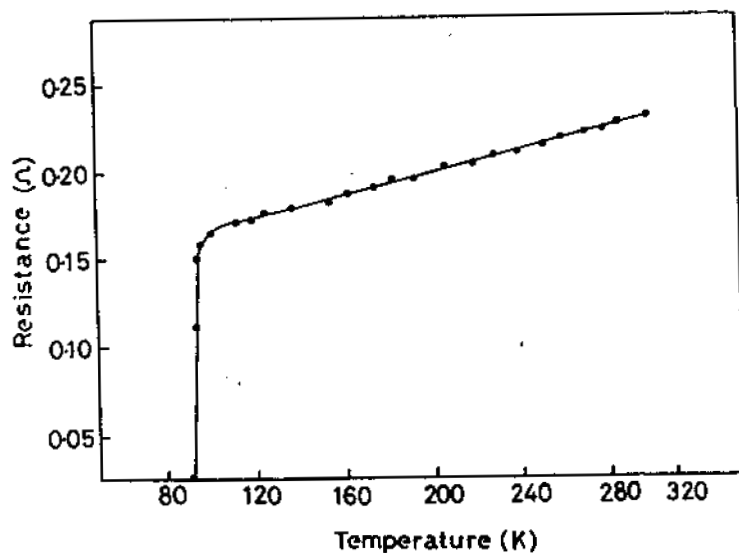


Figure 4.5 (a): Temperature-Resistance Curve for dip-coated YBCO film on  $\text{Ba}_2\text{LaZrO}_{5.5}$  Substrate

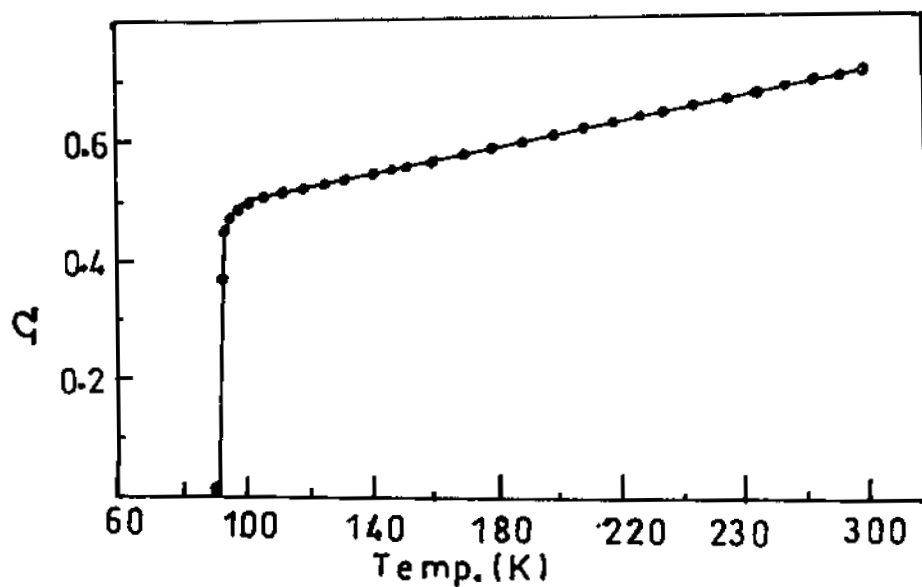


Figure 4.5 (b): Temperature-Resistance Curve for dip-coated YBCO film on  $\text{Ba}_2\text{EuZrO}_{5.5}$  Substrate

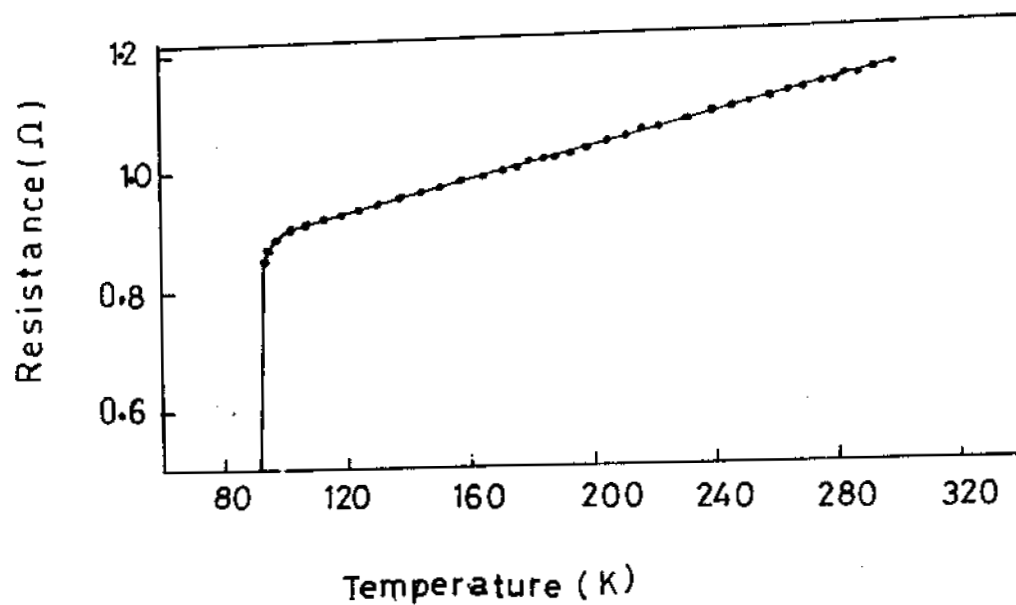


Figure 4.5 (c): Temperature-Resistance Curve for dip-coated YBCO film on Ba<sub>2</sub>YbZrO<sub>5.5</sub> Substrate.

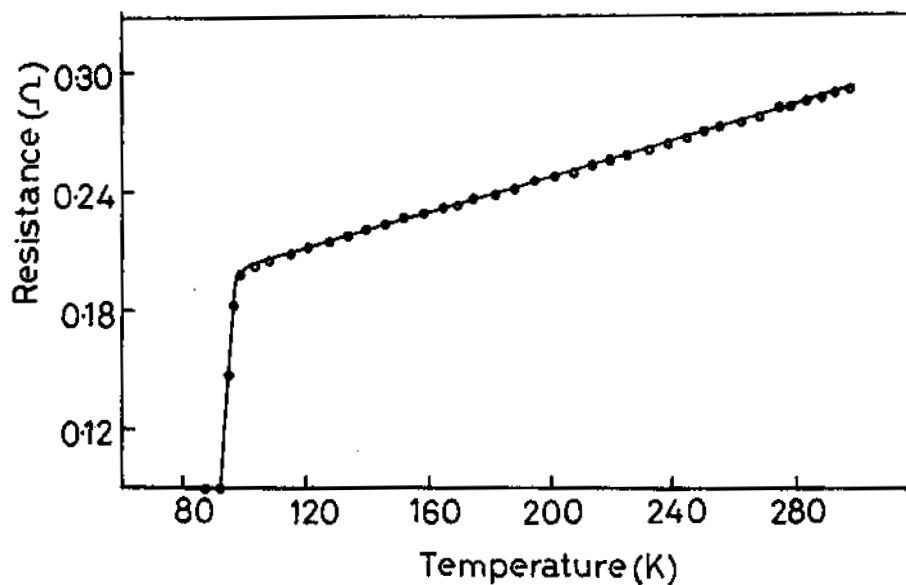


Figure 4.5 (d): Temperature-Resistance Curve for dip-coated YBCO film on Ba<sub>2</sub>HoZrO<sub>5.5</sub> Substrate.

#### 4.6 Conclusions

The results of chemical reactivity studies between  $\text{Ba}_2\text{REZrO}_{5.5}$  and YBCO superconductor indicate that the newly developed materials are chemically non-reacting with the YBCO superconductor even at the extreme processing conditions. The XRD patterns of the  $\text{Ba}_2\text{REZrO}_{5.5}$ -YBCO composite do not show any additional phase other than those of  $\text{Ba}_2\text{REZrO}_{5.5}$  and YBCO in the composite even after severe heat treatment. The addition of  $\text{Ba}_2\text{REZrO}_{5.5}$  up to 50-vol.% in YBCO did not show any detrimental effect on the superconducting properties of YBCO. The lattice constant matching of  $\text{Ba}_2\text{REZrO}_{5.5}$  with YBCO is within the tolerable limit for epitaxial growth. The suitability of  $\text{Ba}_2\text{REZrO}_{5.5}$  materials as substrate for YBCO was confirmed by developing superconducting thick films of YBCO on  $\text{Ba}_2\text{REZrO}_{5.5}$  materials by dip-coating and melt texturing. Because of the high processing temperature and partial melting of the YBCO films in the dip-coating and melt texturing process, YBCO films adhered very well to the  $\text{Ba}_2\text{REZrO}_{5.5}$  substrates. A peel off-test carried out using highly adhesive tape confirmed the excellent adhesion of the YBCO films to the substrates. The structure of the dip-coated films was studied by XRD and the superconductivity was studied by temperature-resistance and critical current density measurements. The films showed metallic behavior in the normal state and gave a  $T_{C(0)}$  of  $\sim 92$  K with a transition width of  $\sim 2$  K. The critical current density of the dip-coated and melt textured films were  $\sim 10^4$  A/cm<sup>2</sup> at 77 K under zero applied magnetic field.

**References**

- [1] J. M. Phillips, *J. Appl. Phys.*, **79**, (1996) 1829.
- [2] N. M. Alford, T. W. Button, M. J. Adams, S. Hedges, B. Micholson, W. A. Phillips, *Nature*, **349**, (1991) 680.
- [3] N. M. Alford, T. W. Button, D. Opie, *Supercond. Sci. Technol.*, **4**, (1991) 433.
- [4] N. M. Alford, T. W. Button, *Adv. Mater.*, **30**, (1991) 318.
- [5] N. P. Bensal, R. N. Simons, D. E. Farrel, *Appl. Phys. Lett.*, **53**, (1988) 603.
- [6] N. P. Bensal, *Mater. Lett.*, **13**, (1992) 7.
- [7] E. Saiz, J. S. Moya, *Supercond. Sci. Technol.*, **5**, (1992) 130.
- [8] N. Khare, A. K. Gupta, S. Chaudhury, V. S. Tomer, *Supercond. Sci. Technol.*, **4**, (1991) 433.
- [9] Y. Matsouka, E. Ban, H. Ogawa, A. Suzumura, *Supercond. Sci. Technol.*, **4**, (1991) 62.
- [10] N. M. Alford, S. J. Penn, T. W. Button, *Supercond. Sci. Technol.*, **10**, (1997) 169.
- [11] M. Miyajima, T. Nakamoto, S. Nagaya, I. Hirobayashi, S. Tanaka, *Supercond. Sci. Technol.*, **5**, (1992) 5292.
- [12] E. K. Hollman, O. G. Vendik, A. G. Zaitsev, B. T. Melekh, *Supercond. Sci. Technol.*, **7**, (1994) 609.
- [13] R. G. Humphreys, J. S. Satchell, N. G. Chew, J. A. Edwards, S. W. Goodyear, S. E. Blenkinsop, O. D. Dosser, A. G. Cullis, *Supercond. Sci. Technol.*, **3**, (1990) 38.
- [14] H. J. Scheel, M. Berkowski, B. Chabot, *Physica C*, **185-189**, (1991) 2095.
- [15] H. Koinuma, K. Fukuda, T. Hasimoto, K. Fueki, *Jpn. J. Appl. Phys.*, **27**, (1988) L1216.

- [16] I. Shih, C. X. Qiu, *Processing and Application of High Tc Superconductors*, The Metallurgical Soc. Inc. 1988.
- [17] X. M. Li, Y. T. Chou, Y. H. Hu, C. L. Booth, *J. Mater. Sci.*, **26**, (1991) 3057.
- [18] X. M. Li, Y. T. Chou, Y. H. Hu, C. L. Booth, *J. Mater. Sci. Lett.*, **9**, (1990) 669.
- [19] M. Naito, R. H. Hammond, B. Oh, M. R. Halin, J. W. P. Hsu, P. Rosenthal, *J. Mater. Res.*, **2**, (1987) 713.
- [20] M. F. Yan, W. W. Rhodes, P. K. Gallagher, *J. Appl. Phys.*, **63**, (1988) 821.
- [21] C. T. Cheung, E. Ruckenstein, *J. Mater. Res.*, **4**, (1989) 1.
- [22] L. H. Preng, T. S. Chin, K. Chen, C. H. Lin, *Supercond. Sci. Technol*, **3**, (1990) 233.
- [23] C. D. Brandle, V. J. Fratello, *J. Mater. Res.*, **5**, (1990) 2160.
- [24] E. G. Bauer, B. W. Dodson, D. J. Ehrlich, L. C. Feldman, C. P. Flynn, M. W. Geis, J. P. Harbison, R. J. Matyi, P. S. Peercy, P. M. Petroff, J. M. Phillips, G. B. Stringfellow, A. Zhangwill, *J. Mater. Res.*, **5**, (1990) 852.
- [25] X. Yu, M. Sayer, *Physica C*, **159**, (1989) 496.

## CHAPTER V

### DEVELOPMENT OF SUPERCONDUCTING BI-CUPRATES THICK FILMS ON BARIUM RARE-EARTH ZIRCONATES BY DIPCOATING AND MELT TEXTURING <sup>☆</sup>

#### 5.1 Introduction

The discovery of superconductivity in bismuth-strontium-calcium-copper-oxide (BiSCCO) was accompanied by the claims that these new oxides would soon supplant  $\text{YBa}_2\text{Cu}_3\text{O}_{7.8}$  (YBCO) as their  $T_C$  was higher, they were less dependant on the maintenance of a precise oxygen content, and they were less sensitive to aqueous contamination [1-2]. Since the initial discovery, however, it has become clear that there are several structural forms for this new series of superconducting compounds and that it is particularly difficult to synthesize the phase, which has a  $T_C$  higher than that of YBCO. The oxide which forms most readily has the chemical composition  $\text{Bi}_2\text{Sr}_2\text{CaCu}_2\text{O}_8$  [Bi (2212)] and has a  $T_{C(0)}$  of 85 K. The high  $T_C$  phase ( $T_{C(0)} = 110\text{K}$ ) having the nominal stoichiometry  $\text{Bi}_2\text{Sr}_2\text{Ca}_2\text{Cu}_3\text{O}_{10}$  [Bi (2223)] was formed only as minority phase [3]. It was reported by several workers that the incorporation of Pb in the Bi-Sr-Ca-Cu-O system coupled with a prolonged sintering in a narrow temperature range was essential to obtain a high concentration of the high  $T_C$  phase [4-8]. As in the case of YBCO, the immediate application of BiSCCO superconductors are also in the form of thick and thin films in microwave integrated circuits, transmission lines and other high frequency devices [9-16]. Processing based on thick film technology will have the advantage

---

<sup>☆</sup>Published in *Materials Letters*, 41 (1999) 112

of making large area superconducting films for high Q resonators and superconducting magnetic shields.

As in the case of YBCO superconductor, the most important criteria for the selection of any material as substrate for Bi-cuprate superconducting film is the chemical non-reactivity between the substrate and the film at the processing temperature [17]. Bi (2223) superconductor is found to be readily reacting with the conventional substrates such as  $\text{Al}_2\text{O}_3$ , Si,  $\text{SiO}_2$ , etc. at the processing temperature [18]. MgO is the most widely reported substrate for Bi (2223) superconductor. However, even on MgO substrate, Bi (2223) developed always contained both low Tc Bi (2212) and high Tc Bi (2223) phases [19, 20]. In this chapter, we describe the details of the synthesis of Bi (2212) and Bi (2223) superconductors and their chemical compatibility with  $\text{Ba}_2\text{REZrO}_{5.5}$  (RE = La, Ce, Eu, Yb, Ho and Er) substrates. The development and characterization of superconducting Bi (2212) ( $T_{C(0)} = 85$  K) and Bi (2223) ( $T_{C(0)} = 110$  K) thick films on these newly synthesized substrates are also described in this chapter.

## 5.2 Synthesis of Bi (2212) superconductor

High purity (99.99%)  $\text{Bi}_2\text{O}_3$ ,  $\text{SrCO}_3$ ,  $\text{CaCO}_3$ , and CuO were weighed in the precise stoichiometric ratio  $\text{Bi}_2\text{Sr}_2\text{CaCu}_2\text{O}_x$  and wet mixed using acetone as the wetting medium in an agate mortar and dried in an electric oven. The dried powders are then calcined in air at a temperature of  $820^\circ\text{C}$  for 24 h. The calcined powders were ground well and sintered in air at  $840^\circ\text{C}$  for 40 h. Figures 5.1 (a) and 5.1 (b) show the XRD pattern of the sintered Bi (2212) and the corresponding temperature-resistance curve. The XRD values of Bi (2212) superconductor

comprises of  $d$  values,  $2\theta$ , line strengths, widths and  $hkl$  indices are given in Table 5.1

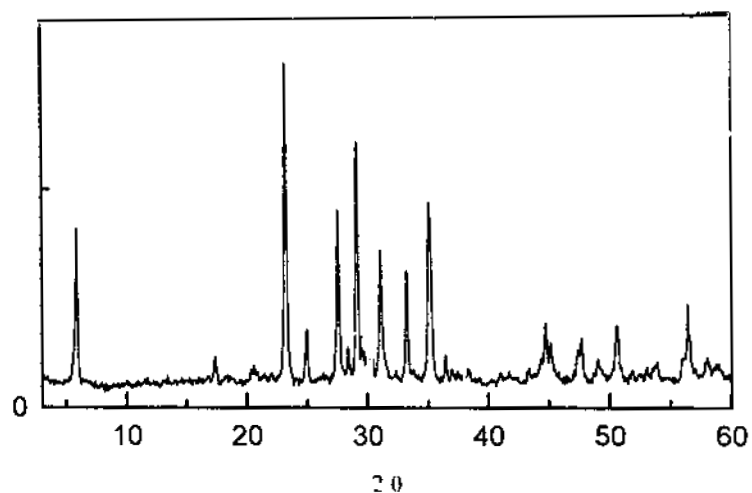


Figure 5.1(a): X-ray diffraction pattern of sintered Bi(2212)

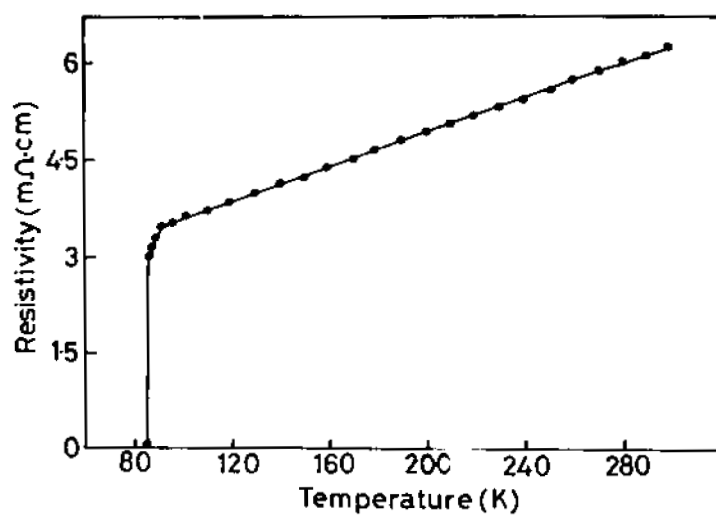


Figure 5.1(b): Temperature resistivity curve of Bi(2212)

**Table 5.1:** X-ray diffraction data of sintered Bi (2212) superconductor:

No	2 $\theta$	d (Å)	Width (deg.)	I / I <sub>0</sub>	hkl
1	5.74	15.39	0.249	50	002
2	17.380	5.098	0.479	14	006
3	23.101	3.847	0.295	100	008
4	24.752	3.594	0.350	21	113
5	27.369	3.256	0.260	55	115
6	29.070	3.085	0.269	75	0010
7	30.905	2.891	0.309	43	117
8	33.090	2.705	0.269	37	020
9	34.953	2.565	0.389	58	0012
10	35.136	2.552	0.389	15	119
11	44.531	2.033	0.460	23	2010
12	45.140	2.007	0.700	17	1113
13	47.437	1.915	0.480	14	220
14	48.700	1.857	0.480	12	2012
15	50.404	1.809	0.490	21	1115
16	57.756	1.595	0.399	27	2210

### 5.3 Chemical reactivity between Ba<sub>2</sub>REZrO<sub>5.5</sub> and Bi (2212)

The most important aspect that makes a material to be suited as a substrate for high T<sub>c</sub> superconductor is the chemical non-reactivity between the substrate and the superconductor at the processing temperature. In order to understand whether Ba<sub>2</sub>REZrO<sub>5.5</sub> are chemically compatible with Bi

(2212) superconductor, chemical reactivity studies between  $\text{Ba}_2\text{REZrO}_{5.5}$  and Bi (2212) were carried out in detail up to a temperature of  $850^\circ\text{C}$ . For the chemical reactivity studies, single phase Bi (2212) and  $\text{Ba}_2\text{REZrO}_{5.5}$  powders were thoroughly mixed in different volume ratio and pressed in the form of circular discs of 13 mm diameter and  $\sim 1.5$  mm thickness by applying a pressure of 300 MPa. These discs were then annealed in air at  $850^\circ\text{C}$  for 15 h and then furnace cooled to room temperature. The chemical reactivity between Bi (2212) and  $\text{Ba}_2\text{REZrO}_{5.5}$  was studied by XRD.

Figures 5.2 (a-f) show the XRD pattern of the composite mixture consisting of different volume ratio of Bi (2212) and  $\text{Ba}_2\text{REZrO}_{5.5}$  and annealed at  $850^\circ\text{C}$  for 15 h. In all the figures the XRD pattern of the annealed mixture is compared with pure Bi (2212) and pure  $\text{Ba}_2\text{REZrO}_{5.5}$ . If Bi (2212) reacted with  $\text{Ba}_2\text{REZrO}_{5.5}$  under such annealing conditions, additional phases besides Bi (2212) and  $\text{Ba}_2\text{REZrO}_{5.5}$  or change in lattice constant would be observed in the XRD pattern of the annealed mixture. On the other hand if Bi (2212) does not react with  $\text{Ba}_2\text{REZrO}_{5.5}$  under such annealing conditions, the crystalline phases after annealing will be just two identical phases of Bi (2212) and  $\text{Ba}_2\text{REZrO}_{5.5}$ . It is clear from those figures that Bi (2212) and  $\text{Ba}_2\text{REZrO}_{5.5}$  remained as separate phases in the composite mixture and there was no indication of any change in lattice parameter of either Bi (2212) or  $\text{Ba}_2\text{REZrO}_{5.5}$ . These observations clearly confirm that  $\text{Ba}_2\text{REZrO}_{5.5}$  materials are chemically compatible with Bi (2212) superconductors.

The effect of  $\text{Ba}_2\text{REZrO}_{5.5}$  addition on the superconducting properties of Bi (2212) was studied by temperature-resistance measurements. Superconducting Bi (2212) and  $\text{Ba}_2\text{REZrO}_{5.5}$  were thoroughly mixed in

different volume ratio 0- 50 % of the superconductor and pressed in the form of pellets at a pressure of 250 MPa. These discs were sintered at 850°C for

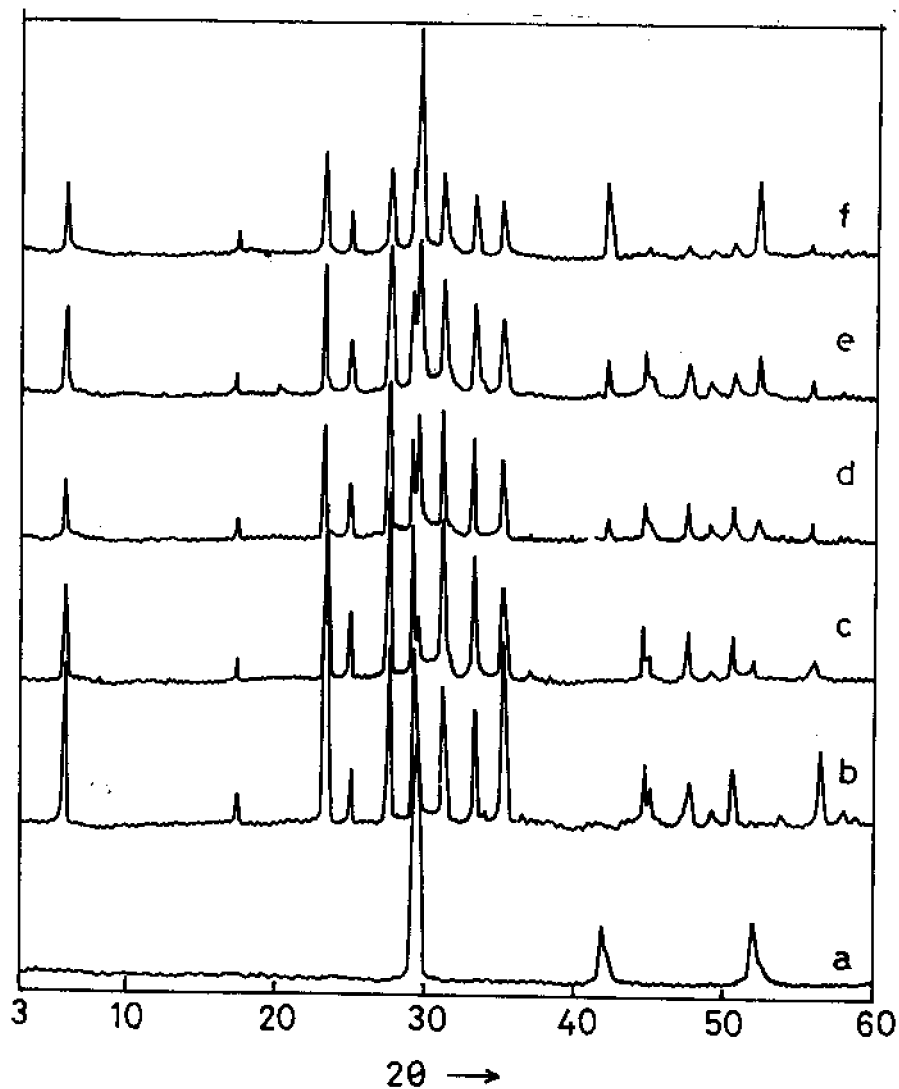


**Figure 5.2 (a).** X-ray diffraction pattern of (a) pure  $\text{Ba}_2\text{CeZrO}_{5.5}$  (b) pure  $\text{Bi}(2212)$  (c)  $\text{Bi}(2212)$  -10 vol.%  $\text{Ba}_2\text{CeZrO}_{5.5}$ , (d)  $\text{Bi}(2212)$  -20 vol.%  $\text{Ba}_2\text{CeZrO}_{5.5}$ , (e)  $\text{Bi}(2212)$  -30 vol.%  $\text{Ba}_2\text{CeZrO}_{5.5}$ , (f)  $\text{Bi}(2212)$  -50 vol.%  $\text{Ba}_2\text{CeZrO}_{5.5}$  composite systems after annealing at 850°C for 15 h.

15 h and then furnace cooled to room temperature. The resistance measurements of the composite compacts were made by standard four-probe technique using a nanovoltmeter (model 181, Kiethley Instruments, Cleveland, OH) and a current source (model 220, Kiethley). The temperature of the sample was measured by a calibrated copper Constantine thermocouple

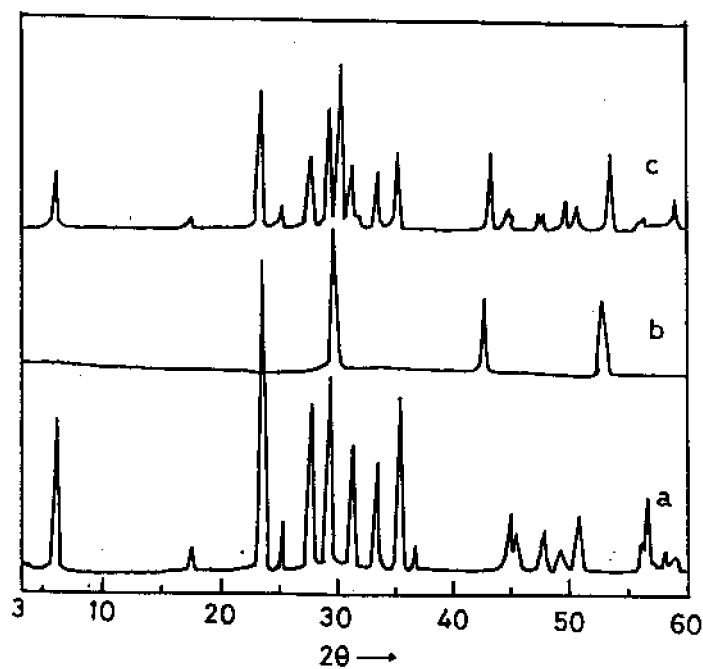


**Figure 5.2 (b):** X-ray diffraction pattern of (a) pure Bi (2212) (b) pure  $\text{Ba}_2\text{LaZrO}_{5.5}$  (c) Bi (2212) -50 vol.%  $\text{Ba}_2\text{LaZrO}_{5.5}$  composite systems after annealing at  $850^\circ\text{C}$  for 15 h

calibrated with a RF 800 rhodium-iron resistance sensor with an accuracy of  $\pm 0.2\text{K}$ . Figures 5.3 (a-f) show the resistivity versus temperature curves for the Bi (2212)-  $\text{Ba}_2\text{REZrO}_{5.5}$  composites containing different volume ratio of  $\text{Ba}_2\text{REZrO}_{5.5}$  annealed at  $850^\circ\text{C}$  for 15 h. A superconducting transition of 85 K was obtained for all the composites. This indicates that a substantial addition of  $\text{Ba}_2\text{REZrO}_{5.5}$  in Bi (2212) did not have any detrimental effect on

the superconducting transition temperature of Bi (2212) even after severe heat treatment.

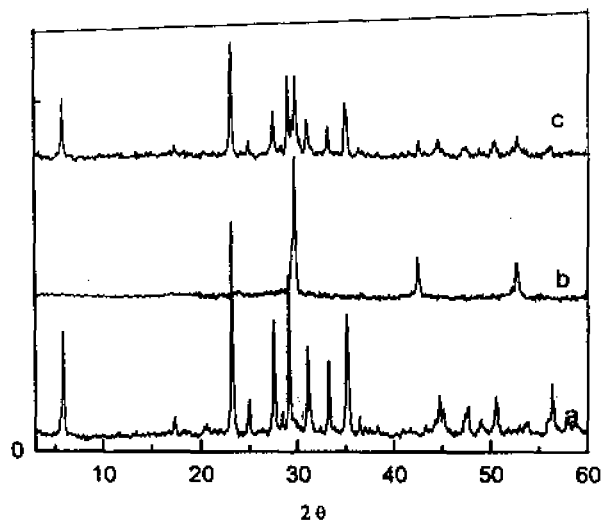


**Figure 5.2 (c):** X-ray diffraction pattern of (a) pure Bi (2212) (b) pure  $\text{Ba}_2\text{EuZrO}_{5.5}$  (c) Bi (2212) -50 vol.%  $\text{Ba}_2\text{EuZrO}_{5.5}$  composite system after annealing at 850°C for 15 h.

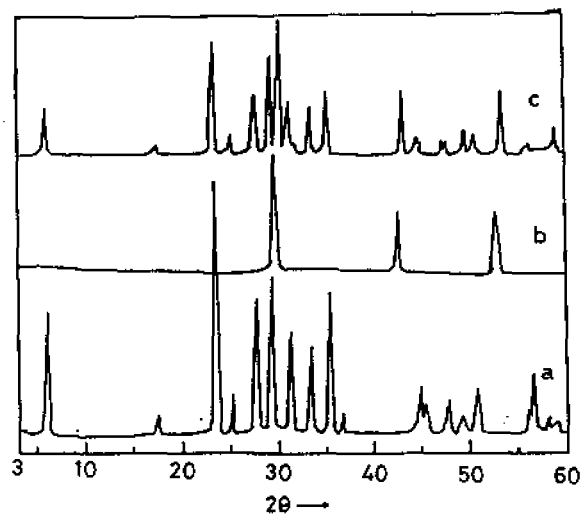


**Figure 5.2 (d):** X-ray diffraction pattern of (a) pure Bi (2212) (b) pure  $\text{Ba}_2\text{YbZrO}_{5.5}$  (c) Bi (2212) -50 vol.%  $\text{Ba}_2\text{YbZrO}_{5.5}$  composite systems after annealing at 850°C for 15 h.

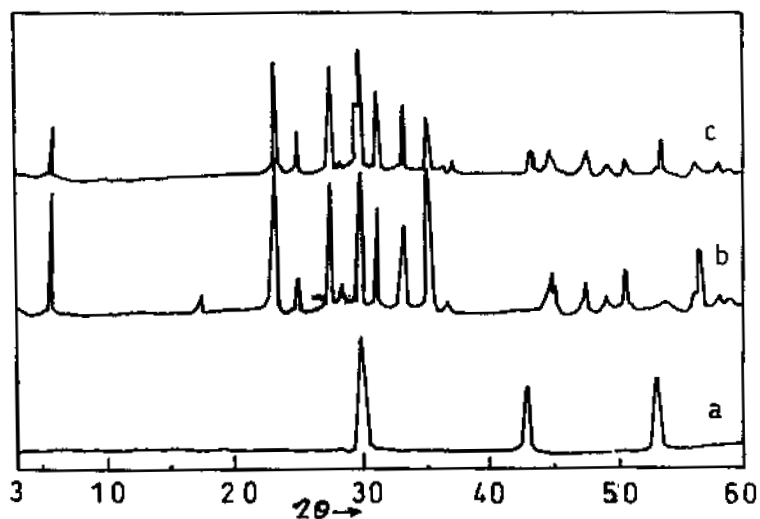


**Figure 5.2 (e):** X-ray diffraction pattern of (a) pure  $\text{Ba}_2\text{ErZrO}_{5.5}$  (b) pure Bi (2212) (c) Bi (2212) -50 vol.%  $\text{Ba}_2\text{ErZrO}_{5.5}$  composite systems after annealing at  $850^\circ\text{C}$  for 15 h.

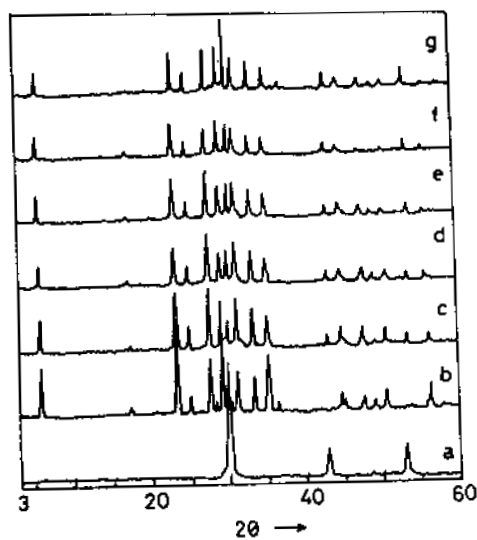


**Figure 5.1 (f):** X-ray diffraction pattern of (a) pure  $\text{Ba}_2\text{HoZrO}_{5.5}$  (b) pure Bi (2212) (c) Bi (2212) -10 vol.%  $\text{Ba}_2\text{HoZrO}_{5.5}$ , (d) Bi (2212) -20 vol.%  $\text{Ba}_2\text{HoZrO}_{5.5}$ , (e) Bi (2212) -30 vol.%  $\text{Ba}_2\text{HoZrO}_{5.5}$ , (f) Bi (2212) -50 vol.%  $\text{Ba}_2\text{HoZrO}_{5.5}$  composite systems after annealing at  $850^\circ\text{C}$  for 15 h.

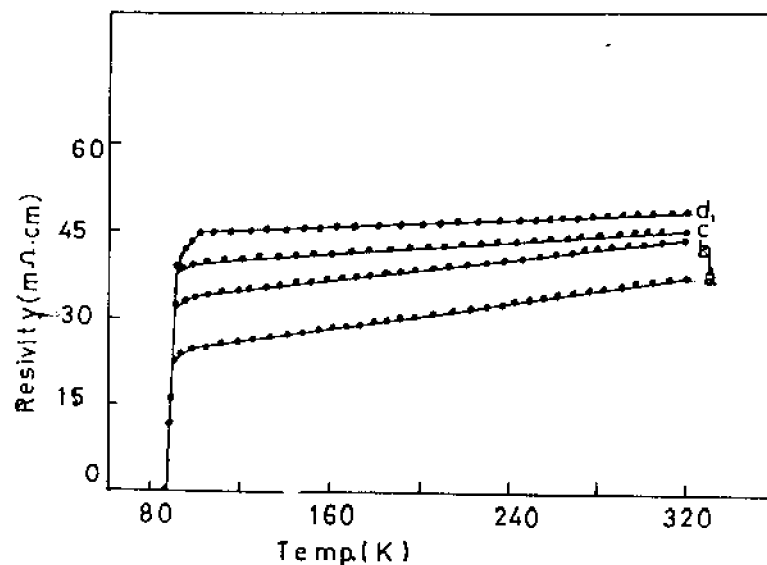


**Figure 5.3 (a):** The electrical resistivity vs. temperature curve for (a) 10 vol.% of  $\text{Ba}_2\text{CeZrO}_{5.5}\text{-Bi}$  (2212), (b) 20 vol.% of  $\text{Ba}_2\text{CeZrO}_{5.5}\text{-Bi}$  (2212), (c) 30 vol.% of  $\text{Ba}_2\text{CeZrO}_{5.5}\text{-Bi}$  (2212), (d) 40 vol.% of  $\text{Ba}_2\text{CeZrO}_{5.5}\text{-Bi}$  (2212), and (e) 50 vol.% of  $\text{Ba}_2\text{CeZrO}_{5.5}\text{-Bi}$  (2212) composites after at annealing at  $850^\circ\text{C}$  for 15 h in air.

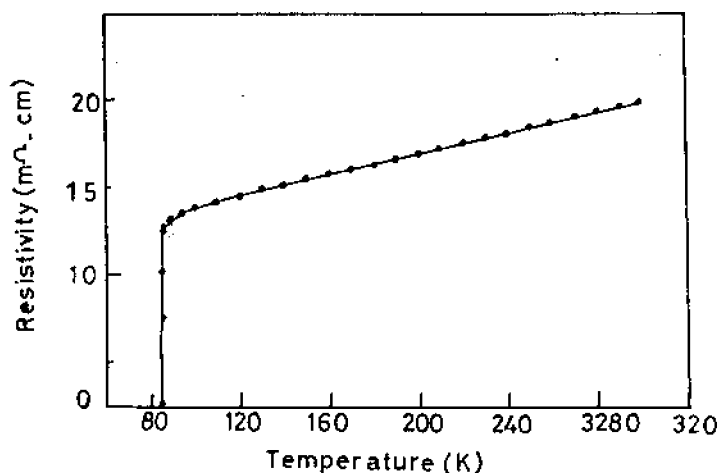


**Figure 5.3 (b):** The electrical resistivity vs. temperature curve Bi (2212)- $\text{Ba}_2\text{LaZrO}_{5.5}$  composite containing 20 vol.% of  $\text{Ba}_2\text{LaZrO}_{5.5}$

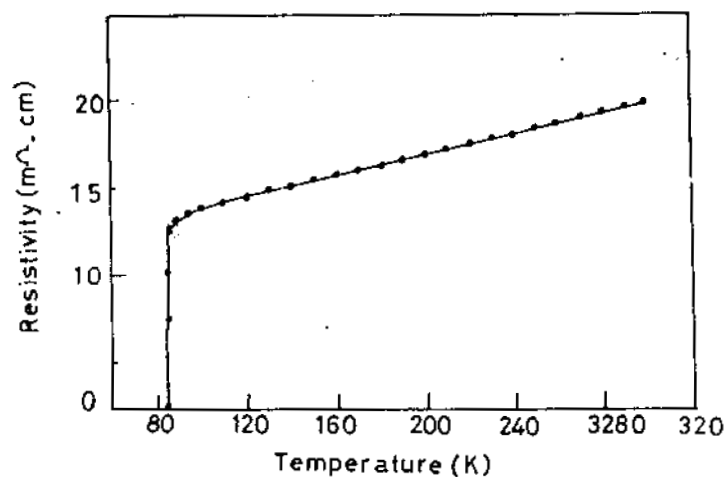


Figure 5.3 (c): The electrical resistivity vs. temperature curve Bi (2212)-Ba<sub>2</sub>EuZrO<sub>5.5</sub> composite containing 20 vol.% of Ba<sub>2</sub>EuZrO<sub>5.5</sub>

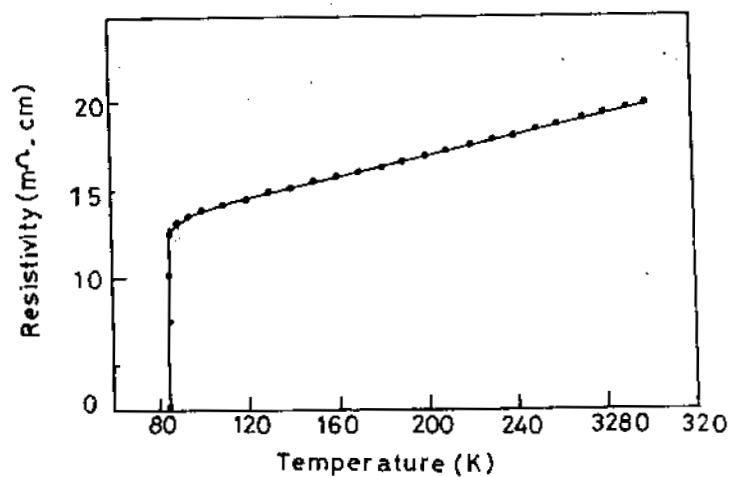


Figure 5.3 (d): The electrical resistivity vs. temperature curve Bi (2212)-Ba<sub>2</sub>YbZrO<sub>5.5</sub> composite containing 20 vol.% of Ba<sub>2</sub>YbZrO<sub>5.5</sub>

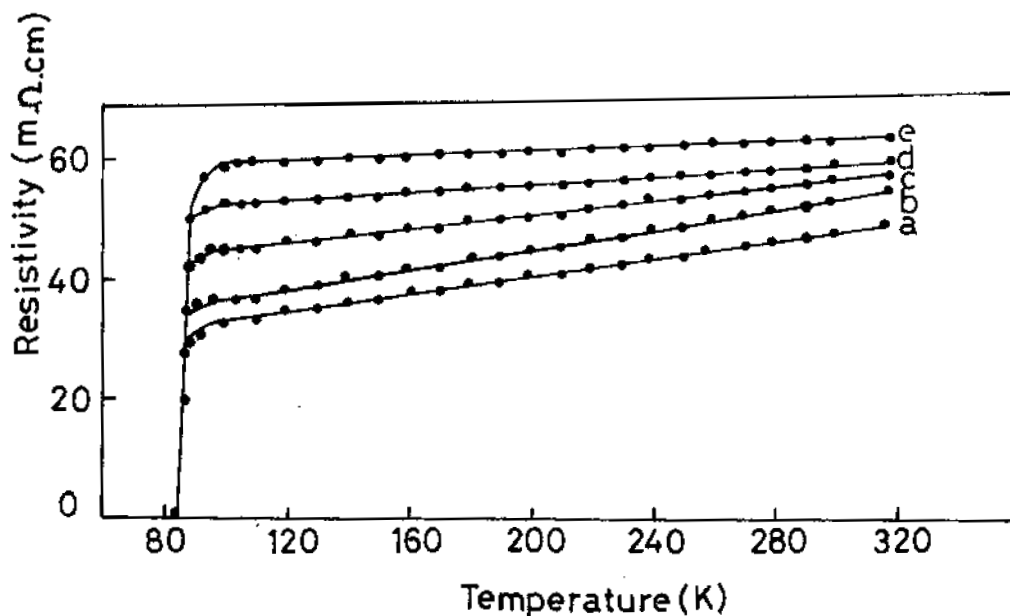


Figure 5.3 (e): The electrical resistivity vs. temperature curve for (a) 10 vol.% of  $\text{Ba}_2\text{HoZrO}_{5.5}\text{-Bi (2212)}$ , (b) 20 vol.% of  $\text{Ba}_2\text{HoZrO}_{5.5}\text{-Bi (2212)}$ , (c) 30 vol.% of  $\text{Ba}_2\text{HoZrO}_{5.5}\text{-Bi (2212)}$ , (d) 40 vol.% of  $\text{Ba}_2\text{HoZrO}_{5.5}\text{-Bi (2212)}$ , and (e) 50 vol.% of  $\text{Ba}_2\text{HoZrO}_{5.5}\text{-Bi (2212)}$  composites after at annealing at  $850^\circ\text{C}$  for 15 h in air.

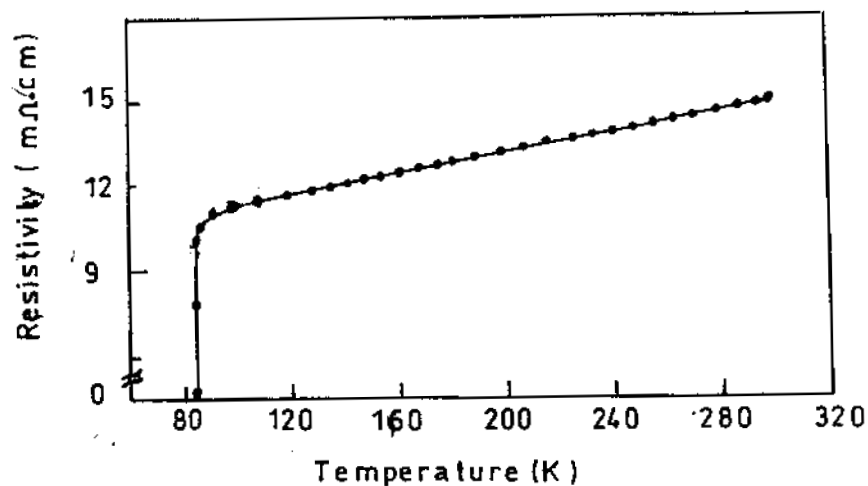


Figure 5.3 (f): The electrical resistivity vs. temperature curve  $\text{Bi (2212)-Ba}_2\text{ErZrO}_{5.5}$  composite containing 20 vol.% of  $\text{Ba}_2\text{ErZrO}_{5.5}$

#### 5.4 Development of Bi (2212) thick films on $\text{Ba}_2\text{REZrO}_{5.5}$

The suitability of  $\text{Ba}_2\text{REZrO}_{5.5}$  materials as substrate for Bi (2212) superconductor was confirmed by developing superconducting thick films on these newly developed substrates. The Bi (2212) suspension for dip-coating was prepared by thoroughly mixing fine superconducting Bi (2212) powder with isopropyl alcohol or n-butanol and the viscosity of the suspension was controlled by the addition of commercially available fish oil. The polished and cleaned  $\text{Ba}_2\text{REZrO}_{5.5}$  substrates were then dipped in the Bi (2212) suspension and dried. This step was repeated till a required thickness is attained. The dip-coated films were then dried in an oven and heated in a programmable furnace at a rate of  $5^\circ\text{C}/\text{min}$  in air up to  $880^\circ\text{C}$  and kept at this temperature for 2 min and then annealed at  $850^\circ\text{C}$  temperature for 6 h. The films were then cooled at a rate of  $1^\circ\text{C} / \text{min}$  up to  $800^\circ\text{C}$  from the annealing temperature of  $850^\circ\text{C}$  and then furnace cooled to room temperature. Heating up to  $880^\circ\text{C}$  was required to get good adhesion between the film and the substrate. Because of the high processing temperature and partial melting of the Bi (2212) films in the dip-coating and melt texturing process the films adhered very well to the  $\text{Ba}_2\text{REZrO}_{5.5}$  substrates. A peel off-test carried out using highly adhesive tape confirmed the excellent adhesion of the Bi (2212) films to the substrates.

The structure of the Bi (2212) films dip-coated on  $\text{Ba}_2\text{REZrO}_{5.5}$  substrates was studied by x-ray diffraction and the superconductivity of the films were studied by temperature-resistance measurements using a standard four probe technique. Figures 5.4 and 5.5 show the XRD patterns of Bi (2212) films dip-coated on  $\text{Ba}_2\text{EuZrO}_{5.5}$  and  $\text{Ba}_2\text{HoZrO}_{5.5}$  substrates respectively. Except for the characteristic peaks of  $\text{Ba}_2\text{REZrO}_{5.5}$  all the other peaks in figures 5.4 and 5.5 are

those of orthorhombic Bi (2212). The temperature-resistance curves for dip-coated Bi (2212) films on  $\text{Ba}_2\text{EuZrO}_{5.5}$  and  $\text{Ba}_2\text{HoZrO}_{5.5}$  substrates are shown in figures 5.6 and 5.7 respectively. The films showed metallic behavior in the normal state and gave a zero resistivity transition of 85 K. The  $J_C$  of the films measured using  $1\mu\text{V}$  criteria was  $\sim 4 \times 10^3 \text{ A/cm}^2$  at 77 K under zero applied magnetic field. This clearly confirms that the newly developed  $\text{Ba}_2\text{REZrO}_{5.5}$  materials are potentially suited for their application as substrates for superconducting Bi (2212) films for various device applications.

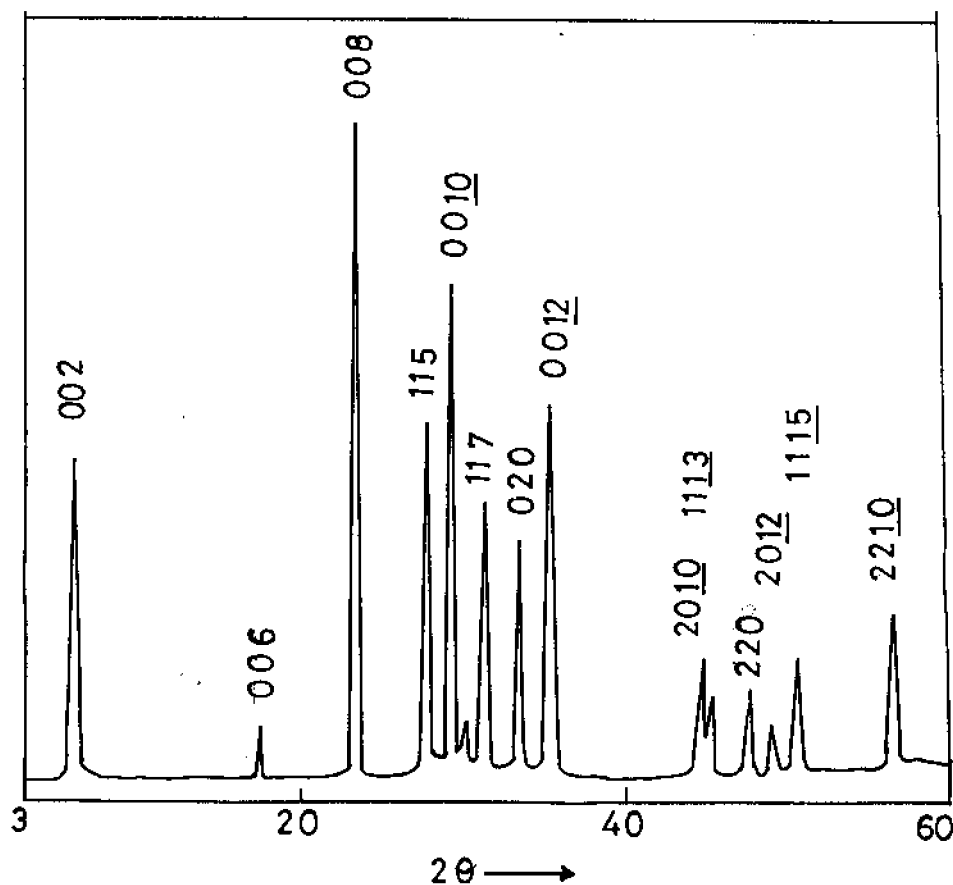


**Figure 5.4:** The XRD pattern of Bi (2212) films dip-coated on  $\text{Ba}_2\text{EuZrO}_{5.5}$  substrate

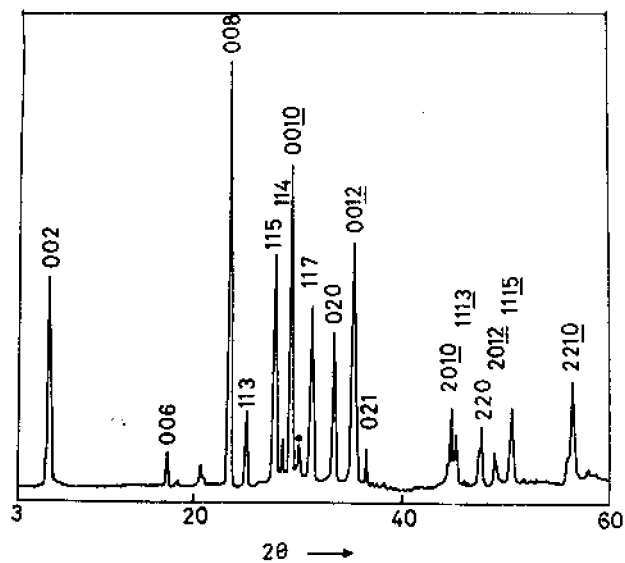


Figure 5.5 : The XRD pattern of Bi (2212) film dip-coated on  $\text{Ba}_2\text{HoZrO}_{5.5}$  substrate

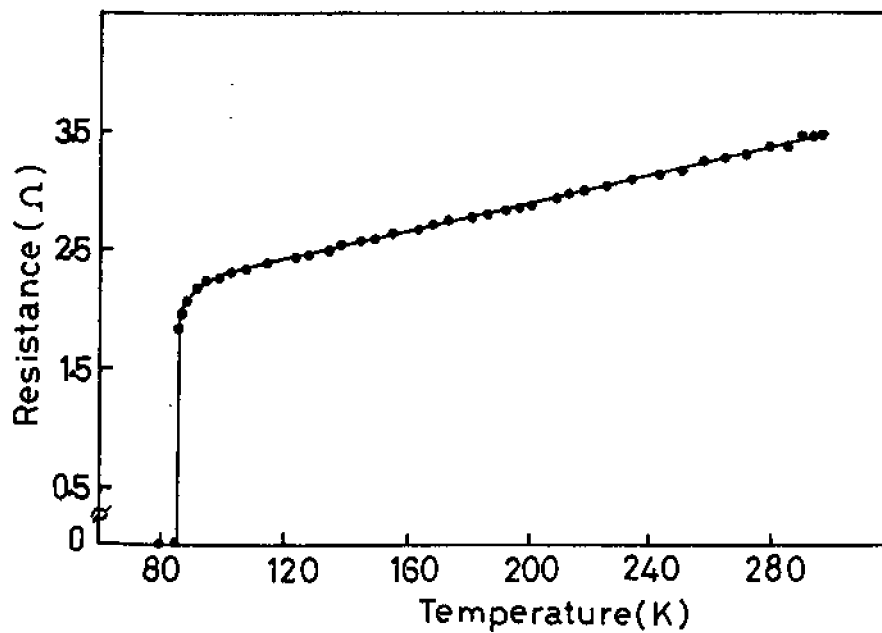
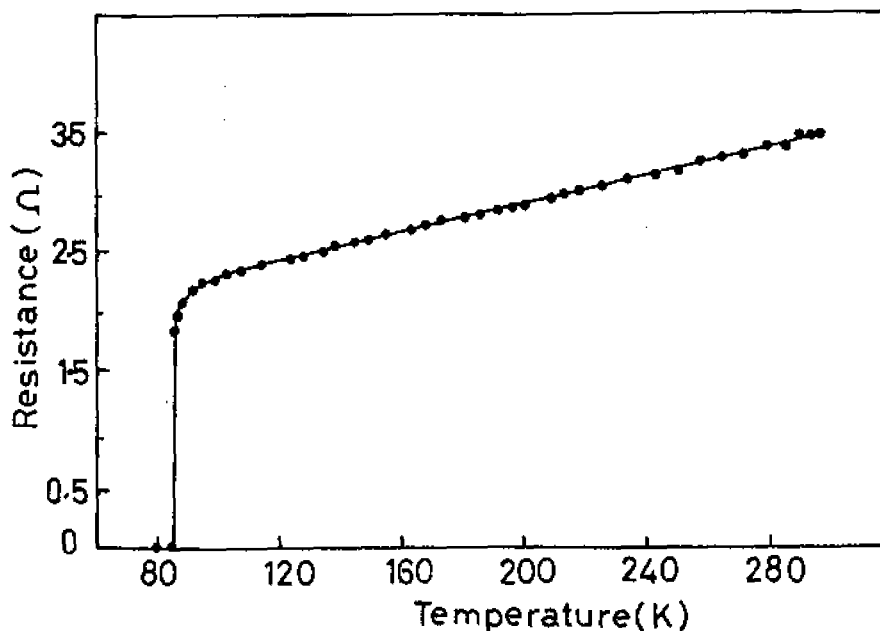


Figure 5.6: Temperature-Resistance curve for Bi (2212) film developed on  $\text{Ba}_2\text{EuZrO}_{5.5}$  substrate



**Figure 5.7:** Temperature-Resistance curve for Bi (2212) film developed on  $\text{Ba}_2\text{HoZrO}_{5.5}$  substrate

### 5.5 Synthesis of Bi (2223) superconductor

Single phase Bi (2223) powder for the present study was also prepared through the solid state route. High purity (99.9%)  $\text{Bi}_2\text{O}_3$ ,  $\text{PbO}$ ,  $\text{SrCO}_3$ ,  $\text{CaCO}_3$  and  $\text{CuO}$  were weighed in the precise stoichiometric ratio of  $\text{Bi}_{1.5}\text{Pb}_{0.5}\text{Sr}_2\text{Ca}_2\text{Cu}_3\text{O}_x$  and the reaction mixture was thoroughly wet mixed in an agate mortar with acetone as the wetting medium. The mixture was dried in an oven and the dried powder was calcined in air at three different temperatures of 800, 805 and 810°C each for 15 h. The finely ground calcined powder was pressed in the form of circular discs with dimensions of ~13 mm diameter and ~ 1.5 mm thickness by applying a pressure of ~ 300 MPa. These discs were then sintered in air at 850°C for 200 h continuously. The sintered samples were then cooled slowly at a rate of 1°C/min from the sintering temperature to 800°C and then finally furnace cooled to room

temperature. The structure of the sintered samples was studied by x-ray diffraction and the superconductivity of the sample was studied by temperature-resistance measurements. The XRD pattern of single-phase Bi (2223) superconductor is shown in figures 5.8 (a) and the XRD values comprising of  $d$  values,  $2\theta$ , line strengths, widths and  $hkl$  indices are given in Table 5.2. The temperature-resistivity curve of the sintered Bi (2223) sample is given figure 5.8(b).

**Table 5.2:** x-ray diffraction data of single phase Bi (2223)

No	$2\theta$	$d$ (Å)	Width	$I/I_0$	$hkl$
1	4.760	18.549	0.423	30	002
2	9.370	9.430	0.420	8	004
3	19.120	4.638	0.465	15	008
4	23.880	3.540	0.540	73	0010
5	26.190	3.402	0.480	41	115
6	28.810	3.097	0.600	100	0012
7	31.840	2.808	0.480	53	119
8	33.110	2.703	0.480	54	200
9	33.780	2.651	0.675	63	1114
10	35.450	2.530	0.450	38	1111
11	44.510	2.033	0.495	11	2012
12	47.560	1.910	0.390	11	220
13	47.990	1.894	0.450	13	1117
14	49.080	1.854	0.465	13	0020

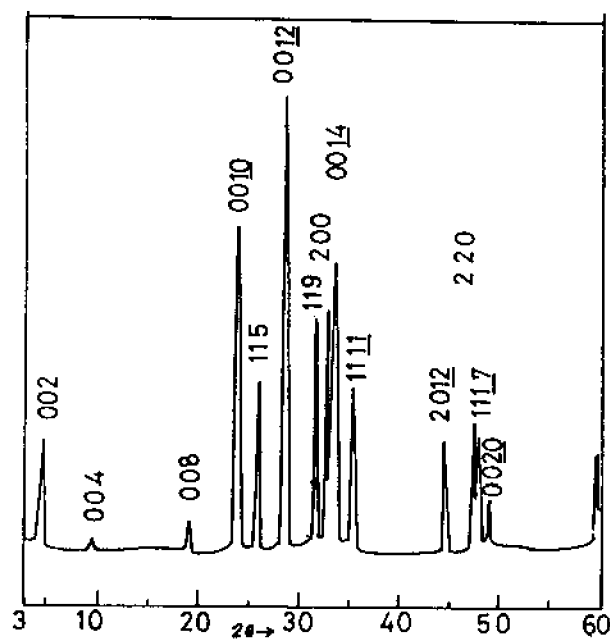


Figure 5.8 (a): XRD pattern of single phase Bi (2223) superconductor

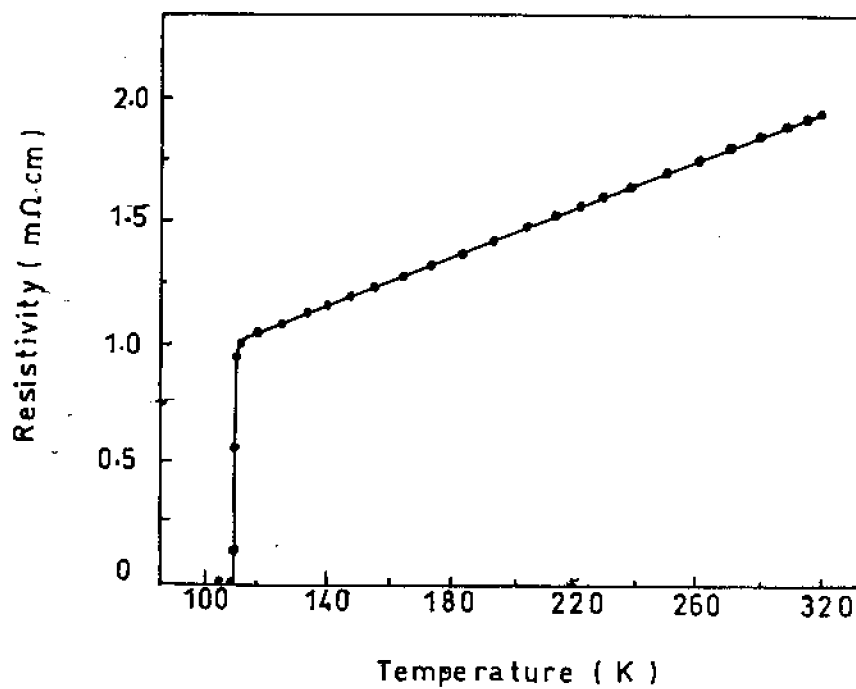


Figure 5.8 (b) : Temperature-resistivity curve for pure Bi (2223) sample

#### 5.4 Chemical reactivity between $Ba_2REZrO_{5.5}$ and Bi(2223)

In order to understand whether the newly developed  $Ba_2REZrO_{5.5}$  ceramics are chemically compatible with Bi (2223) superconductor, the chemical reactivity studies between  $Ba_2REZrO_{5.5}$  and Bi (2223) have been carried out up to a temperature of 850°C. Single-phase  $Ba_2REZrO_{5.5}$  and Bi (2223) were thoroughly mixed in 1:1 volume ratio and the mixture was pressed in the form of circular discs with dimensions ~13 mm diameter and ~1.5 mm thickness by applying a pressure of ~300 MPa. These pellets were then heated in air at 850°C for 15 h and the chemical reactivity was studied by powder XRD. The XRD patterns of Bi (2223)- $Ba_2REZrO_{5.5}$  (RE = La, Ce, Eu and Yb) composites annealed at 850°C for 15 h is shown in figure 5.9. The XRD patterns of the two phases in the annealed samples were compared with those of pure Bi (2223) and  $Ba_2REZrO_{5.5}$  in the  $Ba_2REZrO_{5.5}$ -Bi (2223) composite. It is clear from these figures that two materials in this group with RE = La and Eu are non-reacting with Bi (2223) as judged by the absence of any additional phase other than Bi (2223) and  $Ba_2REZrO_{5.5}$  (RE = La and Eu) phases in these composites. In the case of  $Ba_2CeZrO_{5.5}$  and  $Ba_2YbZrO_{5.5}$ , the Bi (2223) in the composite has decomposed in to a mixture of Bi (2212) and Bi (2223) under such annealing conditions. But when RE = Ho or Er, Bi (2223) present in the composite mixture was fully decomposed in to Bi (2212) on annealing at 850°C for 15 h as shown in figure 5.10. The XRD data comprising  $2\theta$ , d values, line widths, line strengths of the composite after annealing at 850°C is given in Table 5.3 (a-d). The volume fraction of Bi (2223) in the Bi (2223)- $Ba_2REZrO_{5.5}$  composite was calculated from the XRD data using the empirical relation given below [21]

$$V = (Y - 29.07) / (28.81 - 29.07) \quad (5.1)$$

$$28.81 < Y < 29.07$$

where  $V$  is the volume fraction of Bi (2223) and  $Y$  is the  $2\theta$  for peak appearing between 28.81 and 29.07, caused by the interplay of reflection from the crystal planes (0010) of Bi (2212) phase and (0012) of Bi (2223) phase. The volume fraction of

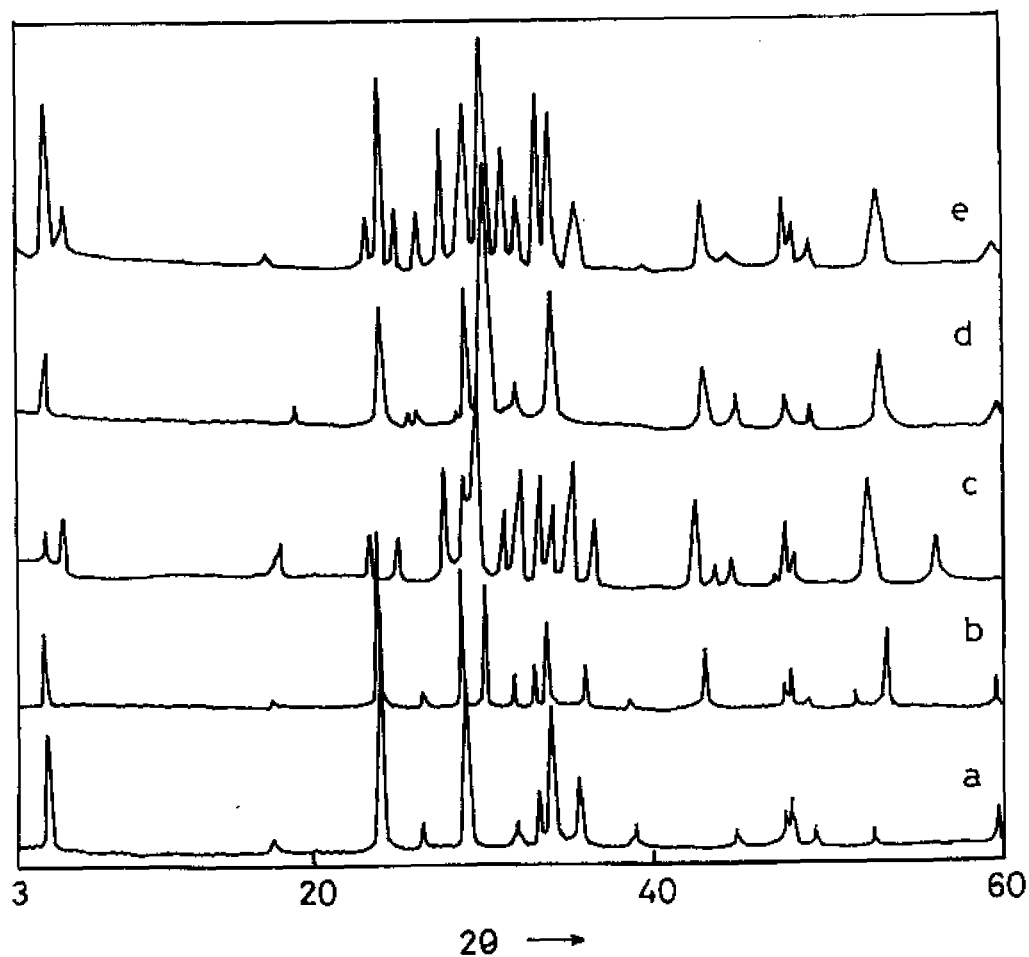


**Figure 5.9 :** Powder X-ray pattern of (a) pure Bi (2223), (b) 1: 1 volume mixture of Bi (2223) and  $\text{Ba}_2\text{LaZrO}_{5.5}$ , (c) 1: 1 volume mixture of Bi (2223) and  $\text{Ba}_2\text{CeZrO}_{5.5}$ , (d) 1: 1 volume mixture of Bi (2223) and  $\text{Ba}_2\text{EuZrO}_{5.5}$ , (e) 1: 1 volume mixture of Bi (2223) and  $\text{Ba}_2\text{YbZrO}_{5.5}$ ; all annealed at  $850^\circ\text{C}$  for 10 h in air.

Bi (2223) in each composite was calculated using the above empirical relation is given in Table 5.4. It is obvious from the tables 5.3 and 5.4 that among  $Ba_2REZrO_{5.5}$  materials, those with RE = La and Eu are potentially suited as substrates for Bi (2223) superconductor.

**Table 5.3 (a):** XRD data of  $Ba_2LaZrO_{5.5}$  - Bi (2223) composite

No	$2\theta$ (deg)	d (Å)	width (deg.)	Hkl	I / I <sub>0</sub>
1	4.760	18.549	0.240	002	30
2	9.370	9.430	0.360	004	3
3	19.120	4.638	0.270	008	8
4	23.880	3.540	0.360	00 <u>10</u>	35
5	26.190	3.402	0.165	115	25
6	28.810	3.097	0.270	00 <u>12</u>	46
7	30.08	2.978	0.645	220*	100
8	31.840	2.808	0.270	119	32
9	33.110	2.703	0.180	200	47
10	35.450	2.530	0.315	11 <u>11</u>	26
11	43.08	2.102	0.360	400*	32
12	43.740	2.067	0.165	00 <u>18</u>	8
13	44.510	2.033	0.150	20 <u>12</u>	21
14	47.560	1.910	0.345	220	24
15	47.990	1.894	0.345	11 <u>17</u>	21
16	49.080	1.854	0.195	00 <u>20</u>	18
17	53.345	1.716	0.465	420*	37

\* Substrate peaks

Table 5.3 (b): XRD data of Ba<sub>2</sub>CeZrO<sub>5.5</sub> - Bi (2223) composite

No	2θ (deg)	D (Å)	width (deg.)	Hkl	I / I <sub>o</sub>
1	4.730	18.549	0.165	002	19
2	5.740	15.384	0.270	002 <sup>●</sup>	20
3	23.101	3.847	0.255	008 <sup>●</sup>	19
4	23.910	3.719	0.285	0010	21
5	24.752	3.594	0.210	113 <sup>●</sup>	16
6	26.190	3.402	0.195	115	7
7	27.369	3.594	0.210	115 <sup>●</sup>	32
7	28.940	3.146	0.390	0012	32
8	29.080	3.068	0.165	0010 <sup>●</sup>	35
9	29.450	3.068	0.165	220 <sup>*</sup>	100
10	31.040	2.878	0.375	117 <sup>●</sup>	19
11	31.860	2.807	0.285	119	32
12	33.100	2.704	0.345	200	32
13	33.750	2.653	0.360	0014	25
14	35.040	2.558	0.180	119 <sup>●</sup>	35
15	35.450	2.533	0.195	1111	17
16	42.180	2.099	0.430	400 <sup>*</sup>	30
17	43.740	2.067	0.165	2010	11
18	44.420	2.033	0.315	2012	14
19	47.540	1.911	0.195	220	21
20	47.990	1.894	0.315	1117	14
21	52.190	1.648	0.575	420 <sup>*</sup>	30
22	55.696	1.648	0.315	315 <sup>●</sup>	18

● Bi (2212); \* Substrate peak

Table 5.3 (c): XRD data of Ba<sub>2</sub>EuZrO<sub>5.5</sub> - Bi (2223) composite

No	2θ (deg)	d (Å)	Width (deg.)	hkl	I / I <sub>o</sub>
1	4.760	18.549	0.240	002	36
2	9.370	9.430	0.360	004	3
3	19.120	4.638	0.270	008	10
4	23.880	3.540	0.360	0010	40
5	26.190	3.402	0.165	115	25
6	28.810	3.097	0.270	0012	46
7	29.265	2.978	0.645	220*	100
8	31.840	2.808	0.270	119	32
9	33.110	2.703	0.180	200	47
10	35.450	2.530	0.315	1111	26
11	42.994	2.102	0.360	400*	32
12	43.740	2.067	0.165	0018	8
13	44.510	2.033	0.150	2012	21
14	47.560	1.910	0.345	220	24
15	47.990	1.894	0.345	1117	21
16	49.080	1.854	0.195	0020	18
17	53.345	1.716	0.465	420*	37

\* Substrate peak

Table 5.3 (c): XRD pattern of Ba<sub>2</sub>YbZrO<sub>5.5</sub> - Bi (2223) composite

No	2θ (deg)	D (Å)	width (deg.)	hkl	I / I <sub>0</sub>
1	4.760	18.549	0.240	002	61
2	5.740	15.384	0.240	002 <sup>●</sup>	30
3	19.120	4.638	0.330	008	21
4	23.100	3.808	0.360	008 <sup>●</sup>	24
5	24.808	3.586	0.300	113 <sup>●</sup>	29
6	26.190	3.402	0.195	115	27
7	28.840	3.582	0.390	0012	60
8	29.180	3.060	0.165	0010 <sup>●</sup>	27
9	30.084	2.968	0.210	220 <sup>*</sup>	100
10	31.040	2.878	0.375	117 <sup>●</sup>	47
11	31.880	2.805	0.315	119	32
12	33.100	2.704	0.345	200	62
13	33.760	2.653	0.360	0014	57
14	35.050	2.558	0.180	119 <sup>●</sup>	29
15	35.410	2.533	0.195	1111	30
16	43.070	2.099	0.430	400 <sup>*</sup>	24
17	44.510	2.033	0.315	2012	20
18	47.540	1.911	0.195	220	31
19	47.990	1.894	0.315	1117	23
20	49.080	1.854	0.210	0020	20
21	53.080	1.724	0.575	420 <sup>*</sup>	33

● Bi (2212); \* Substrate peak

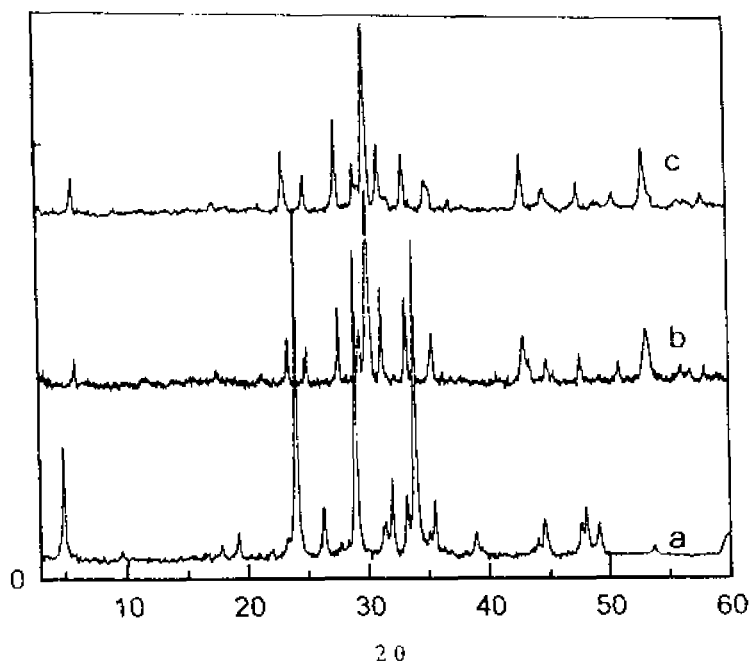


**Figure 5. 10:** (a) 1: 1 volume mixture of Bi (2223) and  $\text{Ba}_2\text{HoZrO}_{5.5}$ ,  
 (b) 1: 1 volume mixture of Bi (2223) and  $\text{Ba}_2\text{ErZrO}_{5.5}$ ,  
 all heated at  $850^\circ\text{C}$

**Table 5.4:** Volume fraction of  $\text{Ba}_2\text{REZrO}_{5.5}$  – Bi (2223) composite

Material	Y	Volume fraction of Bi (2223) (%)
$\text{Ba}_2\text{LaZrO}_{5.5}$	28.81	100
$\text{Ba}_2\text{CeZrO}_{5.5}$	28.94	50
$\text{Ba}_2\text{EuZrO}_{5.5}$	28.81	100
$\text{Ba}_2\text{YbZrO}_{5.5}$	28.84	85
$\text{Ba}_2\text{HoZrO}_{5.5}$	No peak	0
$\text{Ba}_2\text{ErZrO}_{5.5}$	No peak	0

The effect of  $\text{Ba}_2\text{REZrO}_{5.5}$  addition on the superconducting properties of Bi (2223) was studied by temperature-resistance measurements. Superconducting Bi (2223) and  $\text{Ba}_2\text{REZrO}_{5.5}$  were mixed in 4:1 volume ratio and pressed in the form of pellets at a pressure of 300 MPa. These discs were sintered at  $850^\circ\text{C}$  for 15 h and then slow cooled at the rate of  $2^\circ\text{C}/\text{min}$  to  $800^\circ\text{C}$  and then furnace cooled to room temperature. The resistance measurements of the composite compacts were made by standard four-probe technique using a nanovoltmeter (model 181, Kiethley Instruments, Cleveland, OH) and a current source (model 220, Kiethley). The temperature of the sample was measured by a calibrated copper Constantine thermocouple calibrated with a RF 800 rhodium-iron resistance sensor with an accuracy of  $\pm 0.2\text{K}$ . Figure 5.11 (a-f) shows the resistivity versus temperature curve for the Bi (2223)-  $\text{Ba}_2\text{REZrO}_{5.5}$  composites containing 20 vol.% of  $\text{Ba}_2\text{REZrO}_{5.5}$  annealed at  $850^\circ\text{C}$  for 15 h. A superconducting transition of 110 K was obtained for composite containing La, Ce, Eu, and Yb as rare-earth element. This indicate that a substantial addition of  $\text{Ba}_2\text{REZrO}_{5.5}$  (RE= La, Ce, Eu and Yb) in Bi (2223) did not have any detrimental effect on the superconducting transition temperature of Bi (2223) even after severe heat treatment. But the composite mixture gave a  $T_C$  of 85 K when RE = Ho and Er. This reduction in  $T_C$  is due to the decomposition of Bi (2223) in to Bi (2212) when annealed the composite mixture at  $850^\circ\text{C}$  for 15 h.

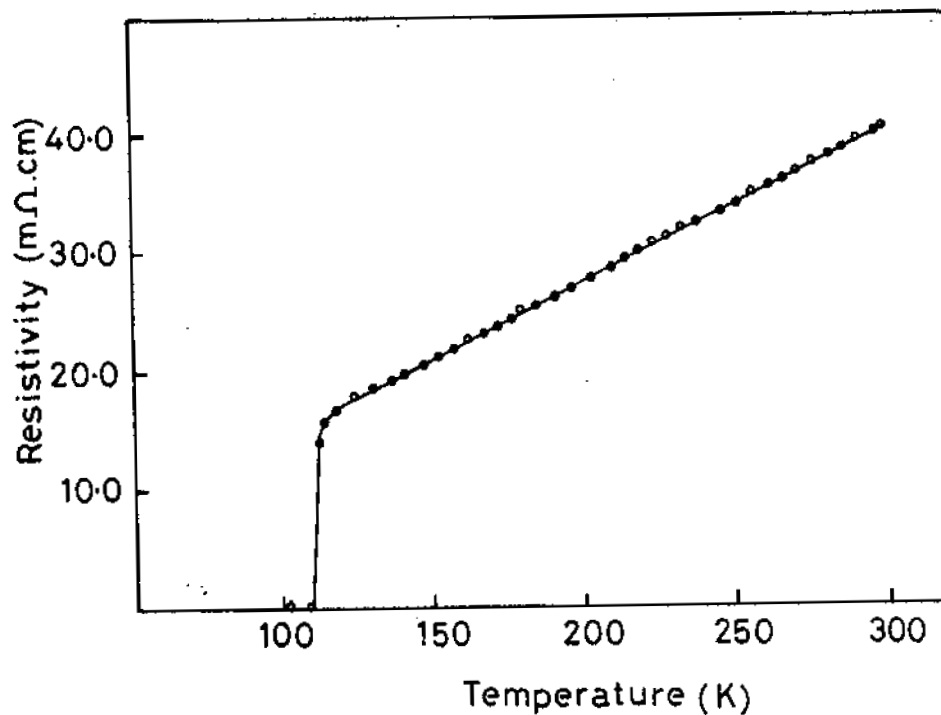


Figure 5. 11 (a): Temperature-resistivity curve for Bi (2223)- $\text{Ba}_2\text{LaZrO}_{5.5}$  composite containing 20 volume % of  $\text{Ba}_2\text{LaZrO}_{5.5}$

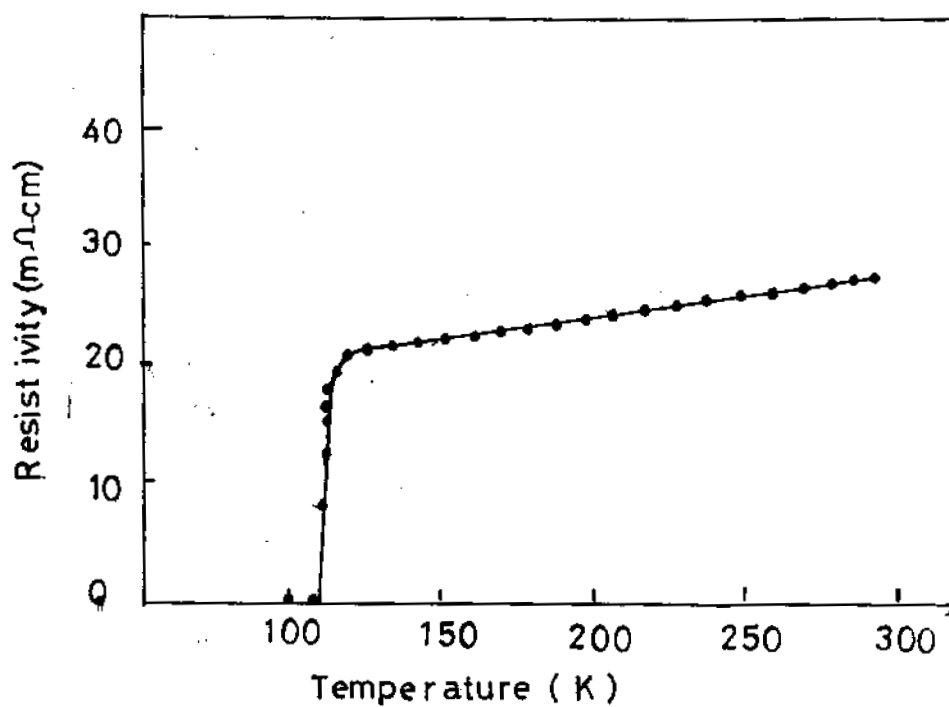


Figure 5. 11 (b): Temperature-resistivity curve for Bi (2223)- $\text{Ba}_2\text{CeZrO}_{5.5}$  composite containing 20 volume % of  $\text{Ba}_2\text{CeZrO}_{5.5}$

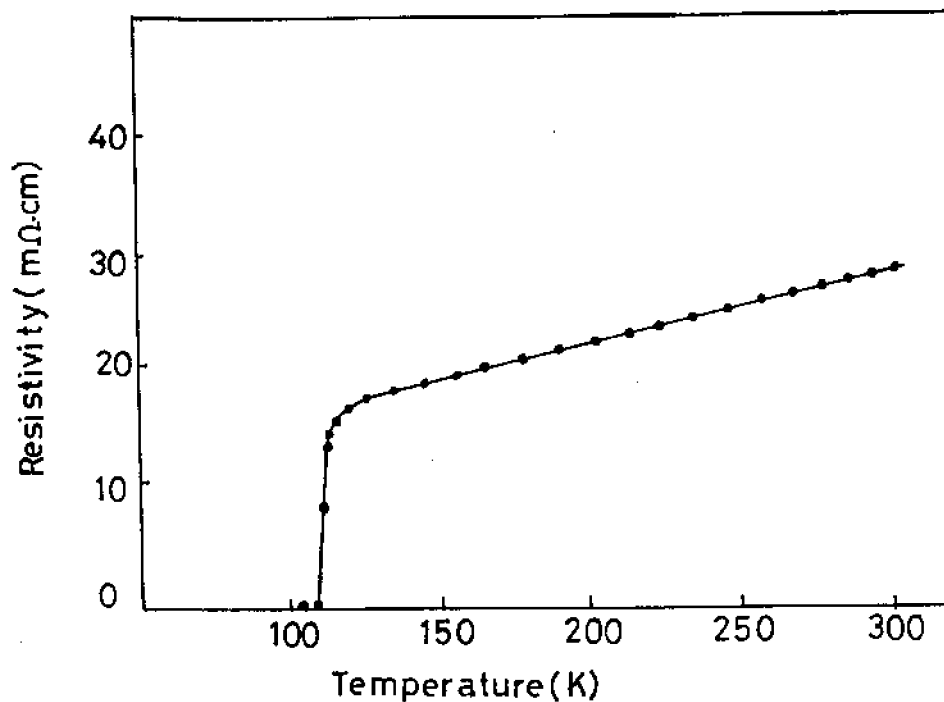


Figure 5. 11 (c): Temperature-resistivity curve for Bi (2223)- $\text{Ba}_2\text{EuZrO}_{5.5}$  composite containing 20-volume % of  $\text{Ba}_2\text{EuZrO}_{5.5}$

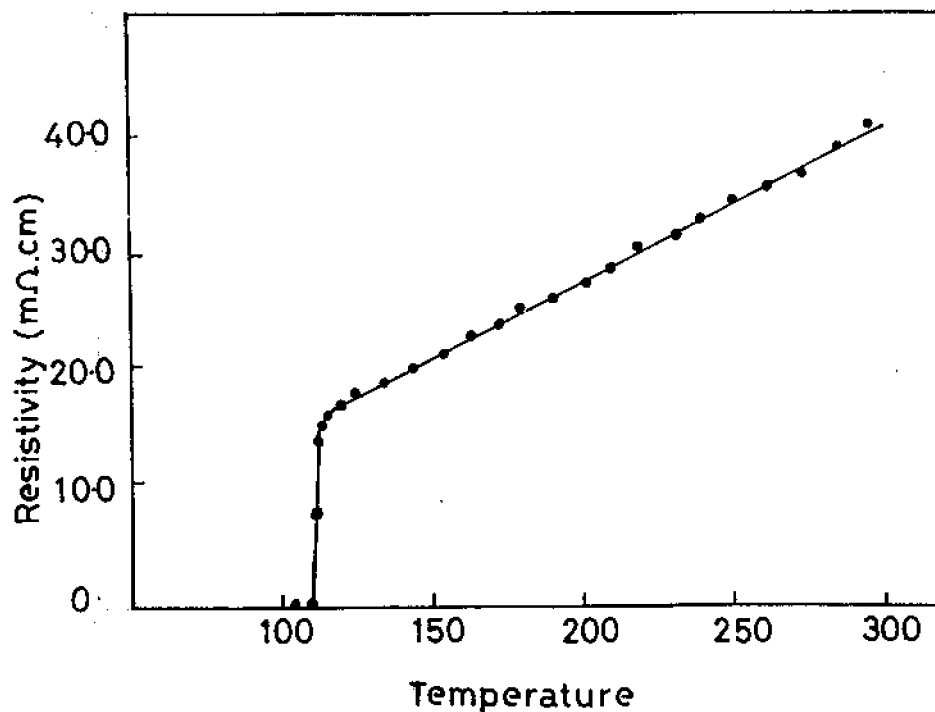


Figure 5. 11 (d): Temperature-resistivity curve for Bi (2223)- $\text{Ba}_2\text{YbZrO}_{5.5}$  composite containing 20 volume % of  $\text{Ba}_2\text{YbZrO}_{5.5}$

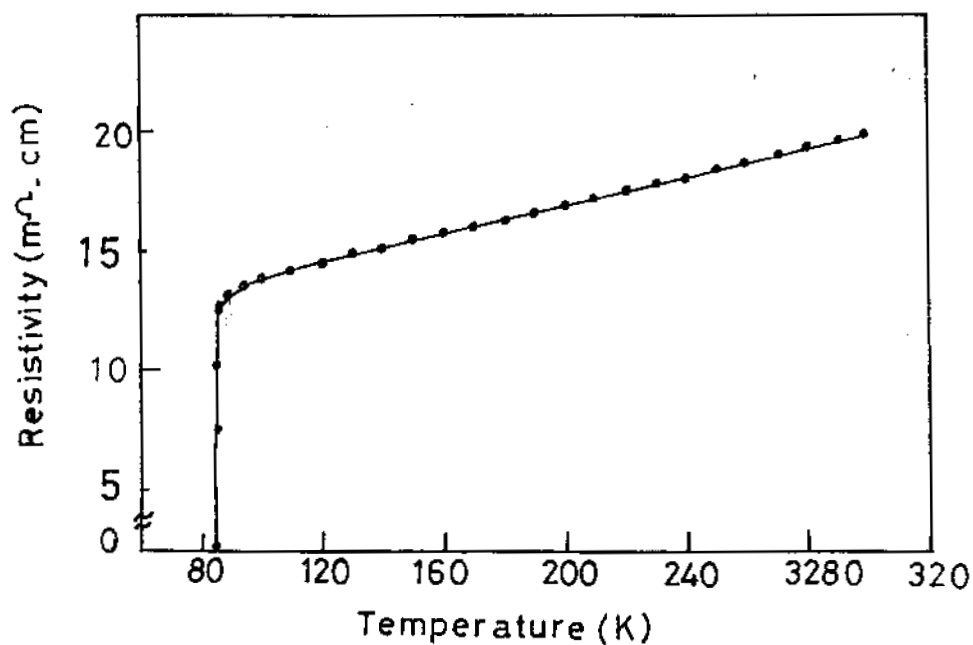


Figure 5. 11 (e): Temperature-resistivity curve for Bi (2223)- $\text{Ba}_2\text{HoZrO}_{5.5}$  composite containing 20 volume % of  $\text{Ba}_2\text{HoZrO}_{5.5}$

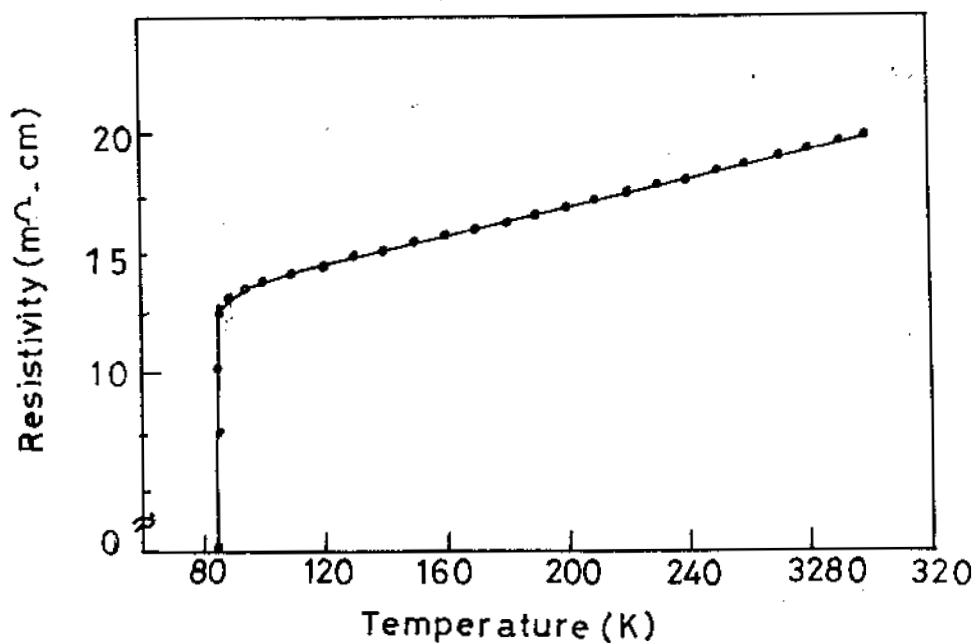


Figure 5. 11 (f): Temperature-resistivity curve for Bi (2223)- $\text{Ba}_2\text{ErZrO}_{5.5}$  composite containing 20-volume % of  $\text{Ba}_2\text{ErZrO}_{5.5}$

## 5.6 Development of Bi (2223) thick films on $\text{Ba}_2\text{REZrO}_{5.5}$ :

The suitability of  $\text{Ba}_2\text{REZrO}_{5.5}$  (RE = La and Eu) as substrate for Bi (2223) superconductor was confirmed by developing superconducting Bi (2223) thick films on them by dip-coating and melt texturing. The Bi (2223) suspension for dip-coating was prepared by thoroughly mixing fine superconducting Bi (2223) powder with isopropyl alcohol or n-butanol and the viscosity of the suspension was controlled by the addition of commercially available fish oil. The polished and cleaned  $\text{Ba}_2\text{REZrO}_{5.5}$  substrate was then dipped in the Bi (2223) suspension and dried. This step was repeated till a required thickness is attained. The dip-coated films were then dried in an oven and heated in a programmable furnace at a rate of  $5^\circ\text{C}/\text{min}$  in air up to  $880^\circ\text{C}$  and kept at this temperature for 2 min and then annealed at  $850^\circ\text{C}$  temperature for 6 h. The films were then cooled at a rate of  $1^\circ\text{C} / \text{min}$  up to  $800^\circ\text{C}$  from the annealing temperature of  $850^\circ\text{C}$  and then furnace cooled to room temperature. The heating schedule adopted for the preparation of Bi (2223) film is given in figure 5.12. Heating up to  $880^\circ\text{C}$  was required to get good adhesion between the film and the substrate. A peel off-test carried out using highly adhesive tape confirmed the excellent adhesion of the Bi (2223) films to the substrates

The structure of the Bi (2223) films dip-coated on  $\text{Ba}_2\text{REZrO}_{5.5}$  substrate were studied by x-ray diffraction and the superconductivity of the films were studied by temperature-resistance measurements using a standard four probe technique. Figures 5.13 and 5.14 show the XRD patterns of Bi (2223) films dip-coated on  $\text{Ba}_2\text{LaZrO}_{5.5}$  and  $\text{Ba}_2\text{EuZrO}_{5.5}$  substrates. Except for the characteristic peaks of  $\text{Ba}_2\text{REZrO}_{5.5}$  all the other peaks in figures 5.13 and 5.14 are those of orthorhombic Bi (2223). The phase purity of Bi (2223) film was further confirmed by calculating the volume fraction of Bi (2223) from the XRD data using the empirical relation given in equation 5.1. The

calculation using the above empirical relation shows that the volume fraction of Bi (2223) in the dip-coated film on  $\text{Ba}_2\text{REZrO}_{5.5}$  is 100%. Figures 5.15 and 5.16 shows the temperature-resistance curve for dip-coated Bi (2223) films on  $\text{Ba}_2\text{REZrO}_{5.5}$  substrates. The films showed metallic behavior in the normal state and gave a zero resistivity transition of 110 K. The Critical current density ( $J_C$ ) of the film measured using  $1\mu\text{V}$  criteria was  $\sim 3 \times 10^3 \text{ A/cm}^2$  at 77 K under zero applied magnetic field. Because of the high processing temperature and partial melting of the Bi (2223) films in the dip-coating and melt texturing process the films adhered very well to the  $\text{Ba}_2\text{REZrO}_{5.5}$  substrates. This clearly confirms that the newly developed  $\text{Ba}_2\text{REZrO}_{5.5}$  materials are potentially suited for their application as substrates for superconducting Bi (2223) films for various device applications.

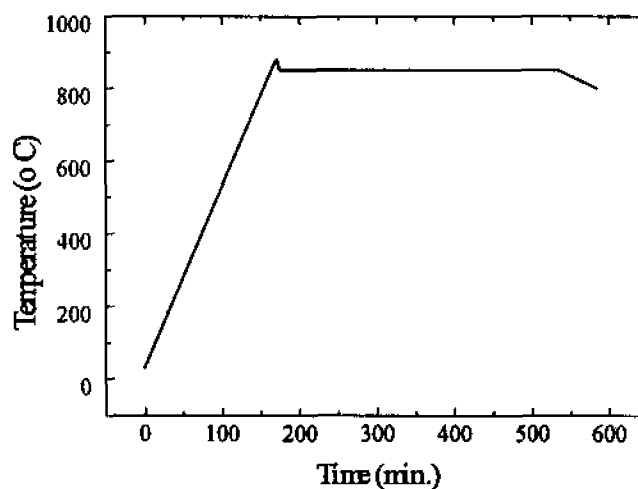


**Figure 5. 12:** Heating schedule adopted for the preparation of Bi (2223) thick films on  $\text{Ba}_2\text{REZrO}_{5.5}$  substrates.

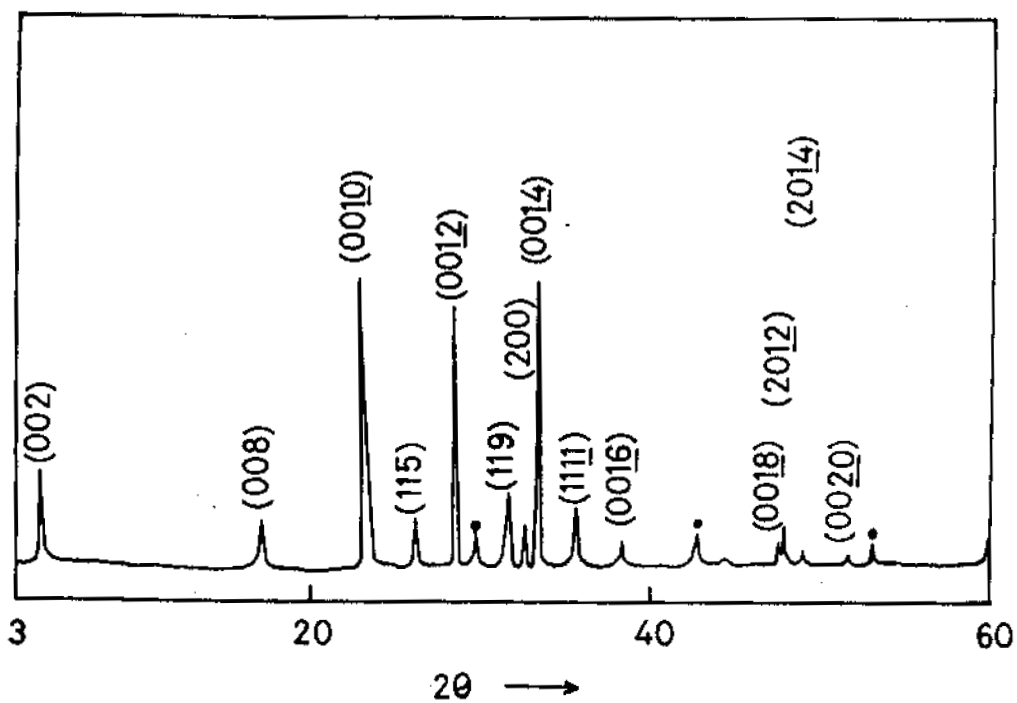


Figure 5.13: XRD pattern of Bi (2223) thick films developed on  $\text{Ba}_2\text{LaZrO}_{5.5}$  substrate.

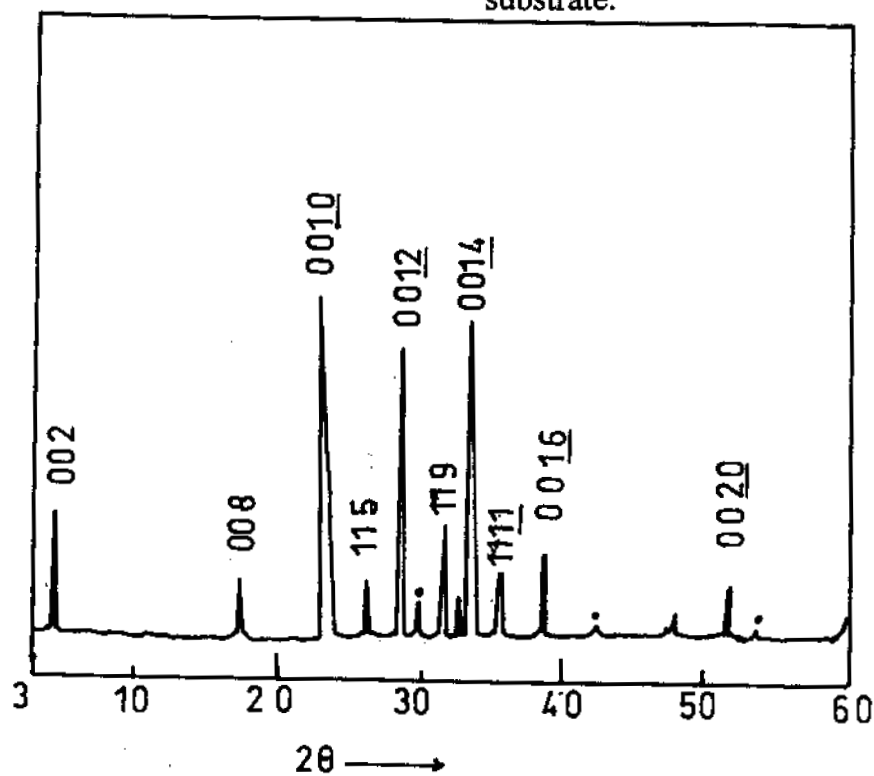
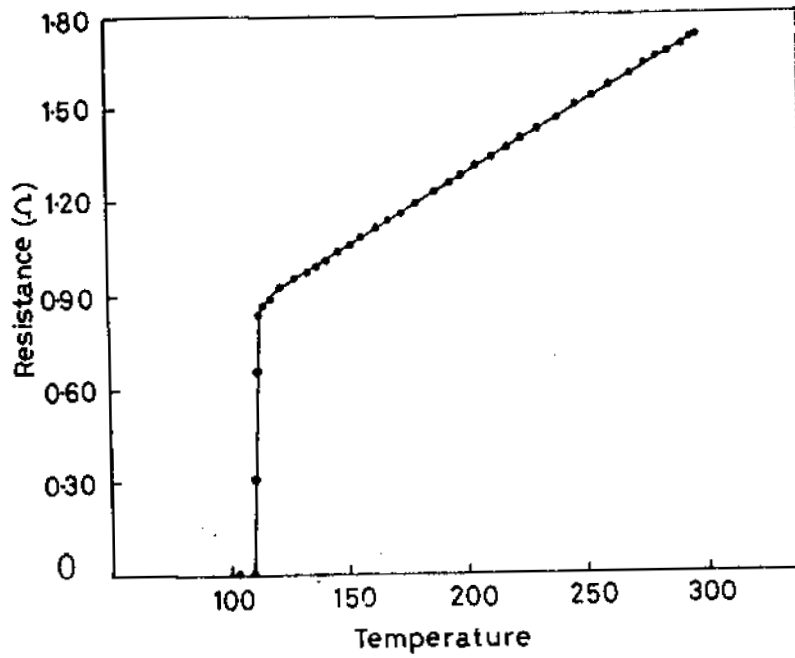
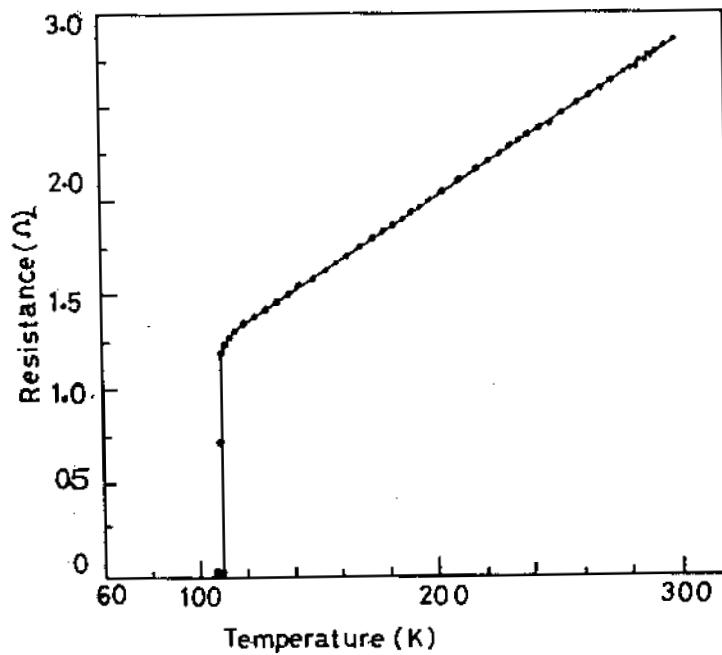


Figure 5.14: XRD pattern of Bi (2223) thick films developed on  $\text{Ba}_2\text{EuZrO}_{5.5}$  substrate



**Figure 5.15:** Temperature-resistance curve for dip-coated Bi (2223) thick film on  $\text{Ba}_2\text{LaZrO}_{5.5}$  substrate



**Figure 5.15:** Temperature-resistance curve for dip-coated Bi (2223) thick film on  $\text{Ba}_2\text{EuZrO}_{5.5}$  substrate

## 5.8 Conclusions

Single-phase  $\text{Bi}_2\text{Sr}_2\text{CaCu}_2\text{O}_x$  [ $T_{C(0)} = 85$  K] and  $\text{Bi}_{1.5}\text{Pb}_{0.5}\text{Sr}_2\text{Ca}_2\text{Cu}_3\text{O}_x$  [ $T_{C(0)} = 110$  K] superconductors were synthesized and sintered through solid state route. X-ray diffraction and resistivity measurements have shown that the newly developed  $\text{Ba}_2\text{REZrO}_{5.5}$  substrates are chemically non-reacting with Bi (2212) superconductors even under extreme processing conditions. A superconducting transition of 85 K was obtained in all the composite mixture consisting of  $\text{Ba}_2\text{REZrO}_{5.5}$  and Bi (2212) containing 0-50 vol. % of Bi (2212) superconductor. The suitability of  $\text{Ba}_2\text{REZrO}_{5.5}$  materials as substrate for Bi (2212) was confirmed by developing superconducting Bi (2212) thick films on  $\text{Ba}_2\text{REZrO}_{5.5}$  materials by dip-coating and melt texturing. The films showed metallic behavior in the normal state and gave a  $T_{C(0)}$  of 85 K and  $J_C 4 \times 10^3$  A /  $\text{cm}^2$  at 77 K under zero applied magnetic field. The suitability of  $\text{Ba}_2\text{REZrO}_{5.5}$  as substrates for Bi (2223) superconductor has also been studied. The results of chemical reactivity studies between  $\text{Ba}_2\text{REZrO}_{5.5}$  and Bi (2223) superconductor indicates that the newly developed materials with RE = La and Eu are chemically non-reacting with the Bi (2223) superconductor even at the extreme processing conditions. Bi (2223) does not react with  $\text{Ba}_2\text{REZrO}_{5.5}$  (RE = La and Eu) even after annealing a 1: 1 volume mixture at 850°C for 10h, and the addition of  $\text{Ba}_2\text{REZrO}_{5.5}$  up to 20 vol.% in Bi (2223) did not show any detrimental effect on the superconducting properties of Bi (2223). The materials with RE = Ce, Yb, Ho and Er were either decomposed fully or partially in to Bi (2212) when annealed at a temperature of 850°C for 15 h. The suitability of  $\text{Ba}_2\text{REZrO}_{5.5}$  materials as substrate for Bi (2223) was confirmed by developing superconducting thick films of Bi (2223) superconductors on  $\text{Ba}_2\text{REZrO}_{5.5}$  materials by dip-coating and melt texturing. The film showed metallic behavior in the normal state and adhered very well with the substrate. The Bi (2223) film dip-coated and melt textured on  $\text{Ba}_2\text{LaZrO}_{5.5}$  gave a  $T_{C(0)}$  of 110 K and  $J_C 3 \times 10^3$  A /  $\text{cm}^2$  at 77 K under zero applied magnetic field.

**References**

- [1] K. Hoshino, H. Takahara, M. Fukutomi, *1st Int. Symp. Supercond., ISS-88, Advances in Superconductivity*, pp. 325 (1988).
- [2] D. P. Almond, B. Chapman, G. A. Saunders, *Supercond. Sci. Technol.*, **1**, (1988) 123.
- [3] P. Bordet, J. J. Capponi, C. Chaillout, J. Chenavas, A. W. Hewat, E. A. Hewat, J. L. Hodeau, M. Marezio, , *Vol. 2*, Nova Publishers 1989.
- [4] H. K. Liu, S. X. Dou, N. Savvides, J. P. Zhou, N. X. Tan, A. J. Bourdillon, M. Kuiz, C. C. Sorrel, *Physica C*, (1989) 93.
- [5] U. Balachandran, D. Shi, D. I. D. Stantos, S. W. Graham, M. A. Patel, B. Tani, K. Vadervoort, H. Claus, R. B. Poppel, *Physica C*, **156**, (1988) 649.
- [6] S. A. Sunshine, T. Seigrist, L. F. Schneemeyer, D. W. Murphy, R. J. Cava, B. Bratlog, R. B. v. Dover, R. M. Fleming, S. M. Glarum, S. Nakahara, R. Farrow, J. J. Krajewski, S. M. Zahurak, J. V. Waszczak, J. H. Marshall, P. Marsh, L. W. Rupp, W. F. Peck, *Phys. Rev. B*, **38**, (1988) 893.
- [7] M. Takano, J. Takada, K. Oda, H. Kitaguchi, Y. Ikeda, Y. Tomii, H. Mazeki, *Jpn. J. Appl. Phys.*, **27**, (1989) 1041.
- [8] Y. Takemura, M. Hongo, S. Yamjaki, *Jpn. J. Appl. Phys.*, **28**, (1989) L916.
- [9] N. M. Alford, T. W. Button, M. J. Adams, S. Hedges, B. Micholson, W. A. Phillips, *Nature*, **349**, (1991) 680.
- [10] N. M. Alford, T. W. Button, D. Opie, *Supercond. Sci. Technol.*, **4**, (1991) 433.
- [11] N. M. Alford, T. W. Button, *Adv. Mater.*, **30**, (1991) 318.
- [12] N. P. Bensal, R. N. Simons, D. E. Farrel, *Appl. Phys. Lett.*, **53**, (1988) 603.
- [13] N. P. Bensal, *Mater. Lett.*, **13**, (1992) 7.
- [14] E. Saiz, J. S. Moya, *Supercond. Sci. Technol.*, **5**, (1992) 130.

- [15] N. Khare, A. K. Gupta, S. Chaudhury, V. S. Tomer, *Supercond. Sci. Technol.*, **4**, (1991) 433.
- [16] Y. Matsouka, E. Ban, H. Ogawa, A. Suzumura, *Supercond. Sci. Technol.*, **4**, (1991) 62.
- [17] J. M. Phillips, *J. Appl. Phys.*, **79**, (1996) 1829.
- [18] S. X. Dou, H. K. Liu, S. J. Guo, K. E. Esterling, J. Mikael, *Supercond. Sci. Technol.*, **2**, (1989) 274.
- [19] A. Agrawal, R. P. Gupta, W. S. Khokale, K. D. Kundra, P. R. Deshmukh, M. Singh, P. D. Vyas, *Supercond. Sci. Technol.*, **6**, (1993) 670.
- [20] W. C. McGinnis, J. J. Briggs, *J. Mater. Res.*, **7**, (1992) 585.
- [21] F. H. Chen, H. S. Koo, T. Y. Tseng, *J. Am. Ceram. Soc.*, **75**, (1992) 96.

## CHAPTER VI

# SYNTHESIS AND CHARACTERIZATION OF NANOPARTICLES OF BARIUM RARE-EARTH ZIRCONATES THROUGH A NOVEL COMBUSTION ROUTE

### 6.1 Introduction

Synthesis of advanced ceramics and specialty materials as nanoparticles, or nanocrystalline materials, is one of the major fields in material-processing technology [1-6]. The specific advantages of nanocrystalline materials are superior phase homogeneity, purity, sinterability and microstructure leading to unique mechanical, electrical, dielectric, magnetic, optical, and catalytic properties [2-6]. A brief write-up on the properties and classification of the nanostructured materials are given in the introductory chapter. By using conventional solid state route, it is not possible to obtain a nanosized powder because the initial sizes of the reactants themselves are much higher.

In earlier chapters, we have described the synthesis of a new group of complex perovskite ceramic oxides,  $Ba_2REZrO_{5.5}$  (RE = La, Ce, Eu, Yb, Ho and Er), through conventional solid state method and characterization for their potential use as substrates for high  $T_C$  superconductors. These materials are found to be non-reacting with YBCO and Bi (2212) superconductors at extreme processing conditions and have attractive dielectric properties for their use as substrates for these high temperature superconductors at microwave frequencies. Two materials in this group with RE = La and Eu are found to be non-reacting with Bi (2223) superconductor also even at extreme processing conditions. But the synthesis of  $Ba_2REZrO_{5.5}$  materials through the conventional solid state method

was found to be tedious due to the repeated calcination of the reaction mixture at high temperatures for prolonged duration. To synthesize these materials as phase pure powders by solid state route, very prolonged heating at temperature  $\sim 1350^{\circ}\text{C}$  were required. In order to achieve high density, the powder compacts were sintered up to an elevated temperature of  $1675^{\circ}\text{C}$  for prolonged duration. A few materials in this group could not be synthesized or sintered as single component materials without the addition of CuO. The high temperature processing leads to the unwanted microstructure coarsening leading to poor sinterability and physical properties [7]. In order to improve the characteristics of the powder, especially their sinterability and phase purity, attempts were made to synthesize  $\text{Ba}_2\text{REZrO}_{5.5}$  materials as nanoparticles. We have now developed a modified combustion process for the synthesis of  $\text{Ba}_2\text{REZrO}_{5.5}$  as nanoparticles. The synthesis of  $\text{Ba}_2\text{REZrO}_{5.5}$  (RE= Y, La, Eu, Ho and Er) as nanoparticles and the characterization of the combustion product by X-ray and electron diffraction, Differential Thermal Analysis, Thermogravimetric analysis, infrared spectroscopy, BET surface area determination, gas adsorption studies, agglomerate size analysis, and high-resolution transmission electron microscopy described in this chapter. The sintering of nanosized  $\text{Ba}_2\text{REZrO}_{5.5}$  powders and structures of the sintered samples are studied in detail and the results are presented. A brief write-up on various wet-chemical methods for the synthesis of nanoparticles of ceramic oxides is also given in this chapter.

## 6.2 Wet Chemical methods:

Wet chemical methods or liquid phase synthesis represents a large number of preparation methods, which in general starting with an inorganic or metal-organic precursor solutions [8]. The most important wet-chemical methods can be

subdivided into five groups. (i) Dispersion methods: This technique is based on the dispersion of a precursor solution in small droplets or atomization prior to drying in air or in a non-mixable liquid. In this way, the distance of phase separation during drying and calcining is limited by the dimensions of the submicron droplets. Individual granular particles of the desired ceramic can be obtained by drying these droplets followed by calcination. Emulsion techniques [1,9,10], spray drying [11], freeze drying [12,13] etc., are the powder preparation routes based on this method. (ii) Immobilization techniques: In this process the solution is immobilized in some way or another. Demixing during the wet chemical preparation is retarded in this way. This immobilization is done by the formation of a glassy or gelatinous matrix in which the precursor is dispersed or by making a polymeric network. For example, the precursor can be immobilized by complexation with organic acids or alcohols. Processing from polymeric precursors [14-16], oxalate route [17-19], citrate route [20-22], etc. are techniques employing this principle. (iii) Precipitation: This procedure is in general based on the controlled hydrolysis of an aqueous solution of metal salts or an alcoholic solution of metal organic compounds. The precursor solution is strongly diluted, while precipitation takes place in strongly basic or neutral medium. In this way it is possible that precursor solution precipitates instantaneously at high nucleation rate. But in the case of multicomponent system it is likely that various components precipitate at different pH values of the solution and this would affect adversely the powder homogeneity. Prior to drying and calcination, the reaction by products such as alcohol, chlorides or nitrates are washed out by water. Washing may selectively remove a precipitated component, which result in change in chemical homogeneity and composition. The filtered precipitate after washing is calcined at high temperatures. Coprecipitation [23-25], hydrothermal synthesis [26-28] etc are

techniques employing precipitation reaction. (iv) Sol-gel processing: Sol-gel process has been proposed to be very effective method for producing ceramic oxides for various structural and electronic applications [29-31]. In sol-gel processing, colloidal particles in a suspension, a sol is mixed with a liquid, which causes the colloidal particles to join together into a network called a gel. A gel can also be formed by extracting part of the solvent from the sol. Polymerization during the gelation step greatly restricts chemical diffusion and segregation. The gel is dried and calcined. Sol-gel is a multi step operation involve the processing of high volume of liquid with relatively low yield has been pointed out as one of its main drawbacks. (v) Combustion synthesis: Recently, another processing technique termed as self-sustained combustion or combustion synthesis has been used to synthesis fine ceramic powders. The process of combustion synthesis involves rapid decomposition of a saturated aqueous solution containing metal salts, an oxidizer and a fuel. Mostly the powder obtained through combustion synthesis is single phase pure without the need for a calcination process. Therefore the method has energy and cost saving advantages. Combustion synthesis was used by Kingsley *et al* [32-34] for the synthesis of ceramic oxides. In this method, mixture of respective metal nitrates (oxidizers) and urea (fuel) were dissolved in minimum quantity of water and heated at 500 °C. Pramanik *et al* have used the thermolysis of a precursor mass consisting of metal nitrate solutions mixed with polymeric polyvinyl alcohol (PVA) in presence of urea at external temperatures of 300 °C to 500 °C to prepare a variety of ceramic oxides [35-39]. Hess *et al* applied combustion synthesis by using glycene as fuel to prepare Yttrium Aluminium Garnet [40]. All these methods of combustion synthesis is limited to the preparation of those compound which have water soluble metal salts.

### 6.3 The modified combustion process <sup>☆</sup>

We have developed a modified combustion process for the synthesis of nanoparticles of ceramic oxide powders using metal salts, which are even insoluble in water. Here a solvent, which dissolves all the metal salts required for the preparation of particular ceramic oxide, is used. The solvent may be ethyl alcohol, methyl alcohol, ethylene diamine tetra acetic acid, water etc. In this new method no calcination step is involved and phase pure nanoparticle powder is obtained at a relatively low temperature ( $\sim 200^{\circ}\text{C}$ ) using a sand bath / hot plate. The details of procedure for the synthesis of ceramic oxides as nanoparticles through the present method comprises of (1) preparation of the solution of all the metal salts in the required stoichiometric ratio, (2) addition of required quantity of an organic complexing agent like citric acid or ethylene diamine tetra acetic acid (EDTA) to the solution, (3) Adjusting the ammonia / nitrate content in the system, and (4) heating the solution on a hot plate/ sand bath. On heating, the solution boils and undergoes dehydration followed by decomposition leading to smooth deflation producing a foam. The foam then ignites giving voluminous and fluffy product of combustion. The salts of metals may be selected from its alkoxides, oxides, nitrates, oxychlorides, carbonates or anything that could be brought in a solution. The ammonia/nitrate content is adjusted by addition of the appropriate reagents. Ammonia/nitrate could be added as  $(\text{NH}_4)\text{NO}_3$  or any of their derivatives depending on the system selected.

In the present combustion method, citric acid or EDTA was used as the complexing agent instead of polyvinyl alcohol and urea or glycine was replaced

---

<sup>☆</sup> *Indian Patent File No. NF 58 / 98 (1999)*

*US Patent File No. 09/ 537 252 dated 28 March 2000*

with ammonia. By this change of complexing agent and the oxidant / fuel system it was possible to obtain single-phase ceramic oxides in a single step combustion process and the usual calcination for prolonged duration at high temperature was not needed. The only heat source used for the present study is a hot plate / sand bath, hence the route has energy and cost saving advantages. The modified combustion route presented here has also avoided the use of any additives for the synthesis of complex perovskite oxides. The method is so versatile that single phase of any ceramic oxide can be synthesized as nanoparticles through this route and is beyond the scope of this thesis.

### 6.3 Synthesis of Nanoparticles of $Ba_2REZrO_{5.5}$ •

Aqueous solution containing the ions of Ba, RE, (RE= Y, La, Ce, Eu, Yb, Ho and Er) and Zr were prepared by dissolving stoichiometric amounts of high purity (99.9%)  $Ba(NO_3)_2 \cdot 5H_2O$ ,  $RE_2O_3$ , and  $ZrOCl_3 \cdot 8H_2O$ . Since  $RE_2O_3$  is insoluble in water, it was dissolved in 0.1 N nitric acid. Since nitrogen containing compounds leads to easier and cleaner burn out than chlorine containing compounds  $ZrOCl_3 \cdot 8H_2O$  solution was boiled with nitric acid until no trace of chlorine was detected by silver nitrate test [41]. The solutions were then mixed together and an appropriate amount of citric acid was added to it. The oxidant/ fuel ratio of the system was adjusted by the addition of ammonium hydroxide and nitric acid. The solution containing the precursor complex was then heated on a hot plate

---

Published in

**Nanostructured Materials, 11 (1999) 623;**

**Journal of Material Synthesis & Processing, 8, (2000) 1;**

**Journal of Materials Research, 15 (2000) 2125**

to about 250°C. Initially the solution boils and undergoes dehydration followed by decomposition leading to smooth deflation with enormous swelling producing a foam. The foam then gets ignited giving a voluminous and fluffy product of combustion.

#### **6.4 Characterization of Ba<sub>2</sub>REZrO<sub>5.5</sub> powders:**

The as-prepared Ba<sub>2</sub>REZrO<sub>5.5</sub> materials obtained by the present combustion route were characterized by different powder characterization techniques. The structure of the as-prepared and subsequently heated powders was studied by X-ray (XRD) and electron diffraction. In order to know whether there is any phase transition is taking place in the as-prepared sample, thermal analyses viz. Differential Thermal Analysis (DTA) and Thermogravimetric Analysis (TGA) have been carried out. The as-prepared samples were also characterized using IR spectroscopy, Gas adsorption studies and agglomerate size analyses. The powder morphology was studied using High Resolution Transmission Electron Microscopy (HRTEM).

##### **6.4.1 Structural Characterization of the combustion product**

The structure and phase purity of the powders were examined by XRD using a Rigaku, Dmax (Japan) X-ray diffractometer with nickel filtered Cu-K $\alpha$  radiation. Figures 6.1 (a) and 6.2 (a) show the XRD pattern of the as-prepared powder samples of Ba<sub>2</sub>LaZrO<sub>5.5</sub> and Ba<sub>2</sub>EuZrO<sub>5.5</sub> for 2 $\theta$  between 20° and 60°. The broad and diffused peak at  $d = 2.96$  and  $2.98$  Å correspond to the major (220) reflection of Ba<sub>2</sub>LaZrO<sub>5.5</sub> and Ba<sub>2</sub>EuZrO<sub>5.5</sub> respectively, indicating that the complex ceramic perovskite phase is formed during the combustion process itself. The near amorphous nature of the pattern suggests the ultrafine nature of the

powders obtained. The as prepared powders of  $\text{Ba}_2\text{LaZrO}_{5.5}$  and  $\text{Ba}_2\text{EuZrO}_{5.5}$  were heated in a muffle furnace at different temperatures between  $500^\circ\text{C}$  and  $1100^\circ\text{C}$  in order to understand their crystallization behavior. The XRD pattern of the subsequently heated powders of  $\text{Ba}_2\text{LaZrO}_{5.5}$  and  $\text{Ba}_2\text{EuZrO}_{5.5}$  are shown in figures 6.1 (b-d) and 6.2 (b-d) respectively. It may be noted that there is no structural change takes place in the samples other than increasing the crystallinity

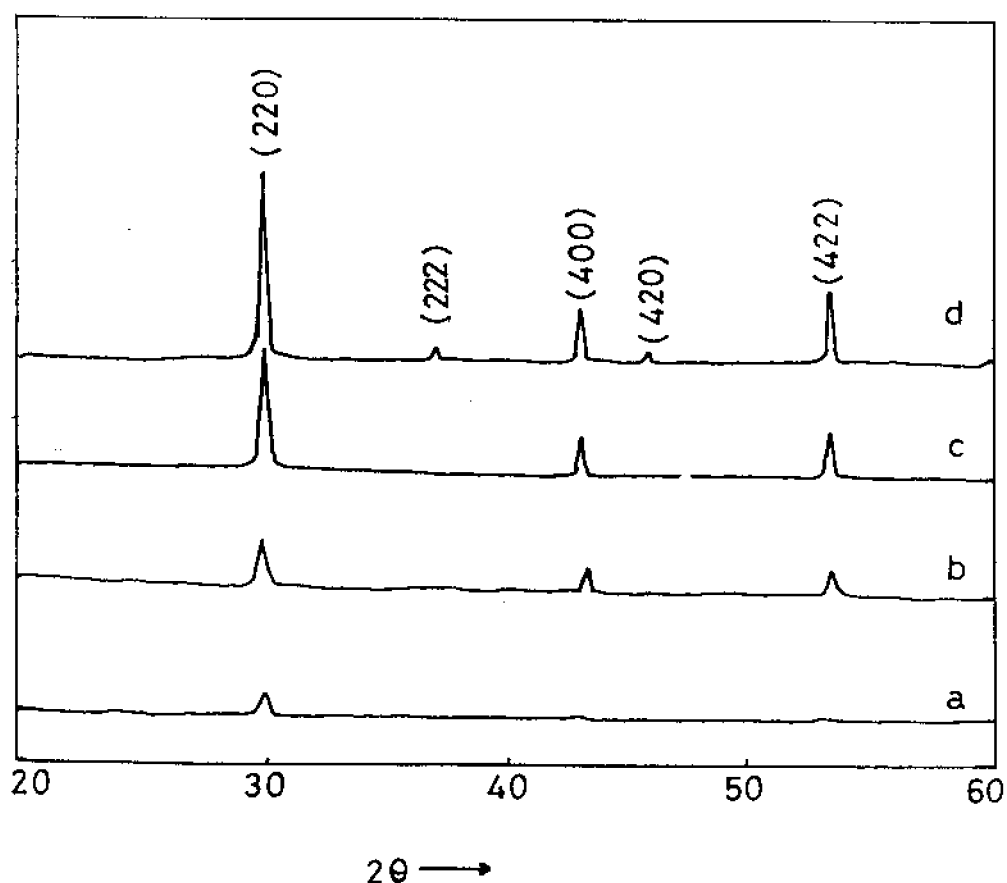


**Figure 6.1:** XRD pattern of  $\text{Ba}_2\text{LaZrO}_{5.5}$  (a) as-prepared, (b) heat treated at  $500^\circ\text{C}$ , (c)  $800^\circ\text{C}$  and (d)  $1100^\circ\text{C}$  each for 8 h in air

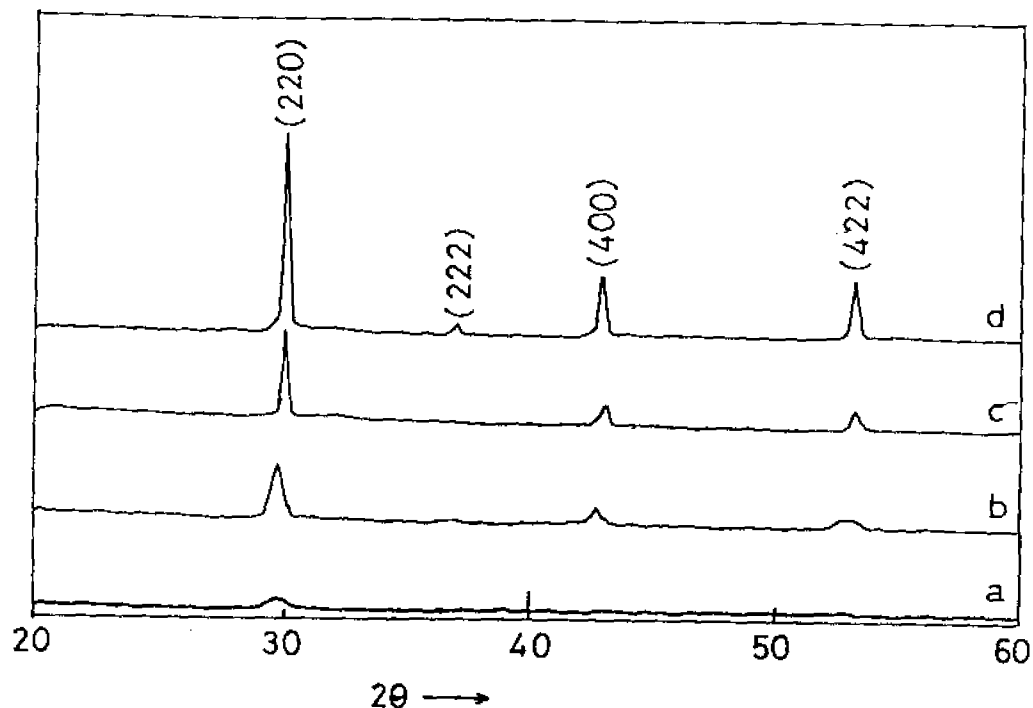


**Figure 6.2:** XRD pattern of  $\text{Ba}_2\text{EuZrO}_{5.5}$  (a) as-prepared, (b) heat treated at  $500^\circ\text{C}$ , (c)  $800^\circ\text{C}$  and (d)  $1100^\circ\text{C}$  each for 8 h in air

of  $\text{Ba}_2\text{LaZrO}_{5.5}$  and  $\text{Ba}_2\text{EuZrO}_{5.5}$  ceramics as the temperature is increased. There is no indication in the XRD patterns of any additional phase other than  $\text{Ba}_2\text{LaZrO}_{5.5}$  and  $\text{Ba}_2\text{EuZrO}_{5.5}$  either in the as prepared or in the heat-treated samples. These observations clearly show that the  $\text{Ba}_2\text{LaZrO}_{5.5}$  and  $\text{Ba}_2\text{EuZrO}_{5.5}$  phase formations was complete during the combustion process itself without the need for a calcination step. It may be noted that single phases of  $\text{Ba}_2\text{LaZrO}_{5.5}$  and  $\text{Ba}_2\text{EuZrO}_{5.5}$  materials can be obtained through solid state reaction route only after calcining the reaction mixture at a temperature of  $1350^\circ\text{C}$  for 72 h with intermediate grindings.

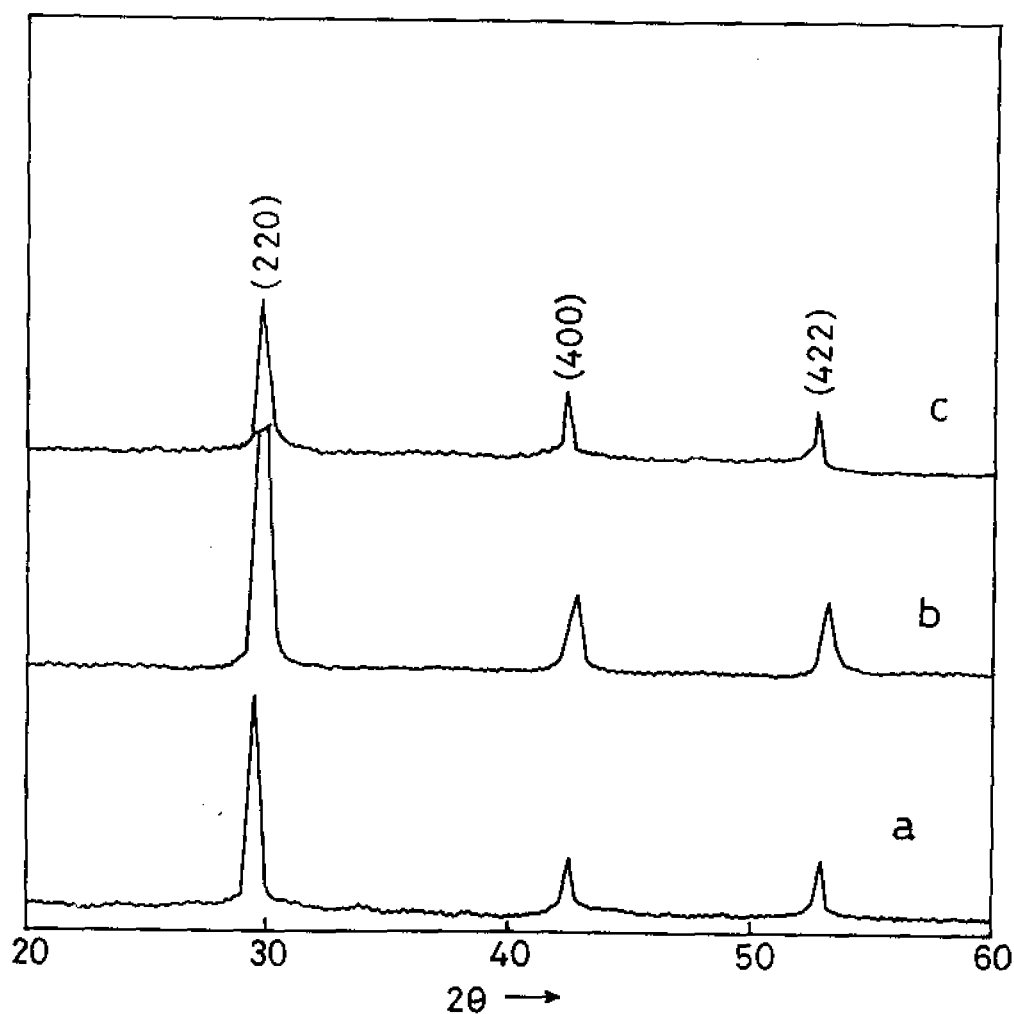


**Figure 6.3:** The XRD pattern of the powder obtained directly after combustion (a)  $\text{Ba}_2\text{YZrO}_{5.5}$ , (b)  $\text{Ba}_2\text{HoZrO}_{5.5}$ , (c)  $\text{Ba}_2\text{ErZrO}_{5.5}$

Figure 6.3 shows the XRD pattern of the as-prepared  $\text{Ba}_2\text{YZrO}_{5.5}$ ,  $\text{Ba}_2\text{HoZrO}_{5.5}$ , and  $\text{Ba}_2\text{ErZrO}_{5.5}$  powders obtained directly after combustion. All the peaks are indexed for a complex cubic perovskite structure corresponding to  $\text{Ba}_2\text{REZrO}_{5.5}$  (RE = Y, Ho and Er) materials. There was no indication in the XRD pattern of any additional phase in the as-prepared powder. In Table 6.1, the lattice constant

values calculated from the XRD patterns of the powders of  $\text{Ba}_2\text{REZrO}_{5.5}$  obtained through the present combustion route are compared with the corresponding powders obtained through the solid state route. These observations clearly show that the phase formation was complete during the combustion process itself, without the need for a calcination step. The broad nature of the peaks in fig. 6.3 indicates the ultrafine nature of the crystallites. As evident from the figure, the solid combustion products were single phase and no intermediate phases or unreacted components were present in the samples. It is interesting to note that  $\text{Ba}_2\text{REZrO}_{5.5}$  (RE = Y, Ho and Er) materials could not be synthesized as single phase materials through solid state route by using the constituent oxides or carbonates and the impurity addition was always required to obtain these material

**Table 6.1:** Lattice constant values and the particle size calculated from XRD pattern of the combustion synthesized  $\text{Ba}_2\text{REZrO}_{5.5}$  powders.

Material	Lattice constant (Å)		Full width at Half Maximum $\times 10^{-3}$ (rad.)	Particle size calculated from XRD (nm)
	Combustion synthesized	Sintered solid state powder		
$\text{Ba}_2\text{LaZrO}_{5.5}$	8.390	8.350	7.557	19
$\text{Ba}_2\text{EuZrO}_{5.5}$	8.453	8.420	13.03	11
$\text{Ba}_2\text{YZrO}_{5.5}$	8.400	8.400	7.976	18
$\text{Ba}_2\text{HoZrO}_{5.5}$	8.428	8.428	11.04	13
$\text{Ba}_2\text{ErZrO}_{5.5}$	8.453	8.445	9.407	15

as single phase. Crystallite size was calculated from the X-ray line broadening of (220) diffraction peak using Scherrer formula [42]

$$D = \frac{0.9\lambda}{\beta \cos\theta} \quad (6.1)$$

where D is the crystallite size in nm,  $\lambda$  is the wave length of the X-ray ( 1.5406Å),  $\beta$  is the corrected half width and  $\theta$  is the diffraction peak angle. The calculated crystallite size by assuming uniform particles are given in table 6.1.

#### 6.4.2 Thermal characterization of the combustion product

The thermal characterization of nanoparticles of  $\text{Ba}_2\text{REZrO}_{5.5}$  synthesized through the modified combustion process has been carried out using differential thermal analysis (DTA) and thermogravimetric analysis (TGA). The DTA was carried out using a Shimadzu DTA-50H differential thermal analysis up to 1100°C at a heating rate of 10°C/min in nitrogen atmosphere. The thermogravimetric analysis was done in the temperature range 30-1100°C using a Shimadzu 50 H unit in nitrogen atmosphere. Figures 6.4 to 6.7 shows the DTA and TGA curves of the as- prepared powders of  $\text{Ba}_2\text{REZrO}_{5.5}$  obtained directly after combustion. In all the cases TGA shows a loss of weight at ~100°C which can be due to the adsorbed moisture present in the sample. This weight change corresponds to an endothermic reaction in the DTA curve at 100°C. Even though the materials were dried initially before recording the DTA and TGA curve, because of its ultrafine nature moisture adsorption occurs immediately on the exposure to the atmosphere. Thereafter neither the weight nor the enthalpy of the samples changed till 1100°C. This implies that the combustion is complete during the process itself and no organic intermediates were present in the

samples. There was also no evidence of any phase transition taking place in the sample up to this temperature.

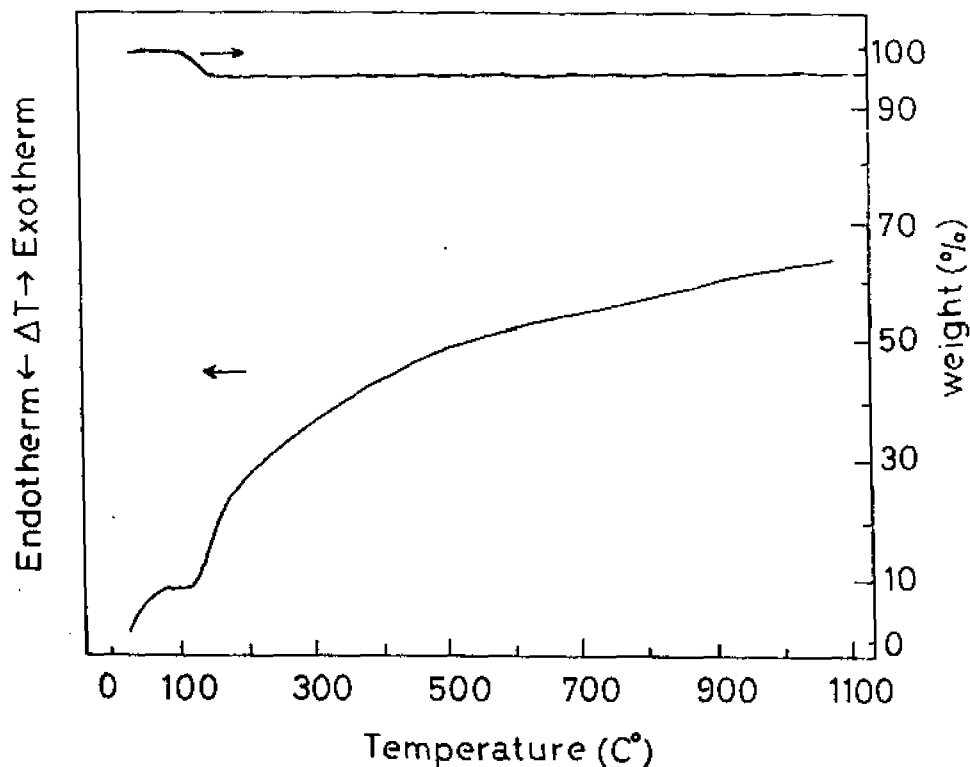


**Figure 6.4:** TGA and DTA Trace of as-prepared  $\text{Ba}_2\text{LaZrO}_{5.5}$  powder between 30 and 1100°C in nitrogen atmosphere at a heating rate of 10°C / min.

#### 6.4.3 FT-IR studies of $\text{Ba}_2\text{REZrO}_{5.5}$ :

Additional information regarding the phase purity and the presence or organic intermediates were obtained by FT-IR spectroscopy. IR spectra of the samples were recorded in the range 400-4000  $\text{cm}^{-1}$  on a Nicolet I 400 D FT-IR spectrometer using KBr pellet method. Figures 6.8 to 6.12 show the FT-IR spectrum of as-prepared  $\text{Ba}_2\text{REZrO}_{5.5}$  compared with that of the sintered specimens. The additional vibrations in the as-prepared powder other than that present in the sintered sample are due to adsorbed moisture. This corroborates the

XRD and thermal analysis results that the combustion is complete and no organic intermediates were present in the sample.

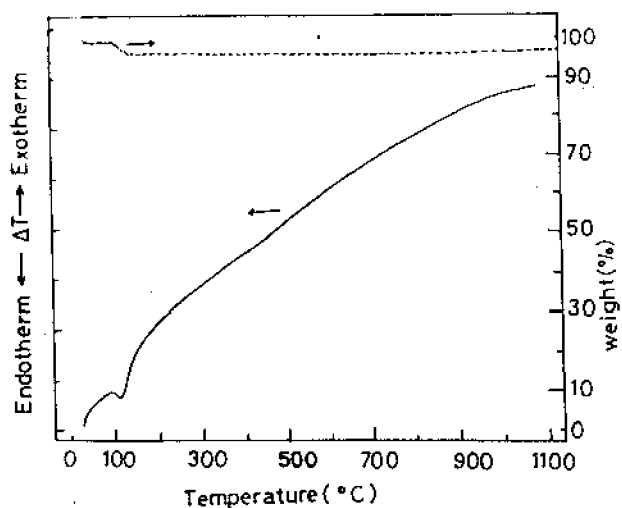


**Figure 6.5:** TGA and DTA Trace of as-prepared  $\text{Ba}_2\text{EuZrO}_{5.5}$  powder between 30 and 1100 $^{\circ}\text{C}$  in nitrogen atmosphere at a heating rate of 10 $^{\circ}\text{C}$  / min.

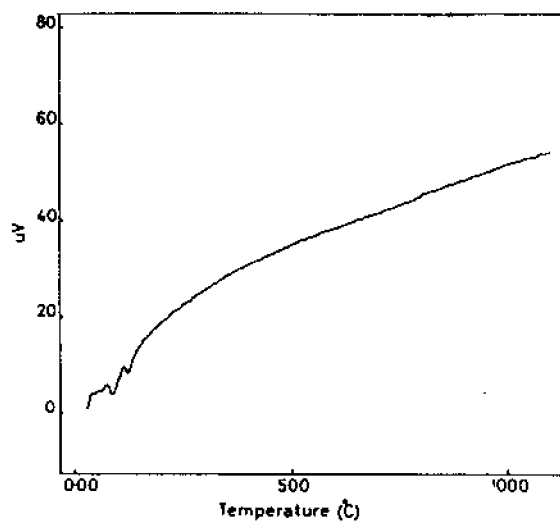


**Figure 6.6:** DTA Trace of as-prepared  $\text{Ba}_2\text{YZrO}_{5.5}$  powder between 30 and 1100 $^{\circ}\text{C}$  in nitrogen atmosphere at a heating rate of 10 $^{\circ}\text{C}$  / min.

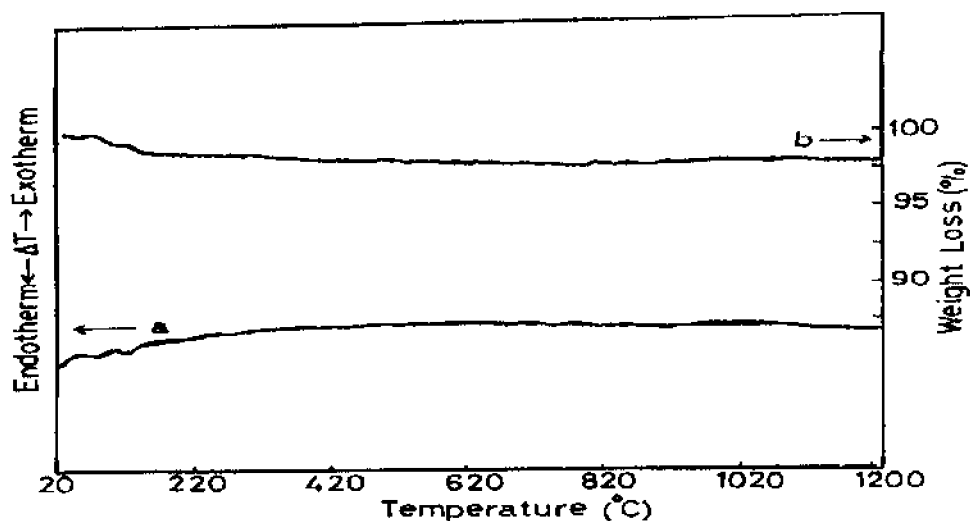


Figure 6.7: TGA and DTA Trace of as-prepared  $\text{Ba}_2\text{HoZrO}_{5.5}$  powder between 30 and  $1100^\circ\text{C}$  in nitrogen atmosphere at a heating rate of  $10^\circ\text{C} / \text{min}$ .

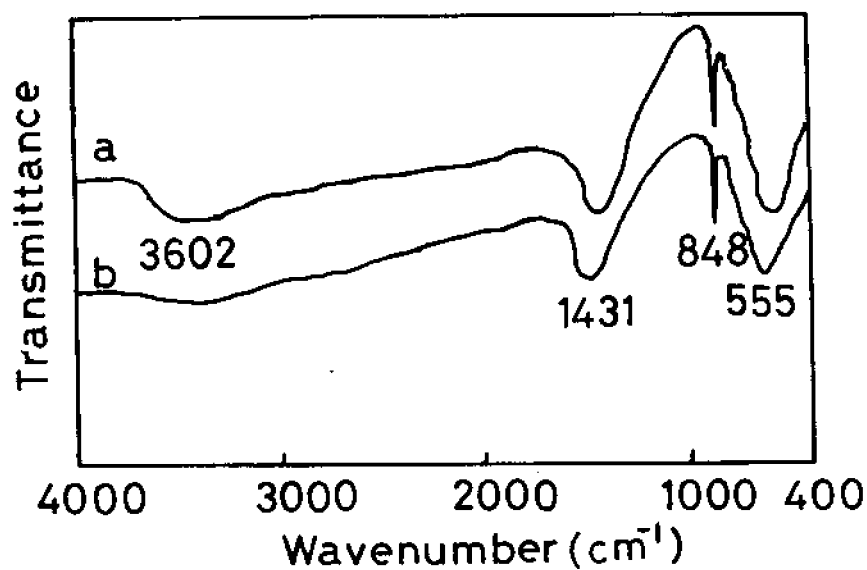


Figure 6.8: FT-IR spectrum of (a) as-prepared  $\text{Ba}_2\text{LaZrO}_{5.5}$  powder obtained through combustion synthesis and (b)  $\text{Ba}_2\text{LaZrO}_{5.5}$  heated at  $1350^\circ\text{C}$ .

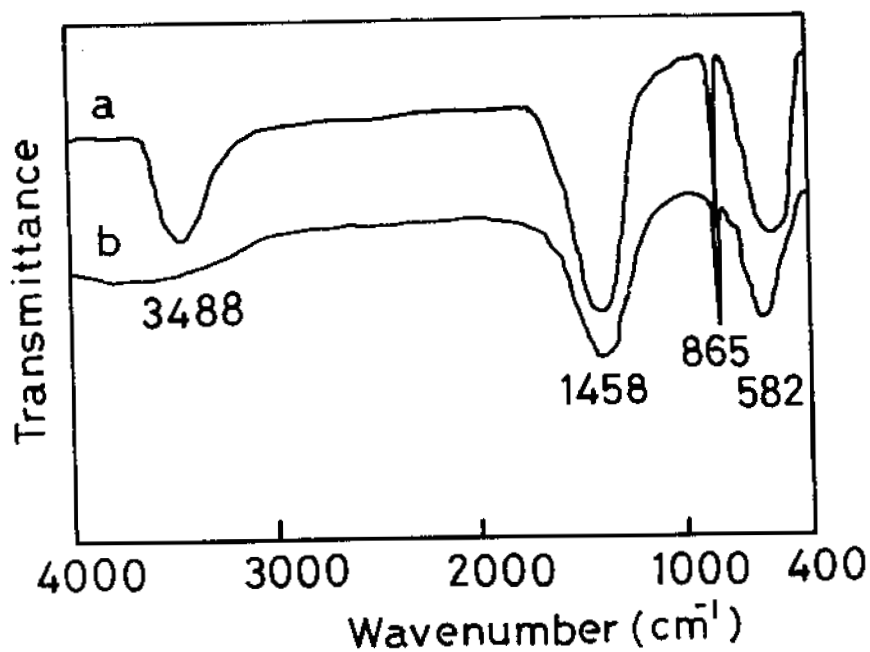


Figure 6.9: FT-IR spectrum of (a) as-prepared Ba<sub>2</sub>EuZrO<sub>5.5</sub> powder obtained through combustion synthesis and (b) Ba<sub>2</sub>EuZrO<sub>5.5</sub> heated at 1525°C.

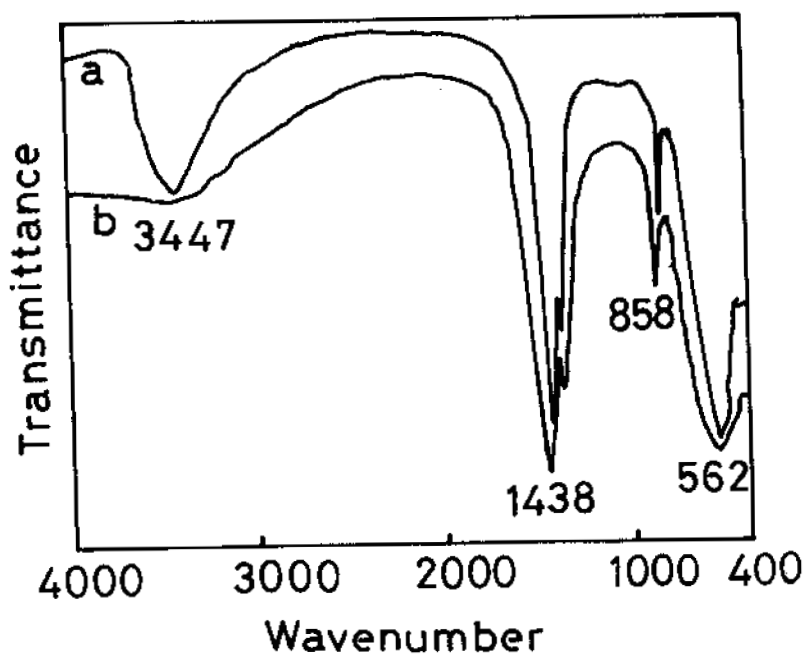
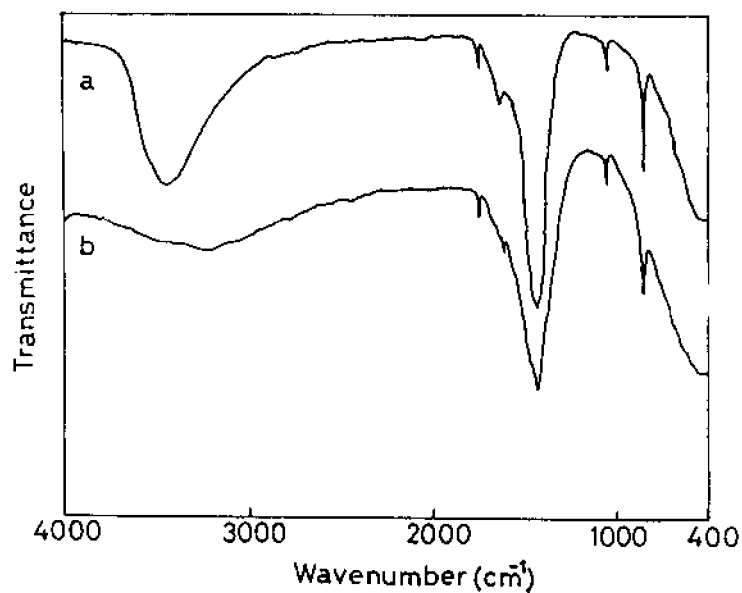
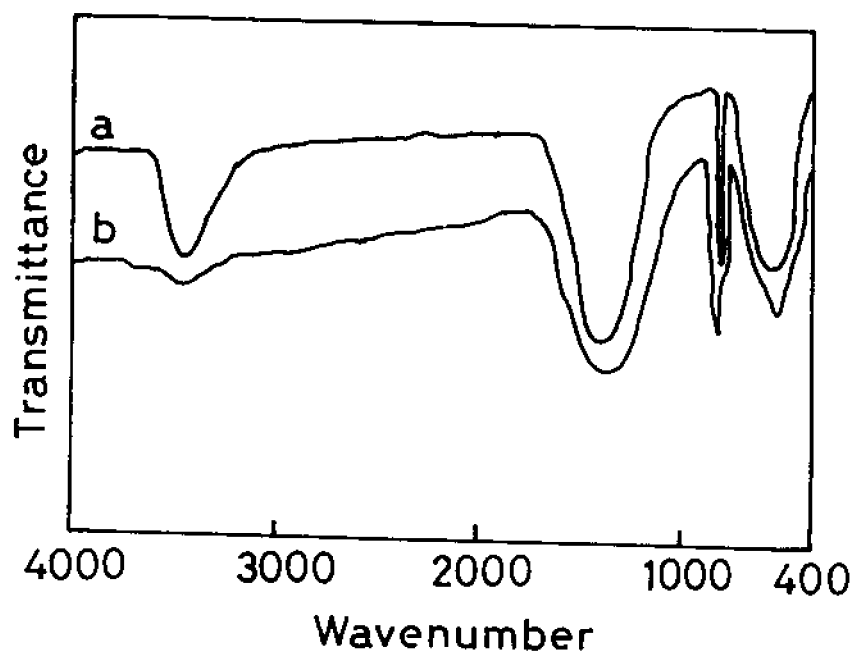


Figure 6.10: FT-IR spectrum of (a) as-prepared Ba<sub>2</sub>YZrO<sub>5.5</sub> powder obtained through combustion synthesis and (b) Ba<sub>2</sub>YZrO<sub>5.5</sub> heated at 1500°C.



**Figure 6.11:** FT-IR spectrum of (a) as-prepared  $\text{Ba}_2\text{HoZrO}_{5.5}$  powder obtained through combustion synthesis and (b)  $\text{Ba}_2\text{HoZrO}_{5.5}$  heated at  $1600^\circ\text{C}$ .



**Figure 6.12:** FT-IR spectrum of (a) as-prepared  $\text{Ba}_2\text{ErZrO}_{5.5}$  powder obtained through combustion synthesis and (b)  $\text{Ba}_2\text{ErZrO}_{5.5}$  heated at  $1600^\circ\text{C}$ .

#### 6.4.4 Gas adsorption studies of the combustion product:

The powder characteristics like adsorption isotherm and specific surface area of the powder was studied using nitrogen adsorption studies. The surface area and gas adsorption studies of the samples were carried out on a Micromeritics unit model Gemini 2360 using nitrogen as adsorbent. The powder samples for this study was degassed at 300°C for 2 h and the adsorption studies were done at liquid nitrogen temperature using analar nitrogen. Table 6.2 gives the BET surface area and the equivalent particle size of Ba<sub>2</sub>REZrO<sub>5.5</sub> calculated by assuming that they are all consists of discrete monosized particles using the formula.

$$t = 6 / \rho A \quad (6.2)$$

where  $t$  is the particle,  $\rho$  is the density of the materials and  $A$  is the specific surface area. The adsorption isotherm of nanoparticles of Ba<sub>2</sub>REZrO<sub>5.5</sub> powders is shown in figure 6.13 . The adsorption behavior of all the material in the group are identical and corresponded to type II isotherm [43]. Type II isotherm is usually encountered for non-porous powder with average pore diameter larger than micropores. The knee of the isotherm indicates the completion of the first adsorbed monolayer and with increasing relative pressure, the higher layers being filled until at saturation, the number of adsorbed layers become infinite

**Table 6.2:** BET surface area, particle size calculated from surface area and pore size of the combustion synthesized  $\text{Ba}_2\text{REZrO}_{5.5}$  powder.

Material	BET surface area ( $\text{m}^2 / \text{g}$ )	Particle size calculated from surface area (nm)	Pore diameter ( $\text{cc} / \text{g}$ )
$\text{Ba}_2\text{LaZrO}_{5.5}$	10	90	0.0543
$\text{Ba}_2\text{EuZrO}_{5.5}$	19	49	0.0636
$\text{Ba}_2\text{YZrO}_{5.5}$	21	48	0.0483
$\text{Ba}_2\text{HoZrO}_{5.5}$	20	43	0.0536
$\text{Ba}_2\text{ErZrO}_{5.5}$	46	40	0.0517

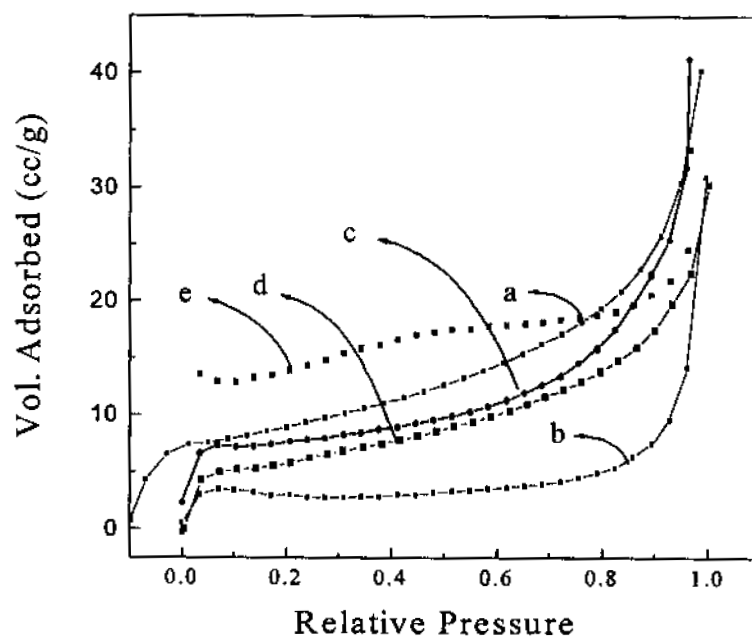


**Figure 6.13:** Adsorption isotherm of (a)  $\text{Ba}_2\text{YZrO}_{5.5}$ , (b)  $\text{Ba}_2\text{LaZrO}_{5.5}$ , (c)  $\text{Ba}_2\text{EuZrO}_{5.5}$ , (d)  $\text{Ba}_2\text{HoZrO}_{5.5}$ , (e)  $\text{Ba}_2\text{ErZrO}_{5.5}$

#### 6.4.5 Agglomerate size analysis of the combustion product

The agglomerate size distribution of the as-prepared nanoparticles of  $\text{Ba}_2\text{REZrO}_{5.5}$  was studied using a Micromeritics sedigraph model 5100. The powder particles were dispersed in water and agitated ultrasonically for 10 min for recording the agglomerate size distribution curve. The agglomerate size distribution of  $\text{Ba}_2\text{REZrO}_{5.5}$  is shown in figure 6.14. It is clear from the particle distribution curve that the majority of the as-prepared powder lies in a smaller particle range ( $<1\mu\text{m}$ ). A few percentage of the as-prepared powder have a larger particle range between 5-10  $\mu\text{m}$ . The maximum size of the agglomerate as seen from the agglomerate size distribution data was  $\sim 10\mu\text{m}$ .

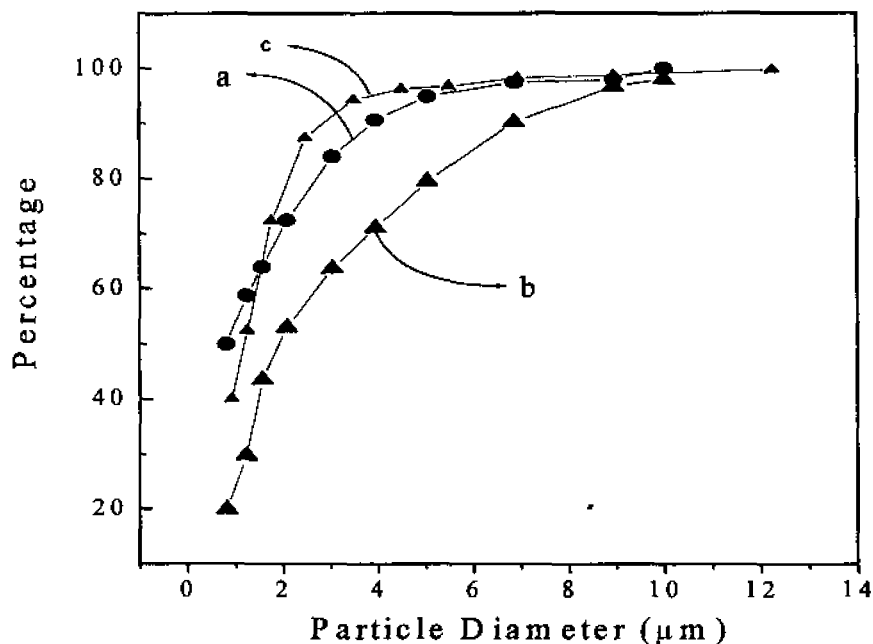
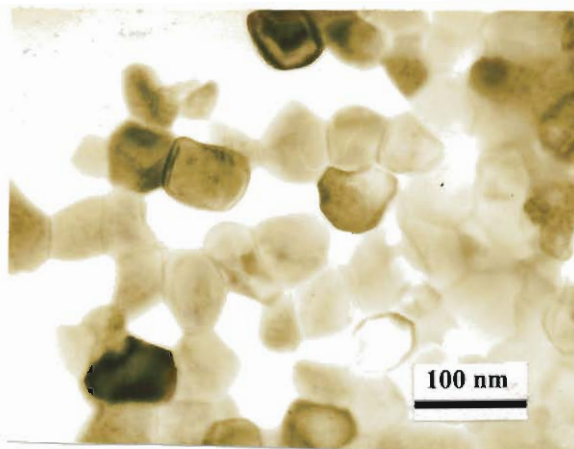


Figure 6. 14: The agglomerate size distribution of the as-prepared powder (a)  $\text{Ba}_2\text{YZrO}_{5.5}$ , (b)  $\text{Ba}_2\text{LaZrO}_{5.5}$ , and (c)  $\text{Ba}_2\text{EuZrO}_{5.5}$

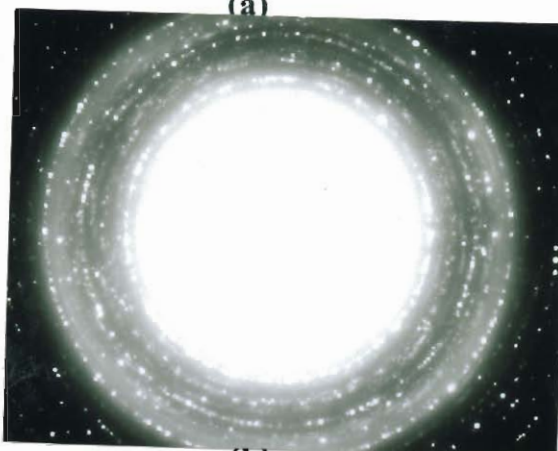
#### 6. 4.5 TEM studies of the combustion product

The powder morphology of the as-prepared powder like particle size, size distribution, shape, shape distribution, degree of particle agglomeration etc were obtained from High-Resolution Transmission Electron Microscopy (HRTEM). The samples for HRTEM was prepared by ultrasonically dispersing the powder particles in methanol and allowing a drop of this to dry on a carbon coated copper grid. The carbon films were developed by vacuum coating technique using an Edward 303 instrument. The Transmission Electron Micrographs were obtained using a JEOL 2000 HRTEM with a top entry stage operating at 200 kV corresponding to a wavelength of 2.508 pm. Each selected area diffraction (SAD) pattern was recorded at a camera length of 100 cm and the calibration of camera length has been confirmed to be within 5%. The TEM studies of the  $\text{Ba}_2\text{REZrO}_{5.5}$  powder obtained by combustion synthesis showed the powder particles to be submicron-sized aggregates of nanocrystallites.

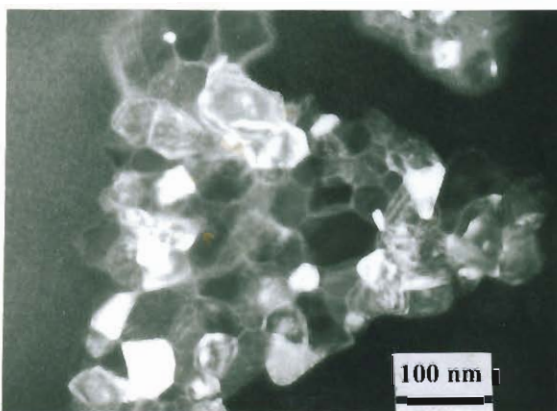
Figure 6.15 (a) is a typical bright field image of the as-prepared  $\text{Ba}_2\text{LaZrO}_{5.5}$  powder particle and figure 6.15(b) is the corresponding SAD pattern. Fig.6.15(c) is a representative powder particle imaged in the dark field mode at a different region. The particles in the system are found to have a bimodal distribution with two size ranges of about 35nm and 65 nm. The SAD pattern obtained has been indexed and is in agreement with the XRD results. Table 6.3 shows the electron diffraction data of  $\text{Ba}_2\text{LaZrO}_{5.5}$  powder obtained through the present combustion route. The ring pattern in the SAED also indicates the nanocrystalline nature of the  $\text{Ba}_2\text{LaZrO}_{5.5}$  powder.



(a)



(b)



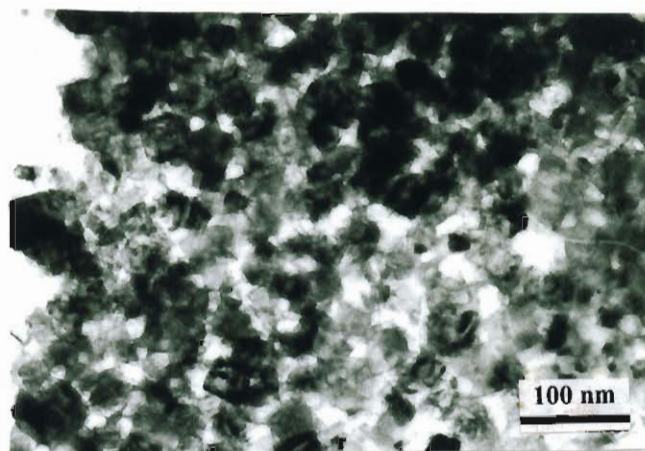
(c)

Figure 6.15: (a) Bright field TEM micrograph of an as-prepared  $\text{Ba}_2\text{LaZrO}_{5.5}$ , (b) corresponding selected area diffraction pattern, and (c) dark-field image of a particle of as-synthesized  $\text{Ba}_2\text{LaZrO}_{5.5}$  powder

**Table 6.3:** Electron diffraction pattern of a powder particle of  $\text{Ba}_2\text{LaZrO}_{5.5}$ 

Ring No	Diameter (mm)	d (Å)	hkl
1	21.68	2.314	222
2	26.26	1.910	420
3	33.72	1.486	440
4	40.42	1.241	444
5	45.02	1.114	642

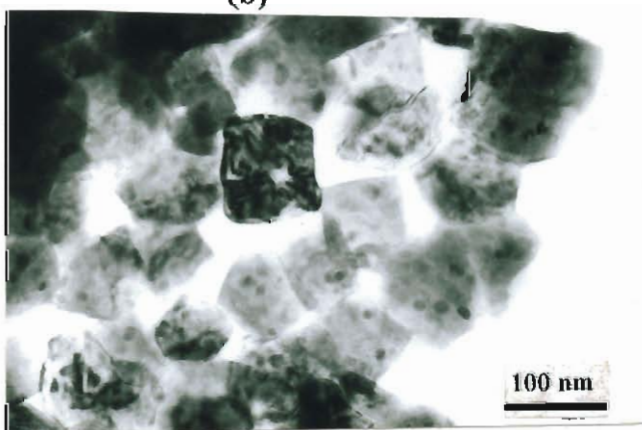
Figure 6.16 (a) shows typical high-resolution electron micrographs of a nanoparticle cluster from the as-prepared  $\text{Ba}_2\text{EuZrO}_{5.5}$  powder. The measured particle size distribution shows a mean particle size of 38 nm with a standard deviation of 12 nm. The particles are of regular cuboidal shape and are submicron aggregates of nanocrystallites. The selected area diffraction pattern of this sample is shown in figure 6.16(b). The electron diffraction data of the pattern shown in figure 6.16 (b) is given in Table 6.4. A small fraction of the as-prepared powder also consists of larger cuboidal particles of about 100 nm size as shown in figure 6.16(c). A closer examination of these larger sized particles reveals that they consist of finer nanocrystallites in the size range 6 nm to 22 nm. The electron diffraction pattern corresponding to this region showed spotty nature which can be due to the fact that the finer crystallites having related orientations are agglomerated together resulting in a limited set of orientations. Figure 6.17 is the high-resolution lattice image of the agglomerate sample in figure 6. 16(c). This lattice image shown in figure 6.17 confirmed the possibility of finer crystallites in the particle having the same orientations. The same set of lattice planes is imaged across nanocrystalline boundaries in the same orientation.



(a)



(b)



(c)

Figure 6.16: (a) Bright field TEM micrograph of an as-prepared  $\text{Ba}_2\text{EuZrO}_{5.5}$ , (b) corresponding selected area diffraction pattern, and (c) bright field micrograph of an as-prepared  $\text{Ba}_2\text{EuZrO}_{5.5}$  powder containing larger particles

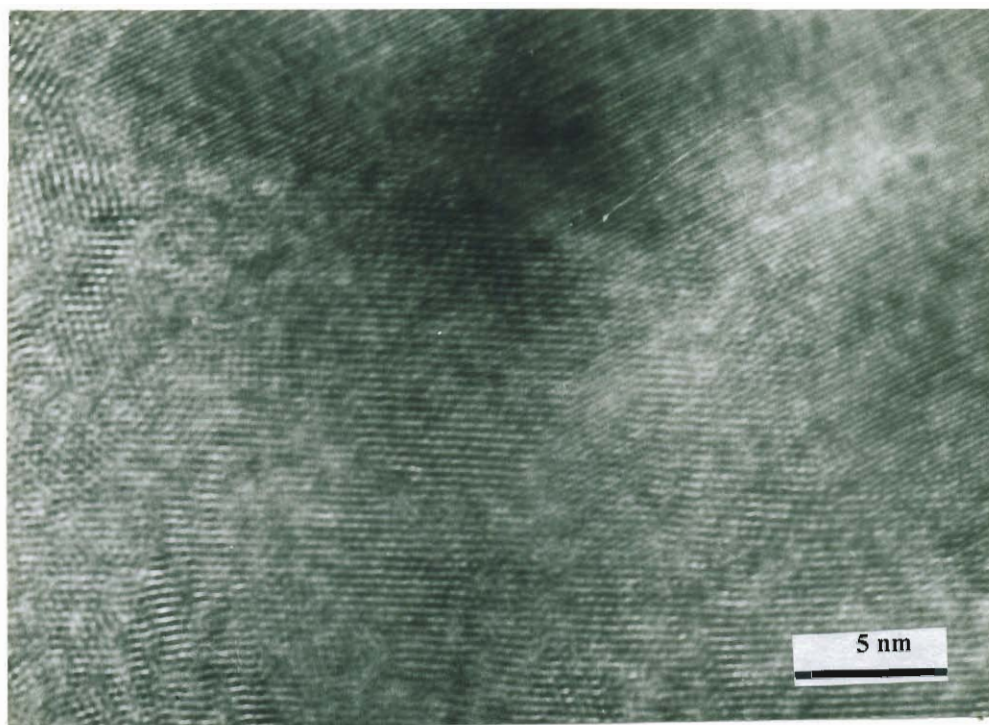


Figure 6. 17: HRTEM lattice image of a powder showing aggregation of finer crystallites in the particle having related orientation

Table 6.4: SAD pattern of a powder particle of  $\text{Ba}_2\text{EuZrO}_{5.5}$

Ring No.	Diameter (nm)	d (Å)	Hkl
1	19	2.639	311
2	22	2.279	400
3	26.5	1.892	420
4	30.5	1.664	511/333
5	34.5	1.453	442
6	40.5	1.238	444

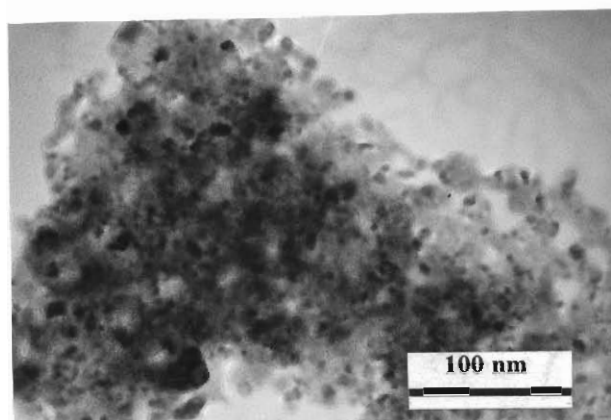
Figure 6.18 (a) shows a typical high-resolution electron micrograph of a nanoparticle cluster from the as-prepared  $\text{Ba}_2\text{HoZrO}_{5.5}$  powder imaged in bright field mode and figure 6. 18 (b) is the corresponding dark field image. The size of

the agglomerates ranged from 200 to 300 nm while the measured nanocrystalline grains are in the range 4 nm to 16 nm with a mean size of 8.2 nm. Both agglomerate and the nanocrystallites are seen to be of irregular shape. The selected area diffraction pattern of this sample is shown in figure 6.18(c). The diffraction data comprising of ring diameter,  $d$  values and  $(hkl)$  values are given in Table 6.5. The electron diffraction pattern is now indexed for a cubic perovskite structure in which the doubling of the basic perovskite unit cell is observed. The SAD pattern is in good agreement to the XRD data.

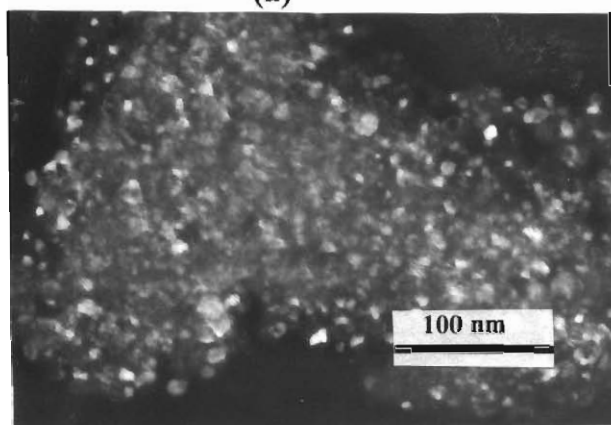
**Table 6.5:** SAD pattern for nanoparticles of  $Ba_2HoZrO_{5.5}$

Ring No.	Diameter (mm)	$d$ (Å)	$hkl$
1	16.9	2.965	220
2	19.0	2.639	311
3	21.0	2.379	222
4	24.0	2.106	400
5	27.0	1.857	420
6	29.5	1.700	422
7	35.0	1.433	440
8	38.0	1.320	620
9	41.0	1.223	642

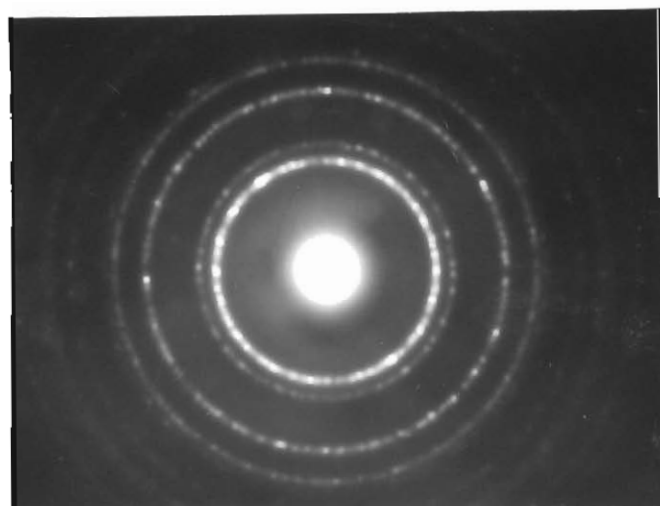
A typical bright field image of a powder particle of as-prepared  $YBa_2ZrO_{5.5}$  is shown in figure 6.19(a) and the corresponding selected area diffraction pattern is given in figure 6.19(b). Aggregate sizes ranged from about 300 nm to more than 1000 nm while the crystallite sizes, as measured in dark field images, ranged from 5 nm to 50 nm. Figure 6.19(c) is a representative powder particle, imaged in the



(a)



(b)



(c)

**Figure 6.18:** (a) Bright field and (b) dark field TEM micrographs of a as-prepared  $\text{Ba}_2\text{HoZrO}_{5.5}$  powder particle, (c) corresponding electron diffraction pattern.

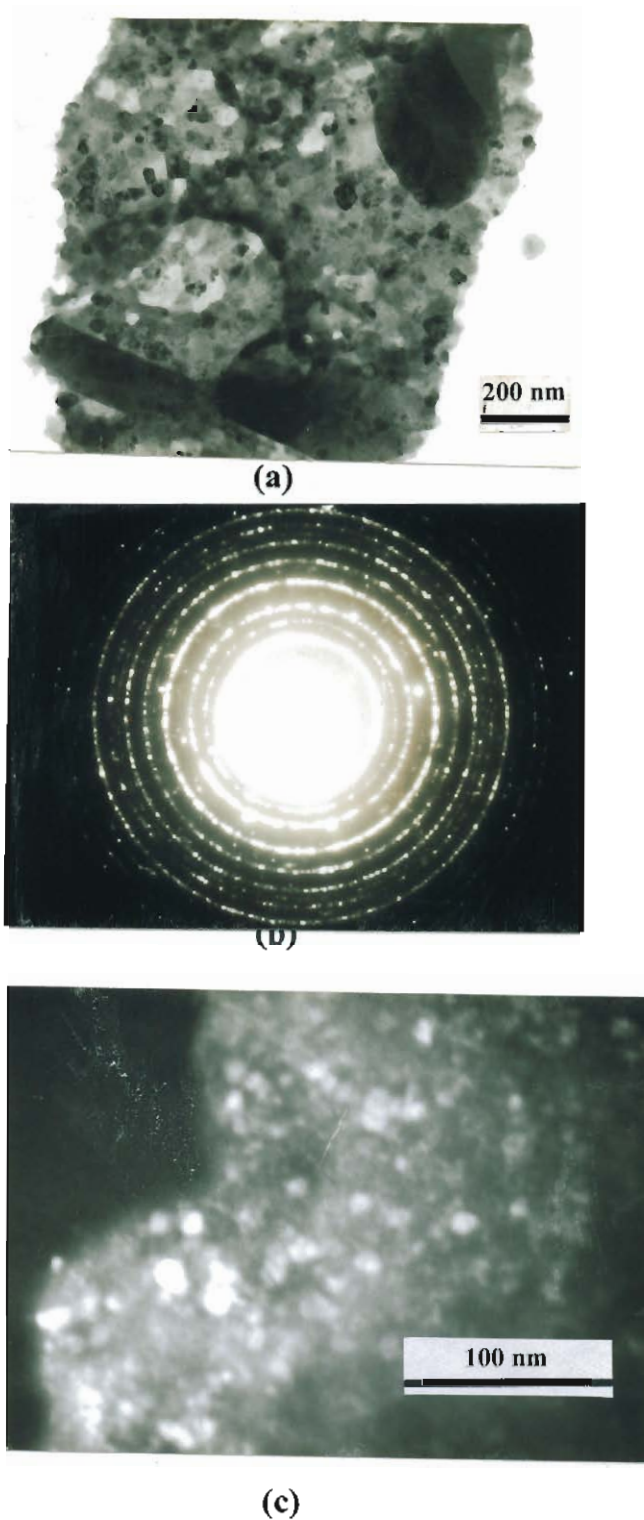


**Figure 6.19:** (a) Bright field TEM micrographs of a powder particle of the as-prepared  $\text{Ba}_2\text{YZrO}_{5.5}$ , (b) corresponding electron diffraction pattern and (c) dark field image of a powder particle of the as-synthesized  $\text{Ba}_2\text{YZrO}_{5.5}$ .

dark field mode using the (220) beams. The electron diffraction pattern obtained for the nanocrystalline particle has been indexed and is given in Table 6.6. The HRTEM lattice imaging of a powder particle is shown in Figure 6.20. An intercrystalline boundary has also been imaged. The lattice image of the nanocrystalline powder showed very little distortion or strain in the lattice and the interface is quite sharp and seems to be without any second phase.

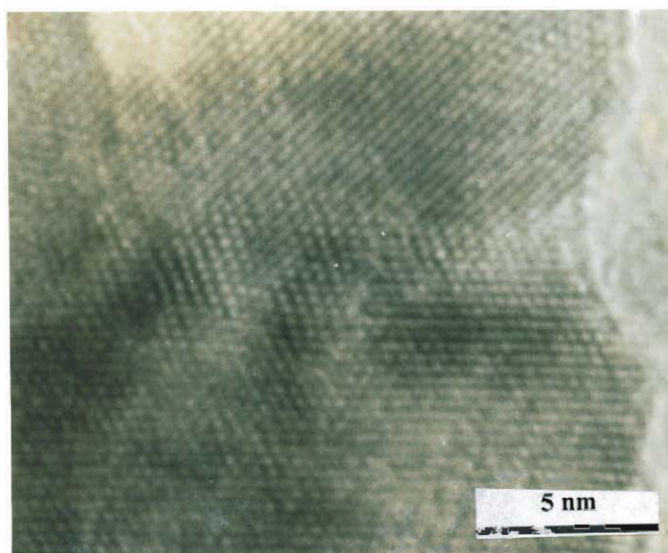


**Figure 6. 20:** HRTEM lattice image of an intercrystalline boundary of  $\text{Ba}_2\text{YZrO}_{5.5}$ .

**Table 6.6: SAD pattern of YBa<sub>2</sub>ZrO<sub>5.5</sub> nanopowder**

Ring No.	Diameter (mm)	d (Å)	Hkl
1	19.7	2.539	311
2	23.0	2.179	400
3	27.0	1.857	420
4	31.5	1.592	511
5	35.0	1.433	440
6	36.5	1.374	531/442
7	38.0	1.320	620
8	41.5	1.208	444
9	47.0	1.067	642
10	49.5	1.013	660

### 6.5 Sintering of nanoparticles of Ba<sub>2</sub>REZrO<sub>5.5</sub>:

The nanoparticulate powders of Ba<sub>2</sub>REZrO<sub>5.5</sub> synthesized through the present method has been sintered to ~ 98 % of the theoretical density. The single phase Ba<sub>2</sub>REZrO<sub>5.5</sub> powders were pressed at a pressure of ~ 450 Mpa in the form of circular discs of dimensions 13 mm diameter and ~ 2.5 thickness and these discs were sintered in air in the temperature range 1375-1525°C for duration ranging from 4 to 10 h. The relative green densities of the samples were 55 ± 2% for this pressure. The individual sintering temperature and time for the nanoparticles of each materials synthesized through the present combustion method compared with the sintering temperature and time of the respective powders obtained through the solid state route is given in Table 6.7. The sintered and relative densities of nanoparticles and coarse-grained powders of Ba<sub>2</sub>REZrO<sub>5.5</sub> materials are also compared in Table 6.7. In all the cases there are a substantial decrease in sintering temperatures of the nanocrystalline powders. The sintering behavior of the nanoparticles of Ba<sub>2</sub>REZrO<sub>5.5</sub> powders synthesized through the combustion route

**Table 6.7:** Comparison of sintering parameters and sintered densities of nano particles obtained through the present method and coarse-grained powders obtained through solid state route of  $Ba_2REZrO_{5.5}$  materials.

Material	Nanoparticles obtained through the modified combustion process				Coarse grained powder obtained through the solid state route			
	sintering		density		Sintering		density	
	Temp. (°C)	Time (h)	Sintered (g / cc)	Relative (%)	Temp. (°C)	Time (h)	Sintered (g / cc)	Relative (%)
$Ba_2LaZrO_{5.5}$	1375	6	6.52	98	1550	10	6.31	97
$Ba_2EuZrO_{5.5}$	1525	6	6.54	97	1625	10	6.49	96
$Ba_2YzrO_{5.5}$	1500	4	6.02	97	1675 *	10	5.96	96
$Ba_2HoZrO_{5.5}$	1500	10	6.72	98	1600 *	10	6.65	97
$Ba_2ErZrO_{5.5}$	1525	6	6.49	98	1650 *	10	6.36	96

\* in presence of 1 wt.% of CuO

is compared with that of coarse-grained powders synthesized through solid state reaction method. Figure 6.21 shows the variation of relative density with temperature for the above two sets of powders. It can be clearly seen from the figures that sinterability of nanoparticle is excellent compared to that of coarse-grained powders synthesized through solid state route. A sintered density of 97 % could be obtained for nanoparticles at a sintering temperature of 1525°C for 6h. In the case of powders prepared through solid-state route, a minimum sintering temperature of 1650°C for 10 h was required to obtain a sintered density of 96% of the theoretical density. This reduction in sintering temperature and time may be attributed to the enhanced kinetics due to the small degree of agglomeration and ultrafine nature of the powder [44].

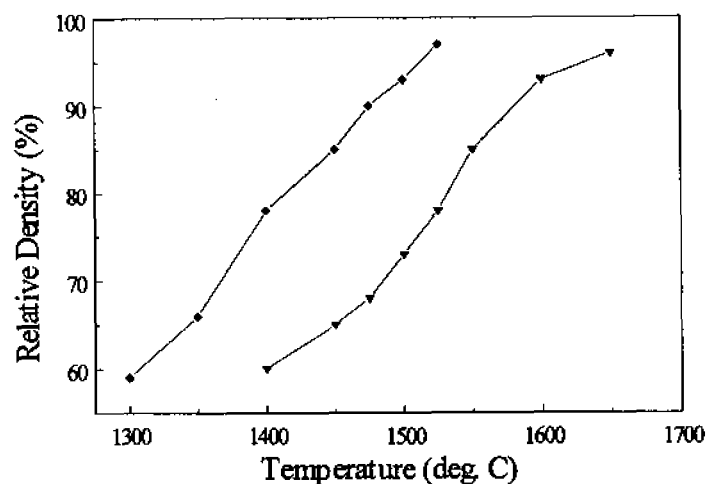


**Figure 6.21:** Variation of Relative density with temperatre of  $Ba_2EuZrO_{5.5}$  nanoparticles

## 6.6 Structural characterization of the sintered Nanoparticles

The XRD pattern for  $2\theta$  between  $5$  and  $90^\circ$  of sintered  $Ba_2REZrO_{5.5}$  samples synthesized through the combustion process is shown in figures 6. 27 (a-b). The sintered samples were single phase and has the same structure as that of the solid state synthesized powders. All the peaks including the minor ones are indexed for a cubic perovskite structure with the general formula  $A_2BB'O_6$ , in which the doubling of the unit cell is observed. The lattice constant values calculated from the XRD patterns of the  $Ba_2REZrO_{5.5}$  material synthesized through the present method agrees very well with the lattice constant values synthesized through the solid state route.

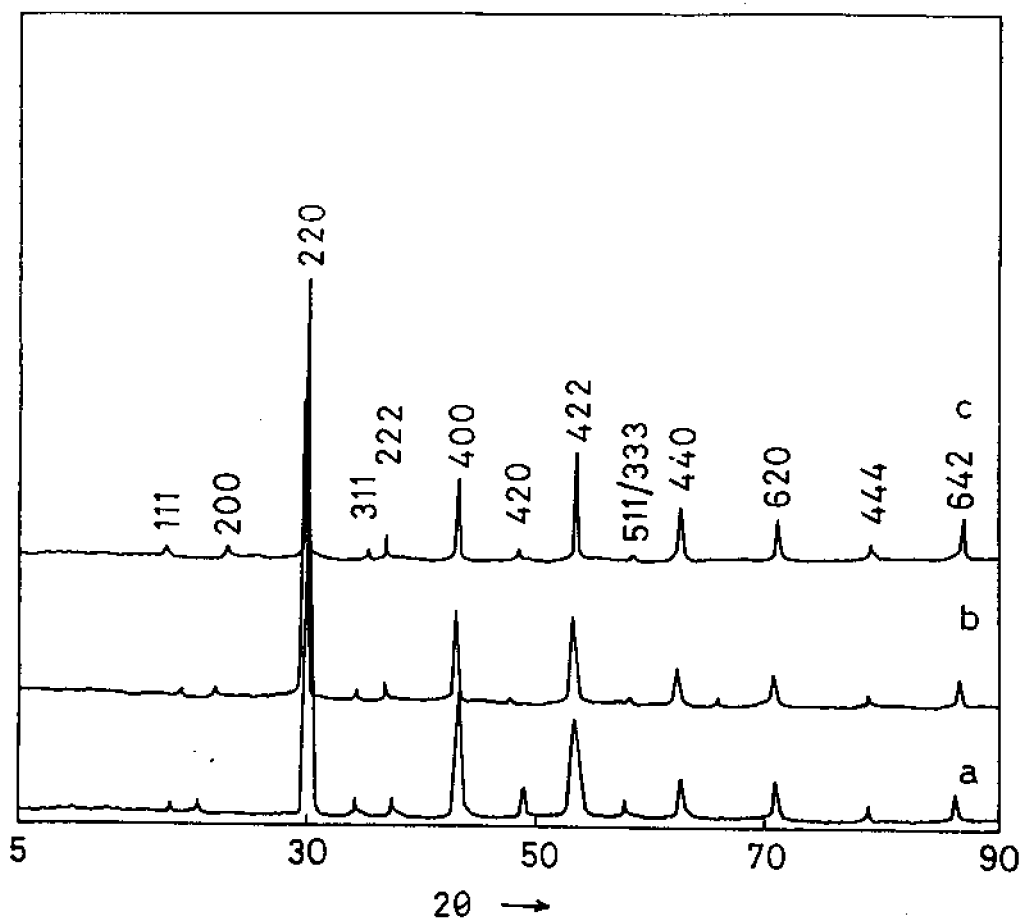
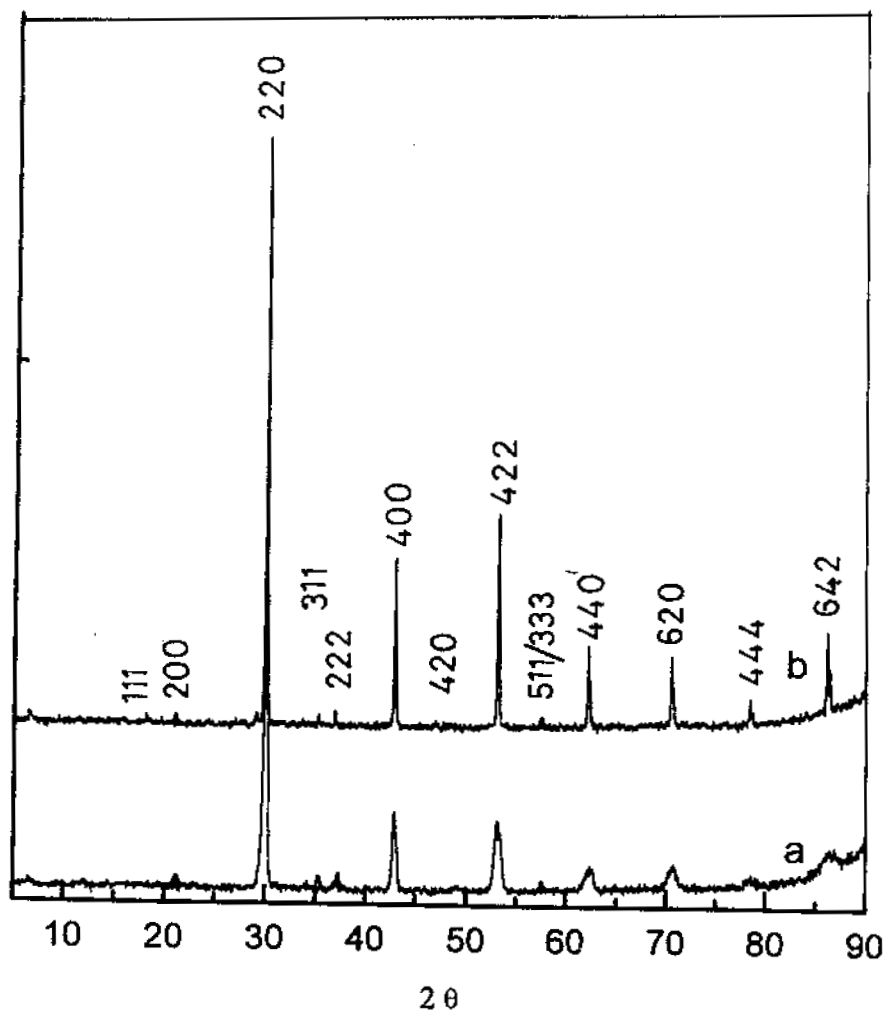


Figure 6.22: The XRD pattern of sintered nanoparticles of (a)  $\text{Ba}_2\text{YZrO}_{5.5}$ , (b)  $\text{Ba}_2\text{LaZrO}_{5.5}$ , (a)  $\text{Ba}_2\text{EuZrO}_{5.5}$



**Figure 6.22:** The XRD pattern of sintered nanoparticles of (a)  $\text{Ba}_2\text{HoZrO}_{5.5}$ , (b)  $\text{Ba}_2\text{ErZrO}_{5.5}$ .

## 6.7 Conclusions

A modified combustion process has been developed for the synthesis of nanoparticles of ceramic oxides. The method is particularly useful for the synthesis of nanosized particles of complex perovskite ceramic oxides. By using the present

combustion route nanoparticles of phase pure materials can be synthesized by heating a precursor solution containing metal salts and a complexing agent in a hotplate / sand bath after adjusting the oxidant / fuel ratio of the initial solution. The newly developed  $\text{Ba}_2\text{REZrO}_{5.5}$  materials were synthesized as nanoparticles through the present modified combustion process. The X-ray and electron diffraction studies revealed that  $\text{Ba}_2\text{REZrO}_{5.5}$  was obtained as single-phase materials without another phase and had a cubic perovskite ( $\text{A}_2\text{BB}'\text{O}_6$ ) structure. The thermal analyses were carried out to study the changes occurring in the sample on heat treatment. The thermal studies revealed that the decomposition is complete during the combustion process itself and there was no evidence of any phase transition at high temperature. Additional information regarding the phase purity and the presence of carbonaceous impurities were obtained from IR spectroscopic studies. The particulate properties such as specific surface area and adsorption behavior were studied using nitrogen gas adsorption technique. The particle morphology of the as-prepared powders was studied by high-resolution transmission electron microscopy. The TEM studies of the  $\text{Ba}_2\text{REZrO}_{5.5}$  powder obtained by combustion synthesis showed the powder particles are submicron-sized aggregates of nanocrystallites. The aggregate / agglomerate size ranged from 100 nm up to 1 microns while the measured nanocrystalline grains ranges from 4 nm to 65 nm. The high-resolution lattice image of the nanocrystalline particle showed very little distortion in the lattice and the intercrystalline boundary was quite sharp without any second phase. The nanocrystalline powders obtained through the present method could be sintered to high density at relatively lower temperature for shorter duration. The sintering behavior of the nanoparticles of  $\text{Ba}_2\text{REZrO}_{5.5}$  powders is excellent compared with the powder obtained through the solid-state reaction method.

## References

- [1] G. H. Beall, L. R. Pinckney, *J. Am. Ceram. Soc.*, **82**, (1999) 5.
- [2] R. D. Shull, *Nanostruct. Mater.*, **7**, (1996) 265.
- [3] C. Suryanarayana, *Bull. Mater. Sci.*, **17**, (1994) 307.
- [4] R. A. Andrievski, *J. Mater. Sci.*, **29**, (1994) 614.
- [5] H. Glieter, *Nanostruct. Mater.*, **1**, (1992) 1.
- [6] H. Glieter, *Acta Mater.*, **48**, (2000) 1.
- [7] J. Wang, J. Fang, S.-C. Ng, L.-M. Gan, C.-H. Chew, X. Wang, Z. Shen, *J. Am. Ceram. Soc.*, **82**, (1999) 873.
- [8] V. Avalacek, J. A. Puszynski, *Ind. Eng. Chem. Res.*, **35**, (1996) 349.
- [9] J. Fang, J. Wang, S.-C. Ng, C.-H. Chew, L.-M. Gan, *Nanostruct. Mater.*, **8**, (1997) 499.
- [10] L.-M. Gan, L. H. Zhang, H. S. O. Chen, C.-H. Chew, B. H. Loo, *J. Mater. Sci.*, **31**, (1996) 1071.
- [11] G. Messing, S. Zhang, V. Jayanthi, *J. Am. Ceram. Soc.*, **76**, (1993) 2707.
- [12] N. J. Ali, S. J. Mline, *Trans. J. Brit. Ceram. Soc.*, **86**, (1987) 113.
- [13] L. A. Xue, F. L. Riley, R. J. Brrok, *Trans. J. Brit. Ceram. Soc.*, **85**, (1986) 47.
- [14] M. Arima, M. Kakihana, Y. Nakamura, M. Yashima, M. Yoshimura, *J. Am. Ceram. Soc.*, **79**, (1996) 2842.
- [15] N. G. Eror, H. U. Anderson, *Mater. Res. Soc. Proc.*, **73**, (1986) 571.
- [16] F. H. Chen, H. S. Koo, T. Y. Tseng, *J. Am. Ceram. Soc.*, **75**, (1992) 96.
- [17] M. Stockenhuber, H. Mayer, J. A. Lercher, *J. Am. Ceram. Soc.*, **76**, (1993) 1185.
- [18] H. S. Potdar, P. Singh, S. D. Deshpande, P. K. Goodbole, S. K. Date, *Mater. Lett.*, **10**, (1990) 112.

- [19] H. Yamamura, A. Watanabe, S. Shirasaki, Y. Moriyoshi, M. Tanaka, *Ceram. Int.*, **11**, (1985) 17.
- [20] J. P. Coutures, P. Odeir, C. Proust, *J. Mater. Sci.*, **27**, (1992) 1849.
- [21] G. A. Hutchins, G. H. Maher, S. D. Ross, *J. Am. Ceram. Soc.*, **66**, (1987) 681.
- [22] B. J. Mulder, *Ceram. Bull.*, **49**, (1970) 990.
- [23] S. Kim, M. Lee, T. Noh, C. Lee, *J. Mater. Sci.*, **31**, (1994) 3643.
- [24] T. Yunkasiri, G. Rujijanagal, *J. Mater. Sci. Lett.*, **13**, (1994) 165.
- [25] T. T. Fang, H. B. Lin, J. B. Hwang, *J. Am. Ceram. Soc.*, **73**, (1990) 3363.
- [26] P. K. Dutta, R. Asiaie, S. A. Akbar, W. Zhu, *Chem. Mater*, **6**, (1994) 1542.
- [27] K. Fukai, K. Hikada, M. Aoki, K. Abe, *Ceram. Int*, **16**, (1990) 285.
- [28] M. Hirano, E. Kato, *J. Am. Ceram. Soc.*, **79**, (1996) 777.
- [29] G. Wilson, R. Heathcote, *J. Am. Ceram. Soc.*, **69**, (1990) 1137.
- [30] M. F. Yan, *Mater. Sci. Engg.*, **48**, (1981) 53.
- [31] M. H. Frey, D. A. Payne, *Chem. Mater*, **7**, (1995) 123.
- [32] J. J. Kinglsey, K. Suresh, K. C. Patil, *J. Mater. Sci.*, **25**, (1990) 1305.
- [33] J. J. Kingsley, K. C. Patil, *Mater. Lett.*, **6**, (1988) 427.
- [34] J. J. Kingsley, K. Suresh, K. C. Patil, *J. Solid State Chem.*, **88**, (1990) 435.
- [35] P. Pramanik, *Bull. Mater. Sci.*, **19**, (1996) 957.
- [36] S. K. Saha, P. Pramanik, *Nanostruct. Mater.*, **8**, (1997) 29.
- [37] A. Pathak, S. D. Kulkarni, S. K. Date, P. Pramanik, *Nanostruct. Mater.*, **8**, (1997) 101.
- [38] R. N. Das, P. Pramanik, *Nanostruct. Mater.*, **10**, (1998) 1371.
- [39] P. Pramanik, *Bull. Mater. Sci.*, **22**, (1999) 335.
- [40] N. J. Hess, D. W. Maupin, L. A. Chik, D. S. Sunberg, D. E. M. Creedy, T. R. Armstrong, *J. Mater. Sci.*, **29**, (1994) 1873.

- [41] S. D. Ramamurthy, Z. Xu, D. A. Payne, *J. Am. Ceram. Soc.*, **73**, (1990) 2760.
- [42] B. D. Cullity, *Elements of X-ray Diffraction*, Addison-Wesley Publishing Co, Inc. 1967.
- [43] S. Lowel, J. E. Shields, *Powder Surface and Porosity*, Chapman and Hall, London 1984.
- [44] W. H. Rhodes, *J. Am. Ceram. Soc.*, **64** (1981) 19

## CHAPTER VII

### SUMMARY AND CONCLUSION

The thesis presents detailed study on (1) the development of a new group of complex perovskite ceramic oxides for their use as substrate for high  $T_C$  superconductors through conventional solid state reaction method, (2) preparation and characterization of high  $T_C$  superconductors films on the newly developed substrates, and (3) synthesis of the newly developed materials as nanoparticles through a modified combustion process.

In the course of this research work, a new group of ceramic oxides with the general formula  $Ba_2REZrO_{5.5}$  (RE= La, Ce, Eu, Yb, Ho and Er) has been synthesized and sintered as single-phase materials by solid state reaction method for the first time. The structure of the materials are studied by XRD and all these materials are found to be isostructural having an ordered complex cubic perovskite structure of general formula  $A_2(BB')O_6$ . The presence of the superstructure lines in the XRD pattern of  $Ba_2REZrO_{5.5}$  indicates the doubling of basic  $ABO_3$  perovskite unit cell. Two materials in this group, viz.,  $Ba_2HoZrO_{5.5}$  and  $Ba_2ErZrO_{5.5}$  could not be synthesized as single-phase materials through solid state reaction method by using only the constituent oxides or carbonates. During high temperature annealing, the development of stable  $BaZrO_3$  and  $BaREO_{2.5}$  (RE = Ho and Er) phases prevented the formation of  $Ba_2REZrO_{5.5}$  (RE = Ho and Er) as a single-phase materials even at  $1650^\circ\text{C}$ . However, an addition of small amount of  $\text{CuO}$  (1 wt.%) in the reaction mixture has resulted in the formation of an ordered complex perovskite phase during the heating process. The lattice parameters of  $Ba_2REZrO_{5.5}$  materials measured by x-ray diffraction are in the range 8.394 - 8.551 Å. Based on the proposed crystal structure, the lattice parameters of the  $Ba_2REZrO_{5.5}$  materials were calculated by using a hard sphere approximation and

is in good agreement with the values observed experimentally. These new materials do not undergo any phase transition in the temperature range 30-1300°C. These materials melt congruently making the single crystals from melt possible and are stable under atmospheric conditions. The dielectric constant and loss factor values of these materials are studied at room temperature and liquid nitrogen temperature and are in a range suitable for electronic applications at microwave frequencies. There was no substantial difference in the value of the dielectric constant measured at room temperature and liquid nitrogen temperature, but the dielectric loss decreased almost by one order of magnitude at liquid nitrogen temperature. The dielectric constant values of the  $\text{Ba}_2\text{REZrO}_{5.5}$  materials calculated using the Classius-Mossotti equation are found to be in agreement with the experimentally observed values.

The results of chemical reactivity studies between  $\text{Ba}_2\text{REZrO}_{5.5}$  and YBCO superconductor indicate that the newly developed materials are chemically compatible with the YBCO superconductor even at the extreme processing conditions. The XRD patterns of the  $\text{Ba}_2\text{REZrO}_{5.5}$ -YBCO composite do not show any additional phase other than those of  $\text{Ba}_2\text{REZrO}_{5.5}$  and YBCO in the composite even after severe heat treatment. The addition of  $\text{Ba}_2\text{REZrO}_{5.5}$  up to 50-vol.% in YBCO did not show any detrimental effect on the superconducting properties of YBCO. The lattice matching of  $\text{Ba}_2\text{REZrO}_{5.5}$  with YBCO is within the tolerable limit for epitaxial growth. The suitability of  $\text{Ba}_2\text{REZrO}_{5.5}$  materials as substrate for YBCO was confirmed by developing superconducting thick films of YBCO on  $\text{Ba}_2\text{REZrO}_{5.5}$  materials by dip-coating and melt texturing. Because of the high processing temperature and partial melting of the YBCO films in the dip-coating and melt texturing process, YBCO films adhered very well to the  $\text{Ba}_2\text{REZrO}_{5.5}$  substrates. A peel off-test carried out using highly adhesive tape confirmed the excellent adhesion of the YBCO films to the substrates. The structure of the dip-

coated films was studied by XRD and the superconductivity was studied by temperature-resistance and critical current density measurements. The films showed metallic behavior in the normal state and gave a  $T_{C(0)}$  of  $\sim 92$  K with a transition width of  $\sim 2$  K. The critical current density of the dip-coated and melt textured films were  $\sim 10^4$  A/cm<sup>2</sup> at 77 K under zero applied magnetic field.

The suitability of Ba<sub>2</sub>REZrO<sub>5.5</sub> as substrate for Bi (2212) and Bi (2223) has been studied in detail using x-ray and electrical measurements. In the present study, single-phase Bi<sub>2</sub>Sr<sub>2</sub>CaCu<sub>2</sub>O<sub>x</sub> [ $T_{C(0)} = 85$  K] and Bi<sub>1.5</sub>Pb<sub>0.5</sub>Sr<sub>2</sub>Ca<sub>2</sub>Cu<sub>3</sub>O<sub>x</sub> [ $T_{C(0)} = 110$  K] superconductors were synthesized and sintered through solid state route. X-ray diffraction and resistivity measurements have shown that the newly developed Ba<sub>2</sub>REZrO<sub>5.5</sub> substrates are chemically non-reacting with Bi (2212) superconductors even under extreme processing conditions. A superconducting transition of 85 K was obtained in all the composite mixture consisting of Ba<sub>2</sub>REZrO<sub>5.5</sub> and Bi (2212) containing 0-50 vol. % of Bi (2212) superconductor. The suitability of Ba<sub>2</sub>REZrO<sub>5.5</sub> materials as substrate for Bi (2212) was confirmed by developing superconducting Bi (2212) thick films on Ba<sub>2</sub>REZrO<sub>5.5</sub> materials by dip-coating and melt texturing. The films showed metallic behavior in the normal state and gave a  $T_{C(0)}$  of 85 K and  $J_C \sim 4 \times 10^3$  A / cm<sup>2</sup> at 77 K under zero applied magnetic field. In the present study it was found that Ba<sub>2</sub>LaZrO<sub>5.5</sub> and Ba<sub>2</sub>EuZrO<sub>5.5</sub> are found to be non-reacting with the Bi (2223) superconductor even at the extreme processing conditions. The materials with RE = Ce, Yb, Ho and Er were either decomposed fully or partially in to Bi (2212) when annealed at a temperature of 850°C for 15 h. The suitability of Ba<sub>2</sub>REZrO<sub>5.5</sub> (RE = La and Eu) materials as substrate for Bi (2223) was confirmed by developing superconducting thick films of Bi (2223) superconductors on Ba<sub>2</sub>REZrO<sub>5.5</sub> materials by dip-coating and melt texturing. The film showed metallic behavior in the normal state and adhered very well with the substrate. The Bi (2223) film dip-coated and melt

textured on  $\text{Ba}_2\text{REZrO}_{5.5}$  gave a  $T_C(0)$  of 110 K and  $J_C$   $3 \times 10^3$  A /  $\text{cm}^2$  at 77 K under zero applied magnetic field.

A new single step process for the synthesis of  $\text{Ba}_2\text{REZrO}_{5.5}$  as nanoparticles is described in detail in the thesis. By using the present combustion route nanoparticles of phase pure materials can be synthesized by heating a precursor solution containing metal salts and a complexing agent in a hot plate/sand bath after adjusting the oxidant/fuel ratio of the initial solution. The X-ray and electron diffraction studies revealed that  $\text{Ba}_2\text{REZrO}_{5.5}$  obtained is single-phase and nanoparticles and had a cubic perovskite ( $\text{A}_2\text{BB}'\text{O}_6$ ) structure. The thermal analyses were carried out to study the changes occurring in the sample on heat treatment. The thermal studies revealed that the decomposition is complete during the combustion process itself and there was no evidence of any phase transition at high temperature. Additional information regarding the phase purity and the presence of carbonaceous impurities were obtained from IR spectroscopic studies. The particulate properties such as specific surface area and adsorption behavior were studied using nitrogen gas adsorption technique. The particle morphology of the as-prepared powders was studied by high-resolution transmission electron microscopy. The TEM studies of the  $\text{Ba}_2\text{REZrO}_{5.5}$  powder obtained by combustion synthesis showed the powder particles are submicron-sized aggregates of nanocrystallites. The aggregate/agglomerate size ranged from 100 nm up to 1 microns while the measured nanocrystalline grains ranges from 4 nm to 65 nm. The high-resolution lattice image of the nanocrystalline particle showed very little distortion in the lattice and the intercrystalline boundary was quite sharp without any second phase. The nanocrystalline powders obtained through the present method could be sintered to high density at relatively lower temperature for shorter duration. The sintering behavior of the nanoparticles of  $\text{Ba}_2\text{REZrO}_{5.5}$

powders is excellent compared with the powder obtained through the solid-state reaction method.

### 7.1 Future Projections

The suitability of the newly developed materials for various structural and functional applications will be explored. The newly developed  $\text{Ba}_2\text{REZrO}_{5.5}$  materials have dielectric properties in the range suitable for their use as dielectric resonators. Other studies will be carried out to examine their potential use as dielectric resonators. In addition, the mechanical properties of  $\text{Ba}_2\text{REZrO}_{5.5}$  will be evaluated for their use for structural applications. The thermal properties of  $\text{Ba}_2\text{REZrO}_{5.5}$  such as thermal conductivity, thermal diffusivity, thermal expansivity, specific heat capacity, etc. will be evaluated to examine whether the thermal properties of these materials are suitable for substrate application. All these studies will be extended for nanoparticles of  $\text{Ba}_2\text{REZrO}_{5.5}$  material synthesized through the modified combustion route and the properties of both coarse-grained and nanoparticles will be compared. For the commercial exploitation of these materials, it is necessary that these materials are to be grown as single crystals. The melting experiments carried out on the single phase  $\text{Ba}_2\text{REZrO}_{5.5}$  revealed that these materials melt congruently, making it possible to grow them as single crystals from melt. One of the major future projections is the growth these materials as single crystals and the development of superconducting thin films on the single crystal substrates. High  $T_C$  superconducting thin films will be developed using pulsed laser ablation on single crystals, polycrystalline coarse grained materials and sintered nanostructured  $\text{Ba}_2\text{REZrO}_{5.5}$  materials.

The growth of single crystal films of  $\text{Ba}_2\text{REZrO}_{5.5}$  on technologically important substrates such as Si,  $\text{SiO}_2$ ,  $\text{Al}_2\text{O}_3$  etc. will be useful as they are commonly available and are widely used for many microelectronic applications.

The successful preparation of single crystal films of  $\text{Ba}_2\text{REZrO}_{5.5}$  epitaxially on Si and the growth of high quality superconducting films on them can have tremendous potential for application in integrating superconductivity with the existing semiconductor technology. As the use of high temperature superconductors in high power electrical application has now taken new turns, the deposits of YBCO on textured metal tapes with suitable buffer layer may be the high temperature superconductor wire technology that enables high field electric power devices at liquid nitrogen temperatures. In this case the successful deposition of  $\text{Ba}_2\text{REZrO}_{5.5}$  on commercially available textured metal tapes and the deposit of either YBCO or Bi cuprate films on these layers would be a breakthrough in superconductivity research. The very recent discovery that  $\text{MgB}_2$  -an intermetallic compound- superconducts at 40 K raised the expectations of superconductor technology. The suitability of  $\text{Ba}_2\text{REZrO}_{5.5}$  materials as substrate for the recently identified  $\text{MgB}_2$  superconductor will be studied in detail with a top priority.

In the present study, the modified combustion processes were applied only for the synthesis of the nanoparticles of the materials described in the present thesis. A lot many ceramic oxides are in use in various devices and their properties will be greatly enhanced/modified if they were synthesized and sintered as nanoparticles. The newly developed modified combustion process will be extended for the synthesis of nanoparticles of such commercially important materials using aqueous and non-aqueous metal salts.